

# **Three-dimensional ultrasound in the management of abdominal aortic aneurysm**

Thesis submitted for the degree of Doctor of Medicine (MD) in  
the Faculty of Biology, Medicine and Health

2016

Christopher Lowe

Faculty of Biology, Medicine and Health

School of Medical Sciences

# CONTENTS

<b>CONTENTS</b>	<b>2</b>
<b>FIGURES</b>	<b>6</b>
<b>TABLES</b>	<b>11</b>
<b>ABBREVIATIONS</b>	<b>12</b>
<b>PREFACE</b>	<b>14</b>
<b>ABSTRACT</b>	<b>15</b>
<b>DECLARATION</b>	<b>16</b>
<b>COPYRIGHT STATEMENT</b>	<b>16</b>
<b>THE AUTHOR</b>	<b>17</b>
<b>DEDICATION</b>	<b>18</b>
<b>ACKNOWLEDGEMENTS</b>	<b>19</b>
<b>PUBLICATIONS AND PRESENTATIONS FROM THIS THESIS</b>	<b>20</b>
<b>SECTION 1: INTRODUCTION</b>	<b>21</b>
<b>CHAPTER 1: ABDOMINAL AORTIC ANEURYSM</b>	<b>22</b>
1.1 Background	22
1.2 Incidence and Prevalence	23
1.3 Pathophysiology	23
1.3.1 Inflammation and Proteolysis	23
1.3.2 Genetics	24
1.3.3 Family history	24
1.3.3 Differences between men and women	25
1.4 AAA presentation and rupture	26
<b>CHAPTER 2: INDICATIONS FOR AAA SURGERY</b>	<b>27</b>
2.1 AAA growth, Screening and Surveillance	27

2.2	Medical management of AAA	27
2.3	Surgical Treatment of AAAs	28
2.3.1	Open Repair	28
2.3.2	Endovascular Aneurysm Repair (EVAR)	29
2.4	When to operate	35
2.4.1	Rupture risk based on maximal diameter	35
2.4.2	Rupture risk based on biomechanical analysis – Peak wall stress estimated by finite element analysis	36
2.4.3	Rupture risk based on biomechanical analysis: wall sheer stress (WSS) estimated by computational fluid dynamics (CFD).	45
2.4.4	Current clinical implementation of biomechanical analysis and potential role of 3D US	48
<b>CHAPTER 3: CURRENT USES OF ULTRASOUND IN THE MANAGEMENT OF AAA</b>		<b>51</b>
3.1	Ultrasound modalities for EVAR surveillance	51
3.1.1	Background	51
3.1.2	Endoleak detection	51
3.1.3	Volume measurements	58
3.2	Ultrasound for rupture risk prediction	62
<b>OVERVIEW OF THESIS AIMS</b>		<b>64</b>
<b>SECTION 2: METHODS</b>		<b>65</b>
<b>CHAPTER 4: METHODS FOR PROGRAMME OF RESEARCH</b>		<b>66</b>
4.1	Duplex ultrasound and three-dimensional ultrasound	66
4.1.1	Ultrasound Generation	66
4.1.2	Three-dimensional ultrasound (3D-US)	66
4.1.3	Types of 3D-US	67
4.2	Sonovue™ contrast	72
4.3	Computed tomographic angiography (CTA)	73
4.4	Digital subtraction angiography (DSA)	73
4.5	Image segmentation for biomechanical analysis	75
4.5.1	Image segmentation	75
4.5.2	Development of the ImFusion Suite prototype	75
4.6	Biomechanical analysis	80
<b>SECTION 3: 3D ULTRASOUND IN THE MANAGEMENT OF ABDOMINAL AORTIC ANEURYSM</b>		<b>82</b>
<b>CHAPTER 5: USE OF THREE DIMENSIONAL CONTRAST-ENHANCED ULTRASOUND IMAGING DURING ENDOVASCULAR ANEURYSM REPAIR</b>		<b>83</b>

5.1 ABSTRACT	84
5.2 INTRODUCTION	86
5.3 METHODS	87
5.4 RESULTS	88
5.5 DISCUSSION	91
5.6 CONCLUSIONS	94
<b>CHAPTER 6: 3D CONTRAST ENHANCED ULTRASOUND IMPROVES THE ACCURACY OF CLASSIFICATION OF ENDOLEAKS FOLLOWING ENDOVASCULAR ANEURYSM REPAIR</b>	<b>95</b>
6.1 ABSTRACT	96
6.2 INTRODUCTION	97
6.3 METHODS	98
6.4 RESULTS	102
6.5 DISCUSSION	114
6.6 CONCLUSIONS	117
<b>CHAPTER 7: MEASUREMENT OF ABDOMINAL AORTIC ANEURYSM VOLUME USING MAGNETICALLY TRACKED 3D ULTRASOUND</b>	<b>118</b>
7.1 ABSTRACT	118
7.2 INTRODUCTION	120
7.3 METHODS	121
7.4 RESULTS	126
7.5 DISCUSSION	139
7.6 CONCLUSIONS	142
<b>CHAPTER 8: MEASUREMENT OF ANEURYSM VOLUME FOLLOWING ENDOVASCULAR ANEURYSM REPAIR USING OPTICALLY TRACKED 3D ULTRASOUND</b>	<b>143</b>
8.1 ABSTRACT	144
8.2 INTRODUCTION	145
8.3 METHODS	145
8.4 RESULTS	149
8.5 DISCUSSION	156
8.6 CONCLUSIONS	161
<b>CHAPTER 9: THE FEASIBILITY AND CHALLENGES OF GENERATING AAA MODELS FOR BIOMECHANICAL ANALYSIS USING 3D ULTRASOUND</b>	<b>162</b>
9.1 ABSTRACT	163
9.2 INTRODUCTION	164
9.3 METHODS	165
9.4 RESULTS	167
9.5 DISCUSSION	175
9.6 CONCLUSIONS	179

<b>CHAPTER 10: COMPUTATIONAL HEMODYNAMICS OF ABDOMINAL AORTIC ANEURYSMS: 3D ULTRASOUND VERSUS COMPUTED TOMOGRAPHY.</b>	<b>181</b>
10.1 ABSTRACT	182
10.2 INTRODUCTION	183
10.3 METHODS	184
10.4 RESULTS	190
10.5 DISCUSSION	195
10.6 CONCLUSIONS	197
<b>CHAPTER 11: WALL STRESS ANALYSES OF ABDOMINAL AORTIC ANEURYSMS: 3D ULTRASOUND VERSUS COMPUTED TOMOGRAPHY.</b>	<b>198</b>
11.1 ABSTRACT	199
11.2 INTRODUCTION	201
11.3 METHODS	202
11.4 RESULTS	206
11.5 DISCUSSION	209
11.6 CONCLUSIONS	211
<b>SECTION 4: OVERALL DISCUSSION</b>	<b>213</b>
<b>CHAPTER 12: DISCUSSION</b>	<b>214</b>
12.1 INTRAOPERATIVE IMAGING	214
12.2 ENDOLEAK DETECTION FOLLOWING EVAR	215
12.3 AAA VOLUME MEASUREMENT	219
12.4 BIOMECHANICAL ANALYSIS	219
12.5 OVERALL CONCLUSIONS	220
<b>REFERENCES</b>	<b>222</b>

# FIGURES

Figure 1: Open repair of a infra-renal abdominal aortic aneurysm using a bifurcated dacron graft.....	29
Figure 2: Types of Endoleak. Reproduced with permission from. <sup>73</sup> Copyright Massachusetts Medical Society. ....	32
Figure 3: Association between maximal aortic diameter and risk of rupture. <sup>48</sup> Reproduced with permission of BMJ publishing .....	36
Figure 4: CTA of a ruptured 8.3cm AAA (left) and a ruptured 5.7cm AAA (right), both in men .....	37
Figure 5: FEARI methodology <sup>119</sup> demonstrating PWS in the anterior aspect of an AAA. The AAA is divided into eight regions, each of which has been assigned an individual tensile strength. Reproduced with permission.....	43
Figure 6: Concept of ‘risk-equivalent diameter’ <sup>95</sup> demonstrating an AAA with a diameter of 4.5cm has a ‘risk-equivalent’ diameter of 6.2cm after biomechanical analysis and should be considered for early repair rather than surveillance. Reproduced with permission. ....	44
Figure 7: Region of low WSS (dark blue) in an AAA, corresponding with the site of rupture on open repair. <sup>134</sup> .....	47
Figure 8: Velocity streamlines in a ruptured AAA. <sup>139</sup> Low velocity values are in blue with higher values in red. Black arrow shows the site of rupture in a zone of low flow velocity and WSS. Red arrow shows the dominant flow channel. Reproduced with permission.....	48
Figure 9: Schematic of a magnetically tracked freehand ultrasound system. <sup>175</sup> Reproduced with permission ©SAGE. ....	68
Figure 10: Liner US transducer adapted for magnetically tracked freehand 3D-US. An electromagnetic sensor is attached in a calibrated position. ....	69
Figure 11: Curefab CS system. <sup>180</sup> Reproduced with permission under CC licencing .....	70
Figure 12: Schematic of an optical tracking system. <sup>175</sup> Reproduced with permission ©SAGE.....	71
Figure 13: Tracking camera used in Piur prototype .....	71
Figure 14: modified US probe with tracking spheres .....	72

Figure 15: Contrast-enhanced ultrasound following EVAR. Contrast is seen contained within the limbs of the stent-graft and there is no endoleak seen. ....	73
Figure 16: Completion uniplanar DSA after EVAR. The left renal artery is not seen in this DSA frame but is patent. ....	74
Figure 17: User defined 'seeds' are placed 'inside' (green) and 'outside' (red) the AAA wall on CTA MPRs of the AAA .....	77
Figure 18: User defined 'seeds' are placed 'inside' (green) and 'outside' (red) the AAA wall on 3D-US MPRs of an AAA.....	77
Figure 19: Initial segmentation results on CT. The yellow line defines the boundary of the segmentation.....	78
Figure 20: Sequence of correcting an error in segmentation. The yellow line does not correspond to the wall of the AAA – left image. This is due to adjacent inferior vena cava – blue arrow. Additional seeds are placed – centre image. The segmentation is re-run and the result improved – right image.....	78
Figure 21: 'Mask image' on CT. This is generated once the user is satisfied with the segmentation result. The pixels inside the structure i.e. AAA wall are labelled green, those outside are labelled red. ....	79
Figure 22: Approach to smoothing. The maximal resolution with no smoothing was selected – left. The mesh was smoothed in stages to achieve an optimal result. ....	79
Figure 23: A type I endoleak (arrow) as seen on the Curefab CS system workstation (Curefab, Munich, Germany) that was not identified on uniplanar angiography. ....	90
Figure 24: Standard US transducer fitted with a tracking sensor.....	101
Figure 25: Volumetric image from 3D-CEUS showing contrast in the stent-graft limbs (red arrow) and a type II endoleak from lumbar artery to lumbar artery (yellow arrow). ....	101
Figure 26: CTA (left) demonstrating a large type II endoleak (yellow arrow). Corresponding CEUS (right ) showing contrast in the stent-graft limbs (red arrows) with a large endoleak seen (yellow arrows) that was reported as a type I or III endoleak. .	104
Figure 27: Type II endoleak seen on catheter angiogram via internal iliac artery .....	104
Figure 28: indeterminate endoleak close to flow divider on CTA(left, arrow). 3D-CEUS diagnosis of type IIb endoleak confirmed on catheter angiography (right, arrow). ....	107

Figure 29: An endoleak is seen on CTA close to the limb of the graft (left, arrow) that cannot be differentiated between type II and III. CEUS was indeterminate. 3D-CEUS diagnosed a lumbar type II endoleak that was confirmed on catheter angiography (right, arrow). .....	108
Figure 30: A possible type II (left, bottom arrow) or III (left, top arrow) endoleak was seen on CTA. Lumbar artery embolisation was performed after a lumbar type II endoleak was diagnosed with 3D-CEUS (right). .....	109
Figure 31: An endoleak on CTA intimately associated with the overlap zone of the main body and left limb of an Endurant stent-graft (left, arrow). Confirmation of type II endoleak seen on 3D-CEUS during catheter angiography (right, arrow). .....	110
Figure 32: Suspected type III endoleak (arrow) seen on CTA associated with the right limb of the graft that had been relined. ....	111
Figure 33: CTA three months following EVAR with an Ovation® stent-graft. There is an indeterminate endoleak associated with the ipsilateral limb and the main body (yellow arrow). .....	112
Figure 35: ITI measurement of AAA diameter in orthogonal sections on CTA.....	122
Figure 36: ITI measurement of AAA diameter in orthogonal sections on 3D-US .....	123
Figure 37: Manual vessel segmentation in each 1mm image slice using the spline tool. ....	124
Figure 38: Completed segmentation on CTA defining 'partial' AAA volume.....	124
Figure 39: Completed segmentation on 3D-US defining 'partial' AAA volume .....	125
Figure 40: Bland-Altman plot of CTA vs 3D-US measurements of AAA volume. Two anomalous results where 3D-US volume was greater than CTA volume are highlighted in red. ....	127
Figure 41: Correlation between CTA and 3D-US AAA volume measurements.....	128
Figure 42: Bland-Altman plot of intra-operator CTA measurements of AAA volume. .	129
Figure 43: Correlation between intra-operator CTA measurements of AAA volume. .	129
Figure 44: Bland-Altman plot of intra-operator 3D-US measurements of AAA volume. ....	130
Figure 45: Correlation between intra-operator 3D-US measurements of AAA volume. ....	131
Figure 46: Bland-Altman plot of inter-operator CT measurements of AAA volume. ....	133



Figure 47: Correlation between inter-operator CT measurements of AAA volume. ...	133
Figure 48: Bland-Altman plot of inter-operator 3D-US measurements of AAA volume .....	135
Figure 49: Correlation between inter-operator 3D-US measurements of AAA volume .....	135
Figure 50: Fusion of CT and 3D-US. The 'colour blending' feature improves visualisation of the 3D-US, which can be faded in and out .....	136
Figure 51: Simultaneous visualisation of CT and 3D-US in each plane demonstrating accurate registration. ....	137
Figure 52: Splines from 3D-US volume measurements overlaid onto CTA data. ....	138
Figure 53: 3D-US spline (left arrow) extending past the AAA wall (right arrow).....	138
Figure 54: Graphical representation of noise and artefact reduction on application of a tracking filter. ....	147
Figure 55: Correlation between CT and 3D-US (optical) AAA volume measurements.	150
Figure 56: Bland-Altman plot of CT vs 3D-US (optical) measurements of AAA volume. .....	150
Figure 57: Correlation between CT and 3D-US (optical) AAA volume measurements.	151
Figure 58: Bland-Altman plot of intra-operator 3D-US (optical) measurements of AAA volume.....	152
Figure 59: Bland-Altman plot of inter-operator 3D-US (optical) measurements of AAA volume.....	155
Figure 60: Correlation between inter-operator 3D-US (optical) measurements of AAA volume.....	155
Figure 61: There is a moderate correlation between increasing AAA volume and the absolute difference between CT and 3D-US measurements.....	158
Figure 62: Weak correlation between increasing AAA volume with difference in 3D-US and CT measurements expressed as a percentage of AAA volume. ....	159
Figure 63: AAA wall geometries derived from CT (left) and 3D US (right) .....	169
Figure 64: Segmentation of wall, lumen and thrombus (left to right) .....	174
Figure 65: Surface meshes of an AAA wall (left –CT, right– 3D-US) using the manual spline segmentation tool. The current software version is not able to include the bifurcation. Smoothing will be required. ....	178

Figure 66: Left – a US image of an AAA. The AAA contains thrombus but it cannot be distinguished from the lumen. Right – same site in the AAA after IV contrast. The lumen and thrombus are now well visualised. ....	179
Figure 67: tool chain employed for the present study. ....	185
Figure 68: Geometry preparation from CT and 3D-US data. ....	187
Figure 69: Mesh used in the CFD analysis (top) full domain, (bottom) cross sectional detail.....	189
Figure 70: Histogram of face aspect ratio for Laplacian, HC Laplacian, and Taubin low pass filter .....	191
Figure 71: Wall sheer stress for each combination of image source and smoothing algorithm.....	192
Figure 72: Axial wall sheer stress for each scanning technique. ....	193
Figure 73: Streamlines and contours of velocity and vorticity for Taubin low pass filter smoothed CT (left) and 3D-US (right) geometries. ....	195
Figure 74: Workflow to prepare models for simulation .....	204
Figure 75: Posterior-anterior view of von Mises stress distribution in CTA (left) and 3D-US (right) derived models. ....	205
Figure 76: Lateral view of von Mises stress distribution in CTA (left) and 3D-US derived models.....	206
Figure 77: Section through AAA models at level of the aortic bifurcation demonstrating von Mises wall stress distributions. Left CTA, right 3D-US. ....	206
Figure 78: Posterior-anterior view of maximal principle stress distribution in CTA (left) and 3D-US (right) derived models.....	207
Figure 79: Section through AAA models at level of the aortic bifurcation demonstrating maximal principle distributions (MPa). Left CTA, right 3D-US.....	207
Figure 80: A type II endoleak seen on post processing of 3D-CEUS. The stent-graft has been segmented in red. The endoleak is clearly seen – yellow arrows. ....	215

# TABLES

Table 1: Summary of studies of duplex modalities for endoleak detection following EVAR .....	52
Table 2: Patient Demographics .....	89
Table 3: Endoleak detection by imaging modality used .....	90
Table 4: Patient demographics .....	102
Table 5: Endoleak diagnosis by each modality. 3D-CEUS most closely reflected the MDT decision.....	103
Table 6: Contingency table for the presence of endoleak - CTA vs. 3D-CEUS/CEUS....	105
Table 7: Contingency table for the presence of endoleak – MDT vs. 3D-CEUS/CEUS..	105
Table 8: Intra-operator variability of AAA volume measurements using 3D-US are within current acceptability of 2D-US diameter measurements using ‘phantom cylinder’ method. ....	132
Table 9: Inter-operator variability of AAA volume measurements using 3D-US are within current acceptability of 2D-US diameter measurements using ‘phantom cylinder’ method .....	134
Table 10: Intra-operator variability of AAA volume measurements using 3D-US (optical) are within current acceptability of 2D-US diameter measurements using ‘phantom cylinder’ method. ....	153
Table 11: Inter-operator variability of AAA volume measurements using 3D-US (optical) are within current acceptability of 2D-US diameter measurements using ‘phantom cylinder’ method. ....	154
Table 12: Main anatomical features seen in 3D-US models.....	168
Table 13: Maximal AAA diameter and body mass index (BMI) in the study group. Patients that failed geometry generation are highlighted in red. ....	175
Table 14: Mesh quality assessment of smoothing algorithms .....	190

# ABBREVIATIONS

AAA	abdominal aortic aneurysm
CEUS	contrast-enhanced ultrasound
CFD	computational fluid dynamics
CIN	contrast-induced nephropathy
CO <sub>2</sub>	carbon dioxide
CPEX	cardio-pulmonary exercise testing
CKD	chronic kidney disease
CT	computed tomography
CTA	computed tomographic angiography
DSA	digital subtraction angiography
DUS	duplex ultrasound
EVAR	endovascular aneurysm repair
FEA	finite element analysis
FEARI	finite element analysis rupture index
FSI	fluid-structure interaction
IMA	inferior mesenteric artery
IC	iodinated contrast
ILT	intra-luminal thrombus
IFU	instructions for use
MMP	matrix metalloproteinases
MPR	multiplanar reconstruction
MRA	magnetic resonance angiography
PWRI	peak wall rupture index
PWRR	peak wall rupture risk

PWS peak wall stress

RCT randomised controlled trial

RPI rupture potential index

TAWSS time-averaged wall shear stress

TUS tomographic ultrasound

US ultrasound

WSS wall shear stress

2D-US two-dimensional ultrasound

3D-CEUS three-dimensional contrast-enhanced ultrasound

3D-US three-dimensional ultrasound

# PREFACE

This thesis is to be submitted in the alternative format as a series of journal papers. This is because the programme of research was designed to produce a number of publications around a common theme. Due to the nature of the work planned, the objective on registering for the degree was to publish papers early in the programme. It was agreed by the supervisory team that the alternative format would be appropriate for this programme of research and this has been approved by the University

The research is, by nature, multi-disciplinary and collaborative as the clinical and technical skills needed for the various projects are not possessed by one single person. Collaborators, therefore, include clinical vascular scientists, vascular surgeons, radiologists and specialists in medical imaging processing. In addition, to complete work relating to finite element analysis and computational fluid dynamics, collaboration with those in the mechanical and bio-engineering field was required.

# ABSTRACT

Christopher Lowe

The University of Manchester

Degree Title: Doctor of Medicine (MD)

Thesis Title: Three-dimensional ultrasound in the management of abdominal aortic aneurysm

Date: June 2016

**Objectives:** Clinical implementation of 3D ultrasound (3D-US) in vascular surgery is in its infancy. The aim of this thesis was to develop novel clinical applications for 3D-US in the diagnosis and management abdominal aortic aneurysm (AAA).

**Methods:** Four principle clinical applications were investigated. 1) *Intraoperative imaging* – The ability of 3D-US to detect and classify endoleaks was compared with digital subtraction angiography in patients undergoing EVAR. 2) *Detection and classification of endoleaks following endovascular aneurysm repair (EVAR)* – The ability of 3D-US to accurately detect and classify endoleaks following EVAR was compared to CTA and the final multi-disciplinary team decision. 3) *AAA volume measurement* – measurements using magnetic and optically-tracked 3D-US were compared to CTA. 4) *Biomechanical analysis* – the challenges of using 3D-US to generate surface models for biomechanical simulation was explored by development of an interactive segmentation technique and comparison of paired CT and 3D-US datasets. Optimal results were used in finite element analysis (FEA) and computational fluid dynamic (CFD) simulations.

**Results:** 3D-US out-performed uniplanar angiography for the detection of endoleaks during EVAR. This approach allowed contrast-free EVAR to be performed in patients with poor renal function. 3D contrast-enhanced ultrasound was superior to CTA for endoleak detection and classification when compared with the final decision of the multi-disciplinary team. Optimal results for AAA volume measurements were gained using an optically tracked 3D-US system in EVAR surveillance. However, there remained a significant mean difference of 13.6ml between CT and 3D-US. Complete technical success of generating geometries for use in biomechanical analysis using 3D-US was only 5%. When the optimal results were used, a comparable CFD analysis under the conditions of steady, laminar and Newtonian flow was achieved. Using basic modelling assumptions in FEA, peak von Mises and principle wall stress was found to be at the same anatomical location on both the CT and 3D-US models but the 3D-US model overestimated the wall stress values by 41% and 51% respectively.

**Conclusions:** 3D-US could be clinically implemented for intra-operative imaging and EVAR surveillance in specific cases. 3D-US volume measurement is feasible but future work should aim to improve accuracy and inter-observer reliability. Although the results of biomechanical analysis using the optimal results was encouraging and provided a proof-of-principal, there are a number of technical developments required to make this approach feasible in a larger number of patients.

# DECLARATION

No portion of the work referred to in this report has been submitted in support of an application for another degree or qualification of this or any other university or other institute of learning.

## COPYRIGHT STATEMENT

- i. The author of this thesis (including any appendices and/or schedules to this thesis) owns certain copyright or related rights in it (the “Copyright”) and s/he has given The University of Manchester certain rights to use such Copyright, including for administrative purposes.
- ii. Copies of this thesis, either in full or in extracts and whether in hard or electronic copy, may be made **only** in accordance with the Copyright, Designs and Patents Act 1988 (as amended) and regulations issued under it or, where appropriate, in accordance with licensing agreements which the University has from time to time. This page must form part of any such copies made.
- iii. The ownership of certain Copyright, patents, designs, trade marks and other intellectual property (the “Intellectual Property”) and any reproductions of copyright works in the thesis, for example graphs and tables (“Reproductions”), which may be described in this thesis, may not be owned by the author and may be owned by third parties. Such Intellectual Property and Reproductions cannot and must not be made available for use without the prior written permission of the owner(s) of the relevant Intellectual Property and/or Reproductions.
- iv. Further information on the conditions under which disclosure, publication and commercialisation of this thesis, the Copyright and any Intellectual Property and/or Reproductions described in it may take place is available in the University IP Policy (see <http://documents.manchester.ac.uk/DocuInfo.aspx?DocID=487>), in any relevant Thesis restriction declarations deposited in the University Library, The University Library’s regulations (see <http://www.manchester.ac.uk/library/aboutus/regulations>) and in The University’s policy on Presentation of Theses



## THE AUTHOR

The author graduated with a BSc(Hons) degree in Physiotherapy from the University of Manchester in 2003. After working for a year as a Physiotherapist, he began his medical training at the University of Liverpool in 2004 on the graduate-entry MBChB programme. After graduation with honours in 2008, he completed his foundation training in the North Western Deanery.

In 2010 he was appointed to core surgical training in General Surgery in the North Western Deanery which he spent at the Royal Preston and Royal Blackburn Hospitals. He became a member of the Royal College of Surgeons of England in May 2011. He was successful in gaining a place as a speciality trainee in General Surgery in 2012 where he completed posts in breast, vascular and colorectal surgery.

He began his period of research in April 2014, where he had the opportunity to present work at a number of international conferences, winning the aortic abstract prize at the British Society of Endovascular therapy meeting in 2015. He returned to clinical training in April 2016 having been accepted to transfer to the new Vascular Surgery training programme. He has a particular interest in the endovascular treatment of abdominal aortic aneurysms.

# DEDICATION

*For Sarah, Lily and Isla*

# ACKNOWLEDGEMENTS

Firstly I would like to thank my supervisory team, Professor Charles McCollum and Mr Jonathan Ghosh for providing an opportunity to pursue these research projects. In particular, I am grateful to the Manchester Surgical Research Trust for providing the necessary funding and the Wellcome Trust for providing a researcher-training grant which funded a very informative visit to Professor Henrik Sillesen's unit in Copenhagen.

I am indebted to my colleagues in the Vascular Studies Unit at University Hospital South Manchester who have accommodated the additional work generated by these studies both in terms of scanning time and image analysis/measurements. Also, the consultant vascular surgeons at University Hospital South Manchester who have made me feel part of the team through my time in research.

I would like to thank my collaborators at the School of Mechanical, Civil and Aerospace engineering (MACE) at the University of Manchester. In particular Drs Alistair Revell and Partha Mandel along with their PhD Students Ben Owen and Wisam Al-Obaidi. I hope this collaboration is able to continue into the future.

Much of this work has relied on the technical support of the team at ImFusion GmbH in Germany. Dr Wolfgang Wein and his colleague Raphael Pravost have always provided the rapid solutions to software problems that were regularly encountered when developing the techniques used in some of these studies. I would also like to acknowledge the input of Robert Bauer and Frederick Bender at Piur Imaging who have always been willing to explore new ideas. I hope the commercialisation of their 3D-US system is a success.

Finally, none of this would be possible without the unwavering support of my family and friends.

# PUBLICATIONS AND PRESENTATIONS FROM THIS THESIS

## Peer reviewed publications

Lowe C, Abbas A, Rogers S, Smith L, Ghosh J, McCollum C. 3D contrast-enhanced ultrasound improves the detection and classification of endoleaks following endovascular aneurysm repair. *Journal of Vascular Surgery* 2016 – *in press*

Lowe C, Rogers S, Ghosh J, Bredhal K, Ghulam Q, Eiberg J, Sillesen H, McCollum C. Three-dimensional ultrasound in the management of abdominal aortic aneurysms – a topical review. *European Journal of Vascular and Endovascular Surgery* 2016 – *ePub ahead of print* – <http://dx.doi.org/10.1016/j.ejvs.2016.06.009>.

Ormesher DC, Lowe C, Sedgwick N, McCollum CN, Ghosh J. Use of three dimensional contrast-enhanced ultrasound during endovascular aneurysm repair. *Journal of Vascular Surgery* 2014; 60(6): 1468-1472. (DO and CL have joint first authorship).

Owen B, Lowe C, Ashton N, Mandal P, Rogers S, Wein W, McCollum C, Revell A. Computational haemodynamics of abdominal aortic aneurysms: ultrasound vs computed tomography. *Journal of Engineering in Medicine* 2016; 2016, 220(3) 201-210.

## Oral Presentations

C Lowe. *3D contrast-enhanced ultrasound improves the detection and classification of endoleaks following endovascular aneurysm repair*. European Society of Vascular Surgery annual meeting. Copenhagen, September 2016

C Lowe (invited faculty) *Clinical Applications of 3D ultrasound in AAA*. Critical issues in aortic endografting, 19<sup>th</sup> International experts symposium. Liverpool, May 2015

C Lowe, A. Revell, L. Smith, S. Rogers, J. Ghosh, C.N. McCollum. *Measuring Peak wall stress by tomographic ultrasound (TUS)*. National AAA Screening Programme Research Meeting. Manchester, February 2015

C Lowe, A Abbas, N Sedgwick, J Armitage, L Smith, S Rogers, J Ghosh, CN McCollum. *3D contrast enhanced ultrasound for endoleak detection after EVAR – a new gold standard?* Vascular Society Annual Meeting. Glasgow, November 2014.

## Poster Presentations

C Lowe. Biomechanical analysis of abdominal aortic aneurysms using three-dimensional ultrasound – is it feasible? European Society of Vascular Surgery annual meeting. Copenhagen, September 2016

# **SECTION 1: INTRODUCTION**

## CHAPTER 1: ABDOMINAL AORTIC ANEURYSM

### 1.1 Background

The term 'aneurysm' is derived from the Ancient Greek word *aneurysma*, meaning 'dilation.'<sup>1</sup> Any artery in the body may develop an aneurysm; however, in the peripheral circulation they are most common in the abdominal aorta and popliteal arteries. They are classified by anatomical location, shape (e.g. sacular or fusiform) and type (true or false). An artery is constituted from three layers – the intima, media and adventitia. A 'true aneurysm' involves all three layers of the artery wall, while a false aneurysm, or pseudo-aneurysm is a leakage of arterial blood from an artery into the surrounding tissue with a persistent communication between the originating artery and the resultant adjacent cavity.

Abdominal aortic aneurysm (AAA) refers to a dilatation of the aorta between the diaphragm and the aortic bifurcation and by convention can be defined as an abdominal aortic diameter of 30mm or more in either anterior-posterior or transverse planes.<sup>1</sup> This threshold was established by the work of Steinberg and Stein who measured aortic diameter on angiograms and found that aortas measuring 30mm at any of four locations were greater than two standard deviations above the mean and therefore considered aneurysmal.<sup>2</sup>

AAAs can occur in differing anatomical locations and are defined by their relation to the renal arteries. Infra-renal aneurysms are most common and involve the aorta below the level of the renal arteries with a variable length of non-aneurysmal infra-renal aorta referred to as the 'neck' of the aneurysm. Juxta-renal abdominal aortic aneurysms are those involving the infra-renal abdominal aorta adjacent to or including the lower margin of renal artery origins.<sup>3</sup> More complex AAAs can involve the renal or visceral arteries or extend into the thoracic cavity as thoraco-abdominal aneurysms.

## 1.2 Incidence and Prevalence

Data on AAA prevalence is dated, however, quite robust as most has been collected as part of randomised controlled trials (RCTs) to investigate the effects of screening. From the UK-based MASS trial,<sup>4</sup> aneurysm prevalence in men aged 65-75 years was found to be 4.9%, however the latest results from the National AAA Screening programme in the UK suggest the current incidence is 1.8%.<sup>5</sup> The prevalence in women is three to four times less at 0.5-1.3%.<sup>6</sup>

## 1.3 Pathophysiology

AAAs can develop due to

- i) connective tissue disorders such as Marfan's syndrome and type 4 Ehlers-Danlos syndrome
- ii) inflammation due to infection such as syphilis (now rare)
- iii) 'late onset' aneurysms – by far the most common.

Risk factors for AAA for both men and women are well established: advanced age, smoking and a family history in first-degree male relatives.<sup>7-10</sup> Evidence suggests that the association between smoking and AAA is stronger in women than men.<sup>11</sup> A number of pathophysiological mechanisms in AAA development have been implicated.

### 1.3.1 Inflammation and Proteolysis

Late onset aneurysm formation is characterised by degradation of the extracellular matrix, inflammatory infiltrate, and proteolysis. Loss of elastin from the arterial media occurs early in aneurysm formation, with a consequent inability to resist the tensile stress of the circulation and subsequent compensatory collagen deposition. The loss of

elastin is mediated by excessive secretion of proteases, particularly matrix metalloproteinases (MMPs), from the activated inflammatory infiltrate. The inflammatory and proteolytic processes appear to be the dominant mechanisms controlling aneurysm expansion, acting in conjunction with other less well characterised mechanisms, including haemodynamic stress, infection and autoimmunity.<sup>12</sup>

### *1.3.2 Genetics*

Given the proteolytic and inflammatory mechanisms outlined above, genetic research has focused on genes governing these mechanisms, in particular those encoding MMPs, human leukocyte antigens (HLAs), interleukins and other inflammatory mediators.<sup>13</sup> Despite over 100 candidate gene association studies, only a small minority of these have been of sufficient power to draw any firm conclusions and few results have been replicated in different sample sets. When coupled with four different genome-wide association studies, six genetic loci have been found to be potentially important. However, no studies have reported results that are consistent with the strong patterns of inheritance in all epidemiological studies. These results also emphasise the importance of environmental factors.

### *1.3.3 Family history*

The familial clustering of abdominal aortic aneurysms (AAA) was reported more than 35 years ago.<sup>14</sup> Although genetic susceptibility is established, it is also well known that individuals with first-degree relatives with AAA have common environmental exposures and cultural habits that may also cause the association.<sup>15</sup> Both the European Society of Vascular Surgery (ESVS)<sup>1</sup> and the Society of Vascular Surgery (SVS)<sup>16</sup> practice guidelines suggest screening of first-degree relatives of patients with an AAA at a younger age than in the standard screening programme. The SVS suggest this should be done 'as early as age 55'. The recommendation of the ESVS is based



mainly on a single population-based case-control study from Sweden where first-degree relatives of AAA cases (1,932) and matched controls (15,943) were analysed.<sup>7</sup> The overall risk of AAA in individuals with a family history was approximately double that of those with no family history (RR 1.9 CI 1.6-2.2).

There have been a total of 20 studies examining US screening in first-degree relatives of AAA patients.<sup>17-36</sup> These trials are generally small with less than 300 participants in each and differ methodologically, though the majority screen both men and women. The two most contemporary studies are those by Linne<sup>33</sup> and Sakalihasan.<sup>34</sup> Linne screened 150 siblings of AAA patients. AAAs were found in eleven (11%) brothers and five sisters (6%). One of these patients was aged <65 years. Six AAAs were >5cm in diameter, none were >5.5cm.

More recently, Sakalihasan screened 186 first-degree relatives aged >50 years. The overall prevalence of AAA (>3.0cms) was 13% (22% in males). When these results were pooled with those from the previous 19 trials, prevalence in first-degree relatives was 12% overall - 20% in males and 5.6% in females.<sup>34</sup>

There are likely to be regional variations in the prevalence of AAAs in relatives as highlighted by the trial from Belfast. They screened 300 relatives > 50 years old and found a prevalence of only 3.3% in their population. This rose to 5% when patients aged <60 were excluded.<sup>32</sup> Brothers of female patients appeared to be at the greatest risk with AAA found in 12.5%.

### *1.3.3 Differences between men and women*

The difference between AAA prevalence in men and women may be attributed to the protective immunomodulative effects of oestrogen, which reduces macrophage MMP production as well as cytokine production, growth factor expression and chronic inflammation.<sup>37</sup> However, once this protective mechanism is removed the growth rate of AAAs in women is more rapid, rupture in surveillance is more likely and the chances of fatal rupture are three times higher than in men. The observation that rupture occurs at smaller diameters in women is likely due to the smaller original diameter in

women. Although intuitive, lowering the treatment threshold for women is contentious as any excess rupture risk in women appears to be offset by increased operative mortality.<sup>38</sup>

#### **1.4 AAA presentation and rupture**

Most AAAs are asymptomatic and detected incidentally or more recently, through screening (see 2.1). Back pain is the most common feature of 'symptomatic' aneurysms, however, this is not consistent and any new abdominal or back pain in a patient with an AAA should be attributed to the aneurysm unless another cause is obvious or ruled out by imaging. Embolism from an AAA is a rare event as, although thrombus is almost universally present in AAAs, it is usually highly organised and stable. If there are symptoms of lower limb emboli in a patient with an AAA the most likely source is an associated aneurysm in the iliac, femoral or popliteal arteries.

When an AAA ruptures, the majority of patients die immediately without reaching hospital. The early survivors may present with severe back or abdominal pain, collapse and hypotension. Those whose bleeding is retroperitoneal may have a better chance of reaching hospital alive due to the tamponading effect of surrounding tissues, however, the majority of patients still die before reaching hospital.<sup>39, 40</sup> The definitive investigation of a CT angiogram should be performed as soon as is practically possible after initial resuscitation measures have been undertaken. This will confirm or refute the diagnosis of a rupture and aid in decision making regarding the suitability of open or endovascular repair. If in symptomatic patients the aneurysm is not ruptured there may be other reasons that urgent repair is indicated such as rapid expansion or inflammatory change around the aneurysm. Despite modern levels of care, the operative mortality of ruptured AAAs has remained unchanged in recent years with mortality rates ranging from 32-80%.<sup>1</sup>

## CHAPTER 2: INDICATIONS FOR AAA SURGERY

### 2.1 AAA growth, Screening and Surveillance

The growth rate of AAAs between 3cm and 5.4cm is 0.2 to 0.3cm per year.<sup>1</sup> Larger diameters are associated with higher growth rates. Until recently, the majority of AAAs were found incidentally during physical examination or investigation for other illness. The Multicentre Aneurysm Screening Study (MASS)<sup>4</sup> was the pivotal trial in the UK, randomising over 67,000 male patients aged 65-74 years to screening or not. The finding of a risk reduction of over 50% in AAA related death was instrumental in the development of the UK National Abdominal Aortic Aneurysm Screening Programme (NAAASP). Further studies have strengthened the view that screening is valuable in preventing death due to rupture. Screening remains cost-effective in the UK, despite incidence in screening being lower than expected.<sup>5, 41-43</sup> This is probably explained by reducing smoking rates and improved primary prevention of cardiovascular disease as a whole. The UK screening programme invites all men aged 65 for an ultrasound scan. If the aortic diameter is  $\leq 2.9$ cm, the patient is discharged. If the diameter is  $\geq 3$ cm, the patient is scanned at regular intervals to monitor progression. This is termed 'aneurysm surveillance.'

### 2.2 Medical management of AAA

Patients with an AAA are at cardiovascular risk,<sup>44, 45</sup> with at least a twofold increase in five year mortality compared with matched controls.<sup>46</sup> Control of cardiovascular risk factors is therefore the mainstay of management for patients in AAA surveillance. The surveillance period provides an ideal opportunity to establish 'best medical therapy.' There is evidence that smoking cessation may reduce AAA growth by up to 20%<sup>47-49</sup> and minimise post-operative complications.<sup>50</sup> Aspirin has been found to significantly reduce coronary events in this cohort, leading to the recommendation that 75mg of aspirin should be taken daily from the time of diagnosis and continued indefinitely.<sup>1</sup> Despite a number of trials of antibiotics, statins<sup>51</sup> and beta-blockers, there is no

convincing evidence that any of these drugs can significantly retard the growth of AAAs.<sup>12, 51, 52</sup>

## **2.3 Surgical Treatment of AAAs**

### *2.3.1 Open Repair*

In the 2<sup>nd</sup> century Galen, physician to the roman gladiators, gave the first true description of an aneurysm writing “when the arteries are enlarged, the disease is called an aneurysm ... If the aneurysm is injured, the blood gushes forth, and it is difficult to staunch it.”<sup>53, 54</sup> The Greek surgeon Antyllus described treatment of aneurysms with proximal and distal ligation of the vessel above and below followed by evacuation of the aneurysm sac. The ‘Antyllus method’ formed the mainstay of treatment until the 19<sup>th</sup> Century. A major advance in treatment came in 1888 with Rudolf Matas' concept of endoaneurysmorrhaphy. After obtaining proximal and distal control, he obliterated the aneurysm sac, oversewing collaterals yet preserving a lumen for blood flow.<sup>55, 56</sup> It was not until 1951 that the first successful AAA resection and allograft reconstruction was reported by Dubost in Paris.<sup>57</sup> The synthetic material Dacron (woven polyethylene terephthalate) was subsequently introduced by DeBakey in 1955 and became the preferred conduit for repair, avoiding problems with aneurysmal deterioration of allografts.

The method of interposition grafting using Dacron was described by Creech in 1966<sup>58</sup> and remains largely unchanged today. The aorta is exposed via a trans-abdominal or less often via a retroperitoneal approach. Specific consideration is given to the anatomy of the aneurysm and the underlying cause to allow adequate exposure and control of the vessels. The retro-peritoneum is opened and the aorta dissected and controlled with clamps above and below the aneurysm. The aneurysm sac is opened and thrombus evacuated. Back-bleeding from lumbar arteries is controlled by suturing. The graft can either be a ‘tube graft’ that is anastomosed to the infra-renal aorta proximally and the aortic bifurcation distally or a bifurcated graft can be used if there is iliac disease or associated iliac aneurysms (Figure 1). A tube graft is preferred

if possible as it is associated with shorter aortic cross-clamping time and less dissection in the region of the ureters, iliac veins and parasympathetic nerves. The abdomen is closed with a non-absorbable monofilament suture in an attempt to avoid incisional hernia. The large majority of patients will require close observation in a level II care environment for the first 48 hours. Contemporary studies from the UK report a 30 day mortality rate for elective open repair of 4-5%.<sup>59, 60</sup>

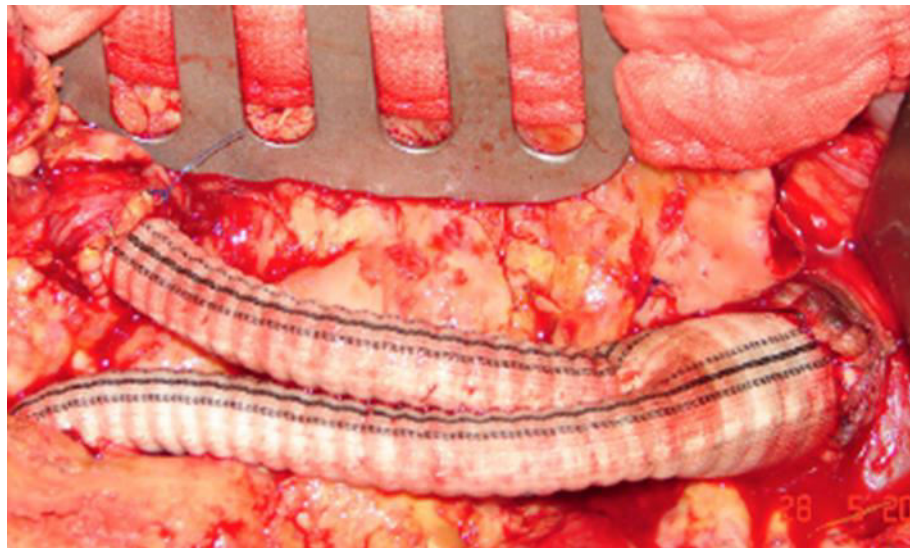


*Figure 1: Open repair of a infra-renal abdominal aortic aneurysm using a bifurcated dacron graft.*

### *2.3.2 Endovascular Aneurysm Repair (EVAR)*

EVAR was pioneered in 1991 by Parodi in his seminal paper 'Trans-femoral Intraluminal Graft Implantation for Abdominal Aortic Aneurysm.'<sup>61</sup> Metal stents were attached to Dacron grafts proximally and distally and mounted on delivery catheters. Balloon inflation provided a friction seal that excluded the aneurysm from the circulation. The advent of EVAR has revolutionised management of AAA and the pace of technological development of EVAR stent-grafts has expanded the number of patients who are anatomically suitable for this method of treatment. EVAR has been the subject of many trials, the most pivotal of which compare EVAR to open repair. The EVAR 1 trial<sup>62</sup> randomised 1082 patients assessed as anatomically suitable for EVAR and fit for open repair to either EVAR or open repair. The initial results found EVAR reduced the

30-day operative mortality by two-thirds in comparison to open repair. However, after long term follow up, no differences were seen in total mortality or aneurysm-related mortality.<sup>60</sup> Similar findings were produced in the United States.<sup>63</sup> Endovascular repair was also associated with increased rates of stent-graft related complications and re-interventions. The EVAR trial II<sup>59</sup> randomised patients not fit for open surgery (i.e. excluded from the EVAR trial I) to EVAR or no intervention. They found that EVAR did not improve survival over no intervention and again was associated with higher rates of re-intervention and increased cost.

It has become clear from the major randomised controlled trials that there remains a significant complication and re-intervention rate associated with EVAR and problems have been reported more than 8 years following stent-graft implantation.<sup>60, 64</sup> The risk of a complication requiring a re-intervention is in the region of 20% with the majority occurring in the first 4 years. This is in contrast to a re-intervention rate of 8% for open repair with the significant majority of these occurring in the first 6 months.<sup>60</sup> For this reason, life long surveillance is recommended to detect stent-graft related complications.<sup>1, 65</sup>

An EVAR device can fail in a number of ways:

### *1. Stent-Graft Migration*

Device migration after EVAR is defined as a movement of >10 mm relative to anatomic landmark with the use of three-dimensional CT reconstruction using a centre-line of flow or any migration leading to symptoms or requiring intervention.<sup>65, 66</sup> It has been observed in all stent-graft designs including those with supra-renal fixation and is more likely to occur more than 24 months after implantation.<sup>66, 67</sup> The underlying cause is multifactorial including aortic neck dilatation after EVAR, accuracy of deployment and initial AAA anatomy (e.g neck angulation, neck length, non-parallel (conical) necks, neck thrombus). The influence of anatomical factors highlights the importance of appropriate patient and stent selection. Stent-graft migration is usually asymptomatic and can dispose to type I endoleaks (see below) with a resultant risk of aneurysm growth and rupture. For the purposes of surveillance, it is vital that plain x-rays are

performed as this complication cannot be reliably detected or measured by ultrasound alone.

## *2. Component Separation*

See type III endoleak, below.

## *3. Limb kinking and occlusion*

Occlusion of stent-graft limbs is more common than open repair.<sup>68</sup> The underlying cause is a stenotic segment of artery distal to the iliac landing zone or a kink in the limb of the stent--. It has been reported to occur in 3.7% of cases.<sup>69</sup> The kink may be symptomatic (e.g. causing claudication) but may also present suddenly as acute limb ischaemia due to occlusion. If detected due to symptoms, it can be treated by balloon dilatation and re-stenting. Detection of asymptomatic kinks that may result in limb occlusion relies on effective surveillance – a kink may be seen directly on CTA or suggested by raised peak systolic velocity on duplex scanning.

## *4. Endoleak*

'Endoleak' is the persistent blood flow within the aneurysm sac but outside the stent-graft<sup>70</sup> and is seen in almost one in four cases following EVAR.<sup>71</sup> As more modern stent-grafts have developed, migration, component separation and stent fracture have become rare and detection of endoleak is now the primary purpose of surveillance. A set of standard definitions has been developed to describe types of endoleak (Figure 2).<sup>65, 70, 72</sup>

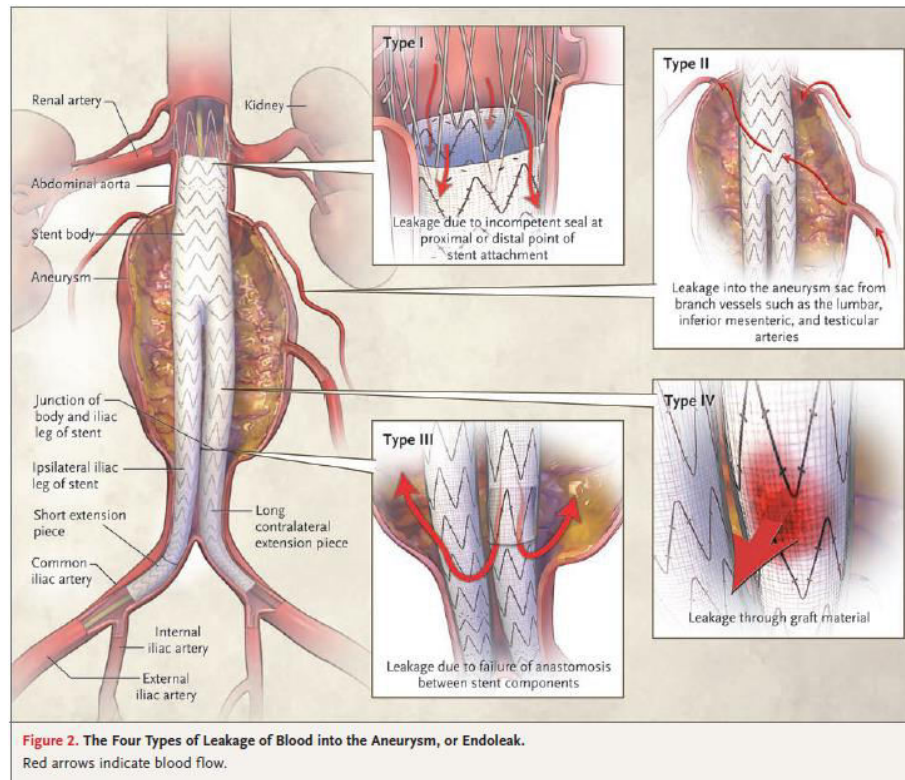


Figure 2: Types of Endoleak. Reproduced with permission from.<sup>73</sup> Copyright Massachusetts Medical Society.

i) Type I endoleak

Type I endoleak is characterised by persistent peri-graft blood flow through the aneurysm due to an inadequate seal at the proximal (type Ia) or distal (Ib) end of the stent-graft. This allows on-going pressurisation of the aneurysm and can lead to expansion and rupture.<sup>74</sup> Type I endoleaks are more common in the presence of 'hostile' anatomy such as short, conical or angulated aneurysm 'necks' - the normal diameter infra-renal portion of the aorta proximal to the aneurysm - or calcified landing zones in the common or external iliac arteries. For the majority of EVAR devices 'seal' is obtained by the radial force of the self-expanding stents in the main body of the graft as they expand against the neck of the aneurysm. The development of a type Ia endoleak in the surveillance period is caused by either a failure to seal due to loss of fixation or dilatation of the aneurysm neck. As the aneurysm contracts following endovascular repair, the morphology of the aneurysm can re-configure and may also dispose to loss of seal.



There is consensus that type I endoleaks should be treated to mitigate the risk of rupture. In type Ia endoleaks without stent-graft migration, it may be possible to re-establish a seal using a moulding balloon or deploy an extension cuff to seal in a more proximal portion of the neck, provided there is adequate infra-renal neck length. If the device has migrated or there is no suitable neck, then conversion to open repair may be needed or complex endovascular revision with a fenestrated or branched stent-graft may be considered.

### *ii) Type II endoleak*

These endoleaks are caused by retrograde perfusion of the aneurysm by aortic branches. A type IIa endoleak has inflow from a single branch vessel and a type IIb endoleak from two or more. The most common sources are the IMA, lumbar and internal iliac arteries. There can also be persistent inflow or outflow from smaller, unnamed aortic side branches. Type II endoleaks are common, and seen in 7.5-44% of patients.<sup>75-78</sup> A large, recent study has shown that spontaneous resolution of type II endoleaks can be anticipated in 35% of patients over a period of 3 months to 4 years.<sup>77</sup>

As type II endoleaks are thought to be low pressure, they may be difficult to detect on imaging and there can also be difficulties differentiating type II endoleaks from other types such as type I and type III. For example, what appears to be a type II endoleak may be the outflow vessel from a type I endoleak and hence multi-modality imaging is often indicated in such cases.

The management of type II endoleaks is also debated as there is insufficient evidence to support any one threshold or indication for intervention.<sup>79</sup> The majority of opinion would suggest that provided the aneurysm size is stable or shrinking no treatment is indicated.<sup>1</sup> The presence of a type II endoleak and increasing aneurysm size is usually an indication for treatment<sup>1, 76, 80</sup> as AAA rupture due to isolated type II endoleaks has been reported.<sup>81</sup> Although increasing size in the presence of a type II endoleak is thought to lead to an increased rupture risk, the recent analysis of 1515 type II endoleaks by Sidloff<sup>77</sup> noted that in 14 ruptures, rupture was preceded by sac expansion in only six patients. This may suggest that aneurysm sac diameter is not a

completely reliable surrogate marker for rupture risk and other parameters, for example, aneurysm volume may be important.<sup>82-84</sup>

If the decision to treat is made, endovascular treatment with embolisation of the inflow and outflow vessels is often first line either via a trans-femoral or trans-brachial approach. Alternatively, a trans-lumbar approach can be used. Both of these procedures are often technically challenging with a 37.5% and 19% failure rate respectively. The trans-lumbar route may have a lower complication rate.<sup>77</sup> Some series have suggested that intervention for type II endoleak does not appear to diminish aneurysm growth, regardless of the approach.<sup>85</sup> Other options such as open or laparoscopic surgery are reserved for when endovascular options have failed and continued sac growth is considered unacceptable.

### *iii) Type III endoleak*

Type III endoleak is due to separation of stent-graft components (IIIa) or tear in the graft fabric (IIIb). They are rare with a reported incidence 0.3-7%.<sup>86, 87</sup> The majority of EVAR devices are modular and rely on a seal formed by the overlap of stent-graft components between the main body and limbs and also between limb components. Type IIIa endoleaks can be due to errors in deployment, however, device migration, stent fracture and aneurysm reconfiguration may also be underlying causes.

Treatment is advised due to the high-pressure nature of type III leaks and cases may be managed by balloon moulding of the causative overlap zone, placement of further components<sup>88</sup> or conversion to aorto uni-iliac repair and femoro-femoral crossover.<sup>89, 90</sup> If the cause is due to stent-graft migration, conversion to open repair may be required.<sup>1</sup>

### *iv) Type IV endoleak*

This is due to porosity of intact stent-graft fabric in the first 30 days after implantation<sup>65, 70, 72</sup> and no treatment is recommended<sup>1</sup>. Past 30 days, these should be considered a type IIIb leak and treated accordingly.<sup>1</sup>

*v) Type V endoleak*

This is the continued enlargement of the aneurysm without a detectable endoleak. If the aneurysm grows more than 10mm following an EVAR and an endoleak cannot be detected, it is recommended that the stent-graft be replaced either with open repair or by re-lining with another stent-graft.<sup>1</sup>

## **2.4 When to operate**

### *2.4.1 Rupture risk based on maximal diameter*

The aim of elective AAA repair is prevention of premature death due to aneurysm rupture. The adoption of maximum diameter as a measure of rupture risk was based, in part, on a retrospective review by Darling<sup>91</sup> of 24,000 consecutive, non-specific autopsies performed over a 23-year period. 40% of AAAs greater than 5 cm in diameter ruptured. Nonetheless, this same report highlights the limitation of aneurysm diameter as a predictor of rupture risk since 40% of AAA between 7 cm and 10 cm had not ruptured, while nearly 13% of patients with aneurysms smaller than 5 cm had ruptured. Nonetheless, it is clear that the risk of rupture increases exponentially with diameter with the risk dramatically increasing at around 6.5cm (Figure 3).<sup>48</sup>

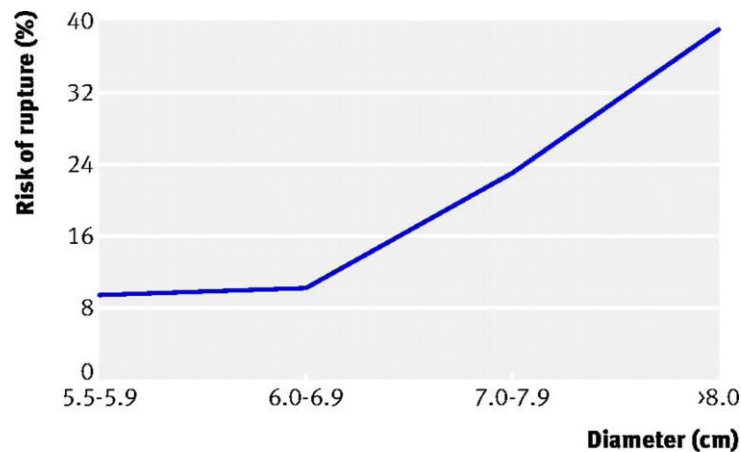


Figure 3: Association between maximal aortic diameter and risk of rupture.<sup>48</sup>

*Reproduced with permission of BMJ publishing*

Currently the maximum aortic diameter is used as the threshold for repair with a diameter of 5.5cm an indication for consideration for surgery. Trials examining the benefits of repairing smaller aneurysms both from the UK<sup>92, 93</sup> and United States<sup>94</sup> have shown no survival benefit on a population basis for the elective repair of aneurysms smaller than 5.5cm. This also applies to patients thought to be fittest for surgery.<sup>94</sup> However, consistent with Darling's work there remains the observation that small aneurysms can rupture and larger aneurysms may remain non-ruptured. This has sparked and maintained interest in other methods of rupture risk assessment such as peak wall stress estimation.<sup>95, 96</sup> Assessment for repair includes imaging to determine the suitability for open repair or EVAR, and functional physiological testing such as cardio-pulmonary exercise testing (CPEX) to assess 'fitness' for surgery.

#### 2.4.2 Rupture risk based on biomechanical analysis – Peak wall stress estimated by finite element analysis

It has been observed that there may be a number of factors other than maximum diameter that may predict the rupture risk of AAA rupture (Figure 4). The applicability of estimates of AAA tensile stress and wall strength or derived parameters to identify patients at risk for rapid growth or rupture, has been identified as a research priority by the American Society of Vascular Surgery.<sup>65</sup>

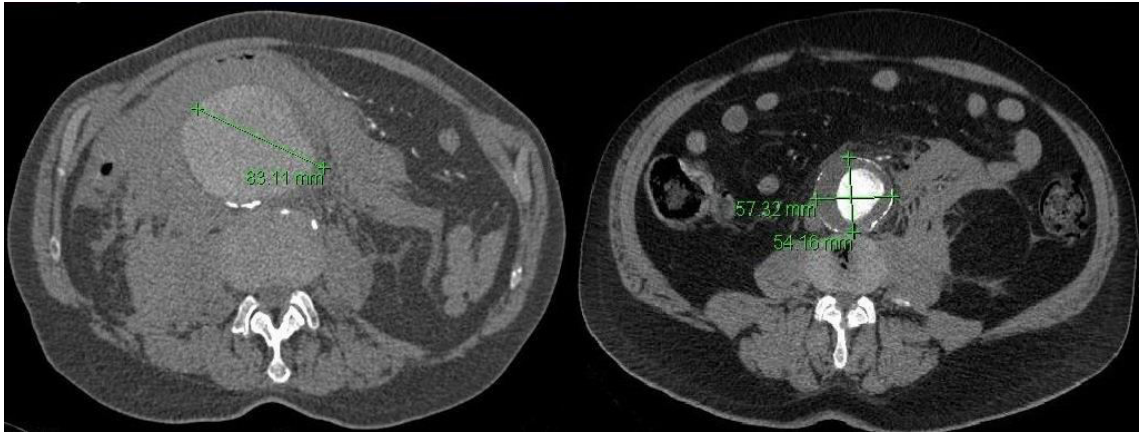


*Figure 4: CTA of a ruptured 8.3cm AAA (left) and a ruptured 5.7cm AAA (right), both in men*

The law of Laplace, which gives a value for circumferential tension in thinned wall structures and forms the basis of diameter-based rupture risk estimations, is inadequate to explain the forces contributing to AAA rupture as AAAs are not a simple cylindrical or spherical shape of uniform radius or curvature:

$$\text{Law of Laplace: } T = \frac{PD}{2t}$$

Where T = wall tension, P = intraluminal pressure, D = diameter, t = wall thickness

From a biomechanical perspective, AAA formation causes an increase in wall stress and a decreasing ability of the AAA wall to withstand such stress. Rupture therefore occurs when wall stress exceeds wall strength.

Finite element analysis (FEA) is a numerical method of solving the differential equations of physics and engineering that was developed in the 1950s. FEA involves breaking down the geometry of the 'problem' (e.g. an AAA) into a finite number of individual regions – 'elements' – that are connected at their corners – 'nodes.' The behaviour of these individual elements is expressed mathematically and combined to give the behaviour of the whole geometry, from which the stress distribution throughout the geometry can be determined. A high degree of accuracy can be achieved if the initial geometry is modelled accurately using a sufficient number of

elements, and the properties of the AAA, such as how the wall responds to stress, are correctly simulated.

Stress analysis for AAAs requires:<sup>97</sup>

- I. The geometry of the AAA under evaluation
- II. A model that explains how the tissue in question behaves (so-called 'material model')
- III. boundary conditions, e.g. blood pressure and points of fixation of the aorta and AAA

In 1987 Stringfellow<sup>98</sup> was the first to employ basic FEA modelling to three theoretical aneurysm geometries. Their FEA demonstrated that cylindrically shaped constant thickness model aneurysms had a higher circumferential stress and comparable maximum longitudinal wall stress when compared with spherical model aneurysms of the same diameter. Further studies in the same era assumed AAAs obeyed the Law of Laplace<sup>99</sup> or assumed axisymmetric geometry<sup>100</sup> though the work by Inzoli was the first to consider the role of intra-luminal thrombus (ILT), reporting that it may reduce wall stress by up to 30%.<sup>100</sup>

The study by Vorp in 1998 was the first to demonstrate the importance of AAA geometry on wall stress estimation.<sup>101</sup> They created 10 hypothetical AAA models with uniform wall strength, uniform peak systolic load of 120mmHg and an elastic modulus that was based on previous ex-vivo tensile tests of AAA tissue. Their key finding was that peak wall stress values in five theoretical AAAs with the same maximal diameter could be up to twice as high due to differences in geometry. This suggested that not all AAAs of the same diameter have the same rupture risk.

Further work by Raghavan's group<sup>102</sup> was the first to perform wall stress analysis using FEA on models derived directly from individual computed tomography (CT) scans. For six patients with AAAs and one control patient, CT scan data with 3-5mm slices was obtained and segmented with a smoothing algorithm applied to smooth surface contours without significantly altering the geometry. The model was pressurised using

the patient's systolic blood pressure with an assumed uniform wall thickness of 1.9mm with the AAA constrained proximally and distally. A nonlinear mathematical model developed specifically for AAA tissue was used.<sup>103</sup> They showed that wall stress within AAAs had large regional variations compared to the control aorta, and that peak wall stress differed by as much as 13% between two patients with the same maximal aortic diameter.

Subsequently, a study by Fillinger was the first to examine the implication of wall stress analysis in 48 patients with electively repaired (n = 30), symptomatic (n= 8) and ruptured (n=10) aneurysms.<sup>104</sup> The creation of the FEA mesh was semi-automated and the updated model accounted for vessel branch points that has previously lead to computational errors. They reported that peak wall stress (PWS – maximal stress in the AAA wall at systolic blood pressure) was significantly different between groups (ruptured,  $47.7 \pm 6$  N/cm<sup>2</sup>; symptomatic,  $47.5 \pm 4$  N/cm<sup>2</sup>; elective repair,  $36.9 \pm 2$  N/cm<sup>2</sup>;  $P = 0.03$ ), with no significant differences in AAA diameter between groups. They included a sub-group analysis of AAAs with identical mean diameters and found again that the ruptured and symptomatic AAAs had significantly higher PWS. In the three rupture cases where the site of rupture was known, the rupture site corresponded to the area of PWS. They were the first to propose the novel idea of 'equivalent stress' with the aim of producing a clinically useable parameter. By using a regression analysis correlating diameter and stress the PWS could be translated into the equivalent diameter of a typical AAA undergoing elective repair. Interestingly, using this method the smallest ruptured AAA in the study of 4.8cm had an equivalent stress to the average electively repaired 6.3cm AAA. The authors acknowledge that at this stage, a number of possible modelling parameters were not accounted for, including wall strength, non-uniform wall thickness, the influence of ILT, and anisotropic wall conditions.

Fillinger's group expanded their analysis in a second study that investigated if PWS was able to more accurately predict rupture than maximal diameter.<sup>97</sup> Using a refined FEA model, they followed up 42 patients with recent CT scans of asymptomatic AAAs for a mean of 28 months. Findings supported the conclusion that PWS in the asymptomatic

period out-performed maximum diameter for predicting AAAs that would require emergent repair for symptoms or rupture. In a striking comparison, 2 patients had asymptomatic AAAs with identical maximal diameters (5.5cm) but with markedly different PWS – 77 N/cm<sup>2</sup> vs 33 N/cm<sup>2</sup>. Both patients refused surgery due to operative risk and were observed. The high PWS AAA ruptured at 18 months post analysis and the lower PWS AAA remained under observation for more than 3 years. Receiver operator characteristic (ROC) curve analysis demonstrated that PWS performed better than diameter in predicting freedom from rupture, and in Kaplan-Meier analysis PWS better predicted freedom from emergency surgery (for rupture or symptoms). These early results indicate that PWS may identify aneurysms that can be safely observed for long periods or those that may need repair to prevent rupture in a relatively short time.

A study lead by McCollum was the first from a UK surgical unit and compared PWS in 12 ruptured and 15 non-ruptured AAAs.<sup>105</sup> They used a crude and time-consuming manual method of segmenting AAAs from CT scan data with a uniform wall thickness of 2.0mm. Material properties were implied from previous studies.<sup>103</sup> They found a significantly higher peak stress in AAAs that had ruptured or went on to rupture. PWS was also related to systolic blood pressure; however when blood pressure was standardised at 120mmHg there remained a significant difference in wall stress between the groups highlighting the importance of aneurysm geometry to rupture risk. Additionally the point of rupture, when known, correlated with the area of peak wall stress in each case. A subsequent study from the same centre<sup>106</sup> using an identical modelling approach analysed 70 patients with infra-renal AAAs (30 acute and 40 elective) to assess the inter- and intra-operator reliability of FEA predictions of peak wall stress as well as the variation in PWS stress between elective and acute cases. Four raters of different experience performed manual image segmentation of the same 10 randomly selected CT scans. They found again that there was no significant difference in the maximal diameter of 'elective' and 'acute' AAAs, however, PWS was significantly higher in 'acute' AAAs.



As few would debate the indication to repair large aneurysms, the paper by Truijers<sup>107</sup> examined the impact of biomechanical analysis of small asymptomatic, symptomatic and ruptured AAAs. Again, an isotropic hyper-elastic non-linear model was employed and the models were pressurised to the patient's systolic blood pressure. ILT was not considered. Again, PWS was significantly higher in ruptured than symptomatic aneurysms. Interestingly, and contrary to other studies, standardisation of blood pressure across the groups to 120mmHg eliminated significant differences in PWS. As the influence of geometry has previously been seen to be the dominant factor, it may be the study of a small group of small aneurysms with comparable geometries failed to produce differences in PWS based on AAA geometry alone.

#### *Influence of AAA wall characteristics and ILT*

As alluded to, other than the initial work of Stringfellow,<sup>98</sup> FEA models in the above studies do not consider the influence of ILT due to controversial effects on PWS and AAA growth and rupture. ILT is a complex three dimensional fibrin structure present in 75% of all AAAs.<sup>108</sup> As the ILT is constantly re-modelled it may have a wall-thinning effect due to a local proteolytic action on the AAA wall.<sup>109</sup> As the intima and media of the AAA wall do not receive a blood supply from the vasa-vasorum, the shielding of the AAA wall from blood flow by ILT may also cause a hypoxic effect.<sup>110</sup> Its mechanical properties have been widely debated, with some authors suggesting that it has no effect on PWS.<sup>99, 111</sup> However work by Vorp's group has shown using mechanical testing that ILT is a nonlinearly elastic material with significant mechanical properties and has a significant 'cushioning' effect on the AAA<sup>112, 113</sup> though this is still disputed.<sup>114</sup> More recent work using biaxial mechanical testing has demonstrated further the complexity of ILT which may have three distinct types of morphologies, each with different mechanical properties. However ILT was found to be mostly isotropic, supporting the current methods of modelling in FEA.<sup>115</sup>

More recent work using refined FEA models now include ILT<sup>96, 114, 116, 117</sup> and a number of studies have focused on the development of clinical indices incorporating

biomechanical parameters in order to improve clinical applicability. This approach was first considered by Vorp's group in 2006<sup>117</sup> who acknowledged that the risk of rupture was dependant on both wall stress distribution and also wall strength distribution. Wall strength was estimated by a previously developed mathematical model using linear regression techniques accounting for local influences of ILT as well as gender and family history.<sup>118</sup> They proposed the 'rupture potential index':

$$RPI = \frac{Stress}{Strength}$$

In the 13 AAAs studied (maximum diameter 5.23cm), they found no differences in PWS or maximal diameter between ruptured and non-ruptured AAAs. Although not statistically significant, perhaps due to small sample size, the *P* value of the peak RPI (0.10) was lower for than the comparisons using PWS (0.62) and maximal diameter (0.26) suggesting the RPI may be better able to identify those AAAs at increased risk of rupture.

More recently, Doyle has proposed the Finite Element Analysis Rupture Index (FEARI).<sup>119, 120</sup> Rather than a statistical model of wall strength, the wall strength data in the FEARI is derived from bench-top mechanical testing of AAA tissue. By combining the results of previous studies,<sup>121-123</sup> 'population mean' wall strength values were derived and divided into eight region-specific values termed 'ultimate tensile strength' (UTS) (Figure 5). For example, the anterior region was given UTS of 0.7744 MPa compared to the posterior at 0.8658 MPa. Therefore:

$$FEARI = \frac{Regional\ PWS}{UTS}$$

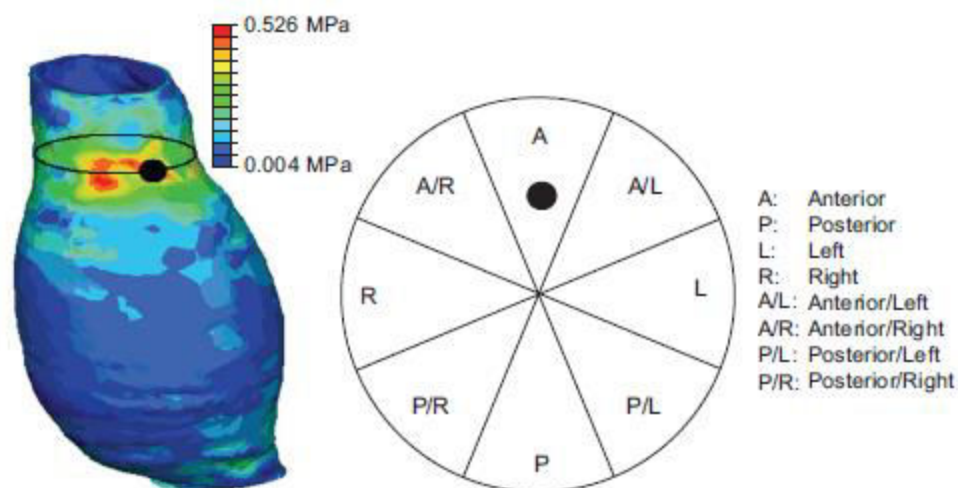


*Figure 5: FEARI methodology<sup>119</sup> demonstrating PWS in the anterior aspect of an AAA. The AAA is divided into eight regions, each of which has been assigned an individual tensile strength. Reproduced with permission.*

They compared groups of ruptured and asymptomatic AAAs using the FEARI and included a subgroup analysis of patients with the same maximal diameter. FEARI was higher in the ruptured/symptomatic group and a poor relationship was seen between FEARI and maximal diameter. Asymmetric AAAs with smaller amount of thrombus were found to have a higher FEARI than fusiform AAAs with larger percentages of thrombus.

The 'Peak Wall Rupture Risk' (PWRR) and 'Peak Wall Rupture Index' (PWRI) proposed by Gasser<sup>114</sup> again accounts for both PWS and differences in wall strength based on ILT thickness, ratio of luminal diameter and healthy infra-renal aortic diameter, gender and family history for rupture. In a recent study, they examined the ability of PWS and PWRR to discriminate between ruptured and non-ruptured AAAs using four different FEA models. Only the most sophisticated model incorporating the effects of ILT, differences in wall thickness and mean arterial pressure (MAP) was able to produce a statistically significant difference in PWS/PWRR to discriminate between ruptured and non-ruptured aneurysms. They reported a 43% better predictive value in identifying ruptures amongst diameter-matched aneurysms for the PWT model, highlighting the importance of ILT and changes in wall thickness. Interestingly, a positive correlation

was seen with both PWS and PWRR with increasing ILT volume suggesting an absence of the protective effects proposed by other authors.<sup>112, 113</sup>

Although the above studies clearly support that FEA modelling may predict AAAs at higher risk of rupture, until the recent work by Gasser and colleagues<sup>95</sup> no clinical trial has investigated threshold values of these parameters for AAA repair and consequently they have limited clinical relevance and impact. Translation of biomechanical criteria to routine clinical practice is problematic as it is perceived as complex and time consuming. Indeed, it has been reported that more than 20% of European vascular surgeons have never come across them.<sup>124</sup> The project by Gasser explores the concept of 'risk-equivalent' AAA diameter, where following biomechanical analysis the rupture risk values are translated to equivalent diameters of the average aneurysm patient such that an AAA is essentially 'up-staged' or 'down-staged' (Figure 6). Using the PWT model previously described,<sup>114</sup> they retrospectively analysed CT scans from 229 patients (40 ruptures and 203 non-ruptured). They reported that in ruptured aneurysms the risk-equivalent diameter ( $D_{PWRI}$ ) was elevated by 14mm ( $P \leq 0.001$ ) and remained statistically significant in males and females.

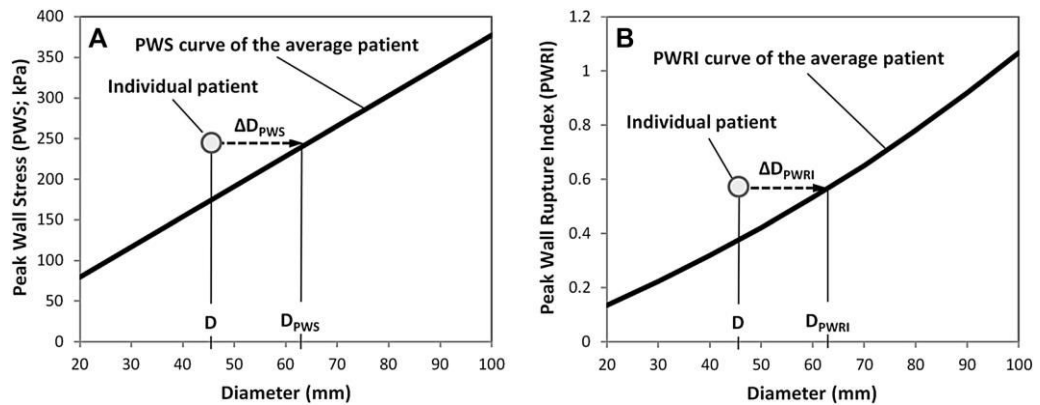


Figure 6: Concept of 'risk-equivalent diameter'<sup>95</sup> demonstrating an AAA with a diameter of 4.5cm has a 'risk-equivalent' diameter of 6.2cm after biomechanical analysis and should be considered for early repair rather than surveillance. Reproduced with permission.

The concept proposed by Gasser has been incorporated into semi-automatic commercial software that is able to perform FEA analysis with minimal user

interaction. It is the first of its type and available as a service on case-by-case basis or as a software package.<sup>125</sup> A recently published meta-analysis highlights that there is continued interest in PWS as a marker for AAA rupture risk. However, there is significant heterogeneity in modelling approaches and software use that makes pooling of results difficult. This remains a challenge to widespread clinical implementation of biomechanical analysis.<sup>126</sup> The influence of ILT, material properties of the diseased tissue wall e.g. anisotropy vs isotropy, wall thickness i.e. uniform vs non-uniform and the effects of wall calcification are all matters of continued debate that require further study. Refinement of these parameters, however, may not significantly affect results or make clinically meaningful differences.

#### *2.4.3 Rupture risk based on biomechanical analysis: wall shear stress (WSS) estimated by computational fluid dynamics (CFD).*

While FEA considers the physical characteristics of the aortic wall and other 'solid' elements, relatively little attention has been paid to the influence of haemodynamic factors on AAA growth and risk of rupture. 'Stress' is a measure of the forces induced in a vessel wall due to blood pressure and blood flow. 'Shear stress' is the stress induced on the vessel intima by the shaving force of blood flow. Stresses in the aorta cannot be directly measured but can be computed if the geometry is known. For simple geometries, e.g a cylinder, the calculation of shear stress is straight-forward:

$$\sigma_{Shear} = \frac{4\mu V}{r}$$

where  $\sigma$  is stress,  $\mu$  is viscosity of flowing blood,  $V$  is the average velocity of flow and  $r$  is the radius of the cylinder.<sup>127</sup>

When the luminal geometry becomes more complex, computational methods such as computational fluid dynamics are required. Similar to the finite element method described above, CFD analysis requires the geometry of the lumen, the material and mechanical properties and appropriate boundary conditions.

Under normal conditions, the shear stress placed on the vessel wall stimulates vascular endothelial cells to produce directly or in directly acting anti-thrombotic mediators such as prostacyclin,<sup>128</sup> nitric oxide,<sup>129</sup> calcium<sup>130</sup> and thrombomodulin.<sup>131</sup> Within aortic aneurysms, altered haemodynamics such as recirculating flow leads to oscillating WSS which may create endothelial injury or lead to inflammatory infiltration. Low WSS has been implicated in processes that degenerate the AAA wall. A wall shear stress (WSS) of <0.4 Pa appears a critical point that leads to inflammatory cell infiltration and endothelial injury.<sup>132</sup>

The exact mechanisms by which changes in WSS may contribute to aneurysm growth and rupture risk is poorly characterised. One possible mechanism is in the relationship of WSS to the formation of ILT. A number of studies have demonstrated a relationship between areas of low WSS and thrombus formation.<sup>133, 134</sup> Studies have suggested that ILT has a protective effect against peak wall stress,<sup>113, 135</sup> however, there is evidence to suggest that ILT has a wall weakening effect due to the local action of proteolytic enzymes and arterial wall hypoxia.<sup>109, 110</sup> There is evidence that the presence of ILT is associated with an increased growth rate<sup>136, 137</sup> however, the overall influence of ILT on AAA growth and rupture risk remains somewhat conflicted.

#### *Clinical use of CFD*

The study by Doyle<sup>134</sup> was the first serial computational study to investigate the development of an AAA over time by using patient specific geometries taken from four CT scans over a 29 month period from a patient who subsequently suffered AAA rupture. Their modelling approach was similar to previous authors using Mimics software (Materialise, Leuven, Belgium) for segmentation and assumptions of Newtonian fluid, rigid walls and laminar flow. A pulsatile inlet boundary condition was applied based on a waveform averaged from AAA patients<sup>138</sup> rather than constant

flow. They found that maximal intra-luminal thrombus accumulated at the region with the lowest time-averaged wall shear stress (TAWSS) and this region corresponded with the site of rupture at open surgery (Figure 7).

The AAA studied in this paper was over 7cm in maximal diameter when rupture occurred and emergency open repair was performed. It is not clear why this patient did not undergo earlier elective repair. Such an approach using multiple CT scans to study the influence of WSS in larger numbers of patient is clearly unfeasible.

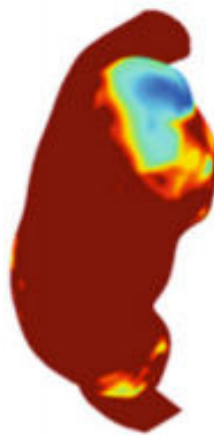


*Figure 7: Region of low WSS (dark blue) in an AAA, corresponding with the site of rupture on open repair.<sup>134</sup>*

Most recently, work by Boyd described CFD simulations in seven ruptured AAAs.<sup>139</sup> The modelling approach was similar to previous studies assuming rigid walls, blood as a Newtonian fluid and constant laminar flow. In six of the seven cases, the clinical site of rupture corresponded to regions of low WSS and a larger amount of thrombus deposition. Only three of these seven cases ruptured in the region of maximal aortic diameter (Figure 8).

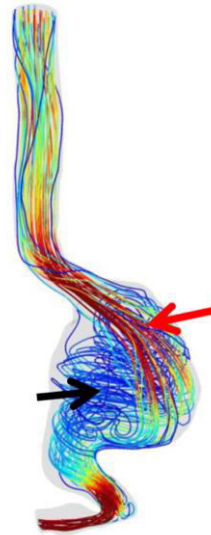


Figure 8: Velocity streamlines in a ruptured AAA.<sup>139</sup> Low velocity values are in blue with higher values in red. Black arrow shows the site of rupture in a zone of low flow velocity and WSS. Red arrow shows the dominant flow channel. Reproduced with permission.

Low WSS is unlikely to cause rupture directly, however, the way in which it appears to promote the formation of ILT and lead to inflammatory infiltration likely increases susceptibility to rupture by causing wall-weakening. In truth, the optimal computational model would couple both FEA and CFD approaches to explore the interaction between the fluid and solid components. This approach, termed fluid-structure interaction (FSI), is likely to be the most sophisticated method of biomechanical analysis.

#### 2.4.4 Current clinical implementation of biomechanical analysis and potential role of 3D US

As detailed above, current techniques for biomechanical analysis of AAAs rely on CT to provide the geometry of the aneurysm, with the material properties of the AAA wall defined by bench-top mechanical testing of explanted aortic tissue or mathematical models.<sup>121</sup>



Since the aim of biomechanical analysis is to identify firstly, small aneurysms that are at higher risk of rupture and secondly, large aneurysms that are at lower risk, any analysis needs to be applicable to the population of patients on AAA surveillance – that is, a cohort of patients with AAAs <5.5cm in diameter. As the only indication for CT in a patient with an asymptomatic AAA is planning for repair, CT scans are not available for the target population. As a result, despite the recent availability of commercial FEA software for AAA (<http://www.vascops.com/en/vascops-home.html>) the approach is not in routine clinical use. Routine use of CT for biomechanical analysis of small AAAs is not feasible due to the number of patients, radiation exposure and cost. Nor would CT be suitable as a research tool to investigate how PWS and WSS evolve in large numbers of patients.

The key data supplied by CT scanning is the geometry of the AAA. Three-dimensional ultrasound (3D-US) has the potential to provide 3D AAA geometries for use in biomechanical analysis. This is a unique application of 3D-US and when compared to CT, is inexpensive and does not involve radiation. If accurate AAA geometries can be produced using 3D-US they may be used in FEA in the same way as CT, widening the applicability of this technique.

Given that 10 AAA repairs are performed to prevent one rupture, more accurate rupture risk data, in the form of peak wall stress derived from widely available modality such as 3D US, would help individualise indications for AAA repair when taken in context with other factors such age, co-morbidity and physiological status. Integration of peak wall stress estimation could be integrated into existing clinical decision aids.

By identifying smaller AAAs at high risk of rupture earlier surgery may be recommended. Smaller aneurysms are more likely to be suitable for EVAR with its associated reduction in mortality. Patients with large AAAs (>5.5cm/>5cm) with significant co-morbidity may be found to be at lower risk of rupture than anticipated, allowing surgery to be safely deferred to allow optimization of co-morbidities or support a decision not to operate. Some patients who are at high surgical risk may

decide not to undergo surgery if they have a 'lower risk AAA'. AAA surgery is expensive – open repair incurs its costs from the need for post-operative critical care and length of hospital stay and EVAR from the cost of the stent-graft, post-operative surveillance and re-intervention. More individualised indications for AAA repair has the potential to make AAA surgery more cost effective

## CHAPTER 3: CURRENT USES OF ULTRASOUND IN THE MANAGEMENT OF AAA

### 3.1 Ultrasound modalities for EVAR surveillance

#### 3.1.1 Background

Surveillance aims to assess the structural integrity and position of the endograft, presence of endoleaks, and stenosis or occlusions in stent-graft limbs and related vessels.<sup>140</sup> Historically, computed tomographic angiography (CTA) has been considered the 'gold standard' for post-EVAR surveillance and formed the basis of follow-up programmes. However, CTA is expensive, delivers a significant radiation dose to patients (as much as 400 chest x-rays)<sup>141</sup> and requires the use of nephrotoxic iodinated contrast media. Duplex ultrasound imaging has been identified as a possible non-invasive, non-toxic and inexpensive modality for detecting complications following EVAR, therefore mitigating the undesirable aspects of CTA.

#### 3.1.2 Endoleak detection

The use of Duplex ultrasound (DUS) in various forms for EVAR surveillance developed quickly after the advent of EVAR and has been described in number of studies summarised in Table 1. Generally, the studies are difficult to compare as a group due to the clear learning curve demonstrated in the earlier studies, development of ultrasound technology, changes in EVAR stent-graft design, and changes in CT scanning protocols (introduction of dual phase/triple phase protocols.) However, a number of good quality reviews and meta-analysis have been completed.

Table 1: Summary of studies of duplex modalities for endoleak detection following EVAR

Author	Year	Type of study	Number of patient/images	Imaging Modalities compared	Findings/Conclusion
Heilberger <sup>142</sup>	1997	Prospective	113 patients	CEUS/CTA	CEUS detected all but one 'major leak.' Useful for detecting type II endoleaks.
Sato <sup>143</sup>	1998	Retrospective	117 patients	CEUS/CTA	CEUS 97% sensitive. Duplex data on flow valuable.
McWilliams <sup>144</sup>	1999	Prospective	20 paired scans	CEUS/CTA	CEUS sensitivity 100%, Specificity 65%.
Wolf <sup>145</sup>	2000	Prospective	76 patients, 166 paired scans	DUS/CTA	DUS 81% sensitive, 95% specific.
Pages <sup>146</sup>	2001	Prospective	120 paired scans	DUS/CTA	DUS 48% sensitive
Raman <sup>147</sup>	2003	Retrospective	281 patients, 495 paired scans	DUS/CTA	DUS sensitivity 49%. PPV 53.9%
Bendick <sup>148</sup>	2003	Prospective	20 patients	DUS/CEUS/CTA	CEUS detected all endoleaks seen on CTA and out-performed DUS
Bendick <sup>149</sup>	2003	Prospective	40 patients	CEUS/CTA	CEUS detected all but one endoleak. CEUS-based surveillance is feasible.
AbuRhama <sup>150</sup>	2005	Prospective	367 paired scans	DUS/CTA	68% sensitivity of DUS. DUS not recommended as primary surveillance modality for EVAR.
Ashoke <sup>151</sup>	2005	Systematic Review and Meta analysis	711 patients, 1335 paired scans	DUS/CTA	Sensitivity of DUS 69%. DUS not accurate enough to use routinely.
Iezzi <sup>152</sup>	2009	Prospective	84 paired scans	DUS/CEUS/CTA	Sensitivity of duplex much

					improved by addition of contrast (97.5 vs 67.5%).
Mirza <sup>153</sup>	2010	Systematic review and Meta analysis	DUS vs. CT: 2601 pts CEUS vs. CT: 285 pts	-	Standard duplex has poor sensitivity.
Ten Bosch <sup>154</sup>	2010	Prospective	127 paired scans	CEUS vs. CT	CEUS has better sensitivity for all endoleak than CTA, particularly type II.
Perini <sup>155</sup>	2011	Prospective	395 paired scans	CEUS vs. CT	CEUS and CT are equivalent for endoleak detection.
Cantisani <sup>156</sup>	2011	Prospective	108 patients	DUC/CEUS/CT/MRI	CEUS is markedly better for endoleak detection than DUS and similar to CT and MRI. CEUS classified endoleaks more accurately.
Karthikesalingham <sup>157</sup>	2012	Systematic review and Meta analysis	DUS vs. CTA: 3975 paired scans CEUS vs CTA: 961		DUS is adequate for detection of clinically important endoleaks that is not improved by routine use of CEUS.
Grey <sup>158</sup>	2012	Retrospective	145 patients	DUS/CTA	100% sensitivity of DUS compared to CTA. Significant financial savings by moving to DUS surveillance
Gurtler <sup>159</sup>	2013	Retrospective	200 paired scans	CEUS/CTA	CEUS is at least equivalent to CTA for endoleak detection
Millen <sup>160</sup>	2013	Retrospective	33 patients with diagnostic uncertainty on DUS or CTA	DUS/CEUS/CTA	CEUS clarified endoleak type in difficult cases, including type I leaks. Reserve CEUS for cases of diagnostic uncertainty

The study by Heilberger in 1997<sup>142</sup> was the first to describe the use of DUS for EVAR surveillance. Interestingly, each DUS scan was performed using an intravenous contrast agent (now termed contrast enhanced duplex ultrasound (CEUS)). As the study pre-dated any consensus on the definition of endoleak types, they examined for the presence of any leak as the main outcome with a descriptive analysis. Even in this early experience, CEUS detected all but one of the 'major leaks' when compared with CTA. In this one case, the distal leak from an iliac landing zone (i.e. type Ib) was thought to be obscured due to overlying bowel gas. From a technical standpoint, the authors found analysis of some scans difficult due to the extensive artefact produced by the combination of contrast and colour Doppler. This study lacked blinding, and any measurement of reproducibility of results. The small sample size restricted it to a descriptive analysis.

The Sato paper included blinded assessment of paired images in a core lab, though again lacked any assessment of inter-observer reproducibility.<sup>143</sup> Only 19% of DUS scans performed were felt to be of adequate quality for endoleak detection, which related to the lack of a standardised scanning protocol specific to surveillance and experience with EVAR. The authors noted that the additional information regarding directionality of flow within the AAA sac could help in determining the type of endoleak and that this was data that could not be gained from CTA. McWilliams *et al.*<sup>144</sup> reported a pilot study of 20 patients revealing a 100% sensitivity of CEUS and reinforced the concept that 'false positives' seen on CEUS are likely to be 'true positives' due to the increased sensitivity of CEUS.

Wolf's study<sup>145</sup> had a more robust methodology including large numbers, blinding and an accredited vascular technologists scanning to a standardised protocol. A smaller proportion of DUS scans were unsuitable for analysis (7%) mainly due to patient factors including obesity and bowel gas. This demonstrates a refinement in technique and development of expertise in DUS for EVAR surveillance. A potential confounder in the analysis was the change in CTA protocol in 1998 to include delayed-phase imaging (57% of cases) that likely improved the sensitivity of the CTA to detect small endoleaks. They noted that the endoleaks missed by DUS were 'small posterior leaks' (likely to represent type II leaks) and probably clinically benign. The small proportion of

endoleaks seen on DUS and not CT were deemed 'false positives' but may have been true 'positives' as some of the CTA did not have delayed phase imaging.

Despite initial promising results in these early papers, other authors failed to reproduce such encouraging results. A large study from a group in the USA analysed 494 same-day CTA and DUS images of post-EVAR patients.<sup>147</sup> They reported a sensitivity of only 43% for detection of all endoleaks. However, as CTA was the 'gold standard' any endoleaks seen on DUS but not CTA were considered false positives, a potentially inaccurate interpretation as the CTA images only included a non-contrast and arterial phase. Further studies between 2000 and 2009 also reported mixed results with some demonstrating poor sensitivity.<sup>146, 150</sup> The view that DUS was not sensitive enough to use in routine follow up after EVAR was supported by a well-conducted systematic review by Ashoke in 2005, although this included unpublished data.<sup>151</sup> However, some reports were more promising and continued to advocate the use of duplex imaging, particularly with the use of intra-venous contrast.<sup>148, 149, 152</sup>

The paper by Bendick<sup>148</sup> is important to consider from a technical aspect. They were the first to describe the use and advantages of 'tissue harmonic imaging' during CEUS. This reduces artefact from surrounding structures and enhances the blood flow signal in the ultrasound image. This has been an important step in the evolution of CEUS and has been employed in each of the more contemporary CEUS studies.<sup>154-156, 160</sup>

A further meta-analysis on this subject was published by Mirza in 2010.<sup>153</sup> They reported that unenhanced DUS had a pooled sensitivity of 0.77 compared to CTA on bivariate analysis for detection of all endoleaks. CEUS performed better with a sensitivity of 0.98 and specificity of 0.88. However, these results were difficult to interpret due to significant heterogeneity in studies including expertise in scanning, scanning protocol, CTA protocol and instrument quality. There was little consideration of inter-observer variability or the diagnostic accuracy of ultrasound images and no trial directly compared DUS to CEUS. They acknowledged that the high false-positive rate of CEUS compared to CTA in some studies may in fact represent its higher sensitivity in detection of true low-flow endoleaks. This will always prove to be an unavoidable issue in comparative studies comparing modalities where no true 'gold-standard' exists.

The authors comment that ultrasound modalities do not provide enough information to be used as the sole method of EVAR follow-up as they are not able to detect stent-graft migration, stent fracture and limb kinking. This is certainly true regarding device migration and stent fracture, through both of these can be easily and reliably assessed with plain abdominal x-rays<sup>1</sup> and stent fracture is not thought to be clinically significant.<sup>161</sup> Significant limb kinking should be detected by increased peak systolic velocity in the limb of the EVAR stent-graft or poor flow distal to the stenosis. Therefore, although ultrasound modalities may not be the sole follow up tool it does not necessarily mean a fall-back to CTA. The included studies and the meta-analysis did not include any sub-group analysis based on the detection of types of endoleak. This is important given the different management strategies pertaining to different types. They concluded that the promising results of CEUS warranted further prospective study.

Between 2010 and 2011, the results from two further prospective studies comparing CEUS with CTA<sup>154, 155</sup> and another comparing DUS, CEUS, CTA and magnetic resonance angiography (MRA)<sup>156</sup> were reported. The study by Ten Bosch<sup>154</sup> failed to include an assessment of inter-observer variability for the CEUS performed by three different vascular technologists but was otherwise well designed. Significantly more endoleaks were detected by CEUS than CTA (in 53% vs 22% of cases respectively) representing an overall poor agreement for endoleak detection between the two modalities ( $\kappa = 0.237$ ). The majority of these were type II endoleaks, however, CEUS also found 2 type I endoleaks not seen on CTA. Both of these type I endoleaks seen on CEUS but not CTA required treatment. The author's reluctance to calculate sensitivity and specificity in this study highlights the lack of a gold standard and they suggest that an endoleak seen on either modality should be considered as genuine. They concluded that CEUS can replace CTA as the primary imaging modality for EVAR follow-up in conjunction with x-ray.

The study from Lille<sup>155</sup> represents the largest prospective series comparing CTA and CEUS including 395 paired examinations. They highlight the radiation exposure of one CTA as 20 milliGreys (mGy), and that CTA-only follow up after EVAR equates to a total effective radiation dose of around 145-205 millisieverts (mSV) over 5 years<sup>162</sup> with a



risk of cancer induction.<sup>163</sup> This is contrasted with the 1mSV exposure required for the abdominal x-rays needed to assess for stent migration, kinking and fracture. The authors emphasise that the increased number of endoleaks detected by CEUS represent higher sensitivity, rather than false positives and CEUS has the advantages of detecting the direction of flow of endoleaks which may be valuable information when planning re-intervention. CEUS has all but replaced CTA at their institution for EVAR surveillance.

These more contemporary studies were combined in a further meta-analysis in 2012.<sup>157</sup> The pooled sensitivity of CEUS compared with CTA was 0.96 for all endoleaks with a specificity of 0.85. This reduction in specificity may be in some part due to a higher sensitivity of CEUS than CTA. Their secondary analysis was unique in comparing CTA with CEUS as the gold standard finding a pooled sensitivity of CTA as 0.70 with a specificity of 0.98. As there are clear economic considerations in performing CEUS in routine surveillance (e.g. material cost of contrast agent, further scanning time) a further analysis comparing the ability of DUS and CEUS to detect type I and type III endoleaks showed no statistical difference in the sensitivity of CEUS and DUS. As the ability of DUS to detect type I and III endoleaks currently seems non-inferior to CEUS, the extra cost of CEUS was not be supported for routine use in EVAR surveillance. This was subsequently supported by another large retrospective series that compared CTA to DUS in 242 cases and found DUS 100% sensitive and 85% specific for all endoleaks when compared to CT, questioning the role of CEUS in routine EVAR follow up.<sup>158</sup> They estimated over £60,000 per year in cost savings to the hospital by switching to a duplex- based surveillance programme.

It is clear from the literature that some centres favour routine use of CEUS<sup>155, 156, 159</sup> over DUS despite the added cost of a contrast agent and a meta-analysis suggesting that CEUS is no better than DUS in detecting clinically important endoleaks.<sup>157</sup> A more pragmatic approach to the use of CEUS has been suggested in a study by Millen who investigated the introduction of CEUS into their surveillance programme between April 2011 and July 2012.<sup>160</sup> They proposed three indications for CEUS:

1. Endoleak classification: CEUS should be used pragmatically to clarify endoleaks that are indeterminate on other modalities
2. Cases of endotension.
3. Target vessel patency after fenestrated endovascular repair in patients with CKD IV and in whom DUS was non-diagnostic.

An almost ubiquitous criticism of duplex ultrasound as a surveillance tool following EVAR is operator dependency, and it is surprising how infrequently this is assessed in the literature. Indeed, 2D ultrasound requires the clinician to sweep the probe back and forth across the subject while mentally visualizing the anatomy from multiple 2D images in 3D, which is likely to produce variability in results. This may be mitigated to some extent by operator experience and scanning to a specific protocol, though it is not always possible to have such expertise readily available.

There is clearly a need for a technique of detecting endoleaks that is sensitive, specific and avoids the drawbacks of CTA imaging as well as minimising operator dependence. 3D ultrasound has the potential to fulfil this role and warrants detailed examination against the current 'gold standard' of CTA.

### 3.1.3 *Volume measurements*

Aneurysm shrinkage, based on maximal diameter is thought to be predictive of freedom from complications after EVAR. Intuitively, as AAAs are 3D structures, measurement of the aneurysm volume should be more sensitive than crude diameter in detecting more subtle changes. Changes in aneurysm morphology are known to alter dimensions at multiple levels and these could clearly be missed by measurement of a single cross section, regardless of whether they are standard transverse measurements or orthogonal to the central luminal line.

The potential value of volume measurements after EVAR was first elucidated by Wever some 14 years ago.<sup>164</sup> They compared CT diameter measurements with volume

measurements after EVAR and found that aneurysm size changes after EVAR were not seen when using maximal diameter measurements in over one-third of cases. This was supported by work by Prinssen<sup>82</sup> in 2003 who studied 347 CT images from 82 patients in an EVAR surveillance programme. They found that measurement of aneurysm sac volume provided earlier evidence of sac shrinkage after EVAR than diameter alone. Significant decreases in sac volume were seen in more than 60% of patients in 6 months compared with diameter measurements that only reached a comparable rate after 2 years. They recommended volume measurements for all patients.

Van Keulen compared CT measurements of maximum diameter, orthogonal diameter and volume measurements in 56 patients following EVAR.<sup>83</sup> Volume measurements were taken using a validated, semi-automated technique. Increases in transverse and orthogonal diameters were associated with an increase in volume in only 38% and 44% of cases. They also demonstrated that diameter measurements increased without an increase in volume in small proportion of patients. Importantly, 63% of volume increases in the presence of type II endoleak were missed by diameter measurements alone. As increase in sac size is generally considered an indication for re-intervention, there may be a group of patients who require treatment for endoleaks that are not detected by simple diameter measurements. The findings of a more recent study by Hahne<sup>84</sup> are contradictory to those outlined above. A retrospective analysis of 220 CT scans from 73 patients after EVAR found a high correlation of volume and diameter ( $r = 0.813-0.905; < 0.01$ ). Additionally, there were associated increases in sac diameter and volume in the presence of endoleaks.

With adoption of ultrasound-based EVAR surveillance, volume measurement using CT is no longer a feasible option for most patients and a number of studies have explored the possibility of AAA volume measurements using 3D-US. A proof of principle was established in 2001 by a group from the USA, where 3D volume meshes of a normal, aneurysmal and stent-grafted aorta were generated using an electromagnetically tracked freehand system (Sonos 5500 ultrasound + 'Flock of Birds™'; AscensionTechnology, Burlington, Vt).<sup>165</sup> Generation of the 3D meshes required manual outlining on each individual image before processing with a separate software package. The purpose of the paper was to demonstrate that such a technique was

possible, rather than assess its accuracy or reproducibility and despite the subsequent interest in volume measurements as outlined above, very little work on volume measurement using 3D-US was published for a number of years, though a number of authors used 3D-US to study AAA diameters.<sup>166, 167</sup>

Some 12 years later, another group from the same institution presented results of seven patients with paired data from 3D US and CT angiography.<sup>168</sup> They utilised the same approach as previously described, though this was refined by ECG gating of the image capture to reduce variations in vessel size with the cardiac cycle, though this extended image acquisition time up to 5 minutes. Again, manual outlining of the aneurysm was required on each modality and took up to 43 minutes for each case. CT and ultrasound data was measured by two independent observers on two separate occasions. Although clearly limited by small numbers, they reported a correlation coefficient for volume measurement of 0.93 and good inter-rater reliability. The time taken for processing each case limits the routine utility of this approach for routine cases in busy vascular surgery departments.

Another approach to volume measurement is detailed by Long and colleagues.<sup>169</sup> They defined a 'partial volume' that could be measured in the absence of standard visible landmarks (such as the renal arteries and aortic bifurcation) as the full AAA anatomy was not within the field of view of the mechanical 3D transducer. In 42 patients, they demonstrated impressive inter-observer reproducibility with an intra-class correlation coefficient of 0.99 when AAA volumes were measured with 3D-US by two blinded raters. Their approach was limited in a number of ways. Firstly, although a high degree of reproducibility was achieved, the volume measurements using 3D-US were not compared with a 'gold standard' (e.g. CT) or validated against a known volume (e.g. using a phantom) and may therefore not be accurate. Secondly, the mechanical probe used had a limited field of view, allowing assessment of a volume only 15mm proximal and distal to the maximal aortic diameter. It is possible therefore that volume changes outside this area may not have been detected.

Bredahl and colleagues subsequently addressed the issue of comparison to CT scanning by using the same scanning protocol, probe and processing software as the Long group to measure AAA volume in 93 patients after EVAR.<sup>170</sup> They found that volume measurements using their 3D US method were within +/- 12ml of CT measurements with a mean difference of 1ml. CT measurements were more reproducible than 3D US measurements (mean of difference for 3D US 2ml) mainly due to the image quality limitations inherent to ultrasound and that the 3D-CT inter-operator variability included only the reading process, whereas the 3D-US inter-operator variability included both a new acquisition and a reading. Despite this, reproducibility of 3D-US volume measurements was still within the current expected variability of diameter measurements using 2D-US.

More recent work by Arsicot failed to produce such accurate results. They again used a mechanical 3D-US probe to measure AAA size following EVAR. Their method for defining the measured volume on CT scan was by loss of the parallelism of the aortic walls and an external diameter greater than 30 mm, but the method for 3D-US measurements was not given. The mean difference between CT and 3D-US measurements was 12.75ml with wide limits of agreement between - 58.43 and 32.91ml. The inter-operator reproducibility calculated on a sample of 45 pairs of examinations was  $r = 0.949$  ( $p < 0.0001$ ) with the mean of the differences between two operators of 3.31ml. This study suffers from methodological limitations including a poor explanation of how the proximal and distal extent of the aneurysm was defined on 3D-US and the use of different software packages to analyse the CT and ultrasound data. It is unclear if the ultrasound system or software used is calibrated or designed for vascular applications. Additionally, the interval between 3D-US and CT scans was often long with the mean interval between 3D-US and CT examinations of  $48.18 \pm 36.52$  days which may have accounted in part for the difference between CT and ultrasound measurements.

The advantage of a freehand tracked 3D-US system for volume measurement would be its ability to image most of the infra-renal aorta, rather than a partial segment that would be hoped to be representative. Before volume measurements using this

systems can be used, it requires validation of its accuracy against a gold standard in the form of CT scanning, and assessment of inter and intra-observer reliability.

### **3.2 Ultrasound for rupture risk prediction**

Two authors have recently used 3D-US for estimation of rupture risk, taking very different approaches.

The study by Bihari<sup>171</sup> is the only study to derive physiological parameters from AAAs using a 3D US modality. In-vitro validation of the system using a pulsatile AAA model with both laser-scan micrometer and video photogrammetry showed that the measured mean differences between 3D-US speckle tracking and the reference methods were under 0.76 mm. They therefore subsequently used 3D-US speckle tracking to investigate strain parameters in 5 patients with AAAs. They were able to demonstrate strong local differences in the biomechanical properties of AAAs, and that the strain response of individual AAAs to similar blood pressures was heterogeneous. Although the paper is the first to describe strain parameters from 3D-US, aside from the small sample size there are a number of criticisms that can be made. Firstly, the 3D system used has been developed and optimised for echocardiography and data required exporting to another system for further processing and analysis. Secondly, 'Strain' is a measure of physical distortion (i.e. stretch) and does not translate to 'stress' (i.e. load) which is thought to be the most important biomechanical parameter.

A recent study by from the Netherlands has been the first to explore this approach,<sup>172</sup> analysing paired 3D ultrasound and CT images from 15 patients. 3D-US was performed using a mechanical array. Due to the limited sweep range of the mechanical transducer, multiple acquisitions were performed to image the AAA in each patient. The US data was then manually segmented before assembling the acquisitions into a single geometry in post-processing. The 3D-US and CT based models were then objectively compared using a similarity index and their performance assessed in finite element analysis.

They experienced difficulties with poor image quality and limited field of view making three patients unsuitable for analysis. Four FEA simulations failed. The geometrical comparisons had a positive trend with a similarity index of at least 0.74. However, when 8 paired geometries were compared in FEA, the 3D-US models over-estimated stress by 23% in high stress regions. One of the main limiting factors was the need to fuse multiple acquisitions together to produce a single geometry, leading to artefacts causing regions of high stress in FEA. This will be difficult to overcome and is a limitation of using a mechanical array, though development of an automated segmentation and fusion process may improve this and enhance clinical applicability. An alternative approach would be to acquire 3D-US data using a freehand system, as this would allow imaging of the aorta in a single acquisition. This would remove the need for such extensive post-processing and may avoid the stress artefact caused by registration of multiple volumes.

# OVERVIEW OF THESIS AIMS

3D-US has a number of emerging applications across different medical specialities. The ability to provide non-invasive, relatively inexpensive and radiation free 3D imaging provides scope for use in a number of different areas of AAA diagnosis and treatment outlined in the above review. The main aim of this thesis is to develop novel clinical applications for 3D-US in the diagnosis and management of AAA. This can be divided into four specific research questions:

Can 3D-US:

1. Provide completion imaging following EVAR that is non-inferior to uniplanar angiography? If so, will it prove to be a clinical tool that could reduce contrast burden in patients with severe chronic kidney disease undergoing EVAR?
2. Improve the detection and classification of endoleaks for patients in EVAR surveillance when compared to CT angiography and 2D contrast-enhanced ultrasound? Does it have the potential to reduce the number of CT scans or catheter angiograms required in EVAR follow-up?
3. Measure AAA volume in an accurate and reproducible fashion when compared to volume measurement using CT angiography?
4. Provide AAA geometries that be used in biomechanical analysis to estimate peak wall stress and wall shear stress? What are the technical challenges in developing this as a useable clinical tool?



## **SECTION 2: METHODS**

## CHAPTER 4: METHODS FOR PROGRAMME OF RESEARCH

### 4.1 Duplex ultrasound and three-dimensional ultrasound

#### 4.1.1 *Ultrasound Generation*

Ultrasound (US) is part of the spectrum of mechanical waves of a typical frequency of >20,000Hz and is generated by passage of an alternating electrical current through piezoelectric crystals. The piezoelectric effect is a *reversible* process such that materials exhibiting the direct piezoelectric effect (the internal generation of electrical charge resulting from an applied mechanical force) also exhibit the reverse piezoelectric effect (the internal generation of a mechanical strain resulting from an applied electrical field).

In an US transducer, application of an electrical voltage causes the crystals to expand and contract to produce mechanical oscillations that are transmitted as longitudinal waves of compression and refraction until an interface is encountered. Reflected waves from interfaces travel back through the medium to piezo-electric crystals which then convert the mechanical oscillations to electrical impulses. The time taken for the reflection to travel back to the probe is used to calculate the depth of the tissue causing reflection.

#### 4.1.2 *Three-dimensional ultrasound (3D-US)*

Three dimensional ultrasound is an evolution of standard US that overcomes a number of limitations of 2D-US imaging.<sup>173</sup>

1. Conventional use of US is very operator dependant as it involves the mental transformation of multiple 2D images into a subjective 3D impression of anatomy and pathology. This is universally considered time consuming, inefficient and a source of significant inter-observer variability. In contrast, 3D images can be reconstructed from data obtained from a single sweep of the probe across the

region of interest. Each ultrasound image and its relative position are known and therefore the exact location between anatomical structures is recorded.<sup>174, 175</sup>

2. With 2D-US, the displayed images are displayed as a 'flat' anatomical section. With 3D-US the data can be presented in a number of ways including multiplaner reconstructions (MPRs), volume rendering and surface rendering.<sup>173-175</sup>
3. Conventional 2D-US is not accurate for monitoring disease progression or for conducting quantitative prospective or follow-up studies due to difficulty in replicating the transducer position so the 2D plane is in the same anatomical site and orientation as the previous study.<sup>173, 175</sup>
4. Volume estimations made using 2D-US are based on measurements that are *approximately* orthogonal to each other which may lead to inaccurate and variable results.<sup>176-178</sup>

#### 4.1.3 Types of 3D-US

There are three main approaches to the acquisition of 3D-US data; mechanical, matrix and freehand.

Mechanical 3D-US transducers consist of a motor contained within the transducer that moves a single array of up to 512 piezoelectric crystals acquiring a series of two-dimensional (2D) images. These 2D images are then placed sequentially into a 3D volume reconstruction. The volume that can be imaged is relatively small compared to a matrix transducer. Hence, only small sections of anatomy can be imaged using this technology.

A typical commercially available matrix 3D-US transducer is composed of grids up to 9000 piezoelectric crystals. The imaging volume is larger than mechanical transducers and image acquisition at around one second is much faster. Due to the grid of crystals and electronic sequencing, image acquisition can be performed in all three image

planes. The image resolution is slightly reduced compared with the mechanical transducer. Similar to mechanical scanning, the fixed crystal grid in matrix scanning can image limited volumes but over a longer and wider range. However, for long vessels the anatomy cannot always be seen in a single acquisition.

'Freehand ultrasound' refers to a method of 3D-US that uses positional sensing to reconstruct 2D US frames in 3D. The position sensor is attached to the ultrasound probe of a standard system and records the trajectory and position of the ultrasound probe as the region of interest is scanned. The system therefore is made up from a standard ultrasound machine, positional sensors and a computer to record and combine the ultrasound and positional data. Most often a magnetic or optical positional sensor is used. Both magnetic and optical tracking are well established techniques for multi-modality image registration used in other surgical specialities, particularly neurosurgery (e.g the Brainlab™ platform. Brainlab AG, Germany).<sup>179</sup>

In magnetic systems, a magnetic field is transmitted from a generator through the volume in which the scan is to be acquired. Sensors attached to the probe pick up the field in three orthogonal directions allowing the position and orientation of the probe to be computed (Figures 9 and 10).

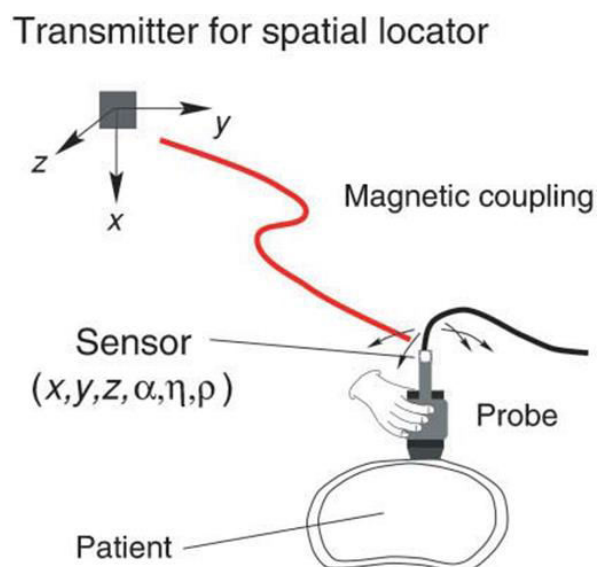


Figure 9: Schematic of a magnetically tracked freehand ultrasound system.<sup>175</sup>

Reproduced with permission ©SAGE.



*Figure 10: Liner US transducer adapted for magnetically tracked freehand 3D-US. An electromagnetic sensor is attached in a calibrated position.*

The main advantage of magnetic tracking over optical tracking is that a line of sight is not required. However, interference from metal objects can affect tracking accuracy and magnetic systems cannot be used in the presence of pacemakers or internal cardiac defibrillators.

The Curefab CS system is a magnetically tracked system. It uses the 3D guidance system "drive BAY" (Ascension Technology Corp., Burlington, USA), which provides positional accuracy of 1.4 mm root mean square (RMS) and rotational accuracy of 0.5° RMS. Tracking sensors are mounted on the ultrasound probe in specific calibrated positions. A high precision frame grabber is used to record the ultrasound image frames, and can be connected to any conventional ultrasound device that has an external analog (VGA) or digital (DVI, HDMI, Display Port) video output (Figure 11).

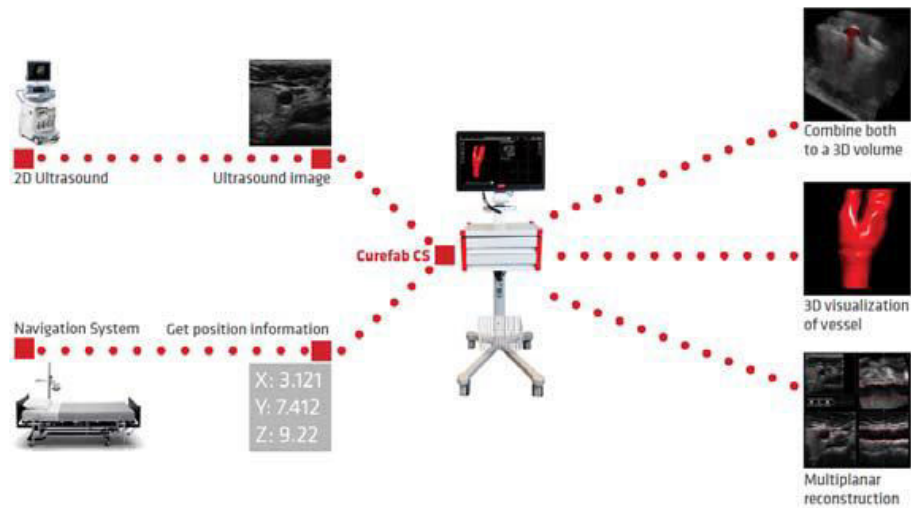


Figure 11: Curefab CS system.<sup>180</sup> Reproduced with permission under CC licencing

In optical tracking (Figure 12), a target is attached to the ultrasound probe. A stereoscopic camera emits infrared light and is able to track the position of the target mounted on the surgical instrument or probe. The Piur Imaging prototype (Piur Imaging GmbH, Vienna, Austria) also utilised in this thesis uses a target consisting of reflective spheres mounted on a 3D printed jig that is attached to the ultrasound transducer. These are then tracked by an infrared camera (Polaris Vicra, NDI Medical, Ontario) (Figures 13-14). Current evidence suggests that optical systems are superior at locating orientations in 3D space and they are not affected by the metallic interference seen in magnetic systems.<sup>175</sup> The main disadvantage is the need for a continuous line-of-sight between the target and the camera. However, this can be easily overcome by appropriate positioning of the patient and the camera.

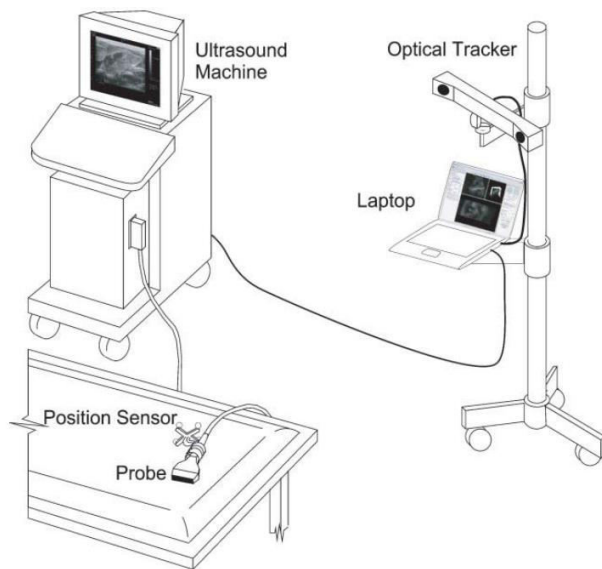


Figure 12: Schematic of an optical tracking system.<sup>175</sup> Reproduced with permission ©SAGE.

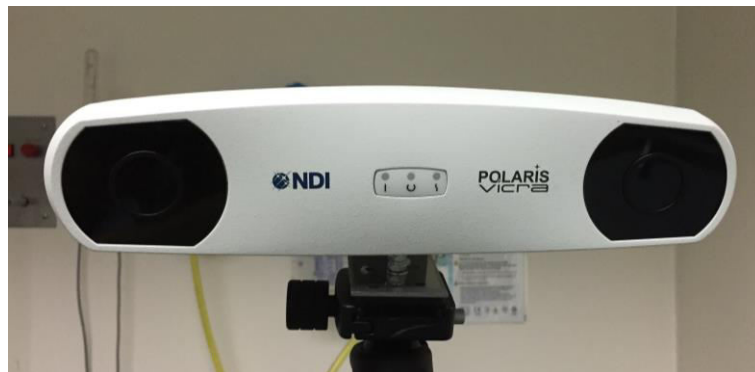


Figure 13: Tracking camera used in Piur prototype



*Figure 14: modified US probe with tracking spheres*

#### **4.2 Sonovue™ contrast**

'Sonovue' (Bracco, Milan) contrast consists of a stable suspension of sulphur hexafluoride micro-bubbles surrounded by a phospholipid shell. It is supplied as a vial containing a lyophilised powder and a syringe pre-filled with 0.9% saline. Once manually mixed, it forms a suspension of sulphur hexafluoride microbubbles in a concentration of 1 to  $5 \times 10^8$ /ml. It is injected directly through a suitable IV cannula ( $\geq 20$  gauge) in a straight path through a three-way stop-cock to avoid destruction of the microbubbles.<sup>181</sup> It is given in bolus doses of 1-2ml followed by a bolus of 5ml of 0.9% saline. The maximum dose is 5ml. Side effects are rare but include headache, paraesthesia and dizziness. Microbubble survival varies between patients – those who quickly metabolise contrast may need further bolus or a larger initial bolus. As the microbubbles are broken down, the sulphur hexafluoride gas is exhaled via the lungs while the phospholipid component of the microbubble shell enters the endogenous phospholipid pathway. It is contraindicated in patients with right to left shunts, severe pulmonary hypertension and adult respiratory distress syndrome.



When insonated at a high frequency, the compressible gas in the microbubbles oscillate, producing a unique echo that enhances the visualisation of the luminal blood flow (Figure 15).



*Figure 15: Contrast-enhanced ultrasound following EVAR. Contrast is seen contained within the limbs of the stent-graft and there is no endoleak seen.*

#### **4.3 Computed tomographic angiography (CTA)**

Each CTA used in this body of work was performed with either a Siemens Sensation 16 slice helical scanner or Siemens Emotion 128 slice helical scanner. In the study involving endoleak detection, both arterial phase and portal-venous phase images were acquired using a dose of 100 mL of the iodinated contrast medium 'Omnipaque 240' (Iohexol, 240 mg/mL) administered intravenously at a flow rate of 3 mL/s using a pump injector. Arterial phase-only images are used in the studies of aneurysm volume and biomechanical analysis.

#### **4.4 Digital subtraction angiography (DSA)**

DSA is a method of fluoroscopy commonly used in interventional radiology and vascular surgery. It allows digital removal of unnecessary structures (e.g bone) to allow more detailed visualisation of vessel anatomy. The acquisition is activated by a foot pedal and timed with the intra-arterial injection of a contrast media through a

multi-holed catheter either using a pump injector at specified volume and rate, or by hand. This is most often an iodinated contrast media such as iodixanol (e.g. Visipaque™). The primary concern when using iodinated contrast during DSA is contrast induced nephropathy (CIN). The risk of CIN is dose-dependent and the minimal amount of contrast should be used in each case. Particular attention should be paid to patients with impaired renal function. Carbon dioxide (CO<sub>2</sub>) offers an alternative to iodinated contrast, avoiding nephrotoxicity but offering inferior imaging quality that is not adequate for 'completion imaging' following stent-graft deployment.<sup>1</sup>

In EVAR, the primary use of DSA is to define the lowest ('target') renal artery to guide stent-graft deployment, and for 'completion' imaging once the stent-graft has been fully deployed. The purpose of completion imaging is 'quality control' to assess for visceral vessel patency and the presence of endoleaks (Figure 16). It is usually performed in a single antero-posterior imaging plane (uniplanar DSA). The sensitivity of uniplanar DSA for detection of endoleaks following EVAR has been criticised,<sup>182</sup> however, additional DSA acquisitions in multiple planes (multiplanar DSA) adds to the contrast dose and increases the risk of CIN.<sup>183</sup>



*Figure 16: Completion uniplanar DSA after EVAR. The left renal artery is not seen in this DSA frame but is patent.*

## 4.5 Image segmentation for biomechanical analysis

### 4.5.1 Image segmentation

The purpose of the image processing applications used in this research is to create 3D surface models of the AAA that can be exported to engineering software for use in biomechanical simulations.

For use in FEA and CFD, an initial surface mesh model must be generated from both the 3D-US and CT data. This initial step is known as 'segmentation'. Segmentation is the process of partitioning a digital image into multiple segments to create contours that outline a structure, e.g. the AAA wall. These contours can then be used to create 3D models with the use of interpolation algorithms. There are a number of different segmentation methods utilised by various software packages.

### 4.5.2 Development of the ImFusion Suite prototype

The ImFusion Suite (ImFusion GmbH, Germany) software prototype was initially developed to improve the accuracy and workflow of carotid plaque volume measurements. Its potential as a tool to provide 3D models of AAAs was recognised by the author. Following collaboration with the software developers, an agreement was reached to develop and refine the software to meet the needs of this project. It had the advantage of being able to simultaneously process both CT and 3D-US data. Multiple software iterations were trialled by the author and refined in collaboration with the software team at ImFusion over approximately six months to produce a version that was suitable for use.

As typical for a number of various segmentation methods<sup>184, 185</sup> the ImFusion Suite uses an interactive image segmentation algorithm that takes as an input two sets of points defined by the user: one that is fully inside the target object, and another completely outside the object – e.g. inside and outside the AAA wall (Figure 17-18). These are known as 'seeds'. Both sets of seeds are used as initial clues for the

segmentation but also act as hard constraints: whatever is labelled inside (with respect to the outside) by the user will stay inside in the final result. This produces an initial result, where the boundaries of the structure (e.g. AAA wall) are defined by the software (Figure 19). Errors can then be manually corrected and refined by the user by placing further seeds. The segmentation process is then re-run and the result re-assessed. Correction is usually needed when the border between two structures is poorly defined. In the case of AAA segmentation using CT, this occurs most often between the right postero-lateral AAA wall and the inferior vena cava as the pixel intensity of the blood in the IVC is similar to that of the intraluminal thrombus in the AAA (Figure 20).

To produce the final result, the “inside” and “outside” regions are then propagated and defused in the whole image.<sup>186</sup> Any unlabelled pixel will be assigned to the segmentation if can be reached "faster" from an “inside” pixel than from any “outside” pixel. Their propagation speed depends on each pixel: if the pixel is on an edge of the image, the propagation speed at this pixel will be very slow. This creates a ‘mask image’ where all of the ‘inside’ pixels are labelled green and the ‘outside’ pixels are labelled red (Figure 21). The ImFusion software then uses then uses a ‘marching cube’ algorithm<sup>187</sup> to convert the contours generated by the segmentation into a surface mesh.

The final step is to decide on the resolution of the mesh and the degree of smoothing. For this work, the mesh resolution was set at maximum. A number of meshes were generated with different levels of smoothing for each case. The optimal result was selected such that anatomical features were retained but extraneous points were removed (Figure 22). Further smoothing may be required when the mesh is prepared for biomechanical simulation.

This process is also summarised in video format at: <https://vimeo.com/156845915>

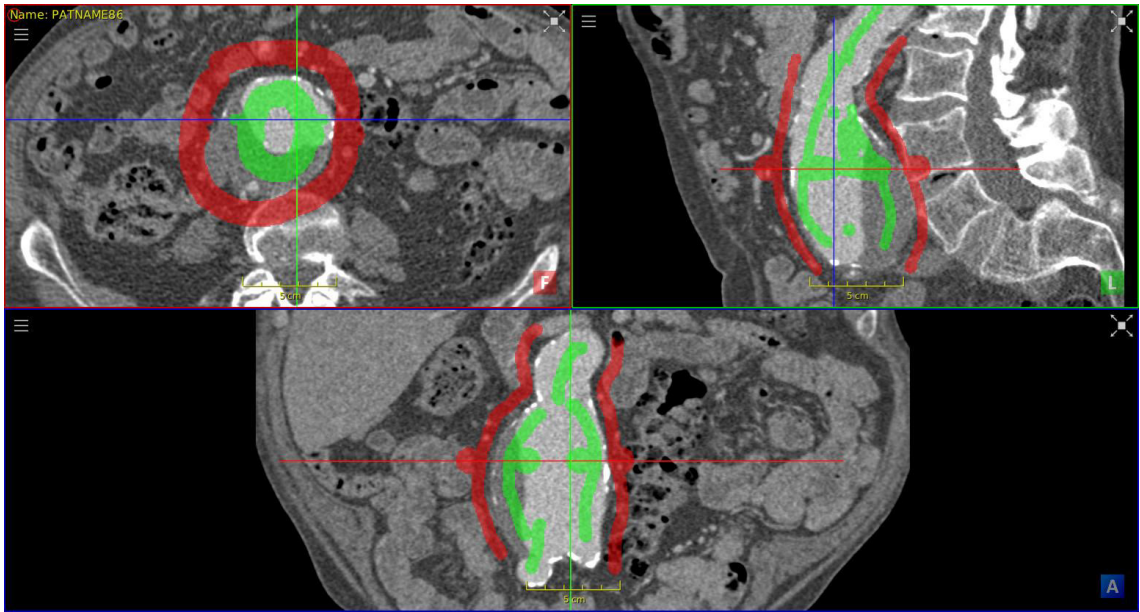


Figure 17: User defined 'seeds' are placed 'inside' (green) and 'outside' (red) the AAA wall on CTA MPRs of the AAA

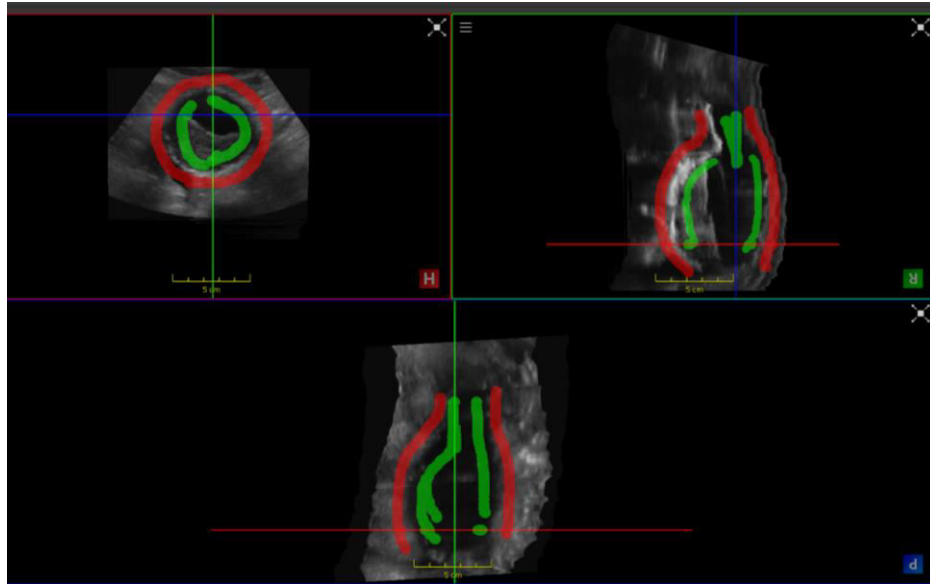


Figure 18: User defined 'seeds' are placed 'inside' (green) and 'outside' (red) the AAA wall on 3D-US MPRs of an AAA

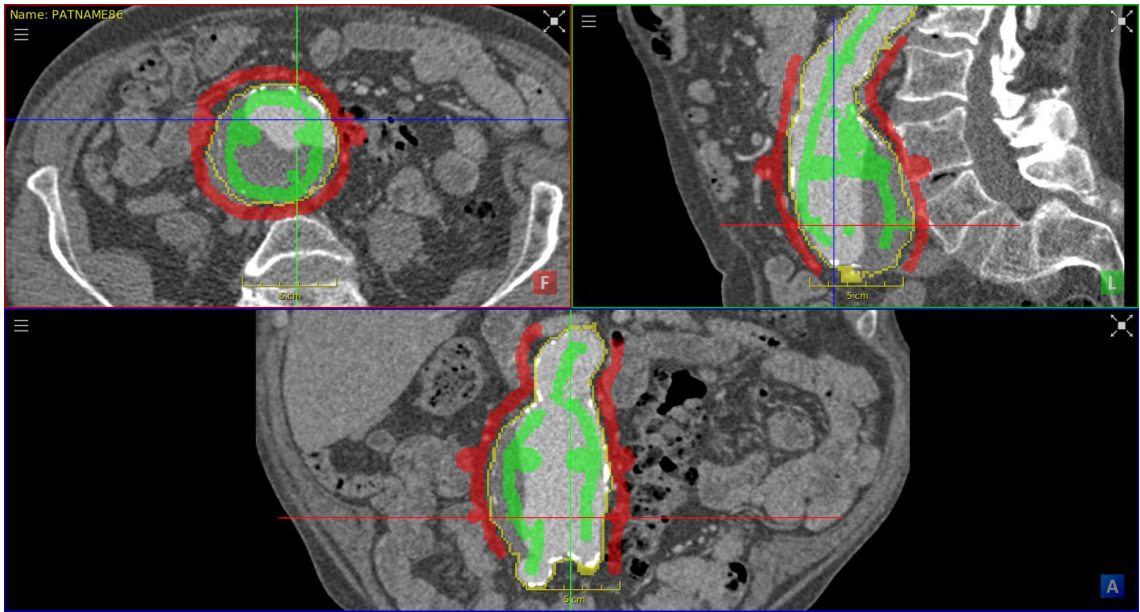


Figure 19: Initial segmentation results on CT. The yellow line defines the boundary of the segmentation.

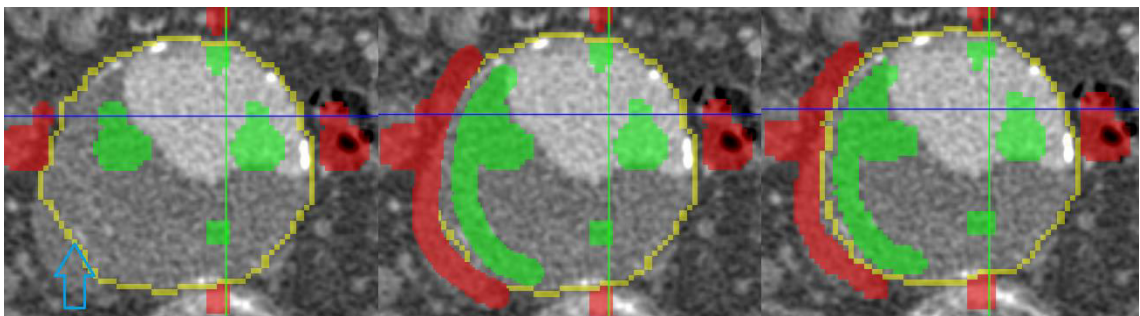
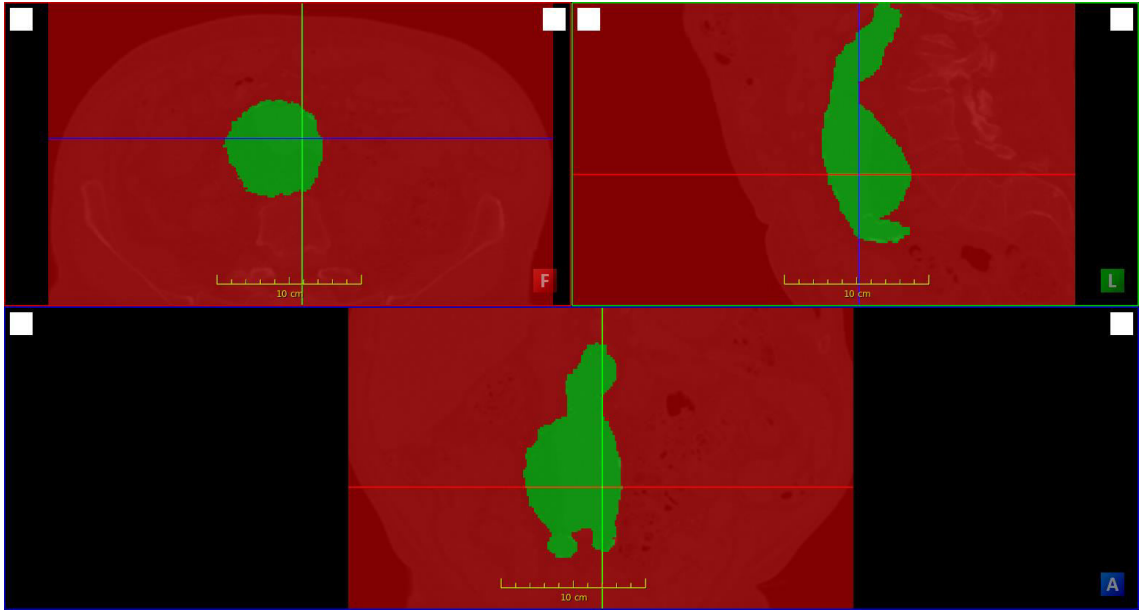
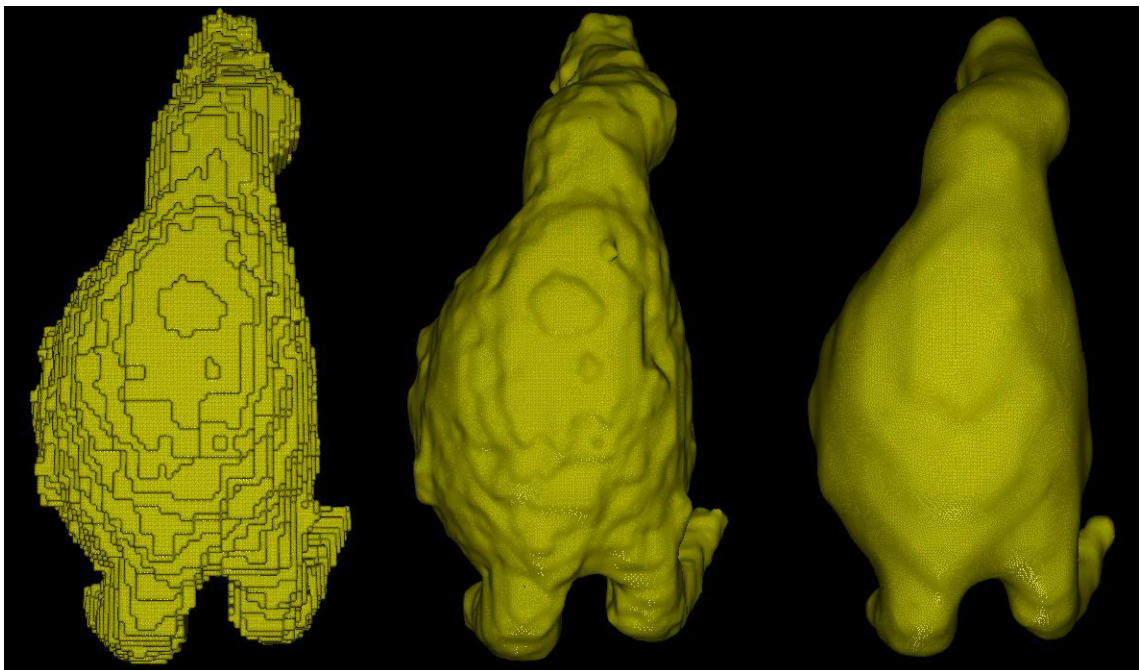


Figure 20: Sequence of correcting an error in segmentation. The yellow line does not correspond to the wall of the AAA – left image. This is due to adjacent inferior vena cava – blue arrow. Additional seeds are placed – centre image. The segmentation is re-run and the result improved – right image.



*Figure 21: 'Mask image' on CT. This is generated once the user is satisfied with the segmentation result. The pixels inside the structure i.e. AAA wall are labelled green, those outside are labelled red.*



*Figure 22: Approach to smoothing. The maximal resolution with no smoothing was selected – left. The mesh was smoothed in stages to achieve an optimal result.*

## 4.6 Biomechanical analysis

Biomechanical analysis (CFD and FEA) was conducted in collaboration with the School of Mechanical Aerospace and Civil Engineering (MACE) at the University of Manchester. For final CFD simulation, the commercial software STAR CCM+ Version 01/15 (CD-adapco Melville, NY, USA) was used. FEA simulation used the commercial software Abaqus v6.14 (Dassault Systèmes, Paris, France).

There are a number of common steps to preparing a model for simulation:

1. **Importing of the geometry/surface mesh from the computer aided design software or segmentation software.** In this case, the facility to export from the ImFusion software in stereolithography (STL, file extension - .stl) was selected. STL files describe the surface geometry of a 3D object and are compatible with a wide range of software packages.
1. **Geometry preparation.** Once imported the surface mesh may require a number of processing operations including increasing in resolution (increasing the number of triangles), repairing, smoothing, or the addition of extra parts. For example, CFD analysis requires the inlet and outlets of each geometry to be extended away from the aneurysm. Each of these steps can be undertaken using specific software packages or within more comprehensive software. In this work, geometry preparation for CFD was performed using MeshMixer (MeshMixer, 2015. [www.meshmixer.com](http://www.meshmixer.com)) and MeshLab (MeshLab, 2015. [www.meshlab.sourceforge.net](http://www.meshlab.sourceforge.net).) Geometry preparation for FEA was performed using 3Matic v10.0 (Materialise, Belgium). Each of these steps is detailed in the relevant chapter.
2. **Boundary conditions.** Parts of the model need to be assigned. For example the different structures in the AAA – lumen, wall, inlet and outlet. Specific conditions, such as the blood velocity profile entering the aneurysm must also be defined. These are described in the relevant chapter.



3. **Meshing.** For CFD and FEA analysis the surface mesh must be converted into a volume mesh so that the haemodynamic characteristics within the aneurysm can be simulated. The volume mesh uses a range of cell types depending on the location within the aneurysm such as smaller prism layer cells close to the aneurysm wall in order to capture the large velocity changes that occur in that location. The meshing types for each simulation are described in the relevant chapter.
  
4. **Assigning physics.** The behaviour of the model structures is assigned. For example, the physical properties of the AAA wall and the blood such as the blood density, blood viscosity and Young's modulus of the aneurysm wall. These are mostly derived from previous studies in the literature.
  
5. **Post-Processing.** The data output from the simulation, can be displayed as various graphical representations and measurements can be defined for various points in the model. These can include the wall shear stress profile along a specified plane cut in the aneurysm and the pressure field at the aneurysm wall.

**SECTION 3: 3D ULTRASOUND IN THE  
MANAGEMENT OF ABDOMINAL AORTIC  
ANEURYSM**

## **CHAPTER 5: USE OF THREE DIMENSIONAL CONTRAST-ENHANCED ULTRASOUND IMAGING DURING ENDOVASCULAR ANEURYSM REPAIR**

### **Chapter contributors and role:**

**D Ormesher:** patient recruitment, data collection and analysis, manuscript writing.

**C Lowe:** patient recruitment, data collection and analysis, manuscript writing.

**N Sedgwick:** 3D-US scanning and analysis.

**Mr J Ghosh:** conception, Co-supervisor.

**Prof C McCollum:** Supervisor

CL and DO are credited with joint first authorship in the Journal of Vascular  
Surgery

*The contents of this chapter are reproduced with permission of Elsevier.*

## 5.1 ABSTRACT

**Background:** Iodinated contrast during EVAR is used with caution in patients with chronic kidney disease. CEUS imaging using non nephrotoxic sulphur hexafluoride microbubble contrast is a novel imaging modality that accurately identifies and characterises endoleaks during EVAR follow-up. We report our initial experience of using three-dimensional (3D)-CEUS imaging intra operatively as completion imaging after endograft deployment. Our aim was to compare intraoperative 3D CEUS against uniplanar angiography in the detection of endoleak, stent deformity, and renal artery perfusion during EVAR.

**Methods:** The study enrolled 20 patients undergoing elective conventional infra-renal EVAR, after which a completion angiogram was performed and the presence of endoleak, renal artery perfusion, or device deformity were recorded. With the patient still under anaesthetic, a vascular scientist blinded to angiographic findings performed 3D-CEUS and reported on the same parameters.

**Results:** Three endoleaks, one type I and two type II, were detected on uniplanar angiography and 13 endoleaks, 11 type II and two type I, were found using 3D-CEUS imaging. Of note, one of these type I endoleaks was not seen on angiography, and this patient underwent balloon moulding of the neck with resolution of the endoleak on repeat imaging. Of the 11 type II endoleaks seen with 3D-CEUS imaging, the inflow vessel was identified in nine cases. No stent-graft deformity or limb kinking was seen in any patient. Both renal arteries could be visualized in 10 patients, whereas the target renal artery was seen in 11 patients. In the remaining patients, the renal arteries could not be visualised, mainly due to intra-abdominal gas or patient body habitus.

**Conclusions:** 3D-CEUS imaging detected endoleaks not seen on uniplanar digital subtraction angiography, including a clinically important type I endoleak, and was also more sensitive than 2D-CEUS imaging for the detection of the source of endoleak. This technology has the potential to supplement or replace digital subtraction angiography

for completion imaging to reduce the use of x-ray contrast. Intraoperative 3D-CEUS has been applied to allow safe EVAR with ultra-low or no iodinated contrast usage in selected cases, without compromising completion imaging.

## 5.2 INTRODUCTION

Endovascular aneurysm repair has reduced the incidence of postoperative mortality compared with open repair,<sup>68</sup> although EVAR may be complicated by acute kidney injury due to mal-deployment, renal micro-embolization, or the use of iodinated contrast (IC) media. IC can result in short-term and long-term contrast-induced nephropathy, particularly in patients with underlying chronic kidney disease (CKD), and is contraindicated in those who are allergic to iodine.<sup>183, 188</sup> Standard endograft deployment technique uses digital subtraction angiography (DSA) with IC media to aid intra-arterial navigation and to provide quality-assurance completion imaging to examine for the presence of endoleaks, visceral vessel patency, and endograft integrity. Although an essential element of safe endograft deployment, completion imaging significantly contributes to the total IC load, especially if several angiographic runs are required. CO<sub>2</sub> has been used as a non-nephrotoxic alternative to IC,<sup>189</sup> but its utility is limited to endograft deployment because CO<sub>2</sub> does not provide adequate image quality for completion quality control.<sup>1</sup>

The role of contrast-enhanced ultrasound CEUS imaging in the context of post-EVAR surveillance has gained acceptability in recent years<sup>153, 155, 156, 159</sup> because it presents a cost-effective alternative to CT that does not necessitate nephrotoxic IC or ionizing radiation. CEUS imaging uses non-nephrotoxic sulphur hexafluoride microbubbles as contrast, which is completely eliminated through the lungs. 3D-CEUS is an evolution of this technology that uses positional information from magnetic field emitters to place and orientate the ultrasound transducer probe precisely in space to allow dynamic interrogation of an endograft from any angle within the aneurysm. A pilot study from our institution showed that 3D-CEUS has accuracy comparable to or better than CT for detecting endoleaks during post-EVAR follow-up.<sup>190</sup>

Intraoperative use of this technology gives the potential to visualise stent-graft positioning and endoleak immediately after deployment while reducing the overall requirement of IC media. Thus, intraoperative 3D CEUS potentially has clinical utility in patients with chronic renal impairment or when CO<sub>2</sub> is used the primary contrast

medium. The aim of this study was to assess the clinical utility of 3D-CEUS for intraoperative completion imaging after EVAR as an alternative to conventional uniplanar catheter angiography for the detection of endoleak, endograft deformity, and renal artery patency.

### **5.3 METHODS**

The study prospectively enrolled 20 patients undergoing elective infra-renal EVAR under the care of a single surgeon. The local ethics committee approved the project, and the patients gave informed consent. All patients were initially seen in the clinic and reviewed by a consultant vascular surgeon. Suitability for EVAR was determined from an initial CT scan using IC. The morphologic characteristics of the aneurysm and access vessels were reviewed at a multidisciplinary team meeting.

All patients underwent EVAR deployment while under general anaesthesia in a vascular operating theatre with mobile C-arm imaging. After endograft deployment, a standard completion uniplanar DSA was performed using 20 mL full strength iodixanol contrast (Visipaque 270; GE Healthcare, Hertfordshire, UK) injected at 10 to 15 mL/s. The presence of endoleak, renal artery perfusion, and device deformity were recorded. Endoleaks were characterised by type and source. Renal artery perfusion and presence of stent-graft deformity were also noted. With the patient still anaesthetised, an accredited vascular scientist with specific training in 3D-CEUS attended the theatre. This individual, who was blinded to the angiographic findings, performed conventional 2D and 3D-CEUS imaging to measure the same parameters.

The 3D-CEUS was undertaken with a Phillips IU22 ultrasound console (Phillips, Amsterdam, Netherlands) using a C5 2-MHz curved array probe. Then, 1-mL boluses of sodium hexafluoride (SonoVue, Bracco, Italy) were administered intravenously to a maximum of 5 mL. The images acquired were processed using a Curefab CS 3D system (Curefab, Munich, Germany) and were replayed and manipulated to identify endoleaks. The 3D-CEUS findings were then verbally relayed to the team performing the EVAR and recorded. If necessary, any interventions based on the 3D-CEUS findings

were then undertaken. The recorded outcome measures were presence of an endoleak, type of endoleak, inflow vessel of endoleak, renal artery visualisation and patency, and evidence of limb kinking. A McNemar's test was used to assess the difference between DSA and 3D-CEUS for detection of endoleaks.

#### **5.4 RESULTS**

The study included 20 consenting patients, and their demographics are given in Table 2. Of these patients, 19 underwent EVAR for infra-renal abdominal aortic aneurysm, including 18 bifurcated stent-grafts and one aorto-uniliac device. One patient had EVAR with a bifurcated stent-graft for a common iliac aneurysm that could not be treated with a straight stent graft. The choice of stent-graft was determined by aneurysm anatomy and was within the manufacturer's instructions for use in all cases.

Three endoleaks - one type I and two type II – were detected on uniplanar angiography. 2D-CEUS imaging found 13 endoleaks: 3 type I, 9 type II, and 1 type III. 3D-CEUS also demonstrated 13 endoleaks, including both type I endoleaks. Of note, one of these type I endoleaks was not seen on angiography (Figure 23) and this patient underwent balloon moulding of the neck, with resolution of the endoleak on repeat 3D-CEUS imaging. Of the 11 type II endoleaks seen with 3D-CEUS imaging, the inflow vessel was identified in nine. 3D-CEUS imaging reclassified two endoleaks described by 2D-CEUS; the type III endoleak was found to be a type II and one type I was found to be a type II. A McNemar's test confirmed a significant difference between DSA and 3D-CEUS for endoleak detection (DSA 3/20, 15% vs 3D 13/20, 65%, McNemar's  $p=0.002$ ).

Table 3 summarizes endoleak detection and classification. No stent-graft deformity or limb kinking was seen in any patient. Both renal arteries could be visualised in 10 patients, whereas the largest (lowest) renal artery was seen in 11 patients. The renal arteries in the remaining patients could not be visualised due to intra-abdominal gas and patient body habitus. Use of the microbubble contrast did not cause any adverse reactions or complications.



Table 2: Patient Demographics

Age	Sex	BMI	Aneurysm size	Smoker	Diabetes	Systolic BP	Diastolic BP	Creatinine	EVAR Device
70	M	33.6	7.2	N	N	128	79	175	Cook LP
86	M	27.8	6	N	N	160	80	109	Endurant II
74	M	26.1	7.8	N	N	171	74	118	Cook Zenith
72	M	30.5	5.6	N	N	130	90	115	Endurant II
77	M	25.2	6.1	Y	N	161	95	213	Ovation
66	M	32.7	5.5	N	N	124	83	71	Endurant II
75	M	30.4	5.7	N	N	127	72	120	Endurant II
68	M	23.1	8.4	N	N	150	70	83	Endurant II
79	M	29.8	6.4	N	N	193	93	102	Ovation
79	M	24.0	5.7	N	N	142	65	59	Endurant II
64	M	30.0	6.7	N	N	151	80	66	Aorfix
86	F	26.4	5.5	N	N	131	63	83	Ovation
84	M	30.1	5.5	N	N	118	68	84	Endurant II
88	F	28.3	5.8	N	Y	110	40	72	Endurant II
74	M	32.2	7.1	N	N	137	68	83	Endurant II
81	M	20.0	4.2 (iliac)	Y	Y	128	64	66	Endurant II
72	M	26.0	5.3	N	N	162	80	129	Endurant II
83	M	27.2	5.7	N	N	165	74	69	Endurant II
86	M	29.0	6.1	N	N	128	61	102	Anaconda
75	M	29.0	9.5	N	N	142	48	107	Endurant II

Table 3: Endoleak detection by imaging modality used

Endoleak Type	Uniplanar DSA	2D-CEUS	3D-CEUS
I	1	3	2
II	2	9	11
III	0	1	0
<b>Total</b>	<b>3</b>	<b>13</b>	<b>13</b>

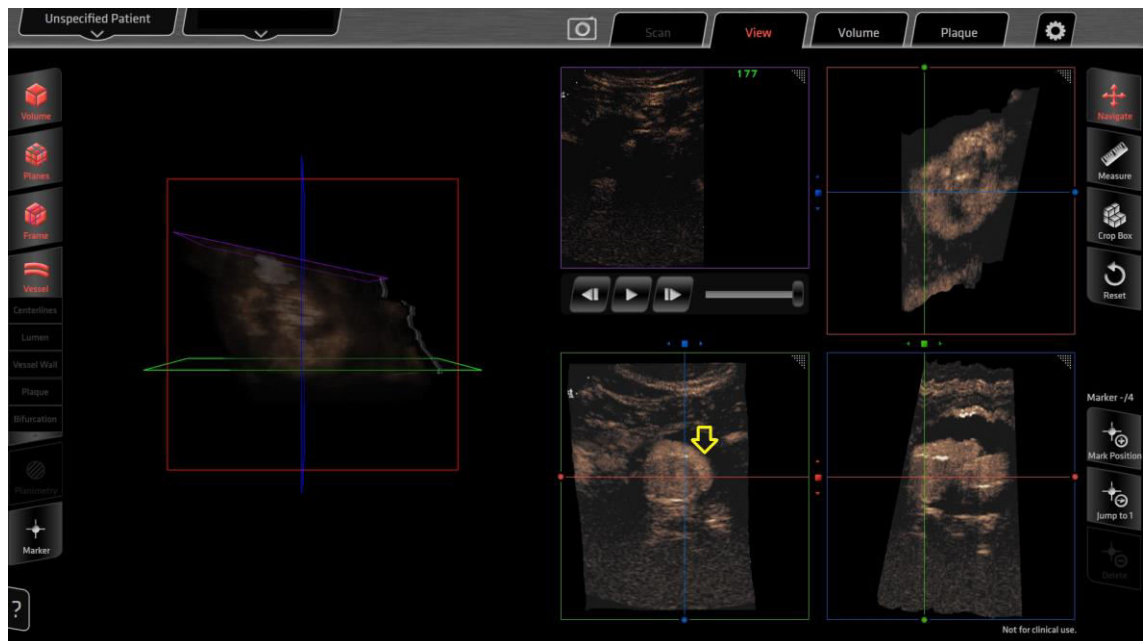


Figure 23: A type I endoleak (arrow) as seen on the Curefab CS system workstation (Curefab, Munich, Germany) that was not identified on uniplanar angiography.

## 5.5 DISCUSSION

Standard uniplanar DSA using IC has been found to miss 4% to 9% of endoleaks.<sup>182, 191</sup> This may be mitigated by multiplanar or rotational angiography but at the expense of increased intra-arterial contrast volume and radiation exposure. A retrospective analysis of 615 EVARs found that duplex scanning within 48 hours of surgery found endoleaks in 53 patients, including 17 type I and eight type III endoleaks, of which 10 of the type I leaks and none of the type III leaks were seen on completion uniplanar angiography.<sup>182</sup>

The Curefab CS system represents an enhancement to standard duplex ultrasound technology by combining contrast-enhanced duplex, a magnetic field emitter, and tracking sensors that can be applied to most standard ultrasound probes. Processing produces a 3D image that can be enlarged and rotated so the aneurysm body and the stent-graft can be identified from all angles. The ability to rotate the 3D reconstruction and scroll through the ultrasound image slice-by-slice, akin to CT images, simultaneously in sagittal, coronal, and transverse planes, allows the operator to ensure that adjacent vessels are not mistaken for endoleaks. An additional benefit of enabling imaging in three planes simultaneously, without manually rotating the transducer, is that the operator does not lose a small area of interest during manual rotation, thus allowing confident identification of even small leaks.

Because images are acquired in the same way as conventional CEUS, 3D-CEUS imaging does not add to the time required for scanning and is completed in 5 minutes. Imaging processing takes seconds, and the time for interpretation depends on the presence or absence of an endoleak. In our experience, the scanning, interpretation, and communication of results added only 10 minutes to the EVAR procedure. Provided the operator has experience with CEUS, we have found 3D-CEUS images are easier to interpret due to the ability to manipulate the images and view them in multiple planes. A pilot study from our institution showed promising results using 3D-CEUS for endoleak detection compared with CT as a gold standard, with encouraging inter-rater reliability ( $k = 0.88$ ; 95% confidence interval, 0.718-1.0).<sup>190</sup>

In this series, 3D-CEUS imaging detected a type I endoleak that was not seen on angiography. This was treated at the same sitting with balloon moulding. We noted that 2D-CEUS imaging found the same number of endoleaks as 3D CEUS imaging, although 3D was superior in delineating the inflow vessel and also reclassified two clinically significant endoleaks - one type III and one type Ia - to type II leaks that did not require any immediate treatment. In each of these cases, the ability to manipulate the 3D images allowed for a more detailed interrogation of the ultrasound data and a more accurate diagnosis. Although it is the experience of endovascular therapists that some type I endoleaks will seal in the postoperative period after reversal of anticoagulation, there is currently no way to predict those that will resolve spontaneously.<sup>182, 192</sup>

The type I leak seen on 2D-CEUS imaging and not on DSA was thought to be significant due to the volume of contrast seen flowing into the sac. We believe that most endovascular specialists would treat an endoleak of this type. Although the renal arteries could not be seen in 50% of cases, in our experience of CEUS imaging, this does not preclude an accurate diagnosis of type I endoleaks due to their characteristic appearance. We previously established that 3D-CEUS imaging has high endoleak sensitivity compared with CT scanning.<sup>190</sup> Although the number of patients limits the present study, it provides scope for a larger-scale study involving a greater number of patients. A paired analysis of completion 3D-CEUS scanning with bi-planar angiography in patients with adequate renal function would further assess the sensitivity to detect endoleaks. The results suggest that 3D-CEUS imaging is either non-inferior or superior to uniplanar angiography in endoleak detection.

The main utility of the addition of a 3D system is the ease of interpretation and image manipulation that is afforded by the volumetric and multiplanar reconstructions. A frequent criticism of US modalities for EVAR surveillance is operator dependency and the difficulties of interpreting 2D images in three dimensions; this may be mitigated by the use of a 3D system. Duplex also affords advantages of hemodynamic

measurements to assess for limb kinking that may be missed due to parallax on angiography, although no limb problems were found in this series.

The main application of 3D-CEUS imaging in this setting is for patients with impaired renal function where there is a priority to avoid IC volume or in emergency cases with a background of CKD where an additional acute kidney injury is a concern due to repeated contrast loads from CT scanning and to hypotension. Intraoperative 2D or 3D CEUS can provide quality control imaging for EVAR performed using CO<sub>2</sub> angiography. CO<sub>2</sub> angiography is an attractive option for arterial navigation and endograft deployment in patients with poor renal function,<sup>189, 193</sup> although it is generally inadequate for completion imaging.<sup>1</sup>

In three cases at our institution, we used CO<sub>2</sub> for navigation and deployment of conventional infra-renal endografts and 3D-CEUS for completion imaging, allowing for contrast-free or ultralow-contrast EVAR. In the first case, we treated a patient with stage IV CKD with an estimated glomerular filtration rate (eGFR) of 20 ml/min/1.73 m<sup>2</sup> using a bifurcated Endurant II (Medtronic, Minneapolis, Minn) stent-graft. We found that CO<sub>2</sub> provided adequate imaging quality to define the renal arteries and the iliac bifurcation. No endoleaks were seen on uniplanar CO<sub>2</sub> angiography, and this was confirmed with intraoperative 3D CEUS, which also demonstrated renal artery patency.

The second patient also had stage IV CKD (eGFR, 30 ml/min/1.73 m<sup>2</sup>) and underwent EVAR using a bifurcated device. In this case, CO<sub>2</sub> failed to adequately demonstrate the target renal artery before deployment and therefore we used a hand-injection of 5 mL contrast to confirm the stent-graft position below the renal arteries. Imaging of the iliac system was clear enough to then allow graft deployment, and completion imaging was performed with 3D-CEUS.

The third patient presented with a ruptured aorto-iliac aneurysm. Intra-arterial contrast was used to define the iliac anatomy and embolise the internal iliac artery; however, graft deployment was performed with CO<sub>2</sub> angiography. Completion imaging with performed with CEUS and limited contrast dose to 25ml. We obtained full

completion imaging in all three patients, and no patient had a postoperative decline in eGFR.

This was a pilot study involving 20 patients and it is appropriate to considering powering for a full-scale trial. This should focus on the detection of only clinically relevant endoleaks (i.e. type I and III endoleaks). Firstly, assuming a non-inferiority study where 3D-CEUS can be up to 5% worse at finding type I and type III endoleaks compared to DSA, there would be 80% power for the lower limit of the 95% CI to be greater than -5% if 350 patients were recruited. This calculation assumes the discordant proportion is 0.13875, the proportion of both tests finding an endoleak is 0.005625 (based on 7.5% endoleak rate from both tests) and the expected difference is 0%. Assuming a superiority trial, using a McNemar's test there would be 80% power at the 5% significance level to detect differences of 5% between 3D and DSA, assuming a discordant proportion of 0.14, with 427 patients.

## **5.6 CONCLUSIONS**

The results of this study suggest that intraoperative 3D-CEUS imaging accurately identifies and characterises endoleaks immediately after stent-graft deployment. Furthermore, 3D-CEUS imaging was able to detect endoleaks not seen on uniplanar DSA, including clinically important type I endoleaks, and has advantages over 2D CEUS imaging in inflow vessel identification and image manipulation. The lowest renal artery could be seen reliably in only 50% of patients; however, by adding CO<sub>2</sub> angiography to guide deployment, this technology has the potential to replace standard completion DSA in patients where renal function is threatened or when the source of an endoleak seen on completion DSA is uncertain. Intraoperative 3D-CEUS combined with CO<sub>2</sub> imaging has been applied to allow safe EVAR with ultra-low IC or no IC usage in selected patients, without compromising completion imaging. The number of patients required likely precludes a full-scale study.

## **CHAPTER 6: 3D CONTRAST ENHANCED ULTRASOUND IMPROVES THE ACCURACY OF CLASSIFICATION OF ENDOLEAKS FOLLOWING ENDOVASCULAR ANEURYSM REPAIR**

### **Chapter contributors and role:**

**C Lowe:** patient recruitment, data collection and analysis, manuscript writing.

**A Abbas:** Pilot data.

**S Rogers:** 3D-US scanning and analysis.

**L Smith:** 3D-US scanning and analysis.

**Mr J Ghosh:** Co-supervisor.

**Prof C McCollum:** Conception, Supervisor.

*The contents of this chapter are reproduced with permission of Elsevier.*

## 6.1 ABSTRACT

**Background:** Three-dimensional contrast-enhanced ultrasound (3D-CEUS) is a novel technology allowing surgeons to view duplex ultrasound images in 3D with ultrasound contrast highlighting blood flow in endoleaks following EVAR. It potentially reduces the need for computed tomographic angiography (CTA) and catheter angiography. This study compares 3D-CEUS with both CTA and the final vascular multi-disciplinary team (MDT) diagnosis using all available imaging. Inter-operator variability for detection of endoleak and the influence of 3D-CEUS on patient management were studied.

**Methods:** 156 consecutive patients undergoing CTA for EVAR surveillance were invited to undergo standard CEUS and 3D-CEUS on the same day with 3D-CEUS reported independently by two blinded vascular scientists. Presence and type of endoleak was compared between CTA, standard CEUS, 3D-CEUS and the final diagnostic decision made in the vascular MDT meeting. Inter-operator reliability of 3D-CEUS was analysed using the kappa statistic.

**Results:** 100 paired CTA, CEUS and 3D-CEUS studies were analysed. When compared with CTA, the sensitivity, specificity, positive, and negative predictive value of 3D-CEUS to endoleak was 96%, 91%, 90%, and 96% respectively. When compared with the MDT decision with access to all imaging modalities, the sensitivity, specificity, positive, and negative predictive value of 3D-CEUS was 96%, 100%, 100% and 96%. The kappa statistic for inter-operator agreement was 0.89. In 7 cases of diagnostic uncertainty on CTA, 3D-CEUS was able to provide a definitive diagnosis

**Conclusions:** 3D-CEUS was more sensitive and accurate than CTA for endoleak detection and classification following EVAR. 3D-CEUS is now our initial investigation of choice in cases of sac expansion during duplex follow-up or diagnostic uncertainty on standard duplex or CTA.



## 6.2 INTRODUCTION

Life-long surveillance is routine following endovascular aneurysm repair (EVAR) to detect stent-graft related complications; endoleak being the most frequent.<sup>1</sup> Endoleaks may pressurise the AAA leading to continued growth and rupture.<sup>1, 65</sup> Surveillance aims to detect device-related complications early, allowing intervention before a complication such as AAA rupture occurs. CT angiography (CTA) is considered the non-invasive 'gold standard' for detection of EVAR-related complications and is used in surveillance programmes worldwide.<sup>1, 16</sup> However, CTA may be insensitive to some endoleaks, is expensive, involves ionising radiation and causes cumulative renal damage due to nephrotoxic iodinated contrast media.<sup>188</sup>

A move from CTA towards ultrasound (US) modalities for EVAR surveillance has been evolving for over a decade. The optimal programme for EVAR surveillance remains uncertain<sup>194</sup> with early reports suggesting standard duplex ultrasound was not sensitive enough to replace CTA for endoleak detection.<sup>150-153</sup> More recently, acceptable detection rates for clinically important endoleaks have been achieved.<sup>157, 158</sup> Contrast enhanced ultrasound (CEUS) involves the intravenous administration of a stable suspension of sulphur hexafluoride micro-bubbles surrounded by a phospholipid shell as an ultrasound contrast enhancing the visualisation of flowing blood. Although CEUS was first reported for EVAR surveillance some 19 years ago,<sup>142</sup> adequate studies demonstrating an improved sensitivity for endoleak to at least a level equivalent to CTA have only recently been done.<sup>155, 156, 159</sup> It has the advantage of avoiding ionising radiation and nephrotoxicity from iodinated x-ray contrast. While CEUS is now used routinely in EVAR surveillance at some institutions,<sup>155</sup> a recent meta-analysis suggested that CEUS detects too few additional type I or III endoleaks for the extra cost of the contrast agent to be justified for every case.<sup>157</sup> Surveillance following EVAR could reasonably be based on standard duplex imaging to measure AAA diameter with CEUS only required if the AAA sac grows or if an endoleak is suspected.<sup>160</sup>

Although the skill of a good vascular laboratory scientist is to interpret standard two-dimensional duplex images, vascular surgeons are more familiar with CTA and relying on simple static 2D ultrasound images or short cineloops saved for later viewing means

some may be reluctant to accept these reports, preferring to see the anatomy for themselves. 3D contrast-enhanced ultrasound (3D-CEUS) uses magnetic position tracking to enable a computer to assemble all the ultrasound reflections into a 3D image that can be interpreted by any clinician. It allows multi-planer reconstruction and image manipulation in any plane as when using a CT workstation. In a pilot study on 30 paired CTA and 3D-CEUS acquisitions, we reported that 3D-CEUS appeared more accurate for the detection and classification of endoleaks than CTA.<sup>190</sup> We have also reported intra-operative use for completion imaging following EVAR.<sup>195</sup>

We now report the final results of a study comparing standard CEUS, 3D-CEUS and CTA for the detection and classification of endoleaks in EVAR surveillance. Inter-operator variability for the detection and classification of endoleak by 3D-CEUS was also studied. Although 3D-CEUS was compared with CTA, the primary endpoint was to compare both standard CEUS, 3D-CEUS and CTA with the final decision of the vascular MDT attended by both vascular surgeons and interventional radiologists after reviewing all the available evidence including catheter angiography when this was needed

### **6.3 METHODS**

Between May 2012 and March 2015, consecutive patients undergoing CTA for EVAR surveillance were invited to take part and underwent 3D-CEUS on the same day where possible. When not feasible, they attended as close to the same date as possible provided that this was within the same month. CTA was reported by the consultant vascular interventional radiologists. Standard CEUS and 3D-CEUS images were acquired by the same experienced vascular scientist for all patients in this study and reported independently by two vascular scientists blinded to each other and the CTA result. The learning curve of around 20 cases for Vascular Scientists reporting in this study was established prior to commencement. Previous studies have compared ultrasound modalities to CTA as the 'gold standard',<sup>155, 156, 159</sup> but no single imaging modality has been shown to be completely accurate. We therefore compared 3D-CEUS reports with the final diagnostic decision made in the vascular multi-disciplinary team

(MDT) meeting including vascular surgeons and interventional radiologists with access to all the available evidence including results from catheter angiography when available. All patients gave informed consent. The study was approved by the National Research Ethics Service (13/NW/0485).

### ***Standard CEUS***

CEUS was performed using the same Phillips IU22 duplex ultrasound (Phillips, Amsterdam) and C5-1 curved array transducer for all patients. A 1ml bolus of sulphur hexafluoride contrast (Sonovue®, Bracco, Milan, Italy) was given into a suitable upper limb vein and flushed with 5ml of 0.9% saline as per our departmental protocol. Further 1-2ml boluses were given as required to maximum of 5ml depending on the complexity of the endoleak and how quickly the contrast was eliminated by each patient. The 'contrast' mode using a low mechanical index, was selected on the duplex instrument to prevent microbubble rupture. The stent graft and AAA were interrogated systematically from neck to limbs. The 'flash' function that dissipates contrast was used to assess the timing, direction of flow and inflow vessel of any endoleak detected.

### ***3D-CEUS***

The 3D-US system used was a prototype magnetically tracked freehand system attached to the same Phillips IU22 ultrasound unit. It incorporated a 3D guidance system ('DriveBay'<sup>TM</sup> Ascension, Vermont, USA) that uses an electromagnetic field generator with tracking sensors attached to the ultrasound probe (Figure 24). It can be fitted to most commercial ultrasound systems. The information generated by moving the sensor in the magnetic field allowed the source of all ultrasound reflections to be interpreted by the computer. Multi-planer reconstructions and a volumetric image were then computed from the ultrasound frames using this positional data.

To acquire the 3D image, the transducer was placed proximally and swept down the aortic aneurysm in an axial orientation from neck to bifurcation. A further bolus of

contrast was given if needed. Multi-planar reconstructions of this ultrasound data were generated in under five seconds. A volumetric image that can be manipulated to improve visualisation of endoleaks was produced simultaneously and could be manipulated on a touch screen (Figure 25).

### ***CT Angiography***

CTA was performed using a Siemens SOMATOM® Perspective scanner (Siemens Medical, Munich). Patients were positioned supine and images at 1mm slices were acquired from the diaphragm to the femoral heads. A dual-phase protocol was used (arterial and delayed) using a bolus dose of 100 mL of the iodinated contrast medium Omnipaque 240™ (GE Healthcare, UK) administered at a flow rate of 3 mL/s. Multi-planar reconstructions were produced and reported by consultant vascular radiologists.

### ***Statistical analysis***

Based on pilot study data, a power calculation suggested a minimum of 67 paired CTA and 3D-CEUS studies were required. Sensitivity, specificity, positive and negative predictive value for endoleak detection were calculated using contingency tables and compare with both CTA and the final MDT decision. CTA was used as a reference as it is commonly to plan endoleak management and has been used as the 'gold standard' in all previous studies. The MDT decision was based on all the available evidence including CTA and catheter angiography where this was indicated. The Kappa statistic was used to determine consistency between two observers to detect and classify endoleaks on 3D-CEUS. Inter-operator agreement for endoleak detection and classification using 3D-CEUS was assessed to include subtypes of endoleak; e.g. agreement was considered negative if the first operator diagnosed a type IIa endoleak and the second a type IIb endoleak. Analyses were performed using SPSS statistics v20 (IBM Corp. Armonk, NY, USA).



*Figure 24: Standard US transducer fitted with a tracking sensor*

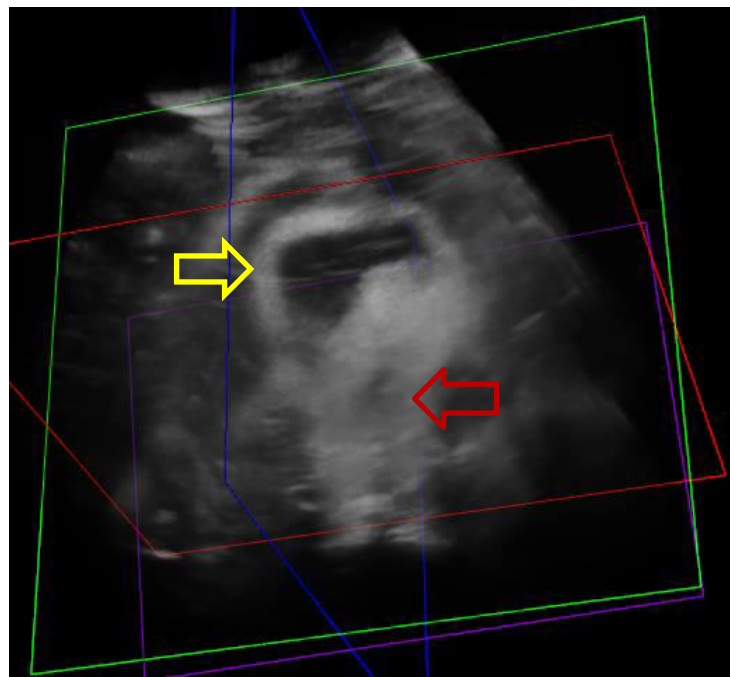


*Figure 25: Volumetric image from 3D-CEUS showing contrast in the stent-graft limbs (red arrow) and a type II endoleak from lumbar artery to lumbar artery (yellow arrow).*

## 6.4 RESULTS

From some 600 patients in our EVAR surveillance programme, 156 consecutive patients due for CTA were invited. 102 matched CTA, CEUS and 3D-CEUS images were acquired from 99 consenting patients. Image quality in two CEUS/3D-CEUS studies was too poor for diagnosis due to bowel gas and/or obesity; 100 paired studies were analysed. There were 86 men and 13 women, mean age of 76, mean body mass index 28. There were no side effects from the use of microbubble or x-ray contrast. CTA and US imaging was on the same day in 52 studies and never more than four weeks apart. Patient demographics are shown in Table 4.

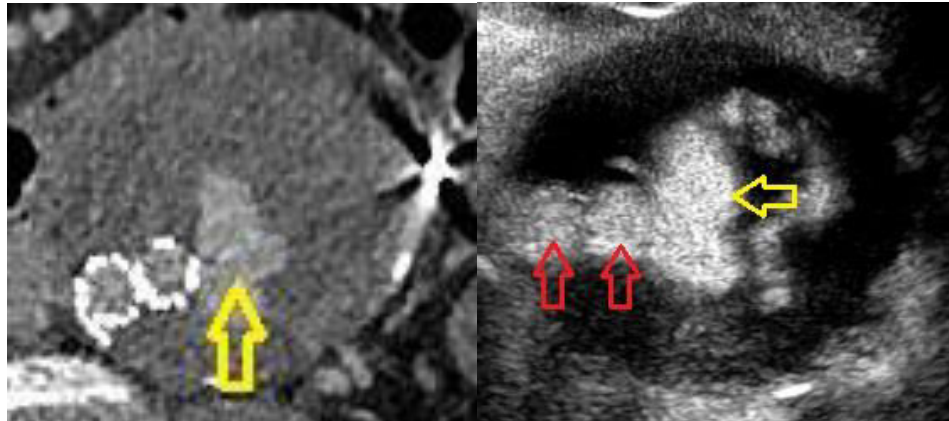
Endoleaks were detected on CTA in 46 patients compared with 49 patients for both CEUS and 3D-CEUS. The final MDT decision determined that there were a total of 51 endoleaks. The frequency of endoleak was higher than in our EVAR surveillance program as patients with potential complications are more likely to be imaged by CTA. The number and type of each endoleak detected by each modality is summarised in Table 5, with each compared to the final diagnostic conclusion reached by the MDT. 3D-CEUS diagnoses compared most closely with the MDT decision. In one case, 3D-CEUS diagnosed a type II endoleak as a type I or III endoleak. A diagnosis of a type I or III endoleak was given due to the amount of contrast in the AAA, the speed of filling when the contrast was obliterated using the 'contrast flash' function and proximity of the contrast to the limb of the stent-graft (Figure 26). This could not be resolved on 3D reconstruction. CTA diagnosed a type II endoleak which was confirmed on subsequent catheter angiography via the internal iliac artery (Figure 27).

Table 4: Patient demographics

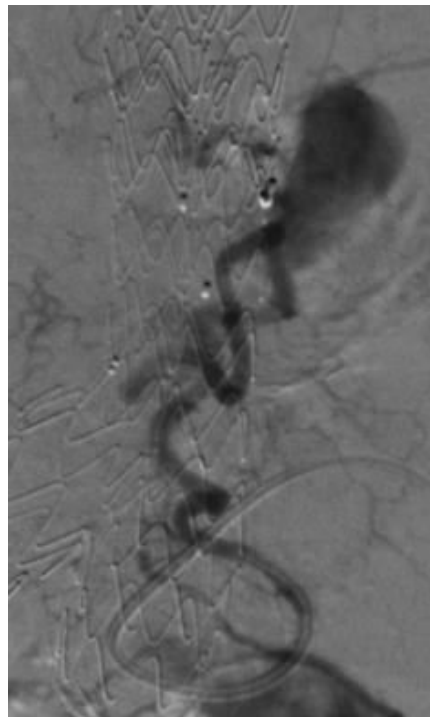
<b>Age (year; mean ± SD)</b>	<b>76 ±7.7</b>
<b>Sex:</b>	
male	86% (86)
Female	13% (13)
<b>BMI (kg/m<sup>2</sup>; mean ± SD )</b>	<b>28 ±5.5</b>
<b>Graft:</b>	
Bifurcated	93% (92)
Aorto uni-iliac	7% (7)
<b>EVAR:</b>	
Elective	93% (92)
Urgent/Emergency	7% (7)
<b>Creatinine (mmol/l; mean ± SD)</b>	<b>85 ± 17.45</b>

Table 5: Endoleak diagnosis by each modality. 3D-CEUS most closely reflected the MDT decision.

Diagnosis	Modality			
	CTA	CEUS	3D-CEUS	MDT
Type I	3	3	2	2
Type II	35	38	46	49
Type III	1	0	0	0
<i>Diagnosis uncertain</i>				
Type II or III	6	4	0	0
Type I or II	1	3	0	0
Type I or III	0	1	1	0
<b>Total</b>	<b>46</b>	<b>49</b>	<b>49</b>	<b>51</b>



*Figure 26: CTA (left) demonstrating a large type II endoleak (yellow arrow). Corresponding CEUS (right ) showing contrast in the stent-graft limbs (red arrows) with a large endoleak seen (yellow arrows) that was reported as a type I or III endoleak.*



*Figure 27: Type II endoleak seen on catheter angiogram via internal iliac artery*

The total number of endoleaks detected by standard CEUS and 3D-CEUS was the same. Therefore compared with CTA, the sensitivity, specificity, positive and negative



predictive value for endoleak detection was 96%, 91%, 90%, and 96% respectively (Table 6). Sensitivity was reduced by the failure to detect two endoleaks seen on CTA, one of which was a type Ia endoleak (small, and seen in the proximal aneurysm neck) and the other a type II leak with no associated increase in aneurysm size.

When standard CEUS and 3D CEUS were compared with the MDT decision the, sensitivity, specificity, positive, and negative predictive values was 96%, 100%, 100% and 96%. (Table 7). A kappa statistic of 0.89 demonstrated consistency in detecting endoleaks and classifying type.

*Table 6: Contingency table for the presence of endoleak - CTA vs. 3D-CEUS/CEUS*

		CTA		
		Endoleak	No Endoleak	
3D-CEUS/CEUS	Endoleak	44	5	<b>PPV 90%</b>
	No Endoleak	2	49	<b>NPV 96%</b>
		<b>Sensitivity 96%</b>	<b>Specificity 91%</b>	

*Table 7: Contingency table for the presence of endoleak – MDT vs. 3D-CEUS/CEUS*

		MDT		
		Endoleak	No Endoleak	
3D-CEUS/CEUS	Endoleak	49	0	<b>PPV 100%</b>
	No Endoleak	2	49	<b>NPV 96%</b>
		<b>Sensitivity 96%</b>	<b>Specificity 100%</b>	

There were seven endoleaks where the diagnosis was unclear on CTA. In six of these, CTA failed to differentiate between a type II and a type III endoleak. In the remaining case, CTA could not distinguish between a type I or II endoleak. One type III endoleak on CTA was re-classified as a type II by CEUS, 3D-CEUS and the MDT. Overall seven patients underwent catheter angiography for diagnostic or treatment reasons but could have been avoided in three patients if the 3D-CEUS diagnosis was accepted, as sac size was stable but CT could not rule out a type III endoleak in two cases and a type I endoleak in another. As high-pressure type I and III endoleaks require urgent treatment and type II endoleaks are usually benign, it is essential that an accurate diagnosis be made. These indeterminate cases seen on CTA are outlined below.

### Case 1

One year following primary EVAR, CTA detected an endoleak closely related to the flow divider of the stent-graft. Both CTA and CEUS was unable to differentiate between a type II or III endoleak. Both 3D-CEUS operators diagnosed a type IIb endoleak. Because of the discrepancy between imaging modalities, catheter angiography was undertaken and a type IIb endoleak confirmed. As the sac size was stable no intervention was performed and the patient continued on duplex surveillance (Figure 28).

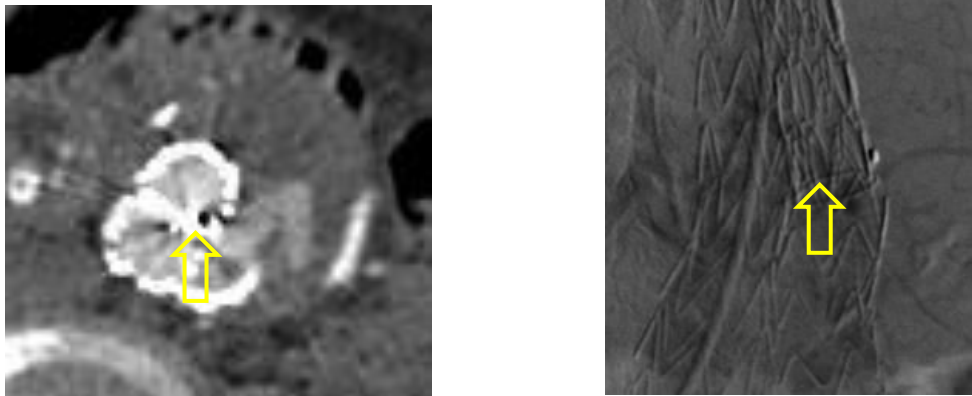


*Figure 28: indeterminate endoleak close to flow divider on CTA(left, arrow). 3D-CEUS diagnosis of type IIb endoleak confirmed on catheter angiography (right, arrow).*

## Case 2

A year following conventional EVAR, a CTA was performed as part of routine surveillance. A type II endoleak was suspected, but a type III endoleak could not be excluded as the endoleak was closely related to the left limb of the stent-graft. The endoleak was associated with a significant increase in sac size (>1cm). A type III endoleak could not be excluded on CEUS. After 3D-CEUS, both operators diagnosed a type II endoleak originating from the IMA. As the patient had an increasing sac size, he underwent catheter angiography where the type II endoleak was confirmed and successful embolisation performed (Figure 29). Sac size remained stable at one one-year follow up.



*Figure 29: An endoleak is seen on CTA close to the limb of the graft (left, arrow) that cannot be differentiated between type II and III. CEUS was indeterminate. 3D-CEUS diagnosed a lumbar type II endoleak that was confirmed on catheter angiography (right, arrow).*

### Case 3

5 years after primary EVAR a significant increase in aneurysm size was noticed on US surveillance. CTA demonstrated an indeterminate type II or III endoleak. CEUS and 3D-CEUS both diagnosed a type II endoleak. 3D-CEUS diagnosed a type II endoleak with lumbar inflow. At catheter angiogram, an endoleak could not be seen; however, lumbar artery embolisation was performed on the basis of the 3D-CEUS finding (Figure 30). The MDT concluded a type II endoleak was present but possibly intermittent. Aneurysm size stabilised on post-embolisation follow up.

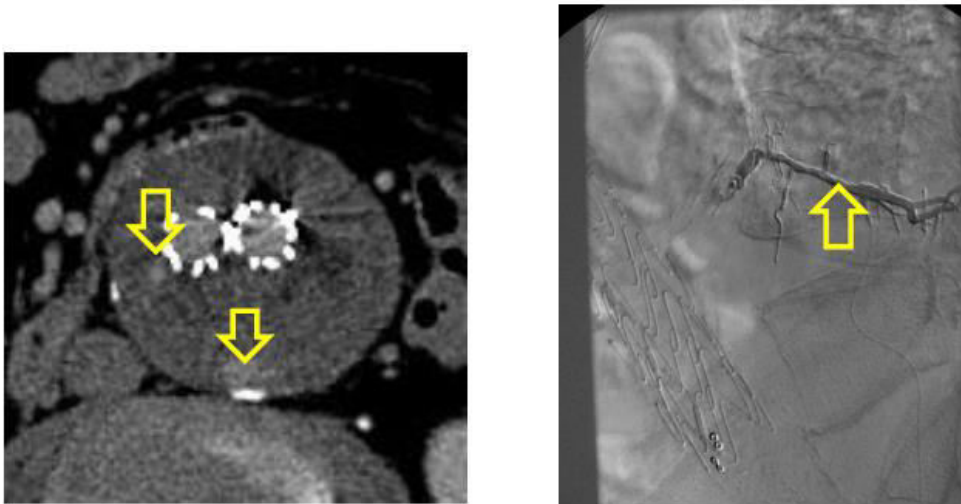


*Figure 30: A possible type II (left, bottom arrow) or III (left, top arrow) endoleak was seen on CTA. Lumbar artery embolisation was performed after a lumbar type II endoleak was diagnosed with 3D-CEUS (right).*

#### Case 4

A routine surveillance CTA at 3 months following EVAR for a 7.2cm AAA detected an endoleak intimately associated with the overlap zone of the left limb of the graft. CEUS confirmed a type II endoleak, however, 3D-CEUS delineated inflow via the IMA. This was confirmed during a catheter angiogram, where the IMA was embolised (Figure 31).

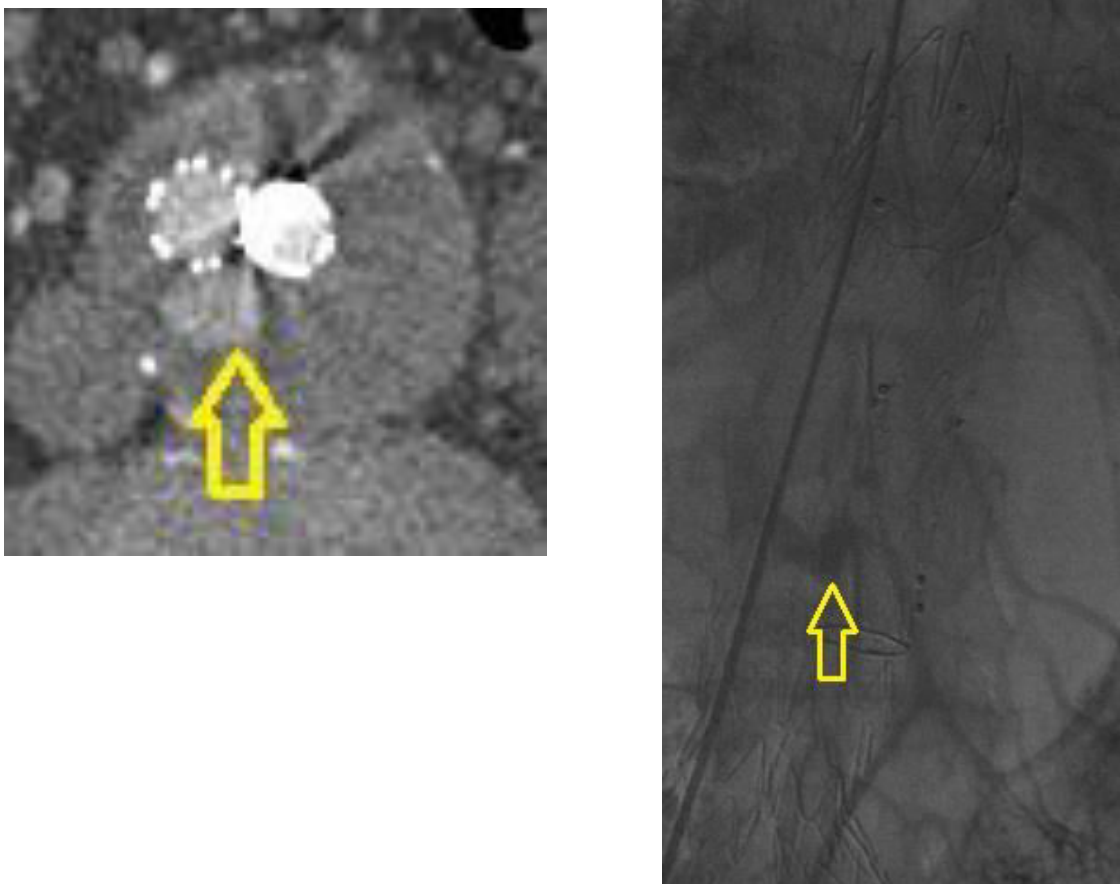


*Figure 31: An endoleak on CTA intimately associated with the overlap zone of the main body and left limb of an Endurant stent-graft (left, arrow). Confirmation of type II endoleak seen on 3D-CEUS during catheter angiography (right, arrow).*

## Case 5

This patient underwent a revision EVAR due to a type Ib endoleak, by re-lining both graft limbs. Four months later, a surveillance CTA was performed and detected a large type III endoleak close to the right limb of the graft (Figure 32). CEUS suggested this was a type II endoleak. 3D-CEUS diagnosed a type IIb endoleak that was confirmed by the MDT. No intervention was performed as the type II endoleak persisted but was not associated with an increase in aneurysm size. On follow up, the endoleak thrombosed spontaneously.

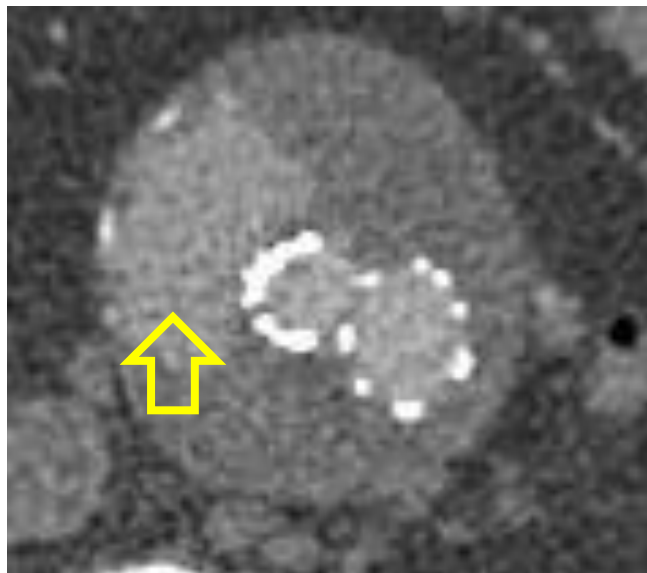


*Figure 32: Suspected type III endoleak (arrow) seen on CTA associated with the right limb of the graft that had been relined.*

### Case 6

This patient underwent EVAR in January 2015 with an Ovation® stent-graft. The surveillance CTA at three months demonstrated an endoleak associated with the ipsilateral stent-graft limb and the main body (Figure 33). Deployment had been difficult due to twisting and rotation of the main body. There was also compression of the contra-lateral limb at the junction with the main body. CTA could not differentiate between a type II or III endoleak. 3D-CEUS diagnosed a type II endoleak. A catheter angiogram was performed to re-stent the compressed limb and investigate the endoleak. No type III endoleak was seen. The contralateral limb was re-stented. The 3D-CEUS diagnosis was supported by the final MDT diagnosis of a type II endoleak.

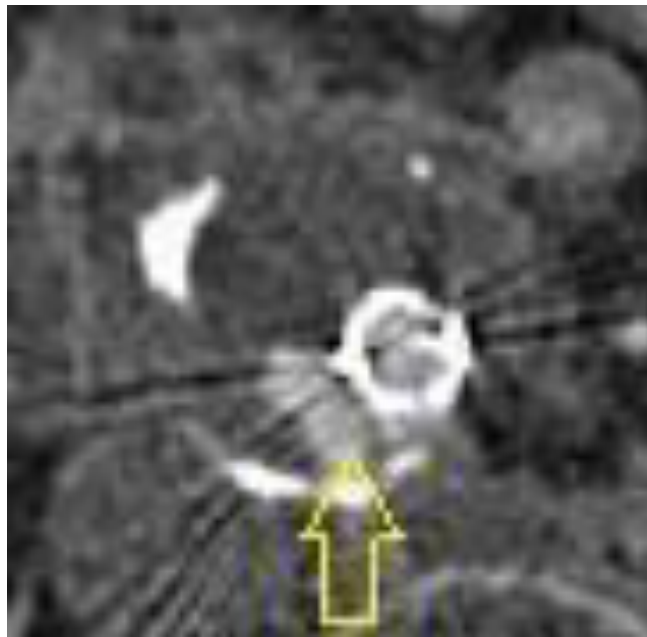


*Figure 33: CTA three months following EVAR with an Ovation® stent-graft. There is an indeterminate endoleak associated with the ipsilateral limb and the main body (yellow arrow).*



### Case 7

A routine surveillance CTA at three months could not be distinguished between a type Ia or type II endoleak. Aneurysm size was stable. CEUS and 3D-CEUS both diagnosed a type II endoleak only. As a potential type I leak was seen on CTA a catheter angiogram was performed, but no endoleak could be demonstrated (Figure 34). The proximal seal zone was balloon moulded based on the CTA result. Repeat CEUS/3D-CEUS post-procedure again demonstrated a type II endoleak. The MDT considered the final diagnosis was a type II endoleak and the patient was returned to routine duplex surveillance.

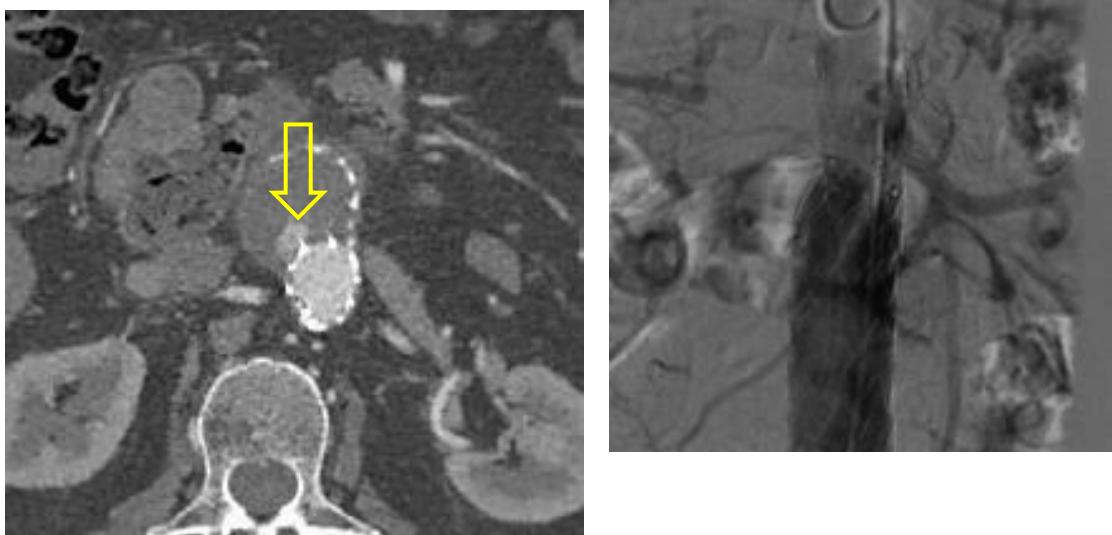


*Figure 34: Possible type I endoleak seen on CTA (left, arrow). No endoleak seen on catheter angiography (right).*

## 6.5 DISCUSSION

This study shows that 3D-CEUS was more sensitive than CTA to endoleak and more accurate at defining the source and type of endoleak. CTA failed to distinguish between type II and III endoleak in six cases and between type I and II in one further patient. These findings are important as type I and III endoleaks are considered to be 'high pressure' leaks that may lead to aneurysm rupture and need urgent repair. Previously, invasive catheter angiography was indicated whenever the endoleak could not be accurately classified by CTA. This carried a risk of complications and was expensive. In this study, 3D-CEUS classified all indeterminate endoleaks on CTA and achieved almost complete agreement with the final decision made by the vascular MDT. Therefore, catheter angiography should be used only when treatment is required.

The sensitivity and specificity of US and CEUS has always been compared previously to CTA.<sup>154-156, 158, 159</sup> Our pilot study showed this to be unsafe as CTA may fail to detect endoleak and frequently fails to classify endoleaks accurately.<sup>190</sup> There is no precedent for using the MDT decision as the 'gold standard', but this was thought to be appropriate for this study as no single imaging modality, including catheter angiography, is 100% sensitive and specific. Obviously, it would not have been ethical to undertake catheter angiography in patients where there was not thought to be a need for treatment. The MDT decision was based on all available imaging including CTA, 3D CEUS and catheter angiography when this was needed. The MDT consisted of vascular surgeons, vascular radiologists and vascular technologists not involved in the study to reduce bias as much as possible.

CEUS is well documented to be more sensitive than CTA to low flow endoleaks, which may still relate to sac growth.<sup>154, 155</sup> In this study, CEUS/3D-CEUS failed to detect only one type I endoleak and one type II endoleak, achieving a sensitivity of 96% when compared with both CTA and the MDT decision. The missed type I endoleak was small and in the very proximal neck – an area often difficult to image on US. The missed type II endoleak was also small and found in a patient where the interval between CTA and 3D CEUS was 14 days; it is possible that this endoleak was intermittent or

thrombosed in the intervening period. In this case, the AAA size was stable and no treatment was needed.

The agreement between operators for both the detection and classification of endoleaks using 3D-CEUS was encouraging ( $\kappa=0.89$ ). This included the identifying the source vessel for every endoleak; the ability to accurately delineate inflow and outflow vessels is important in the planning of interventions.<sup>155</sup> Currently, many vascular surgeons and endovascular therapists are more familiar with CTA as they are able to manipulate the images in three planes, perform reconstructions and take advantage of various visualization tools. As 3D-CEUS achieves multi-planer reconstructions from a single sweep of the transducer, the clinician can view and scroll through the 3D reconstruction slice by slice, akin to CTA images. The images can be interpreted in axial, coronal and transverse planes ensuring that adjacent vessels are not mistaken for endoleaks. An additional benefit of imaging in three planes simultaneously, is that the operator does not miss areas of interest during manual rotation of the transducer; this allows confident identification and classification of even small leaks. Finally, the facility to segment the stent-graft, aneurysm and other structures within the 3D volume adds clarity in difficult cases, although this currently takes around 20 minutes of manual post-processing. A 3D-CEUS study currently takes approximately 20 minutes including reporting, at an approximate cost of 100 GBP/131 USD.

3D-CEUS retains the advantages of dynamic imaging with duplex. Flow velocities through the stent graft can be used to measure severity of stenosis or limb kinking. Plain x-rays are still needed to detect stent fracture or migration, but these are usually treated conservatively unless a complication ensues.<sup>1</sup>

This is the first adequate study on 3D-CEUS for surveillance following EVAR. Recently, Gargiulo and colleagues reported on 'four-dimensional' using a matrix transducer (x6-1; Philips Medical Systems) to investigate endoleak in only 22 patients following EVAR.<sup>196</sup> Although "4D CEUS" was equivalent to CTA for endoleak detection, there were only three endoleaks and the authors fail to explain how their images were acquired. Matrix ultrasound transducers have a limited field of view and we are not told whether single or multiple acquisitions were performed for each patient. As it is essential to image the entire stent graft before endoleak can be confidently excluded,

a tracked freehand system has the advantage that it allows imaging of the entire infra-renal aorta with one sweep of the probe.

Although recruitment was consecutive and non-selective, 57 patients undergoing CTA preferred not to take part or could not be scheduled for CTA and CEUS studies within a month. Additional patients were lost due to instrument failure (failure of tracking sensors) and Sonovue supply problems. The frequency of endoleaks at 51% was higher than expected in a typical surveillance cohort. As our surveillance programme is ultrasound-based, patients undergoing CTA are more likely to have an endoleak as CTA is usually reserved for treatment planning or confirmation of diagnosis made on duplex. A further limitation of this study was that many CTA and 3D-CEUS studies could not be performed on the same day, usually for logistical reasons. It is unlikely that an interval of under four weeks had an important effect on our results, particularly as most patients had paired studies on the same day. We attempted to eliminate bias of the MDT members to an imaging modality by having multiple radiologists, surgeons and vascular scientists within the team, but who were not involved in the study. This study was performed using a prototype system that did not reach the commercial market. However, a CE-marked system (Piur tUS – [www.piurimaging.com](http://www.piurimaging.com)) is now available and works on similar principles. Finally, the clinical applicability of this study may be limited as the use of standard CEUS is not yet global.

3D-CEUS acquisition and display is not "real-time"; this is equally true for CTA. As 3D-CEUS images can be interpreted in the light of the real-time 2D images acquired at the same time, this is not a significant shortcoming. 3D-CEUS is also subject to the same limitations as all ultrasound modalities; bowel gas and obesity can make imaging difficult. An experienced operator can often disperse bowel gas or the scan repeated at another time. Only two CEUS/3D-CEUS images were unsuitable for analysis in our study.

Our practice is now to arrange standard duplex before discharge following EVAR with all patients undergoing CTA at three months. In the absence of type I or III endoleak, subsequent surveillance is by standard duplex and abdominal x-ray. In the event of aneurysm growth >4mm on standard duplex, 3D-CEUS is performed to define any

endoleak although our vascular surgeons still prefer to book CTA before planning treatment. Any new endoleak seen on duplex, even with a stable a AAA diameter, is investigated by 3D-CEUS to classify the endoleak as we not feel standard duplex is satisfactory to accurately classify endoleaks. Proven type II endoleaks are then followed up using standard duplex surveillance. If a type I or III leak is diagnosed, CTA is undertaken to plan treatment. We also use 3D-CEUS selectively after the first follow-up CTA if there is any diagnostic uncertainty. Multi-modality imaging is helpful to the multi-disciplinary team in challenging cases.

## **6.6 CONCLUSIONS**

3D-CEUS was more sensitive for endoleak detection following EVAR than CTA and more accurate in its classification. The inter-operator reliability for reporting both the detection and type of endoleak was excellent. 3D-CEUS is inexpensive, relatively quick to perform and has little or no known risks to the patient. 3D-CEUS is now our initial investigation of choice in cases of aneurysm sac expansion or diagnostic uncertainty following EVAR.

## CHAPTER 7: MEASUREMENT OF ABDOMINAL AORTIC ANEURYSM VOLUME USING MAGNETICALLY TRACKED 3D ULTRASOUND

### Chapter contributors and role:

**C Lowe:** conception, patient recruitment, CT and 3D-US analysis, manuscript writing.

**S Rogers:** 3D-US scanning

**M Ashrafi:** CT and 3D-US analysis

**Mr J Ghosh:** Co-supervisor

**Prof C McCollum:** Supervisor

### 7.1 ABSTRACT

**Background:** Volume measurement may be more sensitive to changes in AAA size after EVAR than diameter but until recently has relied on CT scanning. 3D-US has been proposed as a non-invasive, radiation free modality that may allow volume estimation of AAAs. A number of studies have employed various 3D-US methodologies with varying degrees of success. The aim of this study was to investigate the accuracy of a magnetically tracked 3D-US for measuring AAA volume in native, untreated AAAs compared to CT as the gold standard.

**Methods:** From August 2014 to March 2015, patients undergoing CT for planning of AAA repair had a 3D-US scan performed on the same day. CT and 3D-US data were analysed using a manual segmentation technique. Measurements were repeated at 30 days to investigate the intra-operator reliability of CT and 3D-US measurements. A second blinded operator repeated both CT and 3D-US measurements to investigate inter-operator reliability. Results were assessed using Pearson's correlation and Bland-Altman plots.

**Results:** 22 patients were recruited. The technical success rate was 90% leaving 20 paired CT and 3D-US scans available for analysis. There was a significant difference (mean 25.7ml,  $p=0.03$ ) between 3D-US and CT measurements of AAA. There was no

significant difference between the intra-operator measurements of AAA volume for CT ( $p=0.6$ ) or 3D US ( $p=0.5$ ). For 3D-US, there was a significant difference between the inter-operator measurements (mean 7.82ml,  $p < 0.01$ ).

**Conclusions:** Further research is needed to improve the accuracy of 3D-US measurement of AAA volume compared to CT and its inter-operator reliability. This may be achieved by using a more accurate tracking system, and elimination of the effects of AAA pulsatility by either ECG gating or studying post-EVAR patients.

## 7.2 INTRODUCTION

Aneurysm shrinkage, based on maximal diameter is thought to be predictive of freedom from complications after endovascular aneurysm repair (EVAR). Intuitively, as abdominal aortic aneurysms (AAA) are 3D structures, measurement of the aneurysm volume should be more sensitive than maximal diameter in detecting subtle changes. Changes in aneurysm morphology are known to alter its dimensions at multiple levels and these could clearly be missed by measurement of a single cross section, regardless of if they are standard transverse measurements or orthogonal to the central luminal line.

Aortic volume measurements have been shown to provide earlier evidence of aneurysm shrinkage after EVAR compared to diameter.<sup>82</sup> In one study, 63% of volume increases in the presence of type II endoleak were missed by diameter measurements alone.<sup>83</sup> Therefore, relying on simple diameter measurements when monitoring patients with type II endoleaks has the potential to offer false reassurance of stability due a stable maximal diameter, when in reality there is an increasing aneurysm volume. This may explain the rare phenomenon of AAA rupture with an isolated type II endoleak and stable aneurysm diameter. The potential value of volume measurements after EVAR has been debated in a number of studies but has been hampered by the need to use computed tomography (CT) scans and complex software.<sup>82, 83, 164</sup>

With adoption of ultrasound-based EVAR surveillance, volume measurement using CT is no longer a feasible option. A number of studies have explored the possibility of AAA volume measurements using a range of 3D-US techniques with varying degree of success.<sup>168-170</sup>

Magnetically tracked freehand 3D-US offers the possibility of accurate 3D volume measurements of AAAs. As opposed to other 3D-US methods such as those using mechanical<sup>169</sup> and matrix transducers,<sup>170, 197</sup> this method of 3D-US is theoretically capable of capturing large volumes of ultrasound data such that the majority of the AAA can be imaged in a single acquisition.



The aim of this study was to assess the accuracy and reproducibility of AAA volume measurement using 3D-US by comparison with CT.

### **7.3 METHODS**

Patients due to undergo CTA for treatment planning for AAA repair were invited to take part. The study was approved by the hospital Research and Development department and the National Research Ethics Committee (13/NW/0468). Patients attended for 3D-US on the same day as the CTA or as close to the same day as possible.

#### ***CT Angiography***

CTA was performed using a 128-slice Siemens SOMATOM® Perspective scanner (Siemens Medical, Munich, Germany). Scans were contrast enhanced (100ml 4ml/sec Omnipaque 300) and acquired from the aortic arch to the common femoral arteries. Image acquisition was triggered on contrast enhancement in the distal aortic arch. Images were reconstructed at a nominal slice thickness of 1mm.

#### ***3D-US***

All ultrasound examinations were performed using a Phillips iU22 ultrasound console (Phillips, Amsterdam, Netherlands) using a C5-1 curved array transducer and an attached 3D guidance system “drive BAY” (Ascension Technology Corp., Burlington, USA). In this system, a magnetic field is transmitted from a bedside generator through the volume in which the scan is to be acquired. Sensors attached to the US probe pick up the field in three orthogonal directions allowing the position and orientation of the probe to be recorded. The system had recently been calibrated as described by Feurer.<sup>180</sup> All acquisitions were performed by the same accredited vascular scientist with experience in 3D-US. During a breath-hold to limit movement artefact, the 3D

volume was acquired starting at the most proximal extent of the AAA that could be visualised. The transducer was then steadily moved inferiorly keeping the AAA central in the scanning field to the aortic bifurcation or the most distal point the AAA could be imaged.

### ***3D reconstruction and volume estimation***

The paired 3D-US and CTA data were exported to and analysed using the software package 'ImFusion Suite' (ImFusion GmbH, Munich, Germany), capable of handling both CTA and ultrasound images. As 3D-US did not consistently visualise landmarks from which to start and end measurement (e.g. renal arteries, aortic bifurcation) and the volume of the AAA that could be imaged in each patient varied (due to bowel gas and obesity) the starting point for segmentation was determined as follows:

The axial section of both datasets was scrolled through to define an approximate maximal diameter. Orthogonal views were then obtained in each imaging plane. The section with the largest orthogonal diameter on inner-to-inner (ITI) measurement was defined as the starting point for the segmentation process (figure 35-36).

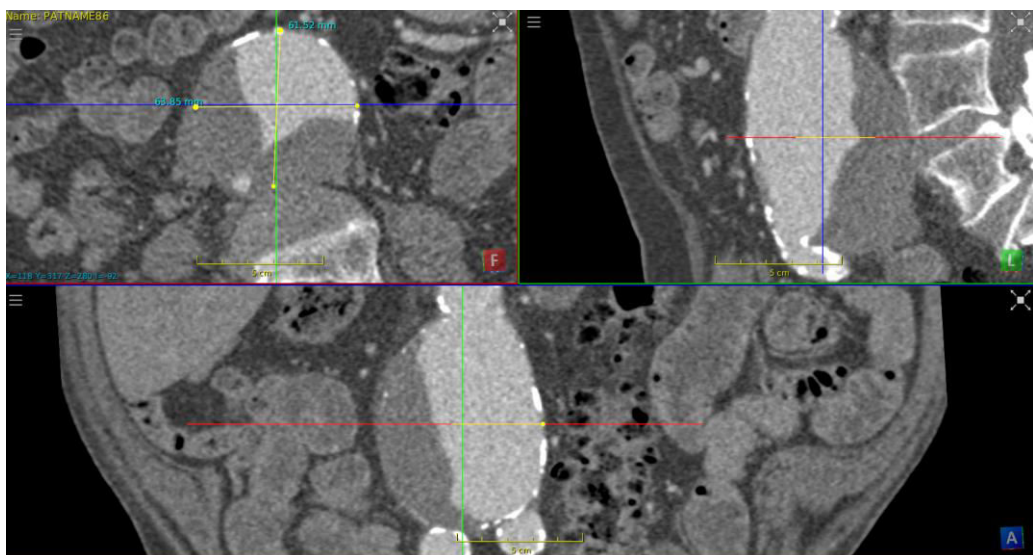


*Figure 35: ITI measurement of AAA diameter in orthogonal sections on CTA*

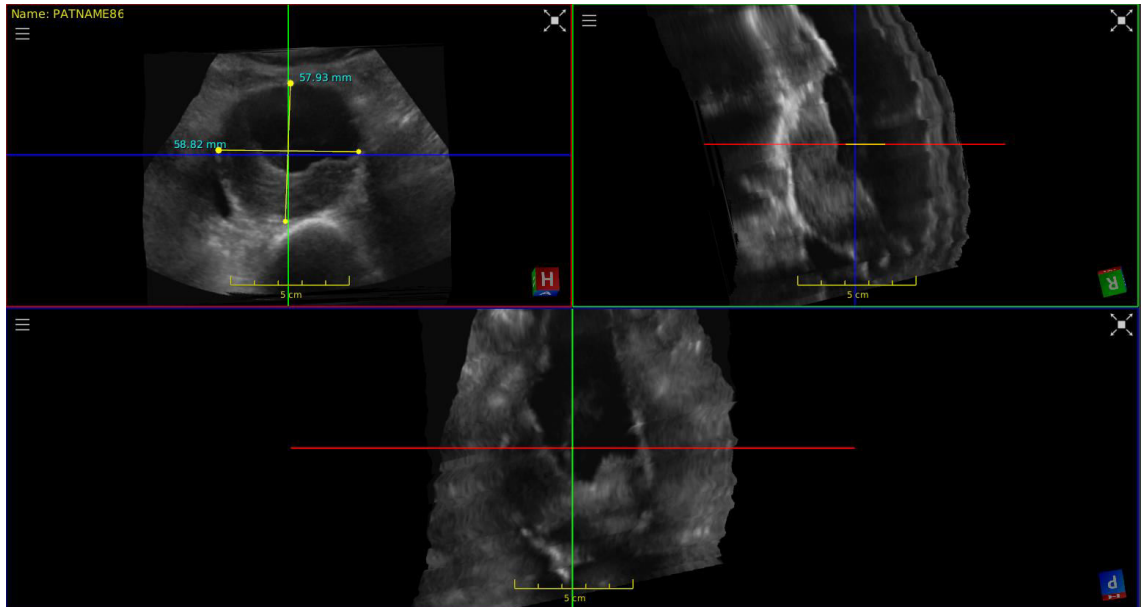


*Figure 36: ITI measurement of AAA diameter in orthogonal sections on 3D-US*

A manual segmentation using a spline tool was utilised. A spline is a curve that connects two or more specific points. The software automatically fits a curve around each of the points that is placed by the user. Spline points were manually placed on the inner vessel wall in both data sets at 1mm slices (Figure 37), 20mm proximal and 20mm distal to the maximal orthogonal AAA diameter. This defined a 'partial AAA volume' of 4cm. Once the splines were placed, the software automatically calculated the volume in the defined region by converting the spline points into a 3D surface mesh (Figure 38-39). Although most 3D-US acquisitions imaged a larger volume of the aneurysm this was a trade-off between the time taken to perform the manual segmentation and having a standardised dataset. Also, due to decreased image quality in the outer range of the acquisition, it would be impossible to choose a longer distance in a number of patients.

A video illustrating this process further is available at: <https://vimeo.com/156839830>

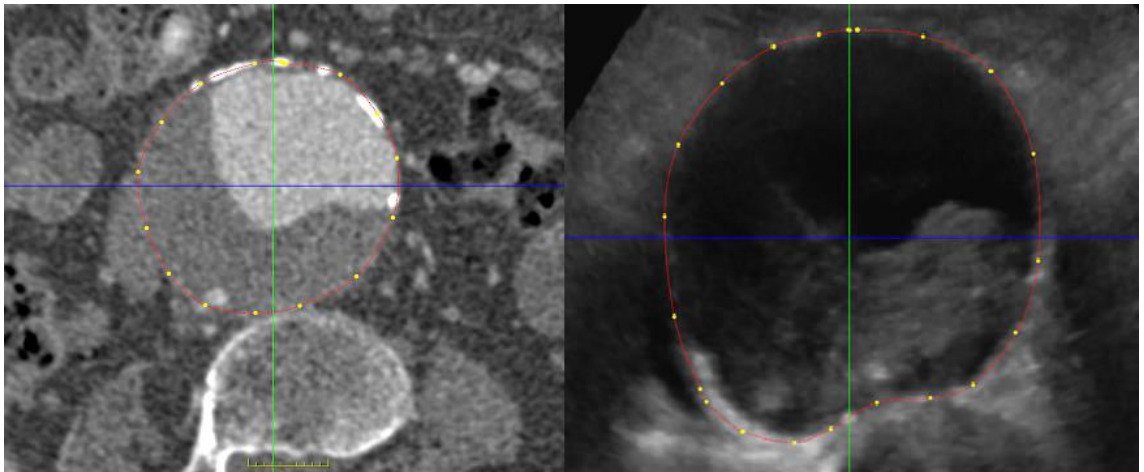


Figure 37: Manual vessel segmentation in each 1mm image slice using the spline tool.

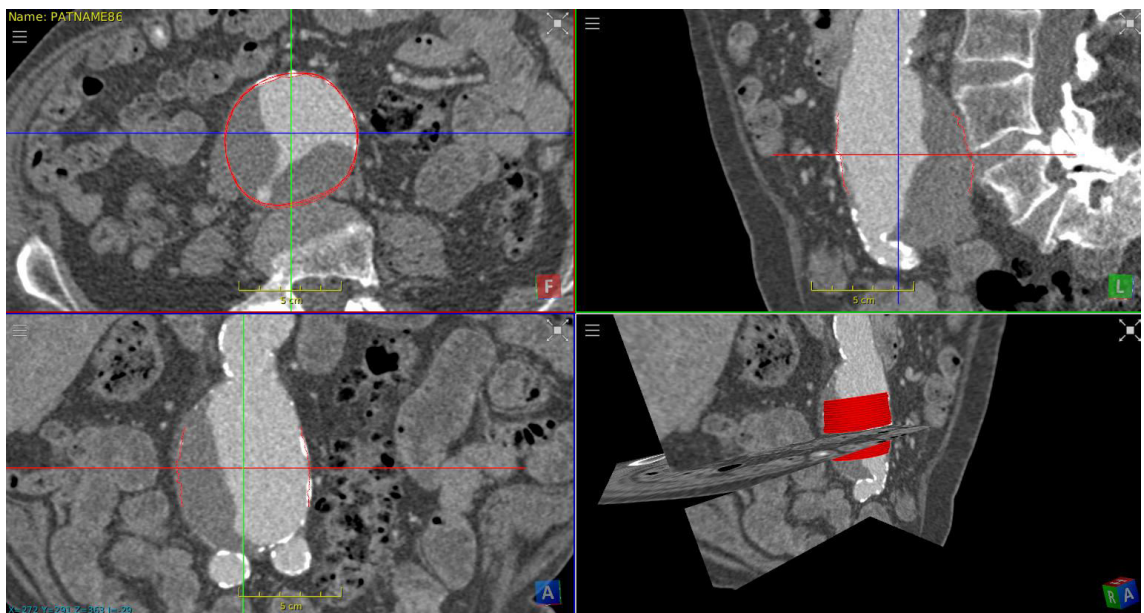
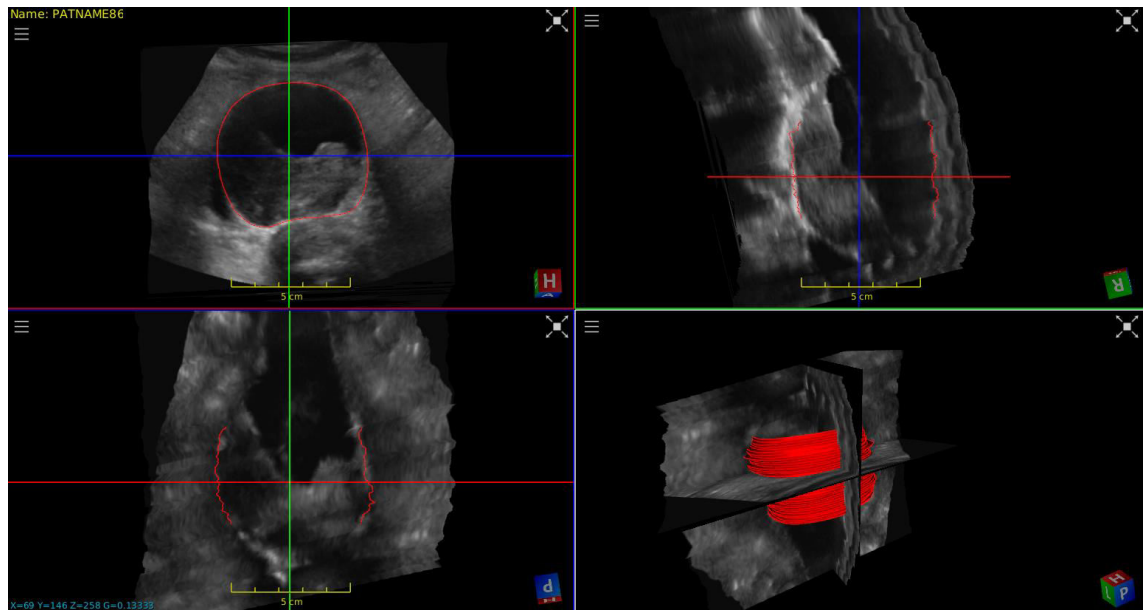


Figure 38: Completed segmentation on CTA defining 'partial' AAA volume



*Figure 39: Completed segmentation on 3D-US defining 'partial' AAA volume*

To assess intra-operator variability of both CTA and 3D-US measurements, volume measurements were repeated on both datasets in random order at least 30 days apart. For assessment of inter-operator variability, a second operator blinded to the results was trained to use the software on two unrelated datasets before performing measurements on the study data.

### **Statistics**

Differences between operator measurements for each modality were analysed using a one-sample T-test. The volume measurements from 3D-US and CTA were compared using Bland Altman plots, where the differences in concurrent measurements on the same subject are plotted against the mean outcome, showing the mean difference and the upper and lower limits of agreements given by the mean  $\pm$  (1.96 x standard deviation (SD)). Correlations between measurements were assessed using Pearson's correlation and scatter plots. Analysis was performed using SPSS statistics v20 (IBM Corp. Armonk, NY, USA).

There is no defined threshold for the reproducibility of 3D-US volume measurement of AAAs. Therefore, the 'phantom cylinder' approach described by Bredahl was used.<sup>170</sup> As the accepted inter-operator variability for 2D-US diameter measurements is  $\pm 5\text{ml}$ , a

'phantom cylinder' was calculated for each measured volume. The diameter was then changed by 5mm and a new volume calculated. This gave the acceptable variation in measurement for each measured volume. For example, for a measured partial volume of 165ml the diameter of the 'phantom cylinder' is  $2 \times \sqrt{(\text{vol}/\pi \times \text{length})} = 73\text{mm}$ . Increasing this diameter by 5mm yields a new volume of  $r^2 \times \pi \times \text{length} = 191\text{ml}$ . Therefore if the range of variability for a partial volume of 165ml exceeds 26ml, the variation exceeds the currently accepted variation in 2D diameter measurement.

#### **7.4 RESULTS**

From August 2014 to March 2015 22 patients were recruited. The technical success of 3D US was 90% as two patients had inadequate image quality (body habitus or bowel gas). Of the 20 patients suitable for analysis 16 male were male and 4 female with a the mean age of 76. The median time between CTA and 3D-US was 0 days (range 0-7).

##### *Volume estimation by 3D-US vs. CTA*

The differences in measured volume were calculated and plotted against the mean. There was a significant difference between the volume measurements on 3D US and on CTA ( $p=0.03$ ). The mean difference was 25.7ml and the limits of agreement 91ml to -40ml (Figure 40). CT and 3D-US volumes were, however, well correlated (Figure 41).

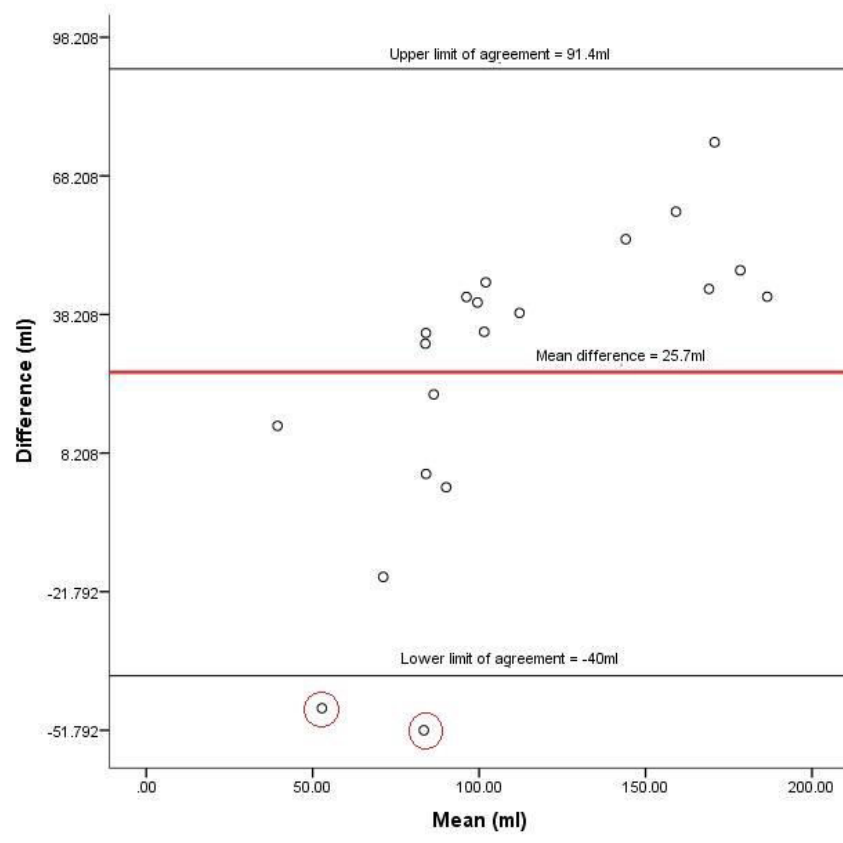


Figure 40: Bland-Altman plot of CTA vs 3D-US measurements of AAA volume. Two anomalous results where 3D-US volume was greater than CTA volume are highlighted in red.

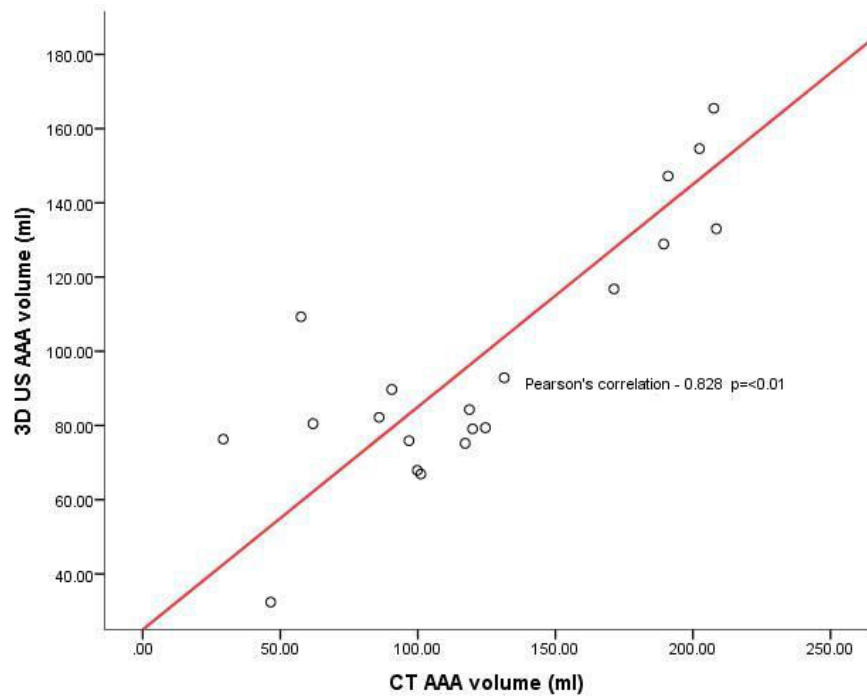


Figure 41: Correlation between CTA and 3D-US AAA volume measurements.

*Reproducibility of CTA AAA volume measurements – Intra-operator*

There was no significant difference between the intra-operator measurements of AAA volume for CTA ( $p=0.6$ ). For CTA the mean difference was  $-0.81\text{ml}$  with limits of agreement  $12.46$  to  $-14.1\text{ml}$ . Correlation was excellent (Pearson's correlation  $0.99$ ,  $p < 0.01$ ) (Figures 42 and 43).



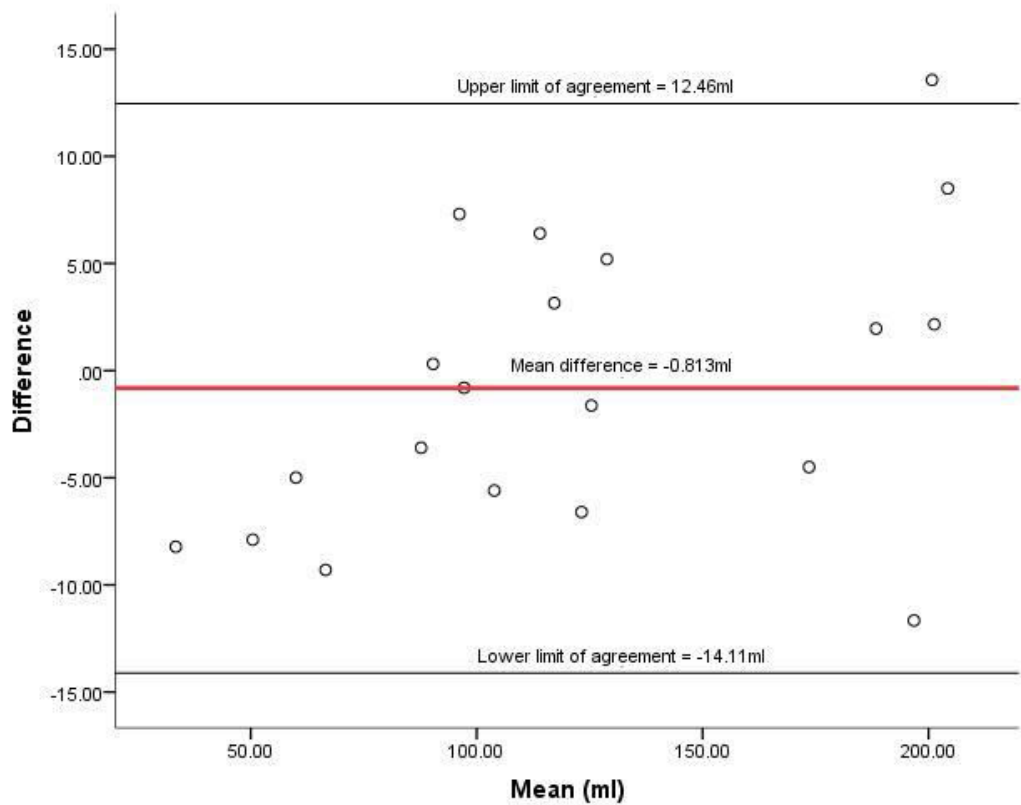


Figure 42: Bland-Altman plot of intra-operator CTA measurements of AAA volume.

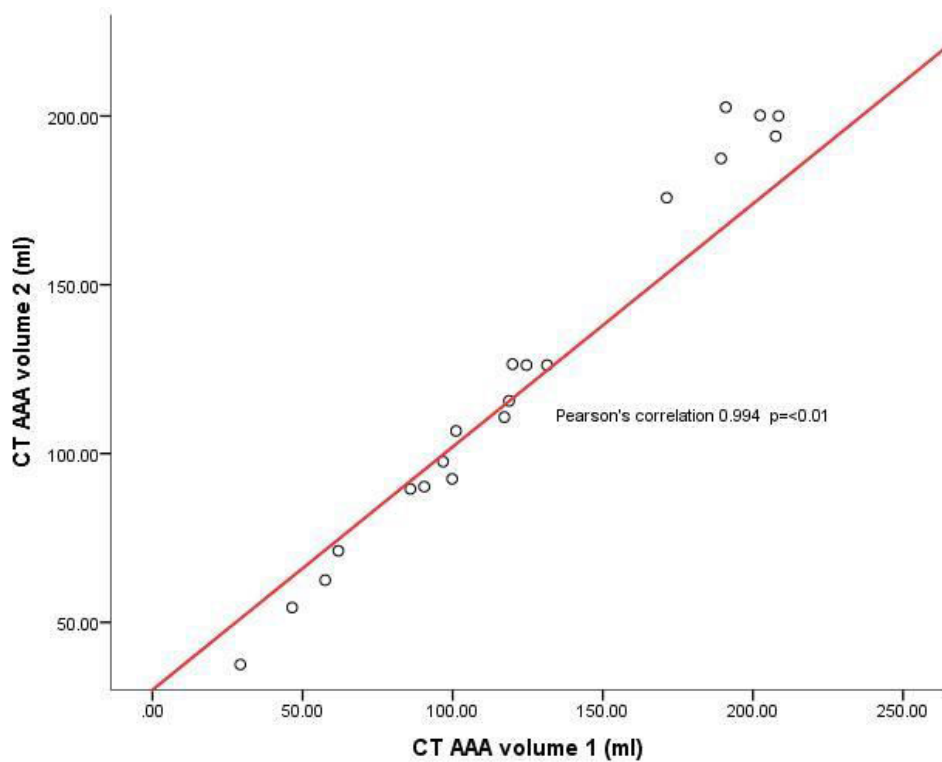
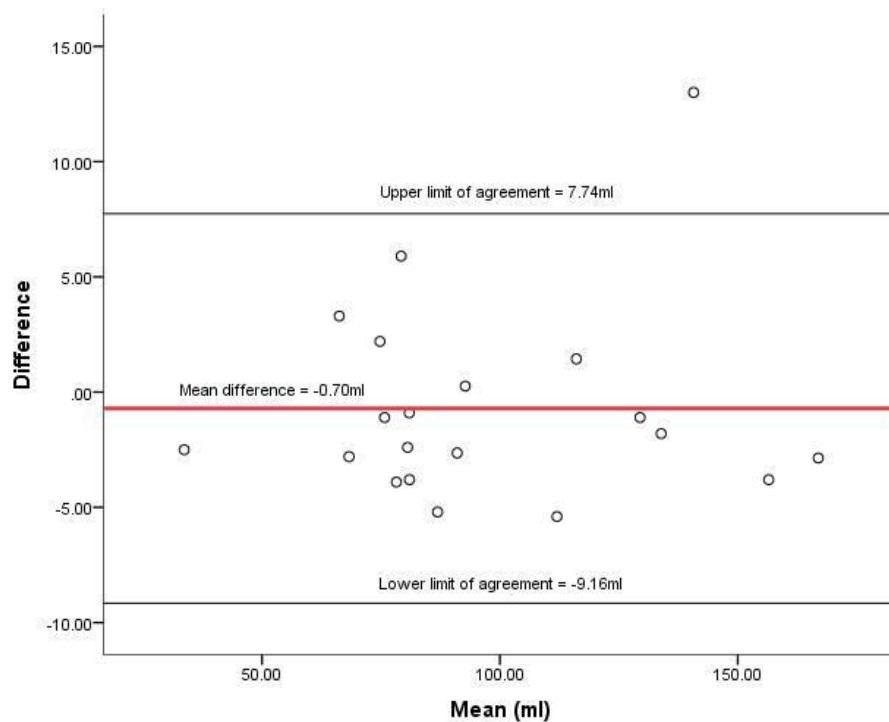


Figure 43: Correlation between intra-operator CTA measurements of AAA volume.

*Reproducibility of 3D-US AAA volume measurements – Intra-operator*

There was no significant difference between the intra-operator measurements of AAA volume for 3D-US ( $p=0.5$ ). For 3D-US the mean difference was  $-0.7\text{ml}$  with limits of agreement  $7.7\text{ml}$  to  $-9.16\text{ml}$  (Figures 44-45). Correlation was high (Pearson's correlation  $0.99$ ,  $p < 0.01$ ). The 3D-US intra-operator variability remained within the range of volume variability that was estimated on the basis of currently accepted diameter measurements (Table 8).



*Figure 44: Bland-Altman plot of intra-operator 3D-US measurements of AAA volume.*

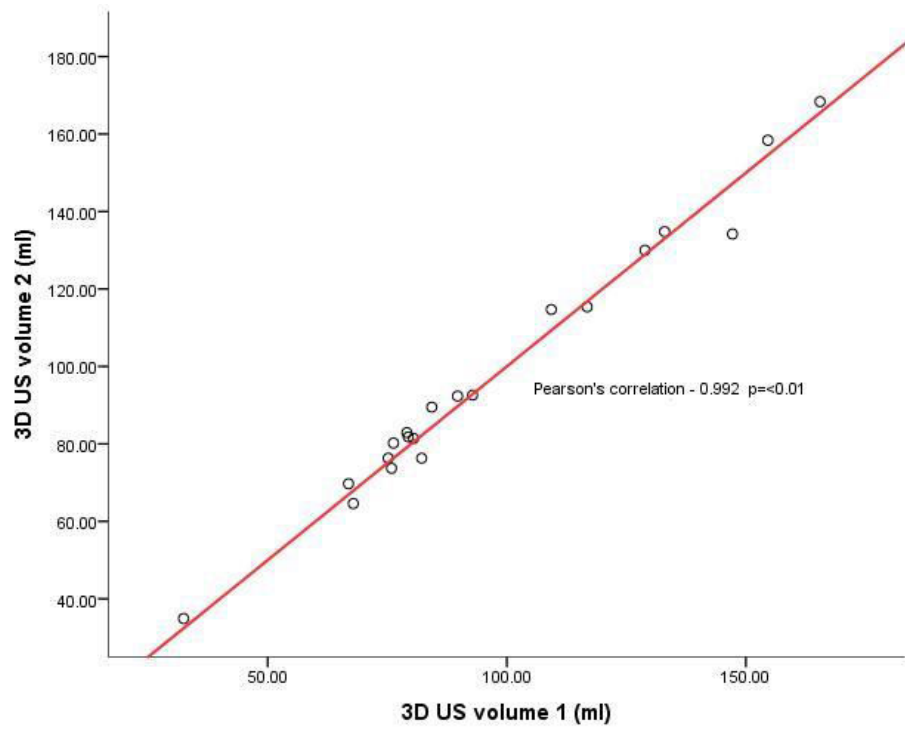


Figure 45: Correlation between intra-operator 3D-US measurements of AAA volume.

*Table 8: Intra-operator variability of AAA volume measurements using 3D-US are within current acceptability of 2D-US diameter measurements using ‘phantom cylinder’ method.*

US Volume 1 (ml)	US volume 2 (ml)	Intra-operator difference (ml)	Error considered acceptable (+/-ml)
76.3	80.2	-3.9	11.7
79.4	81.8	-2.4	15.6
84.3	89.5	-5.2	14.7
154.6	158.4	-3.8	22.1
147.2	134.2	13	24.8
165.5	168.36	-2.86	25.5
128.9	130	-1.1	21.1
89.7	92.342	-2.642	16.3
32.4	34.9	-2.5	10.6
109.3	114.7	-5.4	19.7
133	134.8	-1.8	21
82.2	76.3	5.9	16.8
79.1	82.9	-3.8	19.9
80.5	81.4	-0.9	14.5
116.8	115.36	1.44	20.2
66.9	69.7	-2.8	15.1
75.9	73.7	2.2	16.1
67.9	64.6	3.3	14.1
75.2	76.3	-1.1	16.8
92.86	93	-0.14	16.14

*Reproducibility of CTA AAA volume measurements – Inter-operator*

There was no significant difference between the inter-operator measurements of AAA volume for CTA ( $p=0.176$ ). The mean difference was 2.56ml with the limits of agreement 19.31ml to 14.20ml (Figure 46). Correlation was high (Pearson’s 0.98,  $p<0.01$ ) (Figure 47).

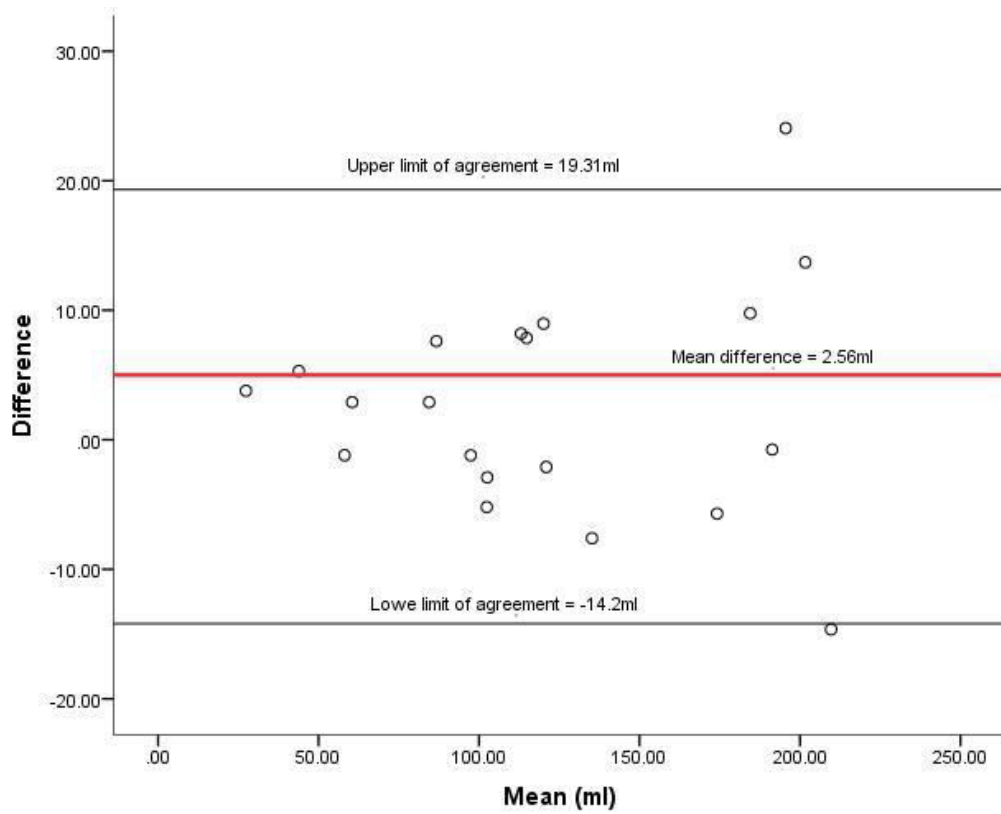


Figure 46: Bland-Altman plot of inter-operator CT measurements of AAA volume.

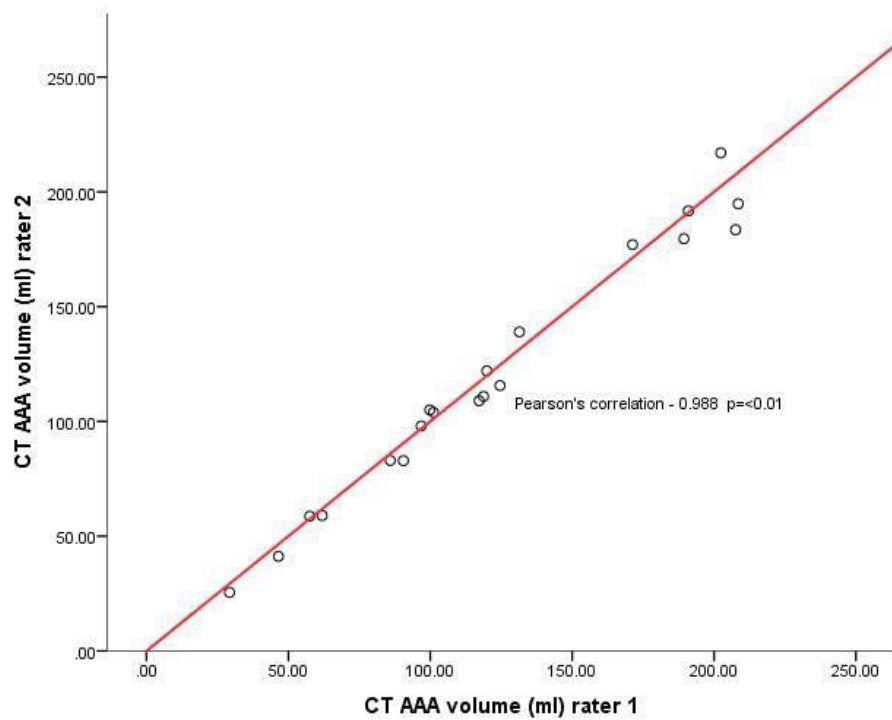


Figure 47: Correlation between inter-operator CT measurements of AAA volume.

*Reproducibility of 3D-US volume measurements – Inter-operator*

For 3D-US there was a significant difference between the inter-operator measurements ( $p=0.001$ ). The mean difference was 7.82ml with limits of agreement 23.5ml to -8.58ml (Figure 48). Correlation was high (Pearson’s 0.97,  $p < 0.01$ ) (Figure 49). Despite the statistical difference found on the inter-operator measurements the 3D-US inter-operator variability remained within the range of volume variability that was estimated on the basis of currently accepted diameter measurements (Table 9).

*Table 9: Inter-operator variability of AAA volume measurements using 3D-US are within current acceptability of 2D-US diameter measurements using ‘phantom cylinder’ method*

<b>US Volume operator 1 (ml)</b>	<b>US Volume operator 2 (ml)</b>	<b>Inter-operator difference (ml)</b>	<b>Error considered acceptable (+/-ml)</b>
76.3	69	7.3	11.7
79.4	79.1	0.3	15.6
84.3	81.3	3	14.7
154.6	146	8.6	22.1
147.2	123	24.2	24.8
165.5	132.5	33	25.5
128.9	114.8	14.1	21.1
89.7	83.5	6.2	16.3
32.4	26.55	5.85	10.6
109.3	105.1	4.2	19.7
133	132	1	21
82.2	78	4.2	16.8
79.1	79	0.1	19.9
80.5	75	5.5	14.5
116.8	115	1.8	20.2
66.9	64	2.9	15.1
75.9	70.9	5	16.1
67.9	57.9	10	14.1
75.2	72.1	3.1	16.8
92.86	77	15.86	16.14

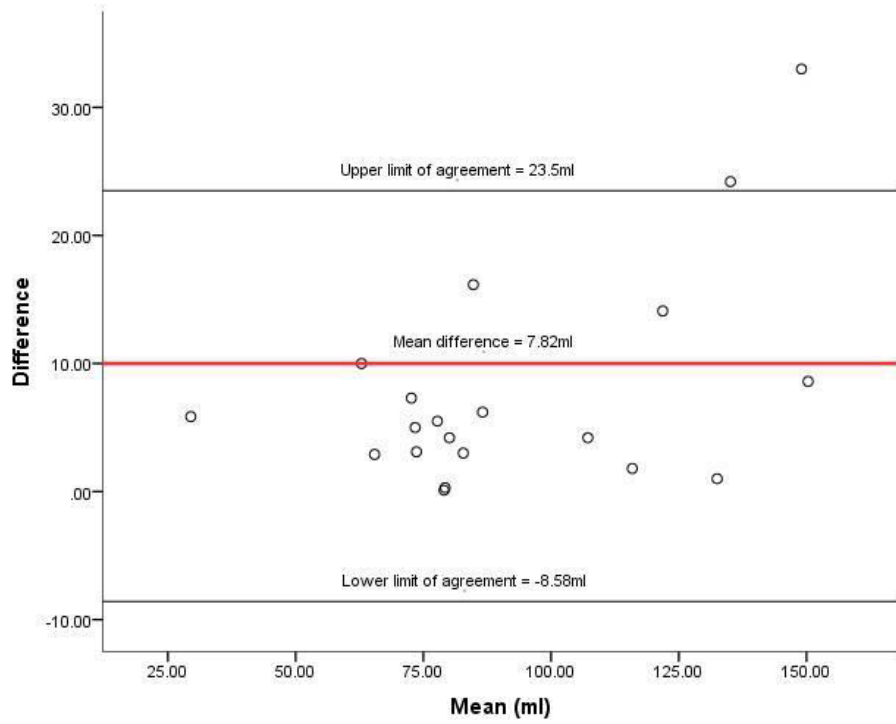


Figure 48: Bland-Altman plot of inter-operator 3D-US measurements of AAA volume

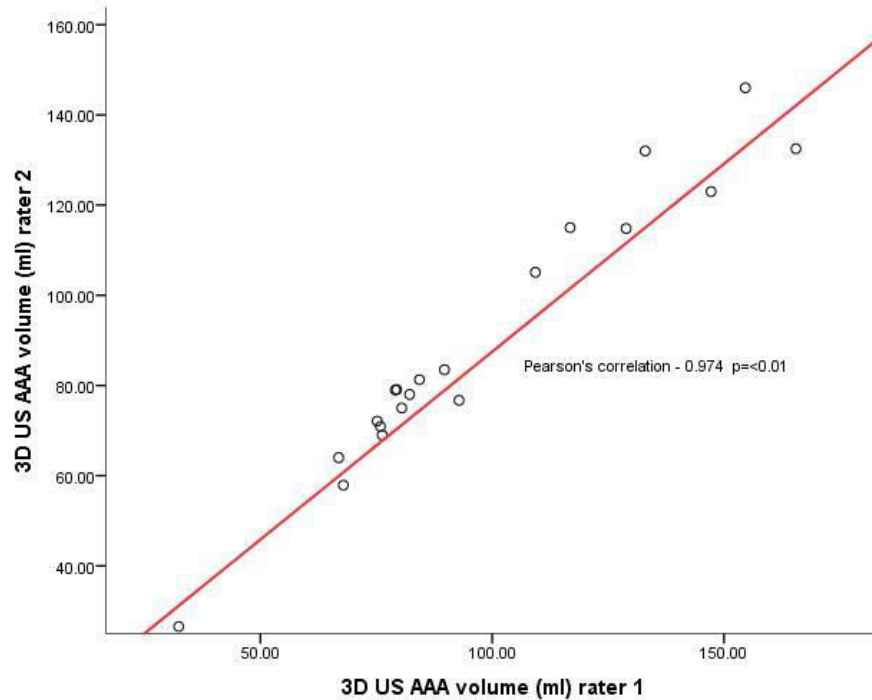
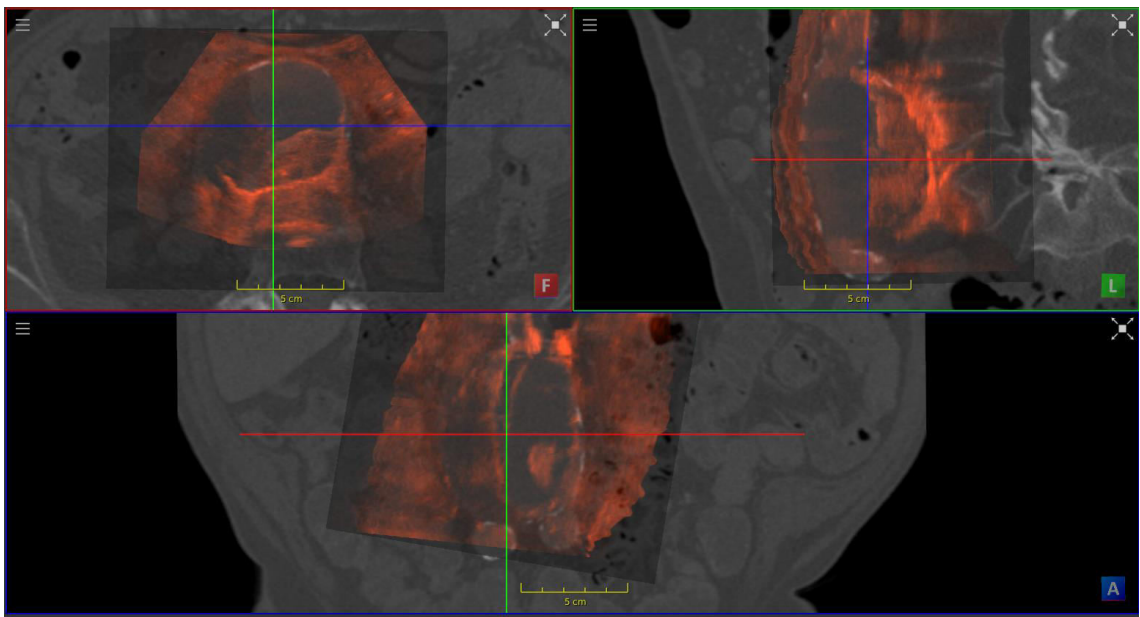


Figure 49: Correlation between inter-operator 3D-US measurements of AAA volume

There were two outlying cases where the 3D-US volumes were significantly higher than CTA (Figure 40). Both of these measurements were reproduced by the second operator. To explore these anomalous results the CTA and US data for both patients was simultaneously loaded onto the ImFusion software and manually 'overlaid'. Following this, an automatic registration algorithm was run to ensure the CTA and 3D US data was accurately fused. Visualisation of the fused 3D-US/CTA data was enhanced by using the 'colour blending' feature and also by viewing the fused data simultaneously in each plane (Figures 50 and 51). Interrogation of the fused data demonstrated excellent accuracy for both patients suggesting that the 3D-US calibration and tracking accuracy was satisfactory.



*Figure 50: Fusion of CT and 3D-US. The 'colour blending' feature improves visualisation of the 3D-US, which can be faded in and out.*



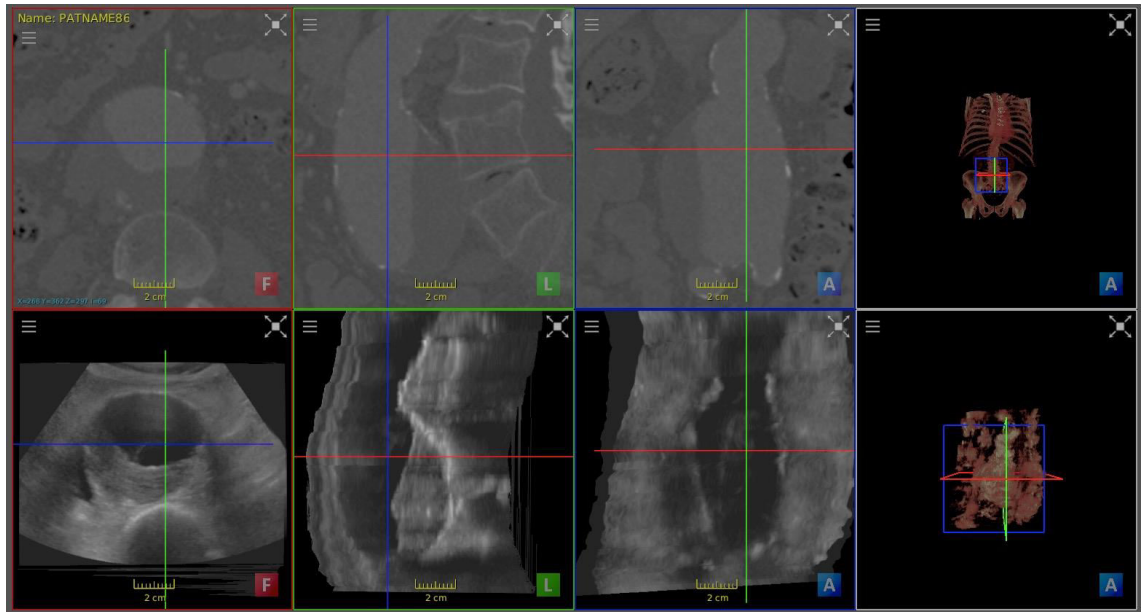


*Figure 51: Simultaneous visualisation of CT and 3D-US in each plane demonstrating accurate registration.*

Following this, the 3D-US annotations were loaded to view the splines outlining the inner AAA wall that had been placed in the 3D-US data for volume measurement. These were compared against the wall of the AAA on CTA for each patient. In the first, the splines from the 3D-US initially appeared well-aligned with the AAA wall on the CTA scan (Figure 52). However, at the proximal portion of the volume there was a significant discrepancy between the wall of the CTA and the 3D-US splines over a distance of 1cm (Figure 53). Examination of the 3D-US images showed loss of definition of the lateral AAA wall and splines had been placed over a larger area, leading to an increase in the measured volume. The 3D-US had been interpreted in the same way by both operators. Analysis of the second patient revealed a similar phenomenon, though the discrepancy was at the distal portion of the AAA. Therefore, it was loss of definition of the lateral AAA wall in both cases that lead the operators to place the splines inaccurately. This phenomenon of poor image resolution of the lateral AAA walls is commonly seen due to the optimal US specular reflection of the outer surface of the anterior wall and the inner surface of the posterior wall.

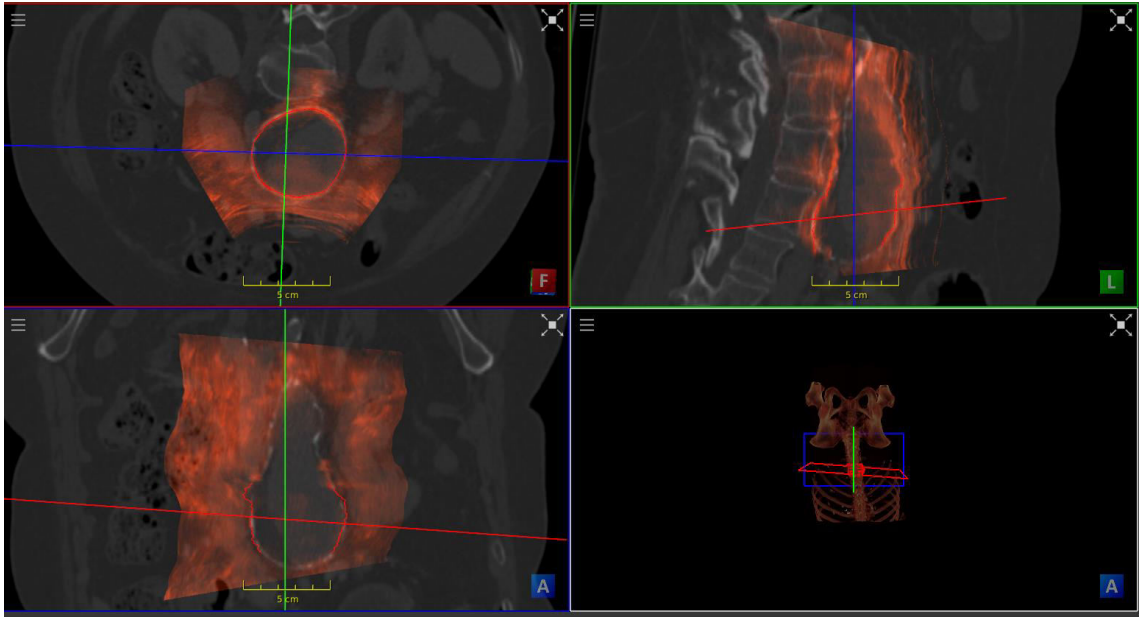


Figure 52: Splines from 3D-US volume measurements overlaid onto CTA data.

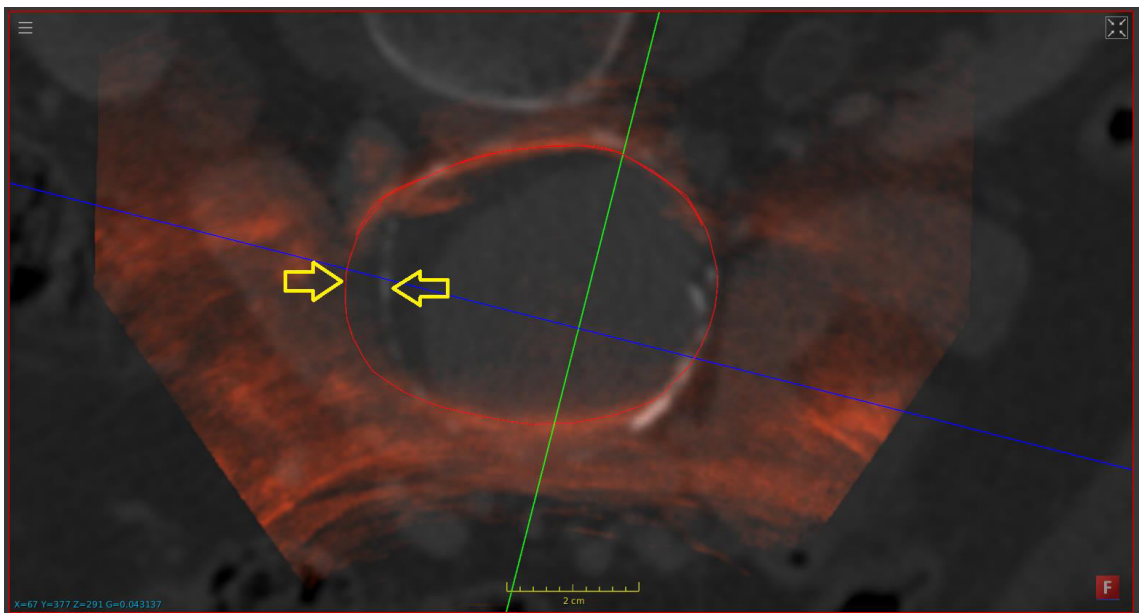


Figure 53: 3D-US spline (left arrow) extending past the AAA wall (right arrow).

## 7.5 DISCUSSION

The results of this study suggest that both CTA and 3D-US measurements of AAA volume had acceptable intra-operator reliability. Additionally, there was acceptable inter-operator variability seen on CTA volume measurements. This provides evidence that the technique used to define the partial volume was reproducible. The most likely cause of the differences in inter-operator variability seen on 3D-US were due to image quality and image artefact. The majority of these problems are difficult to overcome as they are often i) patient related such as obesity or bowel gas or ii) technical, such as the loss of definition of the lateral walls of the aneurysm that makes placing the splines difficult. It is likely that given further training, this consistency could be improved between operators. This being said, the variation in inter-operator volume measurements on 3D-US were still within the range of volume measurement that could be expected based on the phantom cylinder method.

In order to be of clinical value, the 3D-US measurements must correlate to a gold standard measurement. In this study CTA volume was used as this standard. Although a difference in CTA and 3D-US measurements was anticipated, it was statistically significant and in excess of that reported in other studies.<sup>170, 197</sup> The study by Bredahl<sup>170</sup> is the most impressive with a mean difference of 1ml between CTA and 3D-US measurements. There are a number of factors that may have influenced the accuracy of the 3D-US results:

- i) In-accurate calibration of the 3D-US tracking and subsequent reconstruction. Accurate calibration is essential to avoid distortions in the 3D reconstructed geometry.<sup>198</sup> The system's accuracy when properly calibrated has been shown to be adequate<sup>180</sup> and given it had undergone maintenance and calibration prior to the study it is unlikely this was a significant source of error. This was confirmed when the CTA and 3D-US data were co-registered and fused. However, there is evidence to suggest an alternative method of tracking to magnetic, such as optical, may provide more accuracy as there is no effect of metal in the scanning field.<sup>175</sup>

- ii) Use of analysis software non-native to hardware. The on-board software on the magnetic system was not thought to be adequate as it required manual tracing of the AAA wall rather than using a spline tool and it was not able to process CTA data. Based on these results, the ImFusion software was re-tested by the developers and no compatibility issues were identified.
- iii) AAA pulsatility. Maximal AAA diameter is known to vary throughout the cardiac cycle with a mean difference of 1.94mm (range 0-4.7mm) between systole and diastole.<sup>199</sup> This is particularly important given the relationship between diameter and volume. One advantage of the 'freehand' 3D-US approach is the ability to image large volumes, however, this means that the entire AAA cannot be imaged in a single cardiac cycle. The system does not allow for ECG 'gating' where data is acquired only at a specified point in the cardiac cycle. Therefore the AAA was moving as the 3D-US data was acquired. ECG gating is technically challenging, though has been used by some authors in small numbers of patients.<sup>168</sup>

This study compared CT and 3D-US volumes of *untreated* AAA as there was concern that the presence of a stent-graft may reduce image quality. The influence of pulsatility when a stent-graft is in situ is likely to be significantly less or even absent as the AAA is excluded from the circulation and subsequently thromboses. As the clinical application of volume measurement is EVAR surveillance, a dataset of volume measurements with stent-grafts *in situ* should be studied.

- iv) Definition of 'start' and 'end' points. An effort was made to standardise the 'start' and 'end' point of volume measurements on both datasets. The results were favourable for intra and inter-operator variability on CTA and for intra-operator variability on 3D-US. The variation seen in the inter-operator measurements on 3D-US and also between CTA and 3D-US may be due to inconsistencies in selecting different starting points for segmentation as well as inconsistent placing of the splines

Other authors have attempted a number of approaches to defining the volume to be measured. Bredahl reports a method where the maximal aortic diameter on CT and 3D-US is automatically defined by a software algorithm using a central luminal line, which lead to a high level of reproducibility and accuracy in both the measurement of AAA volume and maximal diameter.<sup>170</sup> This software is now almost completely automatic and soon to be offered 'on-cart' as an add-on to a commercialised system (*personal communication with Bredahl et al.*). Arsicot<sup>197</sup> defined the start of the measurement by loss of parallelism of the aortic wall and a diameter >30mm. Given that some AAAs involve the bifurcation and never regain a normal diameter is it difficult to see how this approach is feasible.

In this current work, a manual segmentation process was used, taking a mean of 23 minutes per case. For a volume measurement technique to be clinically feasible, it must be able to be performed rapidly at the bedside. As detailed above, some authors have been able to achieve this with good results. In our experience of the automated segmentation algorithms available to us, none is able to perform to the required accuracy, particularly on the ultrasound data. This however will be key in developing a clinically useable tool. In addition, the time taken to scan a patient multiple times to gain the optimal image in a research setting is not applicable for a busy vascular clinic.

The clinical utility of volume measurements of AAAs in surveillance of small AAAs or after EVAR has not been widely accepted. However, this is possibly due to the need to use CT data and complex software. If ultrasound measurement of volume can be proven to be accurate, reproducible and rapid then it is possible that volume measurement could be become established as the benchmark criterion for AAA and EVAR surveillance. It is possible than a subgroup of patients with benign endoleaks and stable maximal diameters may have increasing AAA volumes and be at risk. However, as successful aneurysm exclusion by EVAR leads to AAA shrinkage and remodelling, it is possible that the site of maximal orthogonal diameter will change over time and lead to altered volume estimations, potentially limiting its applicability for accurate surveillance. How this may be addressed is a matter for further research.

## 7.6 CONCLUSIONS

There was a significant difference in AAA volumes measured on CT and 3D-US with a mean difference of 25.7ml. There was no significant difference in intra-operator measurements of AAA volume for both CT and 3D-US. However, there was significant difference in inter-operator measurements using 3D-US with a mean difference of 7.82ml. Despite this, the 3D-US intra and inter-operator variability remained within an acceptable range based on the currently accepted variability of diameter measurements. Further research is needed to improve the accuracy of 3D-US measurement of AAA volume compared to CTA and its inter-operator reliability. This may be achieved by using a more accurate tracking system and elimination of the effects of AAA pulsatility by ECG gating. This may not be required when measuring post-EVAR patients.

## **CHAPTER 8: MEASUREMENT OF ANEURYM VOULME FOLLOWING ENDOVASCUALR ANEURYSM REPAIR USING OPTICALLY TRACKED 3D ULTRASOUND**

### **Chapter contributors and role:**

**C Lowe:** conception, patient recruitment, CT and 3D-US analysis, manuscript writing.

**S Rogers:** 3D-US scanning, 3D-US analysis.

**Mr J Ghosh:** Co-supervisor.

**Prof C McCollum:** Supervisor.

## 8.1 ABSTRACT

**Background:** Volume measurement may be more sensitive to changes in AAA size after EVAR than diameter but until recently has relied on CT scanning. The aim of this study was to investigate the accuracy of an optically tracked 3D-US for measuring AAA volume in post-EVAR patients compared to CT as the gold standard.

**Methods:** Between March 2015 to December 2015, patients undergoing CT for EVAR surveillance had a 3D-US scan performed on the same day. CT and 3D-US data were measured using a manual segmentation technique. Measurements were repeated at 30 days to investigate the intra-operator reliability of CT and 3D-US measurements. A second blinded operator repeated both CT and 3D US measurements to investigate inter-operator reliability. Results were assessed using Pearson's correlation and Bland-Altman plots.

**Results:** The technical success of 3D-US was 90% (20/22 patients). There was a significant difference (mean 13.64ml) between 3D-US and CT measurements. There was no significant difference between the 3D-US intra-operator measurements with a mean difference of 2.17ml. However, there was a significant difference between the inter-operator measurements (mean 6.89ml).

**Conclusion:** There was a significant difference in AAA volume measured on CT and 3D-US with a mean difference of 13.64 ml. Intra-operator variability was acceptable, but improvements are needed to enhance inter-operator accuracy. This may be achieved by further software features to define the site of maximal diameter and placing of a central-luminal line. The impact of image acquisition by different operators also needs to be assessed in future work.



## 8.2 INTRODUCTION

Aortic volume measurements have been shown to provide earlier evidence of aneurysm shrinkage after EVAR compared to diameter<sup>82</sup> but until recently have relied on CT scanning. 3D-US offers the possibility of volumetric measurements without the well-known drawbacks of CT. A number of studies have been performed recently comparing a variety of 3D-US approaches to CT, demonstrating variations in accuracy and reproducibility.<sup>170, 197</sup> In principle, using a freehand 3D-US approach should allow a greater proportion of the AAA to be imaged, rather than the fixed volumes that are acquired using matrix or mechanical transducers. Previous work (Chapter 7) using magnetically tracked 3D-US to measure AAA volumes in patients awaiting repair demonstrated unacceptable accuracy when compared to CT. Although intra-operator reliability was favourable, there were significant differences in inter-operator measurements.

Optically tracked 3D-US is inherently more accurate than magnetic systems as there is no interference from metallic objects. Scanning patients post-EVAR is likely to reduce the pulsatility of the vessel and application of tracking filter in image processing may also improve results. The aim of this study was to compare the accuracy and reliability of an optically tracked 3D-US system for measurement of AAA volume in patients post-EVAR, compared with CT.

## 8.3 METHODS

Patients due to undergo CTA for follow up after endovascular aneurysm repair were identified from clinical and radiology records. The study was approved by the hospital Research and Development department and the National Research Ethics Committee (13/NW/0468). Patients attended for 3D-US on the same day at the CTA or as close to the same date as possible.

### ***CT Angiography***

CT scans were performed on 128-slice Siemens SOMATOM® Perspective scanner (Siemens Medical, Munich, Germany). Scans were contrast enhanced (100ml 4ml/sec Omnipaque 300) and acquired from the aortic arch to the common femoral arteries. Image acquisition was triggered on contrast enhancement in the distal aortic arch. Images were reconstructed at a nominal slice thickness of 1mm.

### ***3D-US***

All ultrasound examinations were performed using a Phillips iU22 ultrasound console (Phillips, Amsterdam, Netherlands) using a C5-1 curved array transducer. A prototype optical tracking system was used (Piur imaging GmbH, Vienna, Austria) consisting of an infrared tracking camera and a C5-1 transducer modified with matt tracking spheres (Figures 9-11). The infra-red light emitted by the camera is reflected by the spheres and detected by the camera. This allows the US frames to be given x,y,z co-ordinates and a time stamp allowing reconstruction of the 2D ultrasound frames into a 3D volume. All acquisitions were performed by an accredited vascular scientist with specific training in 3D scanning of AAAs for the purpose of this project. During a breath-hold to limit movement artefact, the 3D volume was acquired starting at the most proximal extent of the AAA that could be visualised. The transducer was then steadily moved inferiorly keeping the AAA central in the scanning field to the most distal point the AAA could be imaged.

The paired 3D-US and CTA data were exported to and analysed using the software package 'ImFusion Suite' (ImFusion GmbH, Munich, Germany), capable of handling both CT and ultrasound images. In an attempt to improve accuracy, in this study a tracking filter was applied to the 3D-US data prior to volume reconstruction. Because of tracking inaccuracies, there is usually a jitter in the transformation information, which induces artefacts in the volume reconstruction. Therefore, accuracy may be improved by smoothing both the translation and rotation parameters. The width of the filter was set to five so each parameter is replaced by the average of itself and its two preceding and succeeding neighbours. This removes outliers and noisy

information resulting in artefacts in the resulting volume (Figure 54). In addition to the increased inherent accuracy of optical tracking, it was hypothesised that application of this filter may improve accuracy of the 3D reconstruction compared to the approach used in the previous study (see chapter 7).

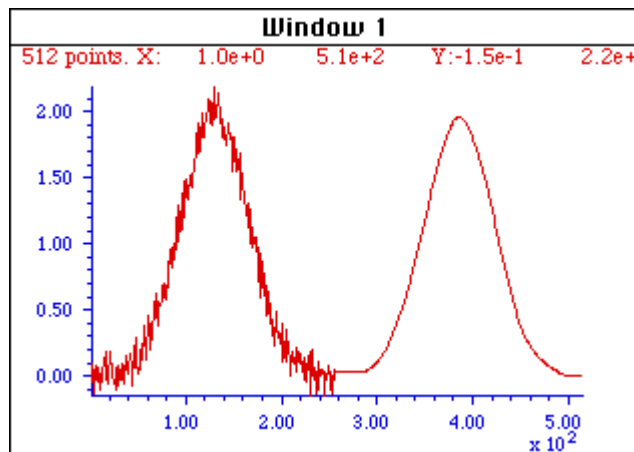


*Figure 54: Graphical representation of noise and artefact reduction on application of a tracking filter.*

As detailed previously, 3D-US did not consistently visualise landmarks from which to start and end measurement (e.g. renal arteries, aortic bifurcation) and the volume of the AAA that could be imaged in each patient varied (due to bowel gas and body shape) the starting point for segmentation was determined as follows:

The axial section of both datasets was scrolled through to define an approximate maximal diameter. Orthogonal views were then obtained in each imaging plane. The section with the largest orthogonal diameter on inner-to-inner (ITI) measurement was defined as the starting point for the segmentation process.

A manual segmentation tool was utilised as previously described. To briefly review, Spline points were manually placed on the inner vessel wall in both data sets at 1mm slices (figure 26), 20mm proximal and 20mm distal to the maximal orthogonal AAA diameter. This defined a 'partial AAA volume' of 4cm. Once the splines were placed, the software automatically calculated the volume in the defined region by converting the spline points into a surface mesh. Again, a 'partial AAA volume' of 4cm was utilised as a trade-off between the time taken to perform the manual segmentation and having a standardised dataset. Also, due to decreased image quality in the outer range of the acquisition, it would be impossible to choose a longer distance in a number of patients.

For comparison with CT, a single operator performed measurements on both the CT and 3D-US. Previous work (see chapter 7) has demonstrated adequate reproducibility of CT measurements of AAA volume using this method. To assess intra-operator variability of 3D-US measurements, volume measurements were repeated on both datasets in random order at least 30 days apart. For assessment of inter-operator variability of 3D-US, a second operator with experience of these methods duplicated measurements on the same 3D-US dataset.

### ***Statistics***

Differences between operator measurements for each modality were analysed using a one-sample T-test. The volume measurements from 3D-US and CT were compared using Bland Altman plots, where the differences in concurrent measurements on the same subject are plotted against the mean outcome, showing the mean difference and the upper and lower limits of agreements given by the mean  $\pm$  (1.96 x standard deviation (SD)). Analysis was performed using SPSS statistics v20 (IBM Corp. Armonk, NY, USA).

There is no defined threshold for the accuracy of US volume measurement of AAA. Therefore, the approach described by Bredahl was used.<sup>170</sup> As the accepted inter-

operator variability for 2D US diameter measurements is  $\pm 5\text{ml}$ , an 'imaginary cylinder' was calculated for each measured volume. The diameter was then changed by 5mm and a new volume calculated. This gave the acceptable variation in measurement for each measured volume. For example, for a measured partial volume of 165ml the diameter of the imaginary cylinder is  $2 \times \sqrt{(\text{vol}/\pi \times \text{length})} = 73\text{mm}$ . Increasing this diameter by 5mm yields a new volume of  $r^2 \times \pi \times \text{length} = 191\text{ml}$ . Therefore if the range of variability for a partial volume of 165ml exceeds 26ml, the variation exceeds the currently accepted variation in 2D diameter measurement.

#### **8.4 RESULTS**

From March 2015 to December 2015 22 patients were recruited. The technical success of 3D US was 90% as two patients had inadequate image quality (obesity or bowel gas). Of the 20 patients suitable for analysis 17 male with a mean age of 81.

##### *Volume estimation by 3D-US (optical) vs. CT*

The differences in measured volume were calculated and plotted against the mean. There was high correlation between CT and 3D-US (optical) measurements of AAA volume (Pearson's correlation 0.95,  $p < 0.01$ ) (Figure 55). However, when statistically compared, there was a significant difference between the volume measurements on 3D-US and on CT. The mean difference was 13.64ml and the limits of agreement 44.8ml to -17.6ml (Figure 56).

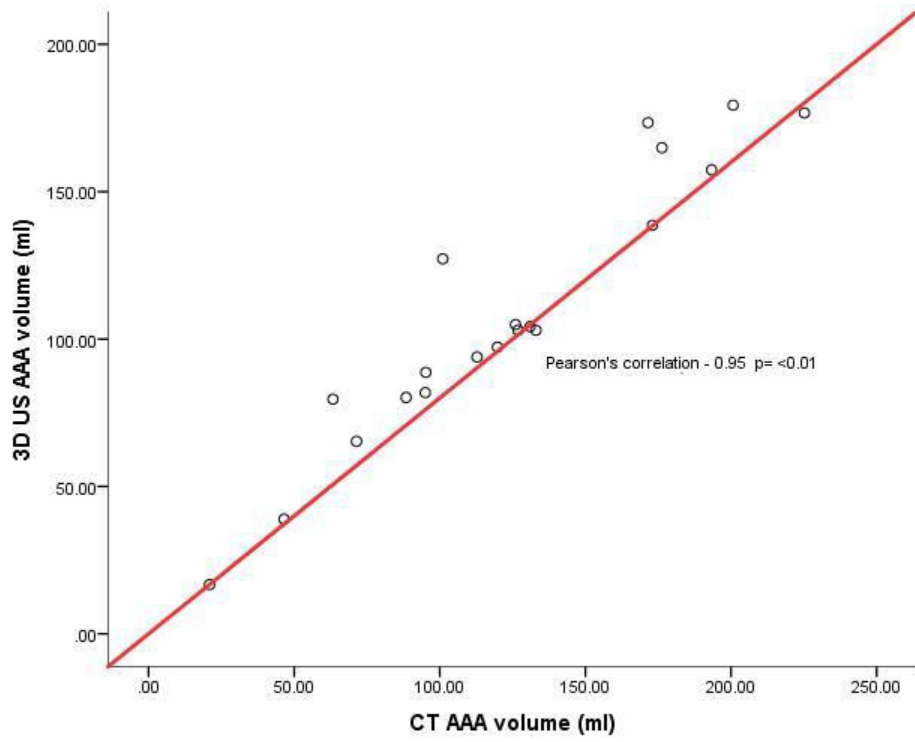


Figure 55: Correlation between CT and 3D-US (optical) AAA volume measurements

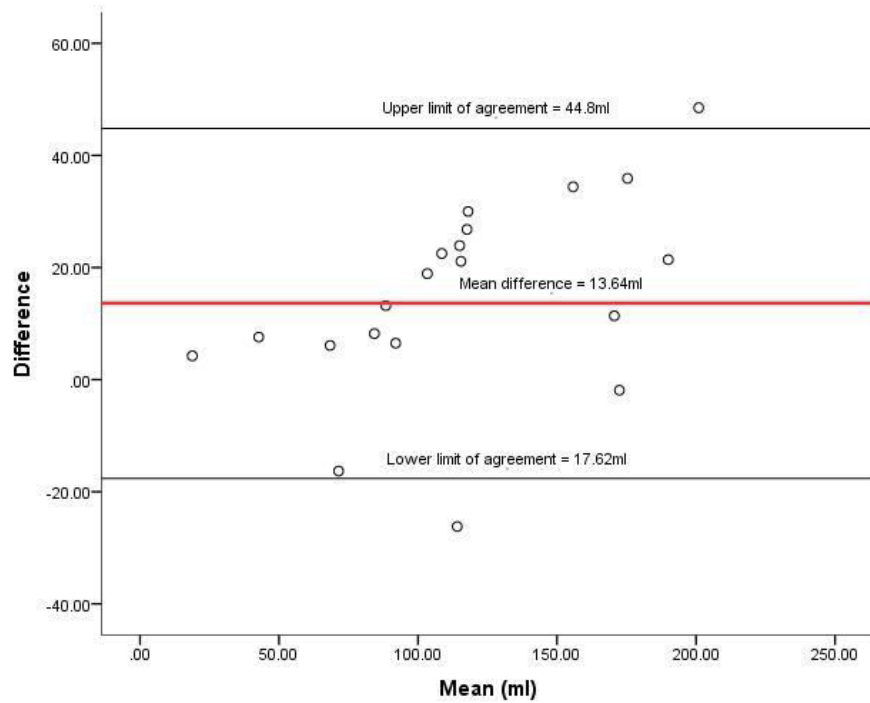
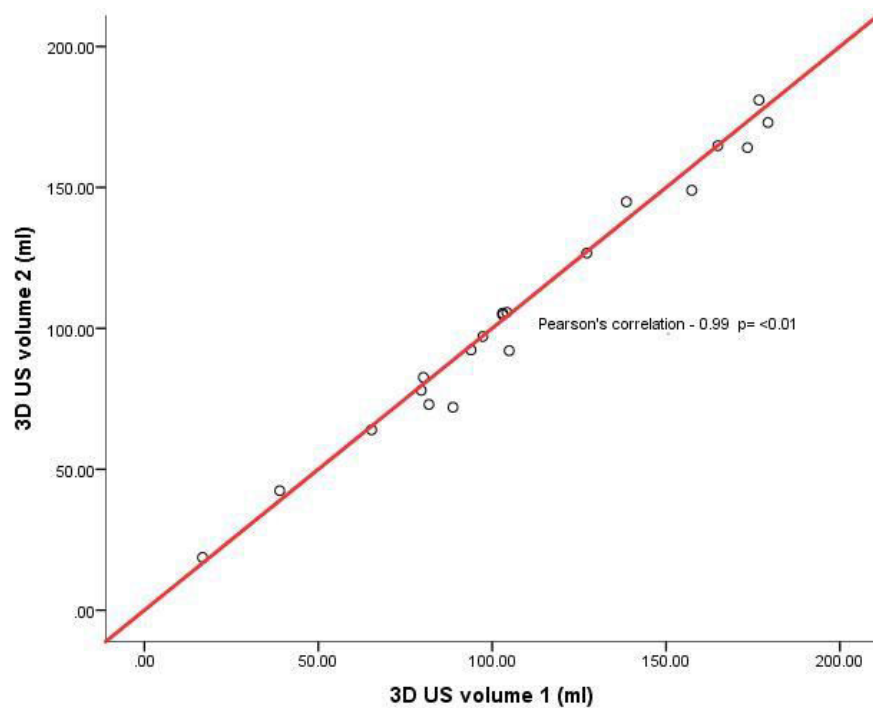


Figure 56: Bland-Altman plot of CT vs 3D-US (optical) measurements of AAA volume.

*Reproducibility of 3D US (optical) AAA volume measurements – Intra-operator*

There was no statistically significant difference between the intra-operator measurements of AAA volume for 3D-US (optical). The mean difference was 2.17ml with limits of agreement 14.2ml to -9.9ml (figures 57-58). There was high correlation (Pearson's correlation 0.99,  $p = <0.01$ ). The 3D-US intra-operator variability remained within the range of volume variability that was estimated on the basis of currently accepted diameter measurements (Table 10).



*Figure 57: Correlation between CT and 3D-US (optical) AAA volume measurements.*

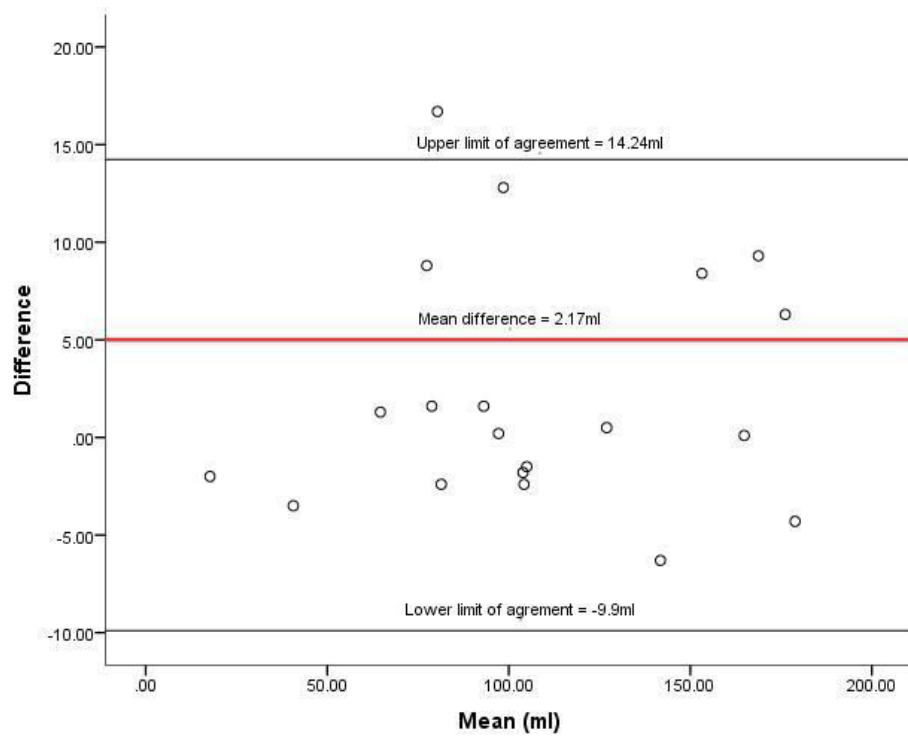


Figure 58: Bland-Altman plot of intra-operator 3D-US (optical) measurements of AAA volume.



*Table 10: Intra-operator variability of AAA volume measurements using 3D-US (optical) are within current acceptability of 2D-US diameter measurements using ‘phantom cylinder’ method.*

US volume 1 (ml)	US volume 2 (ml)	Intra-operator difference (ml)	Error considered acceptable +/- (ml)
173.4	164.1	9.3	22.6
65.3	64	1.3	13.2
93.9	92.3	1.6	19.2
81.8	73	8.8	13.2
138.6	144.9	-6.3	21.4
103	104.8	-1.8	17
38.9	42.4	-3.5	11.3
88.7	72	16.7	16.9
179.3	173	6.3	24.2
157.4	149	8.4	22.6
97.3	97.1	0.2	18.1
79.6	78	1.6	16.4
127.2	126.7	0.5	22.5
80.2	82.6	-2.4	17.8
176.7	181	-4.3	19.3
104.2	105.7	-1.5	16.5
104.9	92.1	12.8	18.6
103	105.4	-2.4	18.5
16.7	18.7	-2	7.9
164.9	164.8	0.1	21.1

*Reproducibility of 3D US (optical) AAA volume measurements – Inter-operator*

There was a statistically significant difference between the inter-operator measurements of AAA volume for 3D-US. The mean difference was 6.89 ml with limits of agreement 23.6 ml to -9.88 ml (Figure 59). There was high correlation (Pearson’s correlation 0.98,  $p < 0.01$ ) (Figure 60). The 3D-US intra-operator variability remained within the range of volume variability that was estimated on the basis of currently accepted diameter measurements (Table 11).

*Table 11: Inter-operator variability of AAA volume measurements using 3D-US (optical) are within current acceptability of 2D-US diameter measurements using 'phantom cylinder' method.*

<b>US volume operator 1 (ml)</b>	<b>US volume operator 2 (ml)</b>	<b>Inter-operator difference (ml)</b>	<b>Error considered acceptable +/- (ml)</b>
173.4	160	13.4	22.6
65.3	63	2.3	13.2
93.9	83.5	10.4	19.2
81.8	78.9	2.9	13.2
138.6	143	-4.4	21.4
103	114	-11	17
38.9	36.3	2.6	11.3
88.7	73	15.7	16.9
179.3	158	21.3	24.2
157.4	158	-0.6	22.6
97.3	90	7.3	18.1
79.6	80.8	-1.2	16.4
127.2	109	18.2	22.5
80.2	78	2.2	17.8
176.7	171	5.7	19.3
104.2	87.9	16.3	16.5
104.9	95	9.9	18.6
103	96	7	18.5
16.7	15.8	0.9	7.9
164.9	146	18.9	21.1

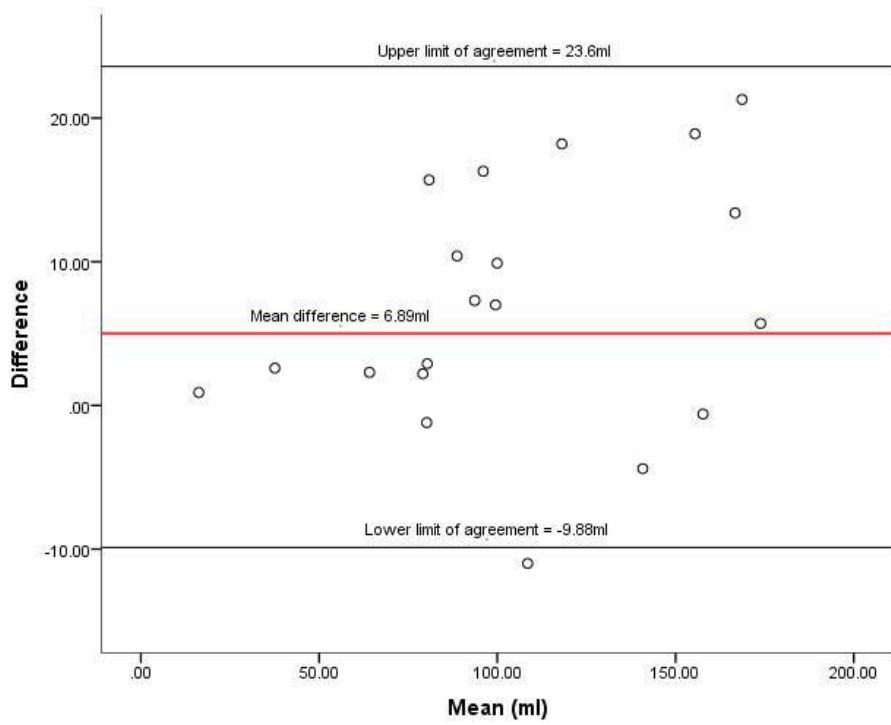


Figure 59: Bland-Altman plot of inter-operator 3D-US (optical) measurements of AAA volume.

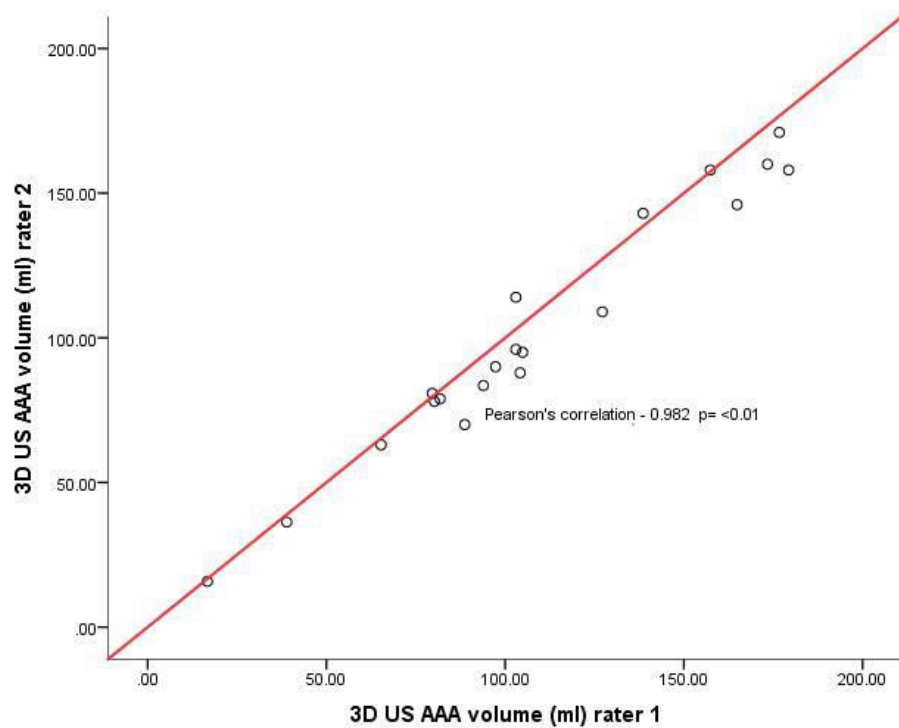


Figure 60: Correlation between inter-operator 3D-US (optical) measurements of AAA volume

## 8.5 DISCUSSION

This study compared measurements of AAA volume in post-EVAR patients using an optically tracked 3D-US system with CTA. The results show that there remains a statistically significant difference in the volumes measured by 3D-US when compared to CTA with a mean difference of 13.64ml. This is in comparison to a mean difference of 25ml in the previous study using magnetic tracking (Chapter 7) in patients with untreated AAAs. Changes to the methodology of this study using optical tracking, applying a tracking filter and scanning post-EVAR patients offer possible explanations for these improvements. However, it is difficult to separate out the individual contributions of each factor entirely. As the tracking-filter function is applied manually in post-processing and before 3D reconstruction, repeating the measurements without applying this step would provide insight into its importance. Optical tracking is widely thought to be more accurate than magnetic tracking<sup>175</sup> and in our recent experience has out-performed the magnetically tracked system for measuring volumes in an *ex vivo* porcine aorta model (currently unpublished data). An ideal experiment would be to scan the same post-EVAR AAAs with both 3D-US systems to validate this *in vivo*. This was the original intention of the research team, however, the calibrated tracking sensor mountings on the transducer for the magnetic system failed when being used for another project. Technical support for the magnetic system was no longer available and the transducer could not be re-calibrated.

The effects of the stent-graft in reducing or eliminating AAA pulsatility is likely to be the most significant reason for the improvement in accuracy. Maximal AAA diameter is known to vary throughout the cardiac cycle with a mean difference of 1.94mm (range 0-4.7mm) between systole and diastole.<sup>199</sup> In the initial study using magnetic tracking and untreated AAAs, there was clearly more motion artefact evident in the 3D reconstruction than observed in the present study. At this point, the optical system was not available to reproduce results. Again, the original plan was to compare the performance of both magnetic and optical tracking in measuring AAA volume in post-EVAR patients but the technical failure of the magnetic system made this impossible.

When compared with contemporary studies on 3D-US AAA volume measurements in post-EVAR patients the accuracy achieved in this work is comparable with the work by Arsicot (mean difference 12.75ml CT vs. 3D-US)<sup>197</sup> but some way behind that from the Copenhagen group (mean difference 1ml CT vs.3D-US).<sup>170</sup> Bredahl reports a method where the maximal aortic diameter on CT and 3D-US is automatically defined by a software algorithm using a central luminal line, which lead to a high level of reproducibility and accuracy in both the measurement of AAA volume and maximal diameter. Arsicot defined the start of the measurement by loss of parallelism of the aortic wall and a diameter >30mm.

The use of CTA as the 'gold standard' in this work is in line with previous studies.<sup>168-170, 197, 200</sup> The first work on CT AAA volume measurements post-EVAR was completed by Wever in 2000,<sup>164</sup> Prinssen<sup>82</sup> in 2005 and Hahne<sup>84</sup> in 2012. Each uses different CT protocols and post processing/segmentation approaches. However, the accuracy of the CT volume methods used in any of these studies has not been established in any published work. Such validation would require scanning a suitable phantom with a known volume, (e.g. determined by water displacement) with both CT and 3D-US.

Similar difficulties in achieving acceptable inter-operator reliability were experienced in this study as in Chapter 7. As previously discussed, the variation seen in the inter-operator measurements on 3D-US could stem from differences in defining the same starting point for measurement. Due to image quality it can be difficult to orientate the MPRs appropriately and ensure orthogonal measurements. There will also be variation in the measurements taken to determine the maximal aortic diameter. In addition, how the observers accommodate for loss of definition of the lateral walls, and image artefacts (such as speckle artefact) will affect how the splines are placed and the reproducibility of the results. The work by Bredahl used a semi-automatic segmentation where the maximal aortic diameter was defined by the software orthogonal to a central-luminal line.<sup>201</sup> They then measured a volume 3cm proximal and distal to this. Automatic vessel detection and segmentation tools are available in the ImFusion software, but are designed for 3D-US datasets of relatively liner vessels such as the long saphenous vein and the carotid artery. Attempts at applying them to AAA datasets was unsuccessful. In addition, the interactive segmentation tool used in

other studies in this work did not allow for accurate definition of the start and end points. Further software development is therefore needed to produce an appropriate tool.

Although the correlation was not strong, there is a relationship between increasing AAA volume and the difference in CT and 3D-US measurements (Pearson's correlation 0.61  $p < 0.01$ , Figure 61).

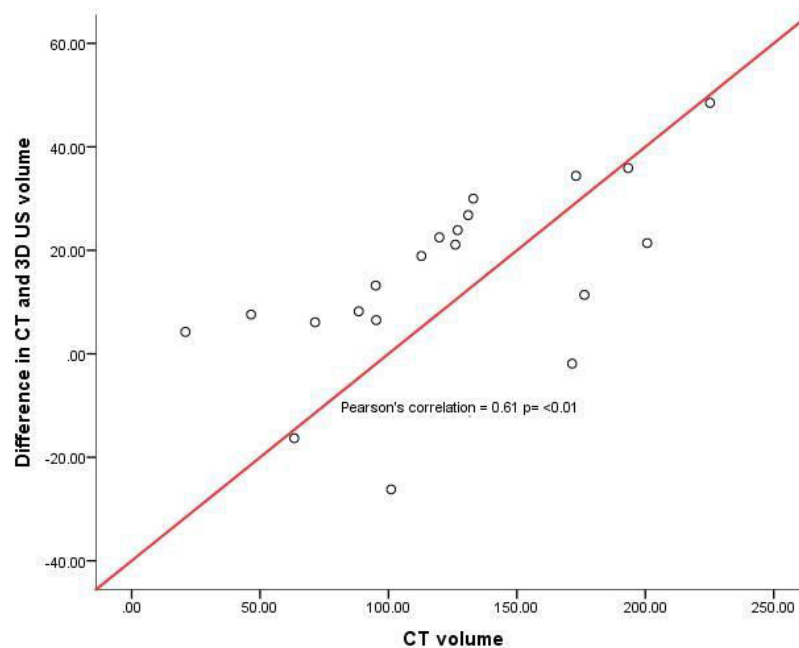


*Figure 61: There is a moderate correlation between increasing AAA volume and the absolute difference between CT and 3D-US measurements.*

This would be expected as any difference in the placement of splines will be magnified with increasing diameter. Given this, it is possible that a correction factor could be applied to reduce this error based on the size of the aneurysm. However, when the difference is expressed as a percentage of the 'true' AAA volume there is no significant correlation and there is clustering between 0-23ml (Figure 62).

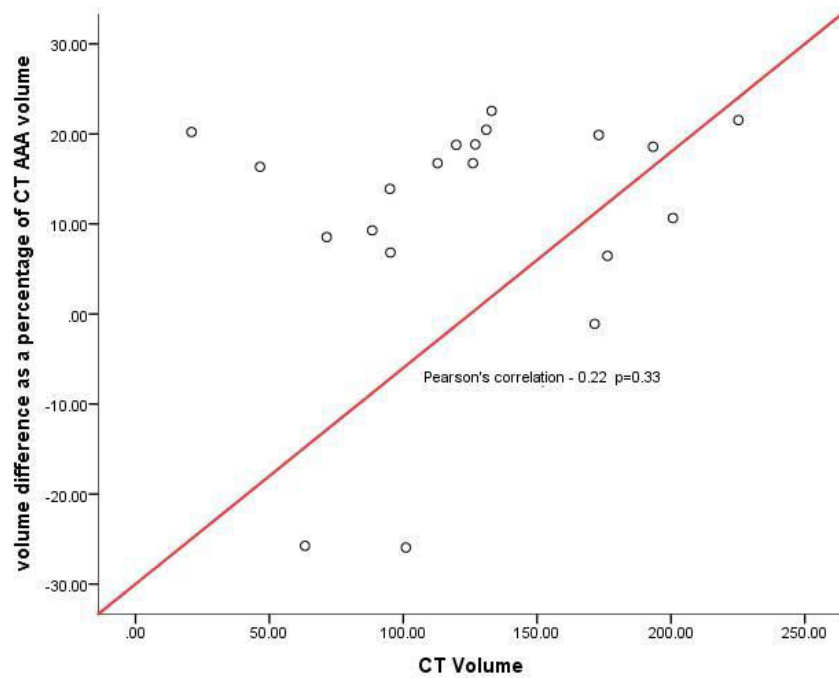


*Figure 62: Weak correlation between increasing AAA volume with difference in 3D-US and CT measurements expressed as a percentage of AAA volume.*

An alternative approach would be to examine the differences between measurements in relation to maximal AAA diameter. In this situation, there is only a weak correlation between increasing AAA diameter and the absolute difference between CT and 3D-US volume measurements (Pearson's correlation 0.36) and no correlation between increasing AAA diameter and the difference expressed as a percentage of the 'true' CT volume (Pearson's correlation -0.5). These relationships would be clarified by a greater number of patients, however, further work should focus on the accuracy of image acquisition and measurement rather than a correction factor.

It was hypothesised that using a freehand ultrasound system would allow measurement of a greater and more representative portion of the AAA than the 'partial' volumes described in other studies.<sup>170, 200-202</sup> This was true for most cases where the AAA could be imaged from neck to bifurcation. Factors such difficult anatomy, bowel gas and obesity often made this impossible in some patients. Furthermore, performing the manual segmentation was time consuming, taking

around 20-30 minutes per case depending on the AAA size. The use of a 4cm partial volume (2cm proximal and distal to the maximal aortic diameter) was selected as a trade-off between the time taken to perform the manual segmentation and having a standardised dataset. For this potential benefit of freehand 3D ultrasound to be realised and for clinical use, further development to at least semi-automate the measurements is required.

In this paper, the accuracy of measurement from a single 3D-US scans acquired by the same operator was assessed. This neglects any variation that could be introduced by different US operators. As US is operator dependent, perhaps a more robust methodology to assess the inter-operator reliability would have been to have two blinded operators perform a 3D-US scan on the same patient and independently measure their own scans. Such an approach has been taken by other authors.<sup>170</sup> However, this would have assessed the reliability of the whole process and made it increasingly difficult to ascertain where the differences in measurement stemmed from. Additionally, error is introduced in 2D AAA measurements by the different transducer orientations and plane selected by each operator. This is mitigated by 3D-US as these differences are accounted for by tracking of the transducer orientation. It is likely therefore that scans performed by different operators would not have affected the results to a significant degree.

As discussed in the previous paper, the clinical value of AAA volume measurements has not been completely elucidated, and how measurements will be affected by aneurysm re-configuration following EVAR is yet to be determined. If the accuracy of the AAA volume technique presented here can be made more accurate and less time-consuming, further studies could be performed on patients in EVAR surveillance to answer these questions.



## **8.6 CONCLUSIONS**

There was a significant difference in AAA volumes measured on CT and 3D-US with a mean difference of 13.64 ml. The optical system out performed the magnetic system however differences in study design make meaningful comparisons difficult. Intra-operator variability was acceptable, but improvements are needed to enhance inter-operator accuracy. This may be achieved by further software features to define the site of maximal diameter and placing of a central-luminal line. The impact of image acquisition by different operators and the effects of AAA reconfiguration following EVAR need to be addressed in future work.

## **CHAPTER 9: THE FEASIBILITY AND CHALLENGES OF GENERATING AAA MODELS FOR BIOMECHANICAL ANALYSIS USING 3D ULTRASOUND**

### **Chapter contributors and role:**

#### **Institute of Cardiovascular Sciences**

**C Lowe:** conception, patient recruitment, CT and 3D-US analysis, manuscript writing.

**S Rogers:** 3D-US scanning

**Mr J Ghosh:** Co-supervisor

**Prof C McCollum:** Supervisor

#### **Imfusion GmbH**

**Dr W Wein:** Software development.

## 9.1 ABSTRACT

**Background:** The current use of a maximal aortic diameter of 5.5cm as an indication for AAA repair is unsatisfactory. There is increasing evidence that biomechanical analysis of AAAs using techniques such as CFD and FEA may be more accurate and patient specific for identifying when AAA repair is indicated. Current methods rely on CT to provide the AAA geometry for biomechanical simulation. This study investigates the feasibility of using 3D-US to provide AAA geometries for FEA and CFD analysis.

**Methods:** From August 2014 to March 2015 20 consenting patients undergoing CT for planning of AAA repair underwent 3D-US on the same day. Both the CT and the 3D-US data was exported to a workstation. Using an interactive segmentation technique, attempts were made to generate a geometrical representation of the AAA wall, intraluminal thrombus (ILT) and lumen. The results from each modality were compared to assess any would be suitable to take to the simulation stage.

**Results:** 20 patients were recruited to the study. There was significant variation in AAA anatomy. In three patients the quality of 3D-US data was too poor to attempt segmentation. Complete AAA wall geometries comprised of the neck, body and bifurcation were gained in only two patients on 3D-US. Only one 3D-US dataset was suitable for segmentation of the wall, ILT and lumen of the entire AAA.

**Conclusions:** Significant software and hardware developments are required to make this a feasible approach. Before CFD analysis is performed an additional smoothing step needs to be applied and the optimal method for this requires investigation. The results of CFD and FEA simulation using the optimal results from this study will be informative for the further development of this technique.

## 9.2 INTRODUCTION

The current use of a maximal aortic diameter of 5.5cm as an indication for AAA repair is unsatisfactory. Although it is clear that increasing AAA size increases the risk of rupture, small AAAs may rupture and large AAAs may not. The law of Laplace is inadequate to explain the forces contributing to AAA rupture as AAAs are not a simple cylindrical or spherical shape of uniform radius or curvature. There is increasing evidence that biomechanical analysis of AAAs using techniques such as CFD and FEA may be more accurate and patient specific for indicating when AAA repair is indicated.

The use of these techniques requires the geometry of the AAA to be extracted from CT scans by means of image segmentation techniques. Despite commercially available software able to perform both semi-automatic segmentation and subsequent biomechanical analysis, these methods have seen very limited uptake by the clinical community.<sup>124</sup> Reasons for this include lack of validation of such techniques, variation in modelling approaches and the lack of agreed or standardised thresholds for repair based on biomechanical parameters. In addition, as CT scanning is only indicated for treatment planning in patients with AAAs of 5.5cm or greater, CT data is not available for the key cohort of patients for whom this technique is relevant – those with ‘sub threshold’ AAAs who may be at greater risk of AAA growth and rupture as suggested simply by diameter. For the same reasons, there are no studies investigating how biomechanical indices such as wall shear stress and peak wall stress evolve during the growth of small AAAs and if they relate to AAA growth rate.

The key data supplied by CT scanning is the geometry of the AAA. Three-dimensional ultrasound (3D-US) has the potential to provide 3D AAA geometries for use in biomechanical analysis. This is a unique application of 3D-US and when compared to CT, is inexpensive and does not involve radiation or nephrotoxic contrast. If accurate AAA geometries can be produced using 3D-US they may be used in biomechanical analysis in the same way as CT, widening the applicability of this technique in both research and clinical environments.

As there can be little justification for not repairing large AAAs in patients fit for surgery, the main clinical utility of this approach would be to identify smaller AAAs at higher risk of rupture than based simply on diameter. Smaller aneurysms may be more suitable for EVAR with its associated reduction in mortality and increasing AAA size is predictive of stent-graft related complications. In addition, patients with AAAs of 5.5-6cm and with significant co-morbidities in who repair would usually be indicated may be found to be at lower risk of rupture than anticipated, allowing surgery to be safely deferred to allow optimization of co-morbidities or support a decision not to operate. Some patients who are at high surgical risk may decide not to undergo surgery if they have a 'lower-risk' AAA. Furthermore, there is no research on how PWS evolves during AAA growth or on whether this predicts growth, the need for repair, or risk of premature rupture. 3D-US has no known risks, is inexpensive and could make biomechanical analysis available to thousands of patients on AAA surveillance and would open up new research opportunities on the development and growth of AAAs.

The aim of this study was to examine the feasibility and identify the challenges of generating 3D AAA models using 3D-US as source data.

### **9.3 METHODS**

#### ***Patients***

Twenty patients at University Hospital South Manchester undergoing CTA for planning of AAA repair or who were in AAA surveillance and had an incidental CT scan for other reasons were identified via the radiology department and gave informed consent.

Ethical approval was granted by the National Research Ethics Committee (13/NW/0468).

### ***3D-US scanning***

3D-US data was acquired using a Phillips IU22 ultrasound console (Phillips, Amsterdam, Netherlands) using a C5-1 curved array transducer. In an attempt to optimise image quality by increasing the frame rate, the sector width was reduced as far as possible and the focus set at the posterior wall of the AAA. An electromagnetic tracking system (Ascension, Vermont, USA) comprising of a field generator and two tracking sensors that attach to the ultrasound probe, is used together with a 3D guidance software. The positional information generated by the movement of the sensors in the magnetic field allows the system to orientate the US probe in time and space. This positional data allows the 2D-US frames to be assembled into a 3D volume.

Patients were not routinely fasted. With the patient lying supine and during a breath hold, the 3D dataset was acquired by moving the transducer along the aorta from the level of the renal arteries to the aortic bifurcation. In the event the renal arteries or bifurcation could not be seen, the acquisition was from the most proximal to the most distal section that could be visualised. All scans were performed by the same vascular scientist with experience of 3D-US. Patients were scanned a number of times acquire the best possible images, with a mean scanning time of 12 minutes.

### **CT scanning**

CT angiography was performed using a 128-slice Siemens SOMATOM Perspective scanner (Siemens Medical, Munich, Germany). Patients were positioned supine and images at 1mm slices were acquired from the aortic arch to the femoral heads. Arterial phase images were acquired as per protocol using a bolus dose of 100 mL of the iodinated contrast medium Omnipaque 240 (GE Healthcare, UK) administered at a flow rate of 3 mL/s.

CT in DICOM format and 3D-US data were exported to prototype analysis software able to perform segmentation on both datasets (ImFusion Suite, ImFusion GmbH, Munich). It was anticipated that for each AAA the lumen, intraluminal thrombus and

wall could be segmented to create surface meshes suitable to export into software for biomechanical analysis.

### ***Image segmentation***

An interactive segmentation algorithm was used within the ImFusion Suite software. This process is covered in detail in Chapter 4.5. Briefly, in both CT and 3D-US datasets the user places 'seeds' inside and outside of the structure to be segmented. For example, when segmentation of the wall was performed, green seeds are placed inside the AAA wall and red seeds outside the wall. The 'inside' and 'outside' regions are then propagated and defused in the whole image, defining the wall from the surrounding structures.<sup>186</sup> Other structures of the AAA (e.g. lumen, thrombus) can also be segmented in the same way. Errors in the segmentation were manually corrected by placing more seeds and the algorithm re-run to produce an optimal result, as determined by the operator. The ImFusion software then uses a marching cube algorithm to convert the contours generated by the segmentation into a surface mesh that can be exported as a stereolithography (STL) file.<sup>187</sup> Time taken for segmentation varied depending on image quality, complexity of the anatomy and which structure within the AAA was being segmented. For the AAA wall, the median time taken for segmentation was 21 minutes for CTA and 32 minutes for 3D-US.

For improved visualisation following segmentation, the STL files were imported into the mesh preparation software 3Matic (Materialise, Belgium).

## **9.4 RESULTS**

20 patients were recruited to the study. Median AAA size was 6.25cm (4.3 – 8.5cm). Mean body mass index (BMI) was 26.3 kg/m<sup>2</sup>. The AAA wall models are shown in Figure 63. There was significant variation in AAA anatomy as demonstrated by the CT derived models. There was significant variation in the completeness of the 3D-US derived models. The anatomical features retained for each patient are summarised in Table 12. In patients 5, 8 and 9 the quality of 3D-US data was too poor to attempt

segmentation. In patients 5 and 8 this was due to a combination of difficult anatomy and high BMI. Patient five had a 8.5cm saccular aneurysm and a BMI of 30 kg/m<sup>2</sup> while patient 8 had 7cm saccular aneurysm with a BMI of 28 kg/m<sup>2</sup>. Although patient 9 had 4.3cm aneurysm and a BMI of 25 kg/m<sup>2</sup> bowel gas prevented adequate visualisation (Table 13).

*Table 12: Main anatomical features seen in 3D-US models*

<b>Features</b>	<b>Patients</b>	<b>Total number</b>
Failed	5, 8, 9	3
Neck, body and bifurcation	10, 14	2
Neck and body	6, 11, 13, 16, 17, 19, 20	7
Body only	1,2,3,4,7, 18	6
Body and bifurcation	12, 15	2
		<b>20</b>

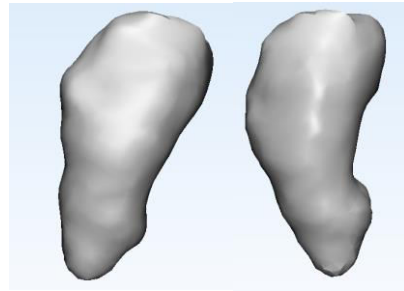
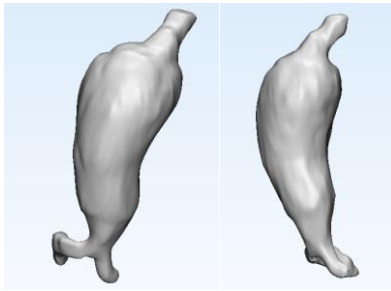
Luminal segmentation was possible in all 20 cases on CT due to the presence of IV contrast. Three AAAs (7, 11, 14) had no ILT. There was variation in the degree to which ILT could be clearly seen on 3D-US, making segmentation of the lumen possible using 3D-US in patients 10 and 12 only (Figure 64).

The most frequent problem was a failure to image the whole geometry of the AAA. There are a number of reasons why this was challenging. Firstly, visualisation of the proximal abdominal aorta was often impaired due to gas in the transverse colon or stomach. In addition, it was also difficult to image the proximal part of the AAA when it had a short infra-renal neck or was truly juxta-renal. Secondly, imaging of the bifurcation was difficult in some cases due to vessel depth and tortuosity such that the common iliac arteries ran posteriorly from the main body of the distal AAA and could not be kept within the scanning field. Bowel gas also made visualisation of bifurcation impossible in some cases.

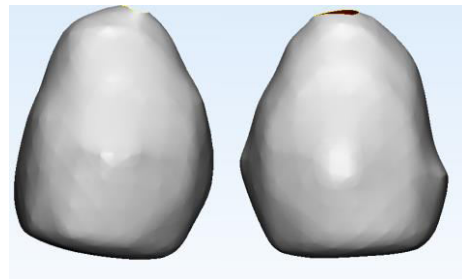
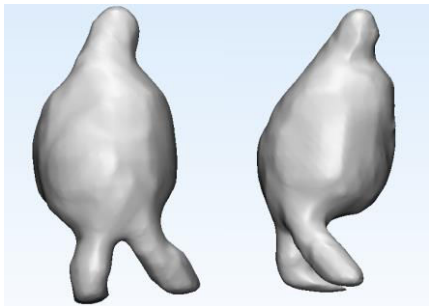


Figure 63: AAA wall geometries derived from CT (left) and 3D US (right)

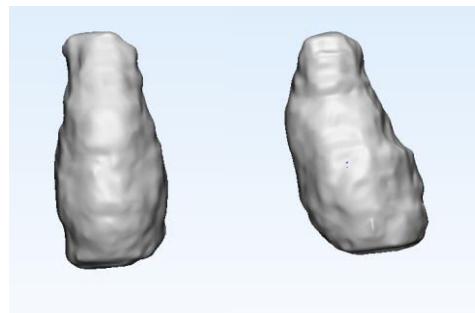
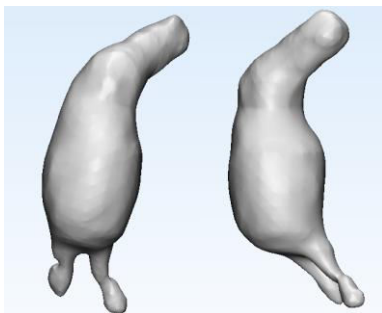
Patient 1



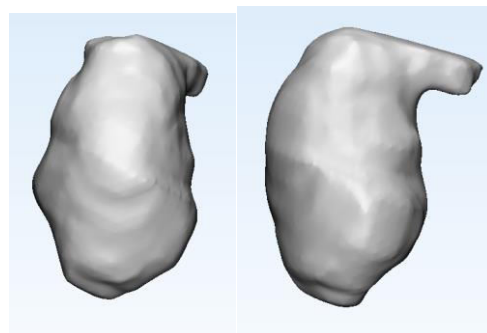
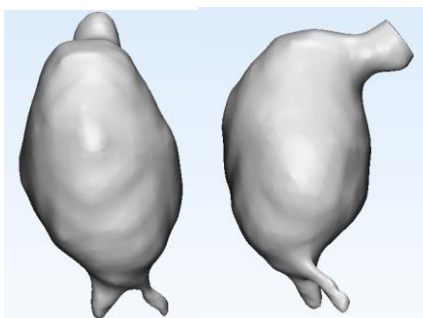
Patient 2



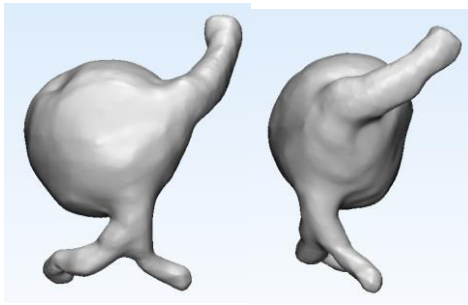
Patient 3



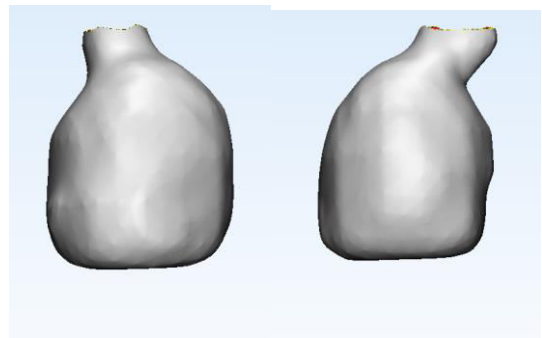
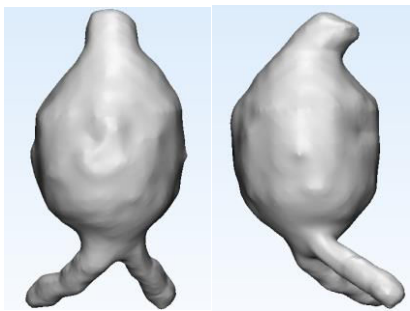
Patient 4



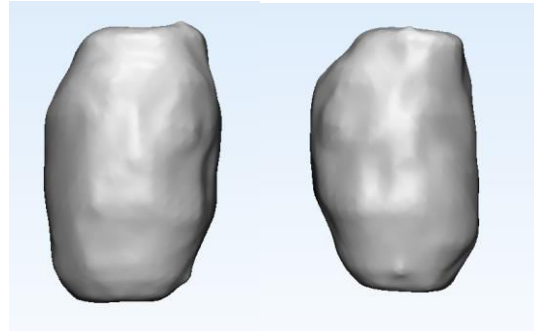
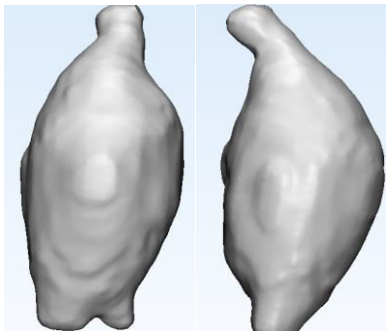
Patient 5



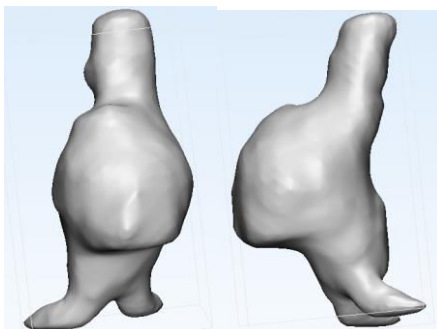
Patient 6



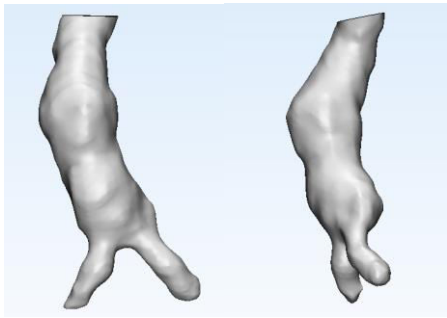
Patient 7



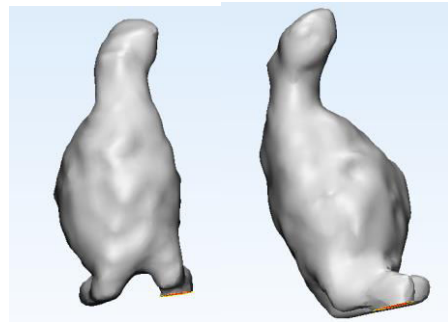
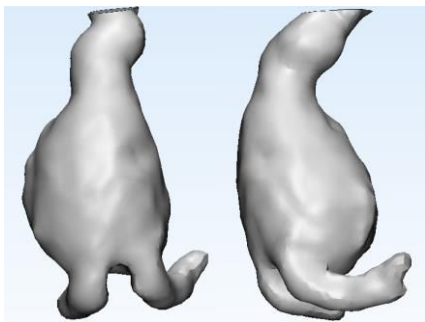
Patient 8



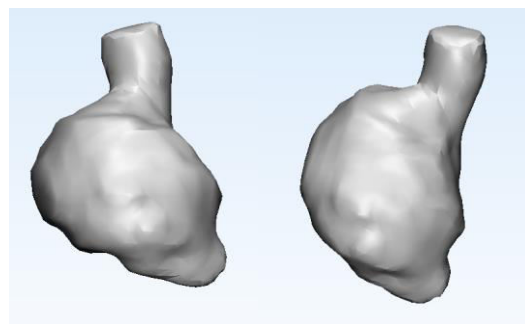
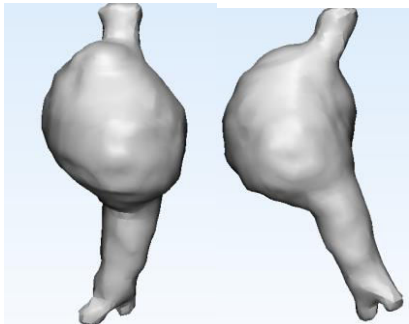
Patient 9



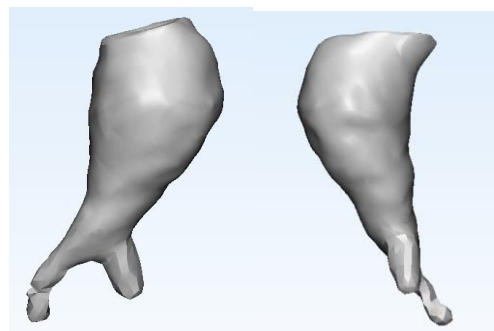
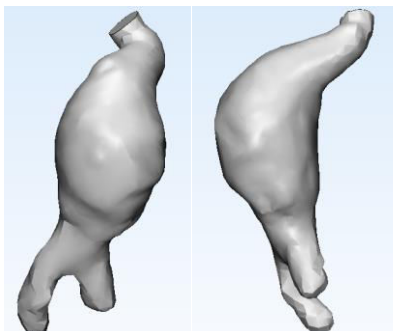
Patient 10



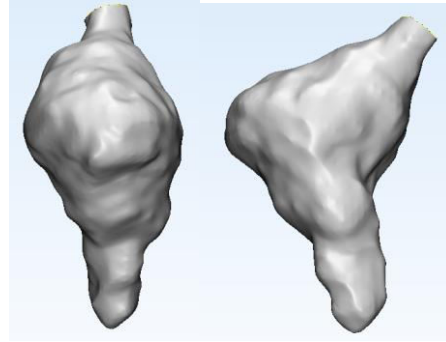
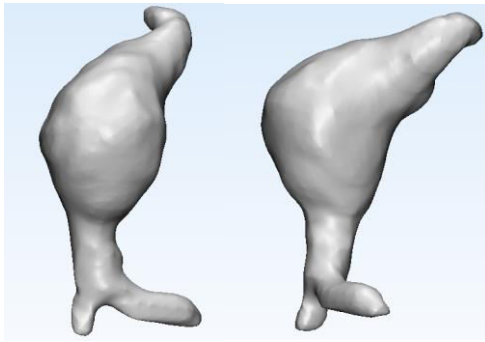
Patient 11



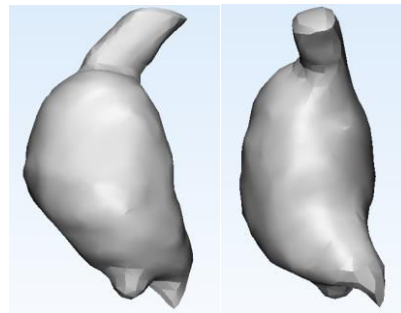
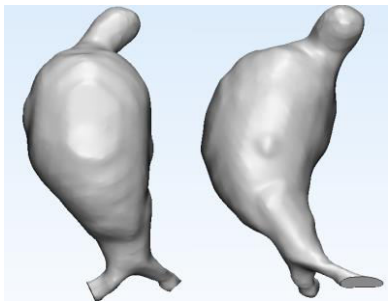
Patient 12



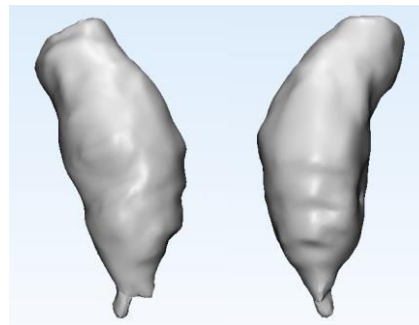
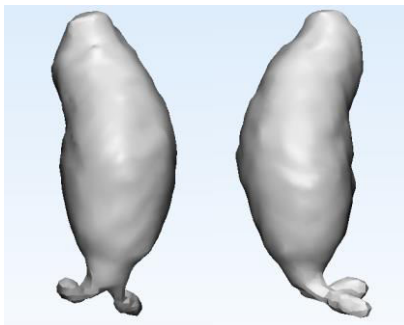
Patient 13



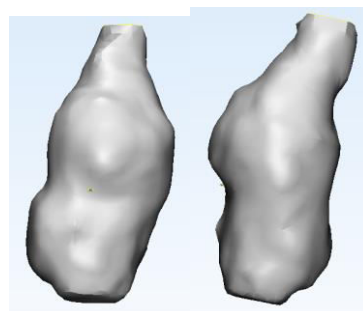
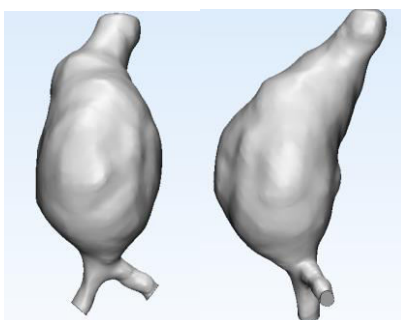
Patient 14



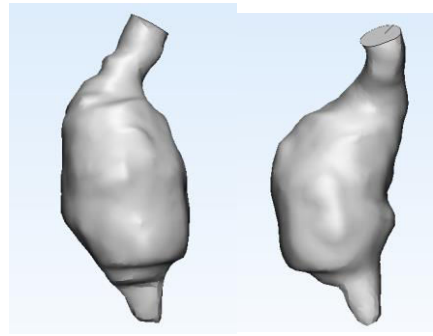
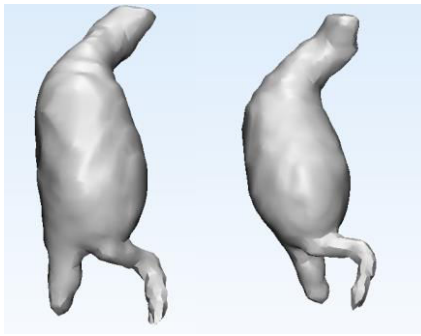
Patient 15



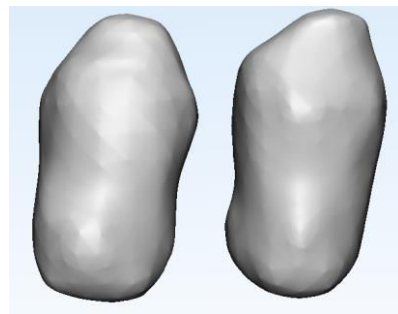
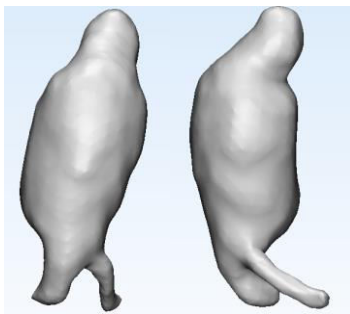
Patient 16



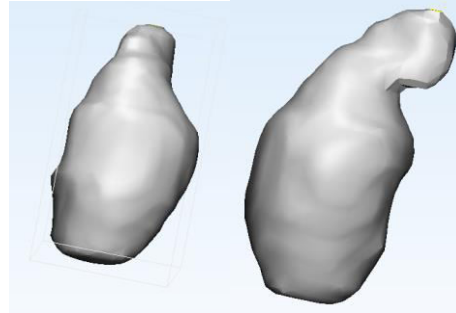
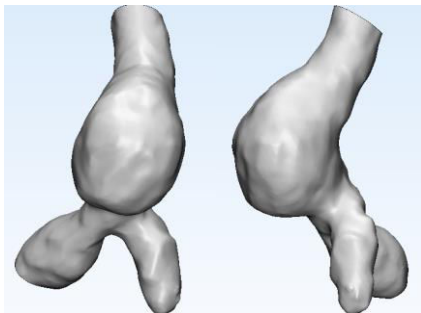
Patient 17



Patient 18



Patient 19



Patient 20

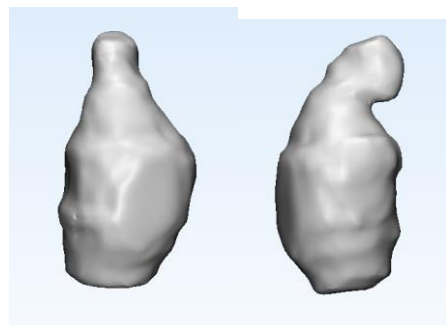
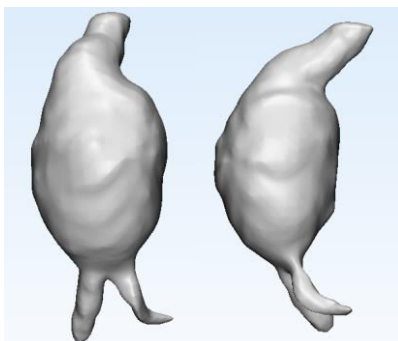
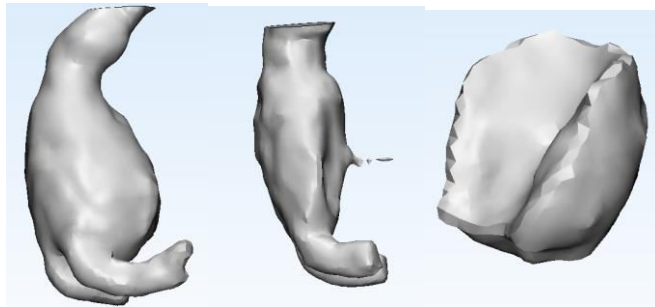
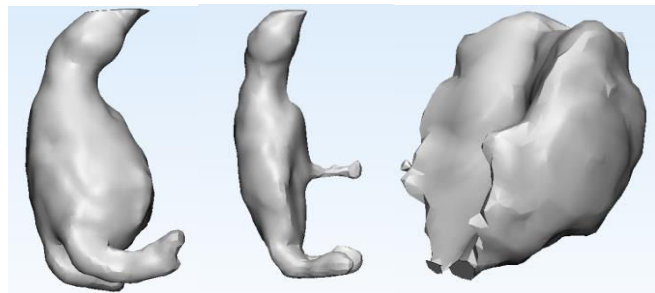


Figure 64: Segmentation of wall, lumen and thrombus (left to right)

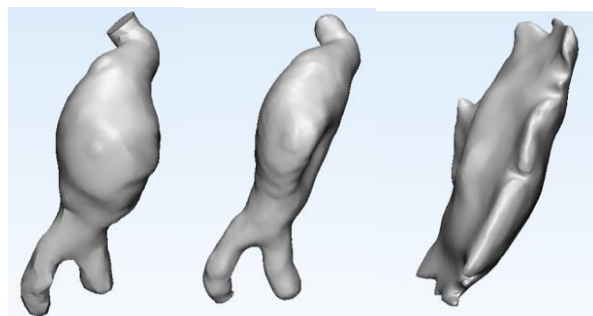
Patient 10 - CT



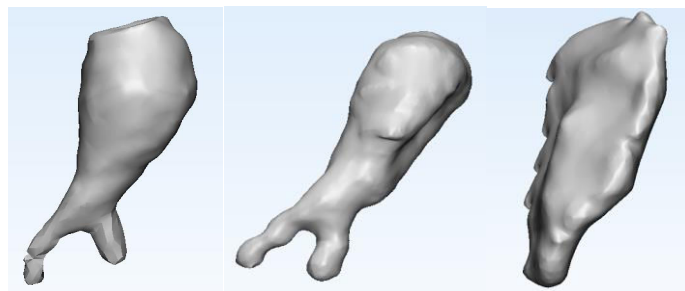
Patient 10 – US



Patient 12- CT



Patient 12 – US



Therefore, only patient 10 had the potential to supply complete geometries of the wall, lumen and thrombus for use in both CFD and FEA.

*Table 13: Maximal AAA diameter and body mass index (BMI) in the study group.  
Patients that failed geometry generation are highlighted in red.*

<b>Patient</b>	<b>Max AAA diameter (cm)</b>	<b>BMI (kg/m<sup>2</sup>)</b>
1	5.1	25
2	6.2	25.5
3	6.1	29.3
4	7.9	24.4
5	8.5	30
6	7.9	23
7	7.2	27.2
8	7	28
9	4.3	25
10	6.9	23.7
11	7.9	28.7
12	5.7	21.9
13	6.3	30.7
14	5.8	20.2
15	7.2	26.6
16	5.6	26.8
17	5.5	25.8
18	5.6	29.3
19	6.3	27.9
20	6.2	28.5

## 9.5 DISCUSSION

Biomechanical simulation of AAAs has been widely studied using CTA as the source data. This unique study evaluated the feasibility of generating geometries suitable for use in CFD and FEA using magnetically-tracked 3D-US and an interactive segmentation technique.

The results show that a number of technical problems currently prevent this from being a widely applicable technique. Complete technical success was achieved in only one case (5%). In a pilot study of 3D-US of 10 normal aortas, it was noted the abdominal aorta could be easily imaged from renal arteries to bifurcation in 90% of cases. In a further pilot study in patients with small AAAs under surveillance, technical success of scanning from the neck to the bifurcation was achieved in 80% of patients. Based on these results, it was anticipated that such an approach would also be feasible in patients with larger AAAs undergoing CTA for treatment planning.

Visualisation of the proximal AAA may be improved in future work by optimising patient positioning such as placing arms above the head or a break in the table. We did not routinely fast patients prior to imaging, given the inconsistent benefit seen on doing this for imaging of the mesenteric vessels. However, three patients were coincidentally fasted as they thought they should be for their subsequent CT scan. This did not appear to significantly improve image quality. It is possible that bowel gas may not have been present if the scan was repeated on a separate day. This was not feasible in this study as patients quickly went on to have surgery.

At least the main body of the AAA was visualised in 17 patients. However, the quality of the 3D reconstruction and the 3D-US derived models was highly variable. The ultrasound images were degraded in some cases, possibly due to vessel pulsatility and tracking inaccuracies. This meant that the software has difficulty in defining the wall of the AAA and required significant user input to make corrections. There are a number of potential ways this may be improved:

1. Optical tracking. Magnetic tracking is known to suffer from interference due to the effect of metal in the scanning field.<sup>175</sup> Use of an optically tracked system may improve results and the application of a tracking filter as described in section 8.3 would help improve accuracy – this feature was not available during recruitment to this study.



2. A method of mitigating vessel pulsatility. As previously discussed, ECG gating is technically challenging as it would require US data to only be acquired at a specific point during the cardiac cycle. This would make the acquisition/scanning time unacceptably long. A second option would be to perform a longer acquisition, for example, over 10 seconds. This would create a large dataset. A software algorithm could then be employed to discard US data at specific time points to provide US slices at the same point in the cardiac cycle.
3. Upgrading of US unit. The IU22 system has now been superseded by the next generation of industry-standard US scanners. These systems offer improved image resolution and quality.
4. Optimisation of scanner settings and transducer. As described in the methods, number measures were taken to try and optimise image quality. However, a number of 3D-US images lacked contrast between the inner and outer wall of the AAA to allow for improved segmentation. Increasing the gain setting as high as possible to provide as optimal definition will be important in future work.
5. Alternative method of vessel segmentation. The application of the segmentation method used in this project for both CT and 3D-US data is unique. In a recent study, a manual segmentation was used to generate 3D AAA models from 3D-US data.<sup>172</sup> This required extensive and time-consuming processing in complex software. A manual segmentation tool is available in the ImFusion suite. It involves manually placing spline contours in each image slice, similar to the process outlined in chapter 7 and 8. Once the splines have been placed, the software creates a surface mesh by interpolating between the contours (Figure 65). This process is not currently able to include the bifurcation, though such a facility is in development. Additionally, this method is very time consuming, taking around 60 minutes to place the required number of splines in the CT or 3D-US data. As the algorithm, essentially 'fills in the gaps' by connecting each spline contour, it creates a 'jagged' surface. Using

this method would also require a smoothing operation before the model could be prepared for simulation.

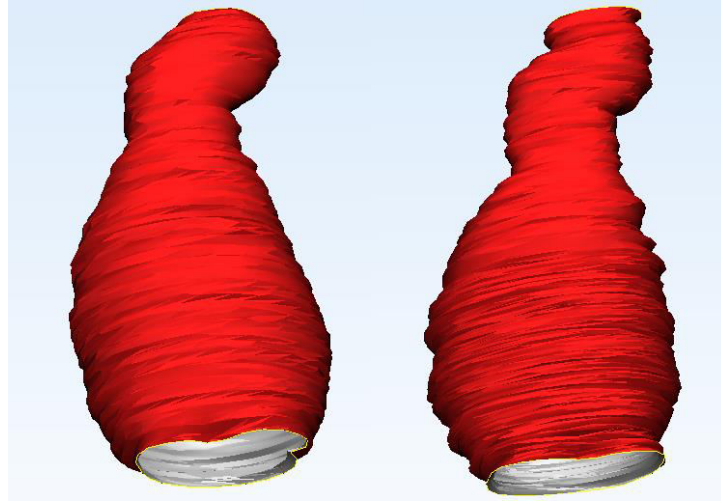


*Figure 65: Surface meshes of an AAA wall (left –CT, right– 3D-US) using the manual spline segmentation tool. The current software version is not able to include the bifurcation. Smoothing will be required.*

In the majority of cases, the flow lumen could not be adequately seen as the ILT could not be clearly defined. In a small number of patients, and after an ethical amendment was approved, a 2ml IV bolus of sulphur hexafluoride microbubble contrast was given. This demonstrated the lumen distinctly from the surrounding thrombus (Figure 66). Although promising, the analysis software was not optimised to process images from contrast-enhanced ultrasound and the results from segmentation were poor. Further development is needed to assess if this will be an effective method of producing a luminal geometry.

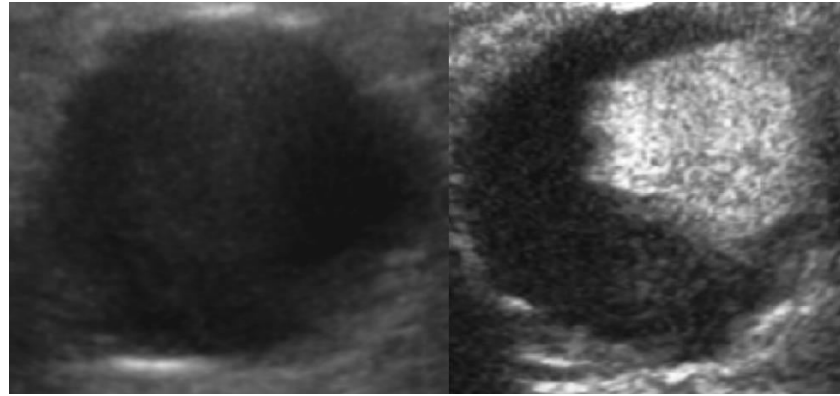


*Figure 66: Left – a US image of an AAA. The AAA contains thrombus but it cannot be distinguished from the lumen. Right – same site in the AAA after IV contrast. The lumen and thrombus are now well visualised.*

CFD simulation is by far the most demanding, as it requires the full luminal geometry – flow is heavily dependent on the neck and the bifurcation. For FEA, neglecting the iliac vessels from the simulation has been shown not to significantly alter wall stress distributions,<sup>97</sup> therefore it is possible that a greater number of 3D-US geometries may be suitable for FEA. In addition, as the main application of the 3D-US approach would be to identify patients with small AAAs at greater risk. This potentially means that the AAAs would be easier to image, and technical success may be higher.

## **9.6 CONCLUSIONS**

AAA geometry generation from 3D-US faces a number of significant challenges, but may be feasible with further methodological and technical development. Complete technical success of a complete wall, lumen and thrombus geometry from AAA neck to aortic bifurcation was achieved in only 5% of patients. Complex anatomy, particularly saccular and bi-lobed aneurysm configurations were the most challenging and lead to complete technical failure. Stomach and bowel gas obscuring the image proximally may be improved by fasting and improved patient position, though this has inconsistent results in the author's experience of renal and mesenteric scanning. Image quality may be improved by updating the US hardware and optimisation of

settings. An alternative segmentation method may be required for 3D-US data. Tracking accuracy may be improved by using an optical tracking system. It is possible that visualisation of the lumen and thrombus may be improved by the use of an IV contrast agent. Further mesh smoothing may need to be applied prior to CFD simulation. The results of CFD and FEA simulation using the optimal results from this study will aid further development.

## **CHAPTER 10: COMPUTATIONAL HEMODYNAMICS OF ABDOMINAL AORTIC ANEURYSMS: 3D ULTRASOUND VERSUS COMPUTED TOMOGRAPHY.**

### **Chapter contributors and role:**

#### **Institute of Cardiovascular Sciences**

**C Lowe:** conception, established collaboration, patient recruitment, CT and 3D-US analysis, manuscript writing.

**S Rogers:** 3D-US scanning.

**Prof C McCollum:** Supervisor.

#### **School of Mechanical Aerospace and Civil Engineering (MACE)**

**B Owen:** CFD simulation and analysis, manuscript writing.

**Dr N Ashton:** Assisted B Owen with CFD simulation.

**Dr P Mandal:** Supervision of B Owen.

**Dr A Revell:** Supervision of B Owen.

#### **Imfusion GmbH**

**Dr W Wein:** Software development.

*The contents of this chapter are reproduced with permission of Sage Publications.*

## 10.1 ABSTRACT

**Background:** The current criterion for surgical intervention in abdominal aortic aneurysms (AAAs), based upon a maximal aortic diameter, is considered conservative due to the high mortality rate in case of rupture. The research community is actively investigating the use of computational mechanics tools combined with patient specific imaging to help identify more accurate criteria. Widespread uptake of a successful metric will however be limited by the need for Computed tomography, which is at present the primary image extraction method on account of the location and complex shape of the aneurysms. The use of 3D ultrasound (3D-US) as the scanning method is more attractive on account of increased availability, reduced cost and reduced risk to patients.

**Methods:** The suitability of 3D-US is assessed for this purpose in the present work; Computational Fluid Dynamics simulations were performed on geometries obtained from the same patient using both Ultrasound and Computed Tomography (CT). The influence of different smoothing algorithms is investigated in the geometry preparation stage.

**Results:** The Taubin Low-Pass Filter was found to best preserve geometry features. Laminar, Newtonian, steady-state simulation analysis identified hemodynamic characteristics to be qualitatively similar in terms of Wall Shear Stress, Velocity and Vorticity.

**Conclusion:** The study demonstrates the potential for 3D-US to be integrated into a more accessible patient specific modelling tool able to identify the need for surgical intervention of AAAs.

## 10.2 INTRODUCTION

The pathogenesis of abdominal aortic aneurysms is complex. Inflammatory and proteolytic processes appear to be the dominant mechanisms controlling aneurysm expansion, acting in conjunction with other less well characterised mechanisms, including hemodynamic stress, infection and autoimmunity.<sup>12</sup> The risk factors for AAA are well established - male sex, advanced age, smoking and a family history in first-degree male relatives.<sup>7-10, 12</sup>

Rupture of an AAA is catastrophic with an overall mortality of 90%,<sup>1, 8</sup> and the cause of over 6000 deaths per year in the UK.<sup>203</sup> The growth rate and rupture risk of AAAs is unpredictable; only smoking (increases growth, doubles rupture risk) and diabetes (slows growth) have been proven as patient-specific factors. The cause of rupture is thought to be due to a number of factors,<sup>204</sup> one of which being low Wall Shear Stress (WSS) in specific areas of the aneurysm.

Based on population studies, a maximal aortic diameter of 5.5cm is considered the threshold for elective repair<sup>205</sup> equating to the point at which risk of rupture is thought to outweigh the risk of surgery. This is clearly not an individualised approach and means that the timing of surgery may not be optimal - currently around 10 AAA repairs are performed to prevent one rupture.<sup>124</sup> There is clearly a need for more patient-specific growth and rupture risk prediction to identify AAA patients at high rupture risk.<sup>16</sup>

Recent attempts to improve this criterion have involved the use of CT scans to obtain 3D models of patient specific geometry, often in conjunction with the application of Computational Fluid Dynamics (CFD) and Finite Element Analysis (FEA) to predict WSS in the aneurysm.<sup>205-209</sup> These attempts have demonstrated the potential benefits of patient specific geometry in the prediction of rupture for AAAs, as the characterisation of aneurysmal flow patterns is most sensitive to aneurysm geometry over other variables.<sup>210</sup> However, this technique has not been widely implemented clinically as CT

scanning is expensive, delivers a significant radiation dose and requires iodinated intravenous contrast, which is associated with cumulative nephrotoxicity.<sup>183</sup> 3D-US is a novel imaging modality that has the potential to overcome these issues and be applied to a wide patient population given that US is already used as the preliminary tool to identify AAAs in patients.<sup>4</sup>

In the current work, additional smoothing is required to prepare the geometry for CFD simulation. A number of different algorithms have been identified as suitable for smoothing of patient specific geometries.<sup>211</sup> We here focus on a paired CT-US data set, both of which are smoothed using each algorithm in turn (Laplacian, HC Laplacian and Taubin Low Pass Filter) in order to assess the importance and effects of geometry smoothing on fluid simulations. In this work, the accuracy of the simulation results using 3D-US geometries will be compared against those obtained through CT scans in order to validate this technique. While most patient-specific approaches reported in previous studies have focussed on structural analysis of the aneurysm wall using FEA, there is an identified need to incorporate effects of the blood flow in order to improve accuracy of rupture prediction and ultimately a coupled fluid-structure approach is sought.<sup>12, 105, 124</sup>

In general, WSS induced by flow simulations will be more sensitive to geometric resolution and inlet/outlet effects than wall stresses obtained by structural analysis alone, whereby loading pressures are generally imposed to be constant. A more stringent test of the potential of 3D-US versus CT scan is thus identified in the comparison of CFD predictions from each source, which forms the focus of the present work.

### **10.3 METHODS**

Figure 67 represents the tool chain for each of the two scanning techniques used in the present study. The current study is limited to a single paired optimal dataset in order to demonstrate the potential and the limitations of using the 3D-US approach, while future and on-going work will aim to quantify this across a wider range of paired



datasets. Patients undergoing CT angiography for planning of AAA repair at University Hospital South Manchester were identified via the radiology department and gave informed consent. Ethical approval was granted by the National Research Ethics Committee (13/NW/0468).

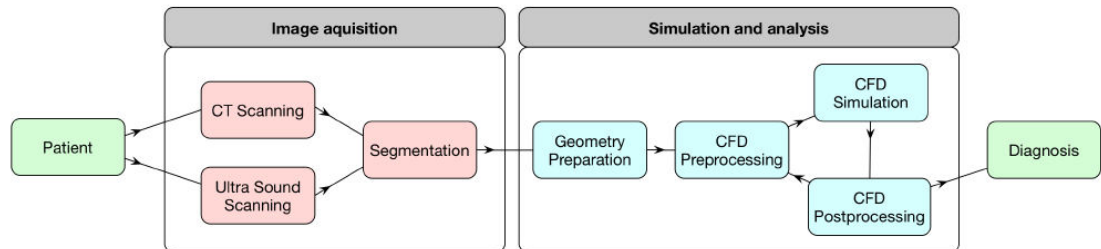


Figure 67: tool chain employed for the present study.

In the following we provide details of the independent steps in the process, as represented by Figure 67. We differentiate between image segmentation and geometry preparation since the former requires physiological knowledge and the latter is associated with facilitation of the simulations.

### ***CT scanning***

CT angiography was performed using a 128-slice Siemens SOMATOM Perspective scanner (Siemens Medical, Munich, Germany). Patients were positioned supine and images at 1mm slices were acquired from the aortic arch to the femoral heads. Arterial phase images were acquired using a bolus dose of 100 mL of the iodinated contrast medium Omnipaque 240 (GE Healthcare, UK) administered at a flow rate of 3 mL/s.

### ***3D-US scanning***

3D-US data was acquired using a Phillips IU22 ultrasound console (Phillips, Amsterdam, Netherlands) using a C5-1 curved array transducer. An electromagnetic tracking system (Ascension, Vermont, USA) comprising of a field generator and two tracking sensors that attach to the ultrasound probe, is used together with a 3D guidance software. The positional information generated by the movement of the sensors in the magnetic field allows the system to orientate the US probe in time and space. This positional data allows the 2D-US frames to be assembled into a 3D volume.

### ***Segmentation***

CT and 3D-US data were exported to prototype analysis software able to perform segmentation on both datasets (ImFusion Suite, ImFusion GmbH, Munich). An interactive segmentation algorithm was used where the operator briefly places seeds inside and outside the lumen in a number of images slices. The 'inside' and 'outside' regions are then propagated and defused in the whole image, defining the lumen from the surrounding aortic wall or thrombus.<sup>186</sup> Other structures of the AAA (e.g. wall, thrombus) can also be segmented in the same way. Errors in the segmentation were corrected by the user and the algorithm re-run to increase accuracy. The ImFusion software then uses a marching cube algorithm to convert the contours generated by the segmentation into a surface mesh<sup>187</sup> that can be exported as a stereolithography (STL) file. Segmentation took less than 10 minutes for CT and less than 20 minutes for 3D-US.

### ***Geometry Preparation***

Before smoothing each geometry, smaller arteries that branch from the abdominal aorta were removed, in this case flow from the lumen into a patent lumbar artery, as seen in Figure 68. By removing these smaller branches, the complexity of the simulation could be reduced. This decision was taken since the error associated with excluding these branches was deemed to be smaller than the effect from the simple

simulation set up for this preliminary study. However, it should be noted that both imaging techniques were able to identify this artery in the same location. The resolution of each geometry was then increased further via the application of the Butterfly Subdivision algorithm.<sup>212</sup> Each geometry was imported into MeshMixer<sup>213</sup> to prepare the inlet and outlets of each aneurysm for fluid simulation.

Due to the high acoustic impedance of bone, US does not pass well through the rib cage and the image can also be obscured by other features such as bowel gas; resulting in difficulty obtaining large portions of the upstream aortic geometry. Furthermore, the aneurysm outlet arteries (iliac arteries) tend to follow the downward curvature of the pelvis, increasing the distance between the skin and the artery. Thus making it challenging to obtain the downstream geometry using US. In an attempt to mitigate these restrictions we restricted our focus on the aneurysm itself, and assumed approximate constant cross-section in both up and downstream directions by extruding planar cuts of the available data as shown in Figure 68.

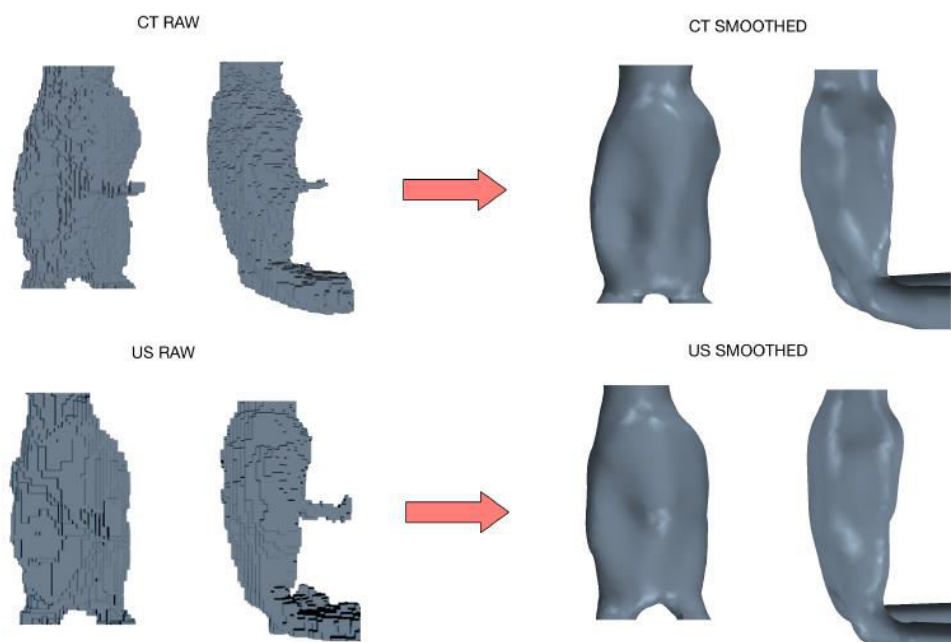


Figure 68: Geometry preparation from CT and 3D-US data.

The aneurysm lumen geometries were then smoothed in MeshLab<sup>214</sup> using Laplacian,<sup>215</sup> HC-Laplacian<sup>216</sup> and Taubin Low-Pass Filter.<sup>217</sup> The Laplacian algorithm is

widely used for a number of applications<sup>218</sup> and is available in most commercial software packages.<sup>219</sup> However, the Laplacian algorithm is known to suffer from shrinkage.<sup>220</sup> Previous research has indicated HC-Laplacian and Taubin Low-Pass Filter are better optimized for medical applications in general<sup>211</sup> however, it was crucial that this be validated for AAA geometries from 3D-US scans.

### ***CFD Pre-processing***

The inlet plane was extruded upstream by a distance of around three times the diameter of the abdominal aorta and an analytical profile was applied at the inlet, as defined by:

$$u_{inlet} = u_{mean} \left( 1 - \frac{r^2}{r_{max}^2} \right)$$

where  $u_{mean}$  is the mean velocity corresponding to the Reynolds number,  $r$  is the radial distance from the centre of the vessel and  $r_{max}$  is the vessel radius. This procedure enables the inlet section to be shortened in order to minimise the effects of boundary conditions, and thereby represent a more realistic blood flow profile in the region of the aneurysm.

The outlets were also extended in a similar manner in order to prevent backflow from affecting the fluid characteristics inside the aneurysm. It was found that the process to prepare the 3D segmented geometry for simulation could be completed by an experienced user in under 10 minutes. The computational grid was generated using 10 layers of prism cells with sufficient resolution to adequately resolve the boundary layer and polyhedral cells used in the remaining domain. A grid refinement study was conducted on a single geometry based on meshes generated with 3 cross-sectional resolutions corresponding to total cell counts of 0.5, 1.7 and 5 million polyhedral cells. It was found that mesh convergence was reached by the second mesh containing 1.7M cells, for which a view of the cross-section is displayed in Figure 69.

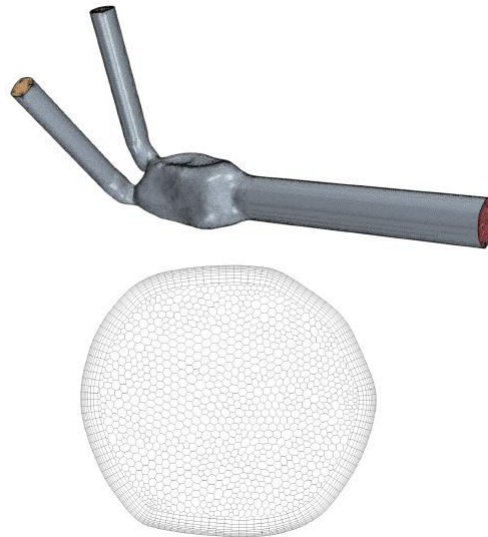


*Figure 69: Mesh used in the CFD analysis (top) full domain, (bottom) cross sectional detail.*

### **CFD Simulation**

All simulations were conducted using the commercial finite-volume code, STAR CCM+. For the purpose of this pilot study, a steady segregated incompressible solver was employed, assuming Newtonian laminar flow. A second-order upwind scheme was used to discretise the convective terms of the momentum equations. Since no patient specific flow velocity data was available, the Reynolds number was assumed to be 660 based upon the average inflow velocity and inlet diameter. The fluid's viscosity was set to  $0.004\text{kg/m/s}$  to represent a Newtonian blood flow and the density was set to  $1050\text{kg/m}^3$ . A Poiseuille Flow was used at the inlet to represent a more realistic blood flow profile<sup>221</sup> while enabling a shortening of the inlet section as described above. The cases were run on 64 cores for 1,700,000 cells (30,000 cells per core). Time per iteration was around 0.5s and the calculation continued until residuals dropped below  $1 \times 10^{-6}$ ; on average this required a total of 5,500 iterations, amounting to a simulation time of 45 minutes.

### ***CFD Post-processing***

The resulting WSS was extracted and compared for both smoothing algorithms to assess the sensitivity of the flow simulation to different smoothing algorithms. The WSS characteristics of the CT and 3D-US scans were then compared to determine the potential viability of 3D-US scans as a basis for surgical intervention for AAAs. The internal flow field was also assessed via a combination of streamlines and contours of both flow velocity and vorticity.

## **10.4 RESULTS**

### ***Assessment of smoothing algorithms***

The geometry from the segmentation stage remains unsuitable for CFD analysis, on account of remaining protrusions and tight internal corners. As such additional smoothing was undertaken using several common approaches employed in the literature and for each algorithm applied, we assessed the quality of the resulting surface mesh. The quality metrics, summarised in Table 14 include the number of faces and vertices, rate of shrinkage and the mean aspect ratios of faces.

*Table 14: Mesh quality assessment of smoothing algorithms*

<b>Metric</b>	<b>Laplacian</b>	<b>HC Laplacian</b>	<b>Low Pass Filter</b>
<b>No. of faces</b>	<b>38 894</b>	<b>39 728</b>	<b>39 614</b>
<b>No. of vertices</b>	<b>19 449</b>	<b>20 010</b>	<b>19 882</b>
<b>Shrinkage %</b>	<b>98.27</b>	<b>99.11</b>	<b>99.85</b>
<b>Mean Aspect Ratio</b>	<b>0.670</b>	<b>0.768</b>	<b>0.778</b>

As mentioned previously, the Laplacian smoothing algorithm is known to suffer from shrinkage.<sup>216</sup> This results in the geometry converging to a single point if applied excessively. Even small amounts of shrinkage can cause geometry detail levels to be significantly reduced as well as artificially reducing the patient specific Reynolds

number through the reduction of the characteristic distance, in this case the aorta diameter.

The face aspect ratio profile of geometries is of particular importance when creating the mesh for CFD analysis. Low aspect ratios can cause mesh distortion resulting in inaccurate solutions and slow convergence. Figure 70 shows the distribution of face aspect ratio for each algorithm when applied to the geometry output from the segmentation stage. The Laplacian smoothing is shown to result in a greater number of faces which have a lower value aspect ratio. Indeed a smearing effect is evident. In contrast, the HC-Laplacian algorithm and Taubin Low Pass Filter retain a superior level of aspect ratio over the entire mesh; both exhibiting a modal face value of around 0.75. The HC-Laplacian algorithm and Taubin Low-Pass Filter were identified as suitable for CFD analysis based upon the superior quality of the resulting smoothed mesh and in the subsequent section we compare the impact of selecting either one or other of these approaches.

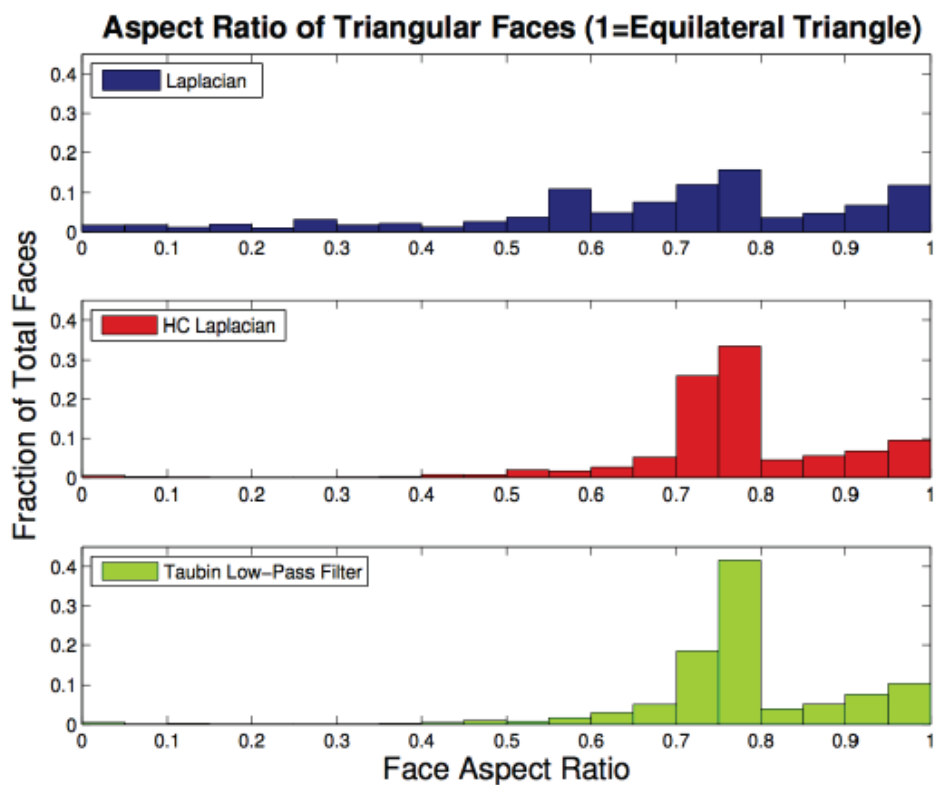
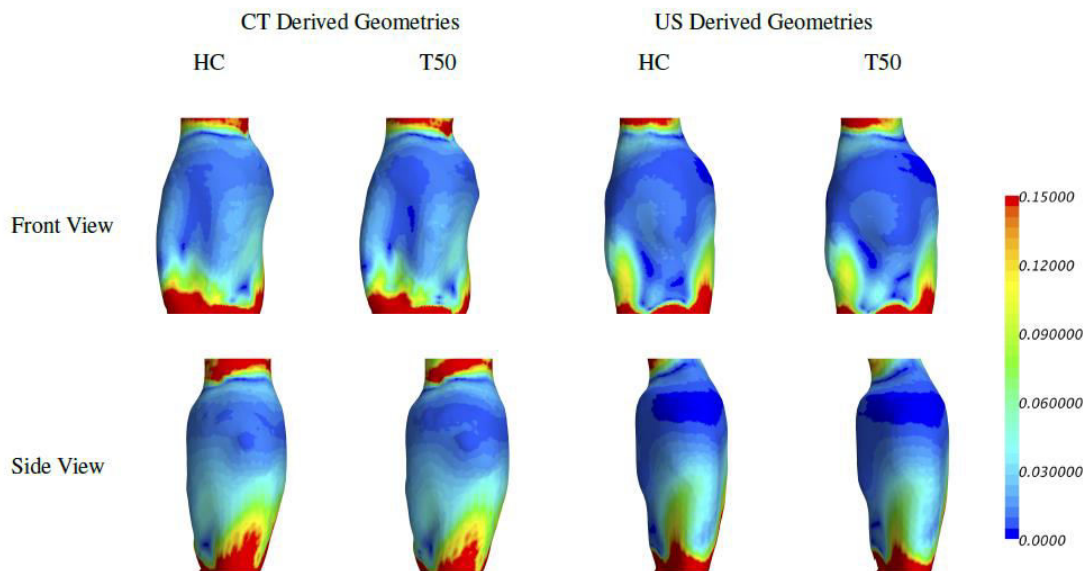


Figure 70: Histogram of face aspect ratio for Laplacian, HC Laplacian, and Taubin low pass filter

### ***Analysis of Wall Shear Stress***

In terms of providing evidence to assess the risk of aneurysm rupture, WSS levels are often deemed to play a crucial role, as reported in the introductory sections. Figure 71 provides a comparison of WSS distribution for the selected combinations of image sources and smoothing algorithms. It can be seen that the differences between geometries resulting from the two smoothing algorithms are minimal when compared to those differences arising from the two methods of scanning. Negative axial WSS is shown in various locations indicating areas of flow recirculation. Encouragingly there are qualitative similarities between the predicted WSS distributions arising from both CT and 3D-US data. Areas of lowest WSS are identified in similar locations for both scanning methods and smoothing algorithms, as demonstrated by the minimum points located in the top right of the aneurysm wall in the front view and located at the top of the side view. In the clinical experience of the authors, the site of AAA rupture is highly variable but has been observed at sites similar to the region of low WSS identified in this simulation. It is therefore feasible to suggest this region may ultimately be the site of rupture and notable that it is unrelated to the site of maximal aortic diameter.



*Figure 71: Wall shear stress for each combination of image source and smoothing algorithm.*



Figure 72 provides the means for a closer inspection of WSS levels. The axial WSS,  $\tau_{wall}$ , is plotted along the artery walls along a probe in both a vertical plane (dark blue) and a horizontal plane (light blue) for all combinations of imaging technique and smoothing algorithm. It can be seen that the range of results all follow a trend, picking up maxima and minima at similar locations. In the vertical plane (on the left of Figure 72 and corresponding to the dark blue plane), there is an initial rise at a distance of 0.02m from the inlet, followed by a drop and a plateau in the region  $0:03 < x < 0:08$ . Beyond this point, the variation of WSS is heavily influenced by the exit and bifurcation region; giving rise to a large negative value corresponding to a flow recirculation. While the qualitative trends are similar, values arising from the 3D-US derived data are higher by a factor of between 1.5 and 2 than values from the CT data.

Differences are expected to be more pronounced at the start and end of the aneurysm, on account of the non-linear influence of small geometric variations in these regions. Nevertheless, away from these locations the agreement is observed to be within 10%. Oscillations in the magnitude of WSS can be seen around the exit of the aneurysm. This is partly caused by the irregularity of the cross sectional area of the aneurysm geometry in this region and also the increased complexity of the flow due to the bifurcation of the aorta into the iliac arteries and the wall between the branches.

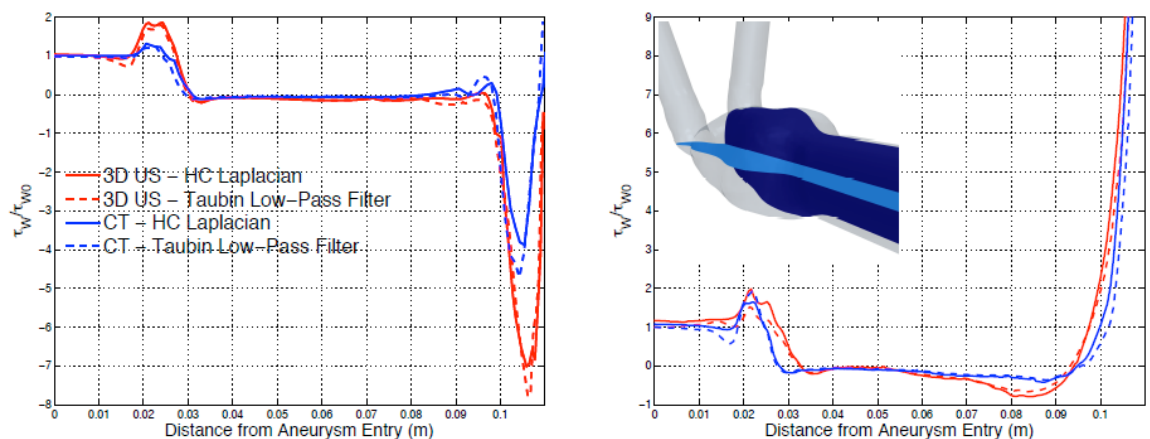


Figure 72: Axial wall shear stress for each scanning technique.

The axial WSS profiles obtained in the horizontal (light blue) plane indicate a somewhat broader variation. Again, the agreement between CT and 3D-US derived

simulations is reasonably close. Peak values are once again predicted at around 0.02m from the inlet, but there is a difference in the subsequent predicted variation in that 3D-US predictions indicate an earlier minima than that from CT simulations. This corresponds to variations in the profile of the aneurysm geometry and the associated distribution of the WSS as seen in Figure 71 (Front Views).

### ***Analysis of predicted flow field***

Switching attention to the internal flow field, we consider here a comparison between CT and 3D-US geometries smoothed using the Taubin Low-Pass Filter only, on account of small details reported in the previous section. Figure 73 displays streamlines of velocity and contours of vorticity plotted at various cross-planes. The streamlines demonstrate once again that the overall bulk flow is comparable between simulations derived from both CT and US sources; with the majority of the flow identified as high velocity bulk flow passing through the middle of the aneurysm. There are notable differences which occur in the lower velocity (blue) streamlines, in the vicinity of the aneurysm walls where geometric inconsistencies are more pronounced. Fortunately, the predicted levels of WSS don't appear to be overly sensitive to these differences. This pattern is also demonstrated in the vorticity contour plots. The flow is observed to become more complex as it reaches the aneurysm outlets, with counter rotating vortices forming inside the aneurysm (shown in vorticity image 1 and 2). These vortices then breakdown as the flow approaches the outlets of the aneurysm resulting in non-uniform flow properties along the aneurysm wall. This results in the variation in the WSS across the wall that were previously identified.

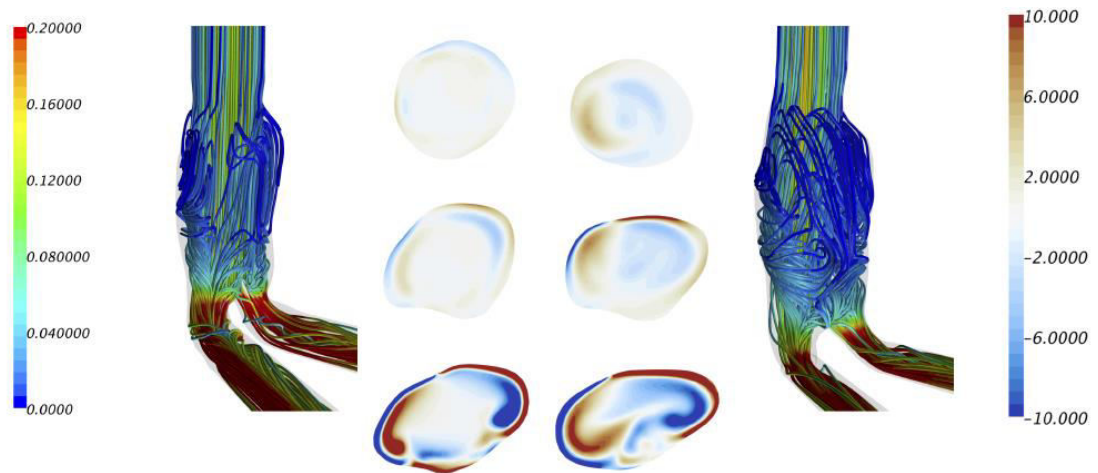


Figure 73: Streamlines and contours of velocity (m/s) and vorticity (l/s) for Taubin low pass filter smoothed CT (left) and 3D-US (right) geometries.

## 10.5 DISCUSSION

Steady CFD simulations of AAA patient specific geometries obtained from a single patient through CT and 3D-US scans were performed and analysis of the derived hemodynamic conditions conducted. In addition, the effects of commercially available smoothing algorithms were assessed with the aim of identifying an optimum algorithm in the fluid simulation of AAAs.

It was found that the basic Laplacian smoothing algorithm was not suitable for AAA applications, creating meshes with higher rates of shrinkage and lower average aspect ratios than the HC-Laplacian and Taubin Low Pass Filter. The Taubin Low Pass Filter provided the highest quality meshes causing no shrinkage to the geometry, the least reduction in visual detail and the highest quality average aspect ratio.

The Taubin Low Pass Filter and HC-Laplacian methods were then selected for CFD simulation. From the results it could be seen that there was little variation quantitatively in the hemodynamic characteristics between the smoothing algorithms. However, given that the HC-Laplacian algorithm causes higher levels of mesh

shrinkage, for future simulations incorporating a patient specific inlet velocity profile, the flow Reynolds number will be artificially reduced using the HC-Laplacian algorithm.

The hemodynamic characteristics exhibited a larger dependence on imaging source, as can be expected. However, it is noted that these geometric differences were not so great as to significantly impact the predicted distribution of wall shear stress, which is commonly understood to be one of the most important metrics in computational hemodynamic analysis of aneurysm rupture. Predictions resulting from the 3D-US derived data identified broadly the same locations of minimum WSS as those from CT scans, with predicted values remaining close across the majority of the flow. In addition, the axial WSS profiles obtained through both scanning techniques indicated very similar qualitative flow characteristics in terms of flow recirculation and the presence of bifurcation. The velocity streamlines and cross sectional contours were again qualitatively similar.

The tool chain for patient-specific geometries obtained through 3D-US methods is more efficient than its CT counterpart, and more practical; and its usage would radically broaden accessibility of patient specific computational haemodynamics analysis. Geometries obtained through CT scan require more outsourced steps in the tool chain, therefore increasing the time before a decision for surgical intervention can take place. Additionally, given the cost and risk to the patient, CT cannot be performed on multiple occasions if the aneurysm grows. This leads to a conservative criterion for surgical intervention given the mortality rate of an aneurysm rupture. In contrast, the 3D-US technique can be performed as and when necessary given the availability and relatively small cost in comparison to CT scanning. This also allows the 3D-US scan to be iterated if the quality of the geometry is not sufficient after the segmentation and smoothing stages.

The research presented in this paper demonstrates the potential for 3D-US to be used as an alternative to CT scanned patient specific geometries in the decision to surgically intervene for AAAs. The hemodynamic characteristics have been shown to be quantitatively similar for a relatively simple CFD simulation. Additionally, the tool chain

for the technique incorporating 3D-US scanning was found to be more favourable to clinicians, allowing more of the method to be conducted bedside and iterated due to the low cost and high availability relative to CT scanning.

Mesh quality analysis found the Taubin Low-Pass Filter to be the most optimal commercially available smoothing algorithm producing high quality faces and preventing shrinkage of the geometry during smoothing iterations. The HC-Laplacian smoothing algorithm also performed favourably.

It should be emphasised that the research presented here is preliminary in nature, and aims only to demonstrate the potential of the 3D-US technique as a viable alternative to CT derived geometry.

## **10.6 CONCLUSIONS**

To this end, it has been shown that careful execution of the segmentation, image smoothing and CFD pre-processing stages can enable comparable analysis under the conditions of steady, laminar and Newtonian flow. Ongoing work will endeavour to repeat simulations for a number of additional pairs of CT and 3D-US derived geometries to understand limitations and the sensitivity to different body types and aneurysm configurations. Furthermore, analysis will incorporate increasing complexity in order to move towards more realistic simulation. Work will continue by assessing the impact on wall shear stress prediction when using a pulsatile velocity inlet condition, as well as a non-Newtonian model for blood. We also plan to incorporate finite element analysis of the artery wall, as well as the thrombus if present, in an attempt to identify a more accurate and efficient metric to indicate the risk of rupture.

**CHAPTER 11: WALL STRESS ANALYSES OF ABDOMINAL AORTIC ANEURYSMS: 3D  
ULTRASOUND VERSUS COMPUTED TOMOGRAPHY.**

**Chapter contributors and role:**

**Institute of Cardiovascular Sciences**

**C Lowe:** conception, patient recruitment, established collaboration, CT and 3D-US analysis, manuscript writing.

**S Rogers:** 3D-US scanning.

**Prof C McCollum:** Supervisor.

**School of Mechanical Aerospace and Civil Engineering (MACE)**

**W Al-Obaidi:** FEA simulation.

**Dr P Mandal:** Supervision of W Al-Obaidi

**Imfusion GmbH**

**Dr W Wein:** Software development.

## 11.1 ABSTRACT

**Background:** Biomechanical analysis using finite element analysis (FEA) to estimate peak wall stress (PWS) has been proposed as superior to maximal aortic diameter as a patient-specific indicator of rupture risk of AAAs. Current approaches to wall stress analysis using FEA rely on CT scans to provide the AAA geometry. Such an approach is not feasible for patients in AAA surveillance and has limited the clinical implementation of this approach. 3D-US may be able to replace CTA for this purpose, though it faces a number of technical challenges. The aim of this study, using one optimal paired 3D-US and CT geometry, was to generate a proof-of-principle and inform further work.

**Methods:** The optimal paired 3D-US and CT scan from a patient being assessed for elective AAA repair was selected from a previous study. An interactive segmentation tool was used to create surface meshes from each dataset. These were exported to 3Matic software and prepared for FEA which was performed using Abaqus. The resulting stress values and distributions in the CT and 3D-US were compared.

**Results:** FEA simulation for both the CT and 3D-US model was successful. The location of PWS was identified in the same region in both simulations, on the right postero-inferior AAA wall. The peak von Mises stress in the CT model was 536 KPa and in the 3D-US model was 761 KPa. Therefore, the 3D-US geometry over-estimated the PWS by 42%. The site of maximal principle stress was also at the same location in both models and was the same site as the region of peak von Mises stress. Maximum principle stress in the CT model was 600 KPa and in the 3D-US model was 911 KPa. Therefore, the site of maximal principle stress was overestimated in the 3D-US model by 51%.

**Conclusion:** Although the FEA simulations were successful and the site of PWS was identified in the same anatomical location in each model, peak von Mises stress and maximal principle stress was overestimated in the 3D-US model by 42% and 51% respectively. Before increasing the complexity of the modelling, further work should concentrate on improving the accuracy of the 3D-US approach, examining the

reproducibility of the CT and US segmentation and validating the segmentation method used against an industry standard.



## 11.2 INTRODUCTION

Selecting the appropriate threshold for AAA repair is critical. Based on population studies, a maximal aortic diameter of  $\geq 5.5\text{cm}$  is considered the threshold for elective repair,<sup>1</sup> equating to the point at which risk of rupture is thought to outweigh the risk of surgery. This is clearly not an individualised approach and means that the timing of surgery may not be optimal - currently around 10 AAA repairs are performed to prevent one rupture.<sup>124</sup> The applicability of estimates of AAA tensile stress and wall strength or derived parameters to identify patients at risk for rapid growth or rupture has been identified as a research priority by the American Society of Vascular Surgery.<sup>65</sup>

The current clinical threshold for repair in men of 5.5cm assumes that AAAs obey the 'law of Laplace,' with the stress on the AAA wall proportional to its diameter. However, AAAs are not simple cylinders or spheres to which the 'law' applies; rather, they have complex three-dimensional geometries.<sup>127</sup> As rupture occurs when wall stress exceeds wall strength, the strength and material properties of the aortic wall are also key issues. There is increasing evidence that estimating PWS using finite element analysis FEA can more accurately predict rupture risk than AAA diameter.<sup>97</sup> Stress is a measure of the internal forces induced in the vessel wall due to blood pressure. PWS describes the region in a structure or geometry where the stress is highest.

FEA is a computational modelling technique that is established in industry to design, prototype and test complex structures and geometries. Current FEA techniques for AAAs<sup>95</sup> rely on CTA to provide the geometry of the aneurysm, with the material properties of the AAA wall defined by bench-top mechanical testing of explanted aortic tissue and mathematical models.<sup>121</sup> However, as CTA is expensive and exposes patients to both ionizing radiation and intravenous contrast that is potentially nephrotoxic, it would be completely inappropriate for patients undergoing AAA surveillance. CTA is only indicated in AAA patients to plan repair. As a result, despite the recent availability of commercial FEA software for AAA (<http://www.vascops.com/en/vascops-home.html>) the approach is not in routine

clinical use. There is no research on how PWS evolves during AAA growth or on whether this predicts growth, the need for repair, or risk of premature rupture.

3D-US has the potential to replace CTA for this purpose and make such analysis possible on a large number of patients. An approach using matrix 3D-US has recently been described, but this approach is hampered by the need to assemble the geometry from multiple acquisitions in lengthy post-processing.<sup>172</sup> Using a tracked freehand ultrasound system avoids this problem, but has also proven to be technically demanding. In a feasibility study, it was identified that complete wall geometry was acquired in 10% of patients (Chapter 9). Nonetheless, when the optimal result was used in CFD simulations, the results were encouraging (Chapter 10).

The aim of this study, using one optimal paired 3D-US and CT geometry, was to generate a proof-of-principle and inform further work.

### **11.3 METHODS**

This current study is limited to a single paired optimal dataset in order to demonstrate proof-of-principle and explore the potential and the limitations of using 3D-US for this application. The optimal results from a single patient in a previous study (Chapter 9) were selected to investigate the feasibility of this approach. The patient had undergone CTA for planning for repair of a 6.9cm AAA at University Hospital South Manchester and was identified via the radiology department records. They gave informed consent. Ethical approval was granted by the National Research Ethics Committee (13/NW/0468).

#### ***CT scanning***

CT angiography was performed using a 128-slice Siemens SOMATOM Perspective scanner (Siemens Medical, Munich, Germany). Patients were positioned supine and images at 1mm slices were acquired from the aortic arch to the femoral heads. Arterial phase images were acquired using a bolus dose of 100 mL of the iodinated contrast medium Omnipaque 240 (GE Healthcare, UK) administered at a flow rate of 3 mL/s.

### ***3D-US scanning***

3D-US data was acquired using a Phillips IU22 ultrasound console (Phillips, Amsterdam, Netherlands) using a C5-1 curved array transducer. An electromagnetic tracking system (Ascension, Vermont, USA) comprising of a field generator and two tracking sensors that attach to the ultrasound probe, is used together with a 3D guidance software. The positional information generated by the movement of the sensors in the magnetic field allows the system to orientate the US probe in time and space. This positional data allows the 2D-US frames to be assembled into a 3D volume.

### ***Segmentation***

CT and 3D-US data were exported to prototype analysis software able to perform segmentation on both datasets (ImFusion Suite, ImFusion GmbH, Munich). The method using an interactive segmentation algorithm has previously been described in detail (Chapter 4.5). To briefly reprise, the operator briefly places seeds inside and outside the wall in a number of image slices. The 'inside' and 'outside' regions are then propagated and defused in the whole image, defining the wall from the surrounding aortic wall or thrombus.<sup>186</sup> Other structures of the AAA (e.g. lumen, thrombus) can also be segmented in the same way. Errors in the segmentation were corrected by the user and the algorithm re-run to increase accuracy. The ImFusion software then uses a marching cube algorithm to convert the contours generated by the segmentation into a surface mesh<sup>187</sup> that can be exported as a STL file. The maximum mesh resolution was selected in each case. A number of meshes were generated with different levels of smoothing. The optimal result was selected such that anatomical features were retained but extraneous points were removed (Chapter 4.5.2). Segmentation took less than 10 minutes for CT and less than 20 minutes for 3D-US.

### ***Geometry preparation***

The STL files were imported into 3Matic software (Materialise, Belgium). Any obvious extraneous points were removed using the 'local smoothing' tool, however, no further smoothing step or algorithm was applied. To create the AAA wall, the surface was

expanded *outwards* by 1.5mm for the 3D-US model and *inwards* by 1.5mm for the CT model using the 'hollow' operation. This was done as the 3D-US segmentation captures the inner wall of the AAA and the CT segmentation captures the outer wall of the AAA. The method of expanding the AAA surface to create the wall, and the assumed wall thickness of 1.5mm is in line with other studies.<sup>172</sup> The influence of ILT was neglected in this study to focus on the accuracy of the wall simulation and due to contention in the literature about its influence on wall stress. The immediate aortic bifurcation was included in the model but not considered further downstream as it was poorly imaged on 3D-US and removal of the iliac vessels from FEA simulations does not appear to significantly influence wall stress distributions.<sup>97</sup>

### ***Mesh generation***

The prepared model was imported from 3Matic to Abaqus v6.14 (Dassault Systèmes, Paris, France). A plug-in within Abaqus, 'Mesh to Geometry', was used to convert the STL model into a native Abaqus part in order to reduce the simulation time. A re-meshing procedure to create a tetrahedral volume mesh on each of the AAA surface meshes was performed. To determine the optimal number of elements and therefore the optimal mesh, mesh independence was performed at a level of  $\pm 2\%$  in peak wall stress. This gave an optimal number of 284,313 elements.

### ***Boundary conditions***

The AAA wall was modelled as a homogenous isotropic hyperelastic material as described by Rhagavan and Vorp.<sup>103</sup> A Poisson's ratio of 0.4 was applied describing an almost incompressible wall. These properties have been used in a number of previous studies.<sup>97, 102, 104, 119, 135</sup> The AAA was constrained proximally and distally to simulate the fixation of the aorta at the renal arteries and bifurcation. A static systolic pressure of 120mmHg (16 KPa) was applied as in most studies. The patient-specific blood pressure was available but was not used to allow better comparison with other studies and keep the simulation straightforward in this preliminary work. Shear stress caused by

blood flow was not considered for the same reasons, but has previously been investigated.

### Post-Processing

The FEA simulation was performed in Abaqus to produce detailed stress distributions on the AAA wall. Peak wall stress (PWS) was reported as von Mises stress (KPa) for means of comparison with other studies. The von Mises stress is a stress index especially suited for failure analysis, as stress is a tensor quantity with nine components, with the von Mises stress being a combination of these components. Maximal principle stress was also calculated for each model.

This process is summarised in Figure 74 below:

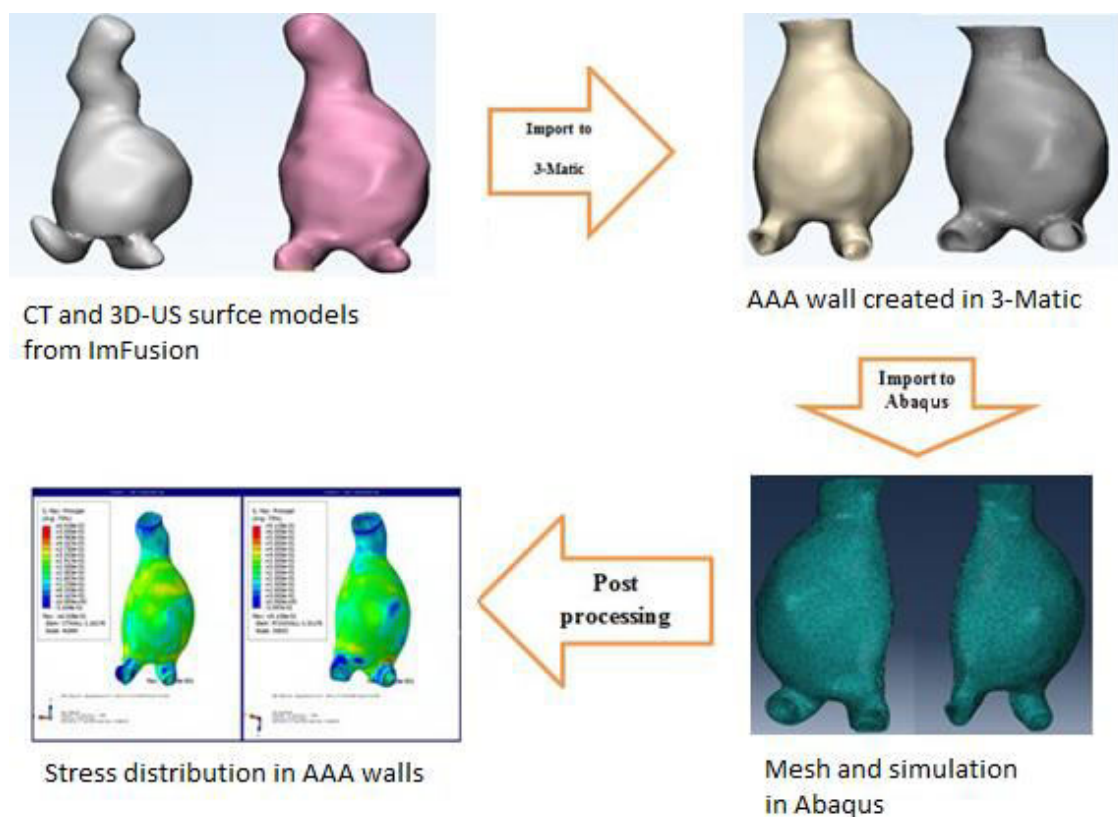


Figure 74: Workflow to prepare models for simulation

## 11.4 RESULTS

FEA simulation for both the CT and 3D-US model was successful. Wall stress distributions and the location of PWS in the CT and 3D-US models is shown in Figures 75-76. The location of PWS was identified in the same region in both simulations, on the right postero-inferior AAA wall. The PWS in the CT model was 536 KPa and in the 3D-US model was 761 KPa. Therefore, the 3D-US geometry over-estimated the PWS by 42%.

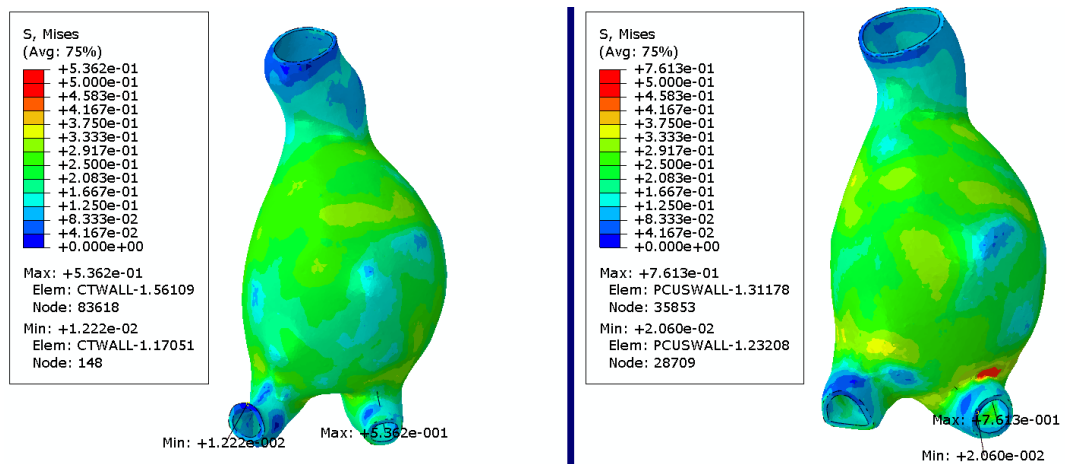


Figure 75: Posterior-anterior view of von Mises stress distribution in CTA (left) and 3D-US (right) derived models.

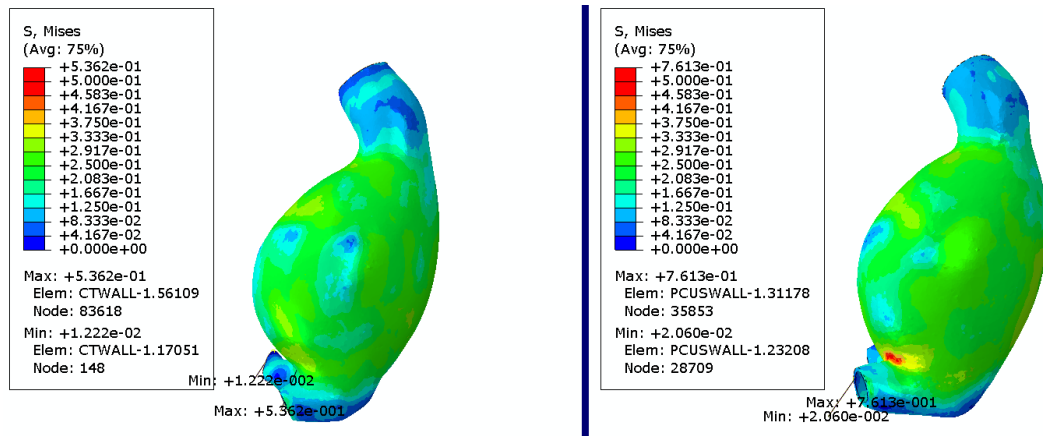


Figure 76: Lateral view of von Mises stress distribution in CTA (left) and 3D-US derived models.

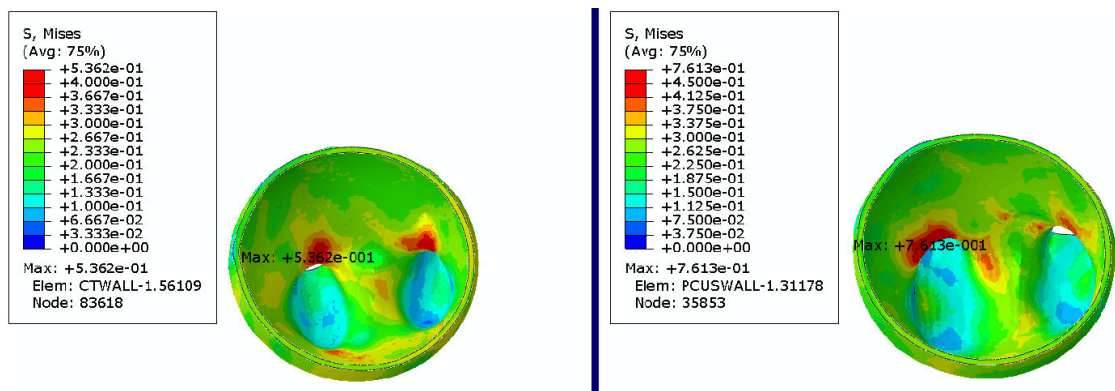


Figure 77: Section through AAA models at level of the aortic bifurcation demonstrating von Mises wall stress distributions. Left CTA, right 3D-US.

The site of maximal principle stress was also at a similar location in both models and was the same site as the region of maximal von Mises stress. Maximum principle stress in the CT model was 601KPa and in the 3D-US model was 911 KPa (Figures 78-79). Therefore, the site of maximal principle stress was overestimated in the 3D-US model by 51%.

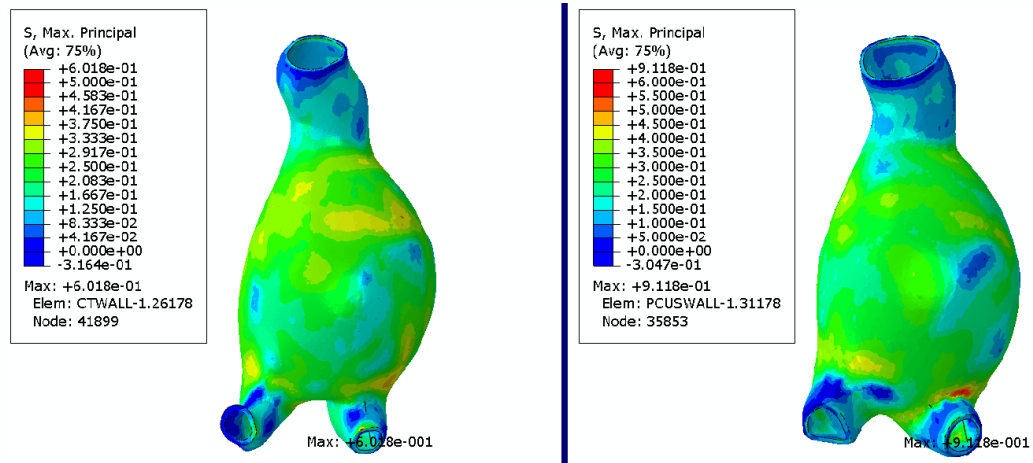


Figure 78: Posterior-anterior view of maximal principle stress distribution in CTA (left) and 3D-US (right) derived models.

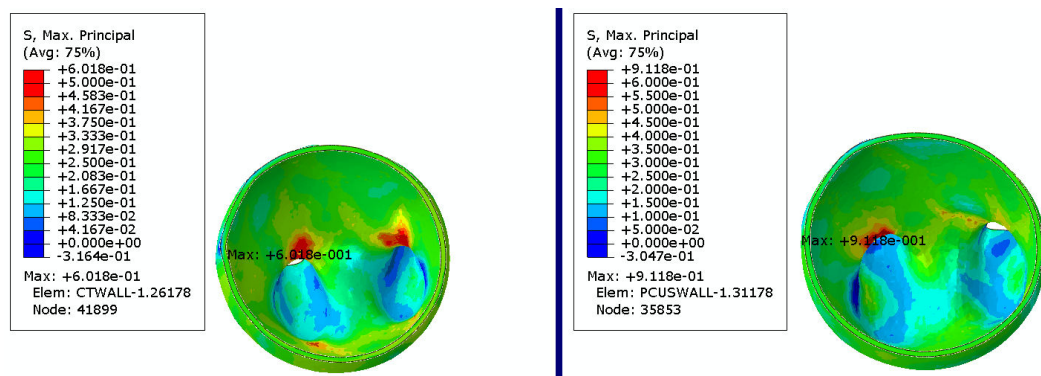


Figure 79: Section through AAA models at level of the aortic bifurcation demonstrating maximal principle distributions (MPa). Left CTA, right 3D-US.



## 11.5 DISCUSSION

This paper compared the performance of a CT and 3D-US derived geometry of the same AAA in FEA. It is the first work to describe the use of freehand 3D-US for this application and acts as a proof-of-principle. The anatomical site of maximal von Mises stress and maximal principle stress was comparable in both models; however, the 3D-US model over-estimated magnitude of the von Mises stress and maximal principal stress by 42% and 51% respectively. The study by Kok is the only study that allows for any comparison.<sup>172</sup> They analysed paired 3D-US and CT images from 15 patients. 3D-US was performed using a matrix transducer. Due to the limited sweep range of the matrix 3D-US transducer, multiple acquisitions were performed to image the AAA in each patient. The 3D-US data was then manually segmented before assembling the acquisitions into a single geometry in extensive post-processing. The 3D-US and CT based models were then compared using FEA. In the eight successful FEA simulations, the 3D-US models over-estimated PWS by an average of 23%.

The differences in PWS and stress distributions observed between the two models in this study relate to the geometrical differences between the two models, which appear minimal on simple inspection but are significant in FEA simulations. This emphasises that the large majority of geometries produced by 3D-US in Chapter 9 are unsuitable for FEA simulation. Other authors have had the facility to directly compare and quantify the differences in the geometries by means of a 'similarity index' and the Hausdorff distance using a custom built graphic user interface (GUI) in MATLAB software.<sup>172</sup> This was not possible in this work but may prove a useful tool for validating future results.

It is notable that the site of PWS was unrelated to the maximum diameter of the aneurysm, a finding that has been replicated in a number of other studies.<sup>96, 97, 126, 134</sup> Indeed, if the wall stress distributions are examined through a plane at the maximal diameter, the wall stress in this region is between 2-3MPa in the CT model and 2-4Mpa in the 3D-US model. This highlights the limitations of maximal aortic diameter as an individual marker of rupture risk. Furthermore, some authors have suggested that the

bifurcation area can be neglected in FEA simulation. Although it is difficult to comment from one case, failure to include the aortic bifurcation in this simulation would have given a misleading location and magnitude of PWS.<sup>97</sup>

As alluded to in previous work, there are a number of developments that may improve the accuracy of the 3D-US simulation at each stage in the process. Firstly, optimisation of scanning technique is essential, including patient positioning and acquiring well-contrasted images using high-gain settings on the console. The benefits of fasting are unclear but may be important to minimise gas in the viscera and allow visualisation of proximal portion of the AAA geometry. Upgrading the ultrasound unit may improve image quality, while using a linear transducer in slimmer patients may be possible and allow a greater US frame-rate and therefore image resolution. Optical rather than magnetic tracking is theoretically more accurate and requires assessment. However, side-by-side comparison will not be possible due to technical failure of the magnetic system. Application of a tracking filter (in the same way as in Chapter 8) may also reduce 'noise' and artefact in the 3D-US reconstruction. There is scope to improve the performance of the interactive segmentation technique, however, as its success is mostly dependant on image quality these are likely to be time-saving features such as increased automation and faster computation times.

This work is clearly limited by the analysis of a single geometry. In addition, the modelling approach excluded the effects of ILT but this can be justified by the on-going contention on how the ILT should be modelled and the need to focus on the basic geometry in this preliminary work. In addition, the interactive segmentation technique used derive the geometries has not been validated. An ideal study would be to derive geometries from CT using the ImFusion software and compare the results in FEA with those from established software such as Mimics (Materialise, Belgium). However, the user-dependency of image segmentation procedures is a problem inherent in the field of computational modelling as a whole at present.

A difficulty comparing the CT and 3D-US models is the assumption the value given by the CT model is correct and the most accurate. Authors have sought to evaluate their modelling approaches experimentally using bench-top testing of silicone models of

patient specific AAAs and FEA simulations.<sup>222, 223</sup> It would be possible to 3D-print physical models of the AAA geometries used in this study and subject them to mechanical testing. This would at least confirm that the wall stress values are correct for each model and also if the location of PWS is ultimately where rupture would occur when wall stress exceeds wall strength. Funding has been secured to conduct these experiments at MACE.

The application of biomechanical techniques to the individualisation of rupture risk faces a number of problems. A significant drawback is the reliance on CT data, which is not available for most patients with AAAs other than those being evaluated for repair – a matter this work aims to address. Secondly, a number of modelling parameters are assumed about the AAA wall, including its thickness (usually assumed to be 1.5-2mm and based on autopsy studies) and mechanical response to stress that is taken to be homogenous with isotropic and linear elastic properties. In reality, the response of the wall to stress will differ across the whole AAA and in multiple directions (i.e. anisotropy). Local differences in wall strength should be acknowledged, and the precise influence of ILT needs to be elucidated. Additionally, the effects of wall calcification are often excluded as there is on-going contention of how it should be modelled in FEA.<sup>126</sup> Thirdly, as alluded to above, a large number of segmentation approaches exist to extract the geometry from CT images and very few have been tested for inter-observer variability. Fourthly, there is no defined and validated threshold or biomechanical parameter that separates an AAA of ‘high-risk’ of rupture from one of ‘low-risk.’ Fifthly, the influence of blood flow and WSS stress is neglected and it is clear an optimal approach utilising fluid-structure interaction modelling should be pursued. Finally, there is no ‘gold standard’ method or consensus to follow when modelling AAA wall stress.<sup>124</sup>

## **11.6 CONCLUSIONS**

Although the FEA simulations were successful and the site of PWS was identified in a comparable anatomical location in each model, peak von Mises stress and maximal principle stress was overestimated in the 3D-US model by 42% and 51% respectively.

This is due to geometrical differences between the models and serves as an indicator of the sensitivity of FEA to these differences. Before increasing the complexity of the modelling, further work should concentrate on improving the accuracy of the 3D-US approach, examining the reproducibility of the CT and US segmentation and validating the segmentation method used against an industry standard.

## **SECTION 4: OVERALL DISCUSSION**

## **CHAPTER 12: DISCUSSION**

This final chapter provides an overarching discussion and assessment of the results in relation to the thesis aims. Potential changes in clinical practice as a result of this work are identified and relevant future work is suggested.

### **12.1 INTRAOPERATIVE IMAGING**

3D-US has been shown to be a robust and accurate modality for detecting endoleaks during endovascular aneurysm repair. Its use as an intra-operative imaging modality is novel and most likely has utility for completion imaging for patients when the minimal or no use of iodinated contrast media is required. It remains to be seen if this will be a viable application with the advent of hybrid operating theatres as studies have shown that both fluoroscopy time and contrast doses can be reduced significantly with the improved image quality and use of image fusion technology.<sup>224</sup> Facilities such as rotational angiography that are integrated into hybrid suites may offer further options for quality control but still require iodinated contrast.

The concept of 'day case' EVAR may be an opportunity to exploit this concept. As CIN manifests 48 hours post contrast administration, performing EVAR with no post-operative monitoring of renal function, especially in patients with established CKD, is unappealing and would restrict the number of patients suitable for this approach. However, the combination of EVAR with favourable anatomy, percutaneous access, a low profile delivery system, CO<sub>2</sub> angiography for stent-graft deployment and 3D-CEUS for completion imaging may make this concept more widely applicable. A further study is underway to compare a new-generation 3D-US system with rotational angiography for completion imaging following EVAR.

The scenario of a type I or III endoleak seen on 3D-CEUS but not seen on DSA warrants further consideration. As highlighted in the paper, the clinical relevance of such endoleaks is debateable, as these endoleaks are likely to be small. It is possible as the heparin anticoagulation reverses and the stent-graft conforms to the proximal and

distal sealing zones, such endoleaks will resolve. However, this has not been investigated in any studies. Therefore, an attempt to treat a type I or III endoleak seen on 3D-CEUS should be made by balloon moulding provided this is thought to be safe. It is difficult to advocate the use of other adjuncts such as proximal extension cuffs or palmaz stenting if balloon moulding is unsuccessful. A trial of conservative treatment and a pre-discharge 3D-CEUS may be an acceptable alternative. However, another possible approach would be to formally reverse the heraparinisation with protamine and see if the endoleak is subsequently obliterated on repeat scanning.

## **12.2 ENDOLEAK DETECTION FOLLOWING EVAR**

3D-CEUS appears more accurate than CT for endoleak detection and classification. However, the additional cost of the contrast agent and the capital cost of the 3D-US unit makes it too expensive to justify use in routine EVAR surveillance. More likely, it should be used to answer specific clinical questions when standard duplex is non-diagnostic (to avoid CTA) or when CTA is indeterminate. The enhanced ability to classify endoleaks is related to i) the ability to view images in MPR format, ii) a 3D volume reconstruction that can be enhanced with post-processing and improve visualisation (Figure 80) iii) the ability to combine findings on 3D-US with dynamic imaging from conventional 2D-US and iv) the reduction in operator dependency.

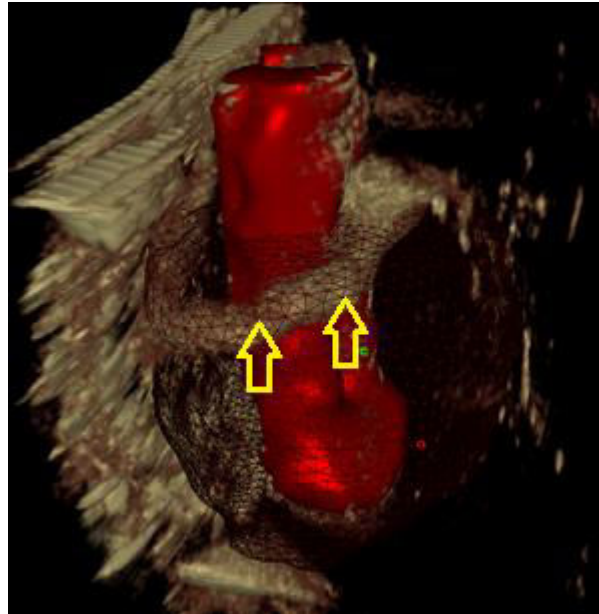


*Figure 80: A type II endoleak seen on post processing of 3D-CEUS. The stent-graft has been segmented in red. The endoleak is clearly seen – yellow arrows.*

The delineation of sub-types of type II endoleak may not have significant clinical implications, however if an interventional procedure is planned for endoleak embolisation then definition of the inflow and outflow vessels may aid in treatment planning.<sup>155</sup> Although not investigated in this study, the possibility of using CT and US fusion has been proposed by some authors.<sup>225</sup> This is technically feasible using the current hardware and software available for this work, but would only have potential value in a very small number of cases and is time consuming. The main utility of 3D-CEUS lies in the classification of indeterminate endoleaks seen on other imaging modalities such as 2D-CEUS or CTA. This work suggests the indication for 3D CEUS in EVAR surveillance are:

- i) Increase in AAA size with no visible endoleak seen on standard DUS.
- ii) New endoleak seen on DUS during surveillance.
- iii) Indeterminate endoleak seen on CTA. Most commonly this will be difficulty differentiating a type II from a type III endoleak.



The availability of this technology at UHSM has generated referrals from other vascular units for assessment. A modified surveillance programme incorporating 3D-US is suggested in Figure 81. The financial implications have not been formally assessed. Other than the capital cost of the 3D-US system, the main cost of performing the scan is the contrast agent. A full financial analysis is beyond the scope of this thesis, however, as this protocol has the potential for reducing the need for CT scanning and catheter angiography this may result in cost savings in the longer term. How quickly this would occur is debateable as the number of patients avoiding CTA or catheter angiography is relatively small. Another option would be to replace the three month CT with 3D-CEUS and an abdominal radiograph. Lack of financial saving may be a barrier to widespread clinical adoption of this technique. Further work should examine the financial implications of integrating 3D-CEUS into the diagnostic armamentarium for patient in EVAR surveillance programmes and if similar results can be replicated in other units.

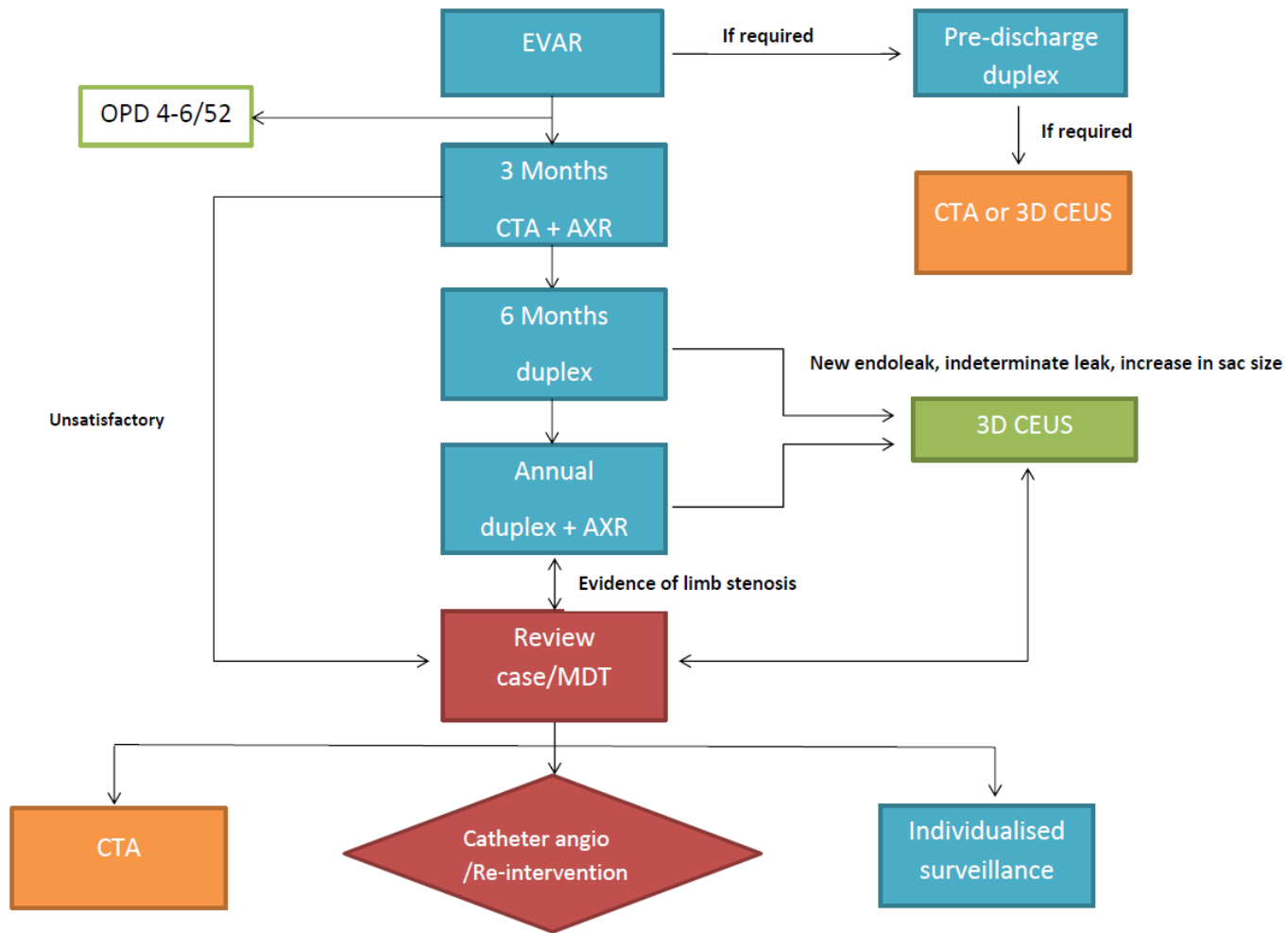


Figure 81: Proposed EVAR surveillance programme integrating 3D-CEUS.

### **12.3 AAA VOLUME MEASUREMENT**

The thesis aims were well addressed by the work in chapters 7 and 8. At present, one would conclude that either 3D-US approach is not yet able to provide sufficiently accurate AAA volume measurements to translate to clinical practice. Also, The value of AAA volume measurement in EVAR surveillance remains a matter of debate with conflicting evidence.

In this work, it appears that optical tracking is likely to be most accurate but it is a weakness of this thesis that both modalities could not be compared side-by-side. Furthermore, the small patient numbers in each study reduces their impact, and they are essentially pilot studies. However, the data will be informative for a larger trial once the necessary technical improvements have been made. In addition, there were significant other methodological differences that made comparing these two studies difficult. The most major of these differences was scanning untreated AAAs in one study and post-EVAR AAAs in the other. The elimination/reduction of pulsatility by the *in-situ* stent-graft is likely to have been the main influence in demonstrating an improvement the accuracy of optical 3D-US measurements when compared to CT. Further work is needed to define a role for AAA volume measurements. Previously, the reliance on CT images has been a major drawback for this concept and 3D-US does offer the potential to make this a clinically applicable technique. In addition to improved accuracy and inter-operator reliability, further automation is needed to reduce the time taken for volume measurement such that it is feasible in a busy vascular clinic and this should form part of any further work.

### **12.4 BIOMECHANICAL ANALYSIS**

Both studies investigating the results of CFD and FEA demonstrate that simulation using 3D-US based models is technically possible. However, even in this optimal paired

dataset, there remained significant differences in the results. This highlights the sensitivity of these techniques and the need for accuracy when both acquiring and segmenting the 3D-US data. Coupled with the difficulties encountered in Chapter 7, when trying to generate comparable geometries in a variety of patients, significant hardware and software development is needed to improve the rate of technical success and accuracy. In addition, there are a number of patient-related factors that will be difficult to overcome such as obesity and bowel gas. The most difficulty was encountered in patients with high BMI and large aneurysms, for example, one patient had a BMI of 30 kg/m<sup>2</sup> and a 8.5cm saccular aneurysm. Given that the intention of biomechanical analysis of AAAs is to identify those that may be at a higher risk of rupture than their diameter would suggest, one could argue that such an approach is most applicable to patients with AAAs of 4.5-6cm. In general, smaller AAAs are less tortuous and may be easier to image on US. For the purposes of this study, a cohort of patients with CT scans was needed, leading to a wide range of AAA sizes with only two patients with AAAs less than 5.5cm in maximal diameter.

There are difficulties relating to AAA modelling in general. As outlined previously, there is no agreed method and significant heterogeneity between studies. There are no clinical trials that have investigated threshold values for any biomechanically derived parameter so the biomechanical approach has little clinical impact to date. Such a study would be difficult as it would essentially involve prospective study of AAA patients from diagnosis until rupture, which clearly unfeasible. However, a number of studies have attempted to bring the concept of PWS estimation to the fore in other ways, with the approach of concept of 'risk-equivalent' diameter proposed by Gasser the most developed.<sup>95</sup> It may be that the biomechanical approach will not stand alone as an independent measure of risk, but be integrated into other clinical decision tools that aim to individualise indications for AAA repair.<sup>226, 227</sup>

## **12.5 OVERALL CONCLUSIONS**

This thesis has explored and developed potential applications of 3D-US that may improve the management of patients with abdominal aortic aneurysm. Overall, this

programme of research has added the currently sparse literature on this emerging imaging technology and developed two applications that are ready for clinical implementation. Further minor technical improvements hold promise for AAA volume estimation, while the use of 3D-US for biomechanical analysis requires significant further development.

## REFERENCES

1. Moll FL, Powell JT, Fraedrich G, Verzini F, Haulon S, Waltham M, et al. Management of abdominal aortic aneurysms clinical practice guidelines of the European society for vascular surgery. *Eur J Vasc Endovasc Surg.* 2011;41 Suppl 1:S1-S58.
2. Steinberg CR, Archer M, Steinberg I. Measurement of the abdominal aorta after intravenous aortography in health and arteriosclerotic peripheral vascular disease. *Am J Roentgenol Radium Ther Nucl Med.* 1965;95(3):703-8.
3. Crawford ES, Beckett WC, Greer MS. Juxtarenal infrarenal abdominal aortic aneurysm. Special diagnostic and therapeutic considerations. *Ann Surg.* 1986;203(6):661-70.
4. Ashton HA, Buxton MJ, Day NE, Kim LG, Marteau TM, Scott RA, et al. The Multicentre Aneurysm Screening Study (MASS) into the effect of abdominal aortic aneurysm screening on mortality in men: a randomised controlled trial. *Lancet.* 2002;360(9345):1531-9.
5. NAAASP. NHS Abdominal Aortic Aneurysm Screening Programme Annual Report. 2013.
6. Svensjo S, Bjorck M, Wanhainen A. Current prevalence of abdominal aortic aneurysm in 70-year-old women. *Br J Surg.* 2013;100(3):367-72.
7. Larsson E, Granath F, Swedenborg J, Hultgren R. A population-based case-control study of the familial risk of abdominal aortic aneurysm. *J Vasc Surg.* 2009;49(1):47-50; discussion 1.
8. Scott RA, Bridgewater SG, Ashton HA. Randomized clinical trial of screening for abdominal aortic aneurysm in women. *Br J Surg.* 2002;89(3):283-5.
9. Vardulaki KA, Walker NM, Day NE, Duffy SW, Ashton HA, Scott RA. Quantifying the risks of hypertension, age, sex and smoking in patients with abdominal aortic aneurysm. *Br J Surg.* 2000;87(2):195-200.
10. Wilmink TB, Quick CR, Day NE. The association between cigarette smoking and abdominal aortic aneurysms. *J Vasc Surg.* 1999;30(6):1099-105.

11. Stackelberg O, Bjorck M, Larsson SC, Orsini N, Wolk A. Sex differences in the association between smoking and abdominal aortic aneurysm. *Br J Surg.* 2014;101(10):1230-7.
12. Thompson MM. Controlling the expansion of abdominal aortic aneurysms. *Br J Surg.* 2003;90(8):897-8.
13. Saratzis A, Bown MJ. The genetic basis for aortic aneurysmal disease. *Heart.* 2014;100(12):916-22.
14. Clifton MA. Familial abdominal aortic aneurysms. *Br J Surg.* 1977;64(11):765-6.
15. Joergensen TM, Houliind K, Green A, Lindholt JS. Abdominal Aortic Diameter Is Increased in Males with a Family History of Abdominal Aortic Aneurysms: Results from the Danish VIVA-trial. *Eur J Vasc Endovasc Surg.* 2014;48(6):669-75.
16. Chaikof EL, Brewster DC, Dalman RL, Makaroun MS, Illig KA, Sicard GA, et al. SVS practice guidelines for the care of patients with an abdominal aortic aneurysm: executive summary. *J Vasc Surg.* 2009;50(4):880-96.
17. Bengtsson H, Norrgard O, Angquist KA, Ekberg O, Oberg L, Bergqvist D. Ultrasonographic screening of the abdominal aorta among siblings of patients with abdominal aortic aneurysms. *Br J Surg.* 1989;76(6):589-91.
18. Bengtsson H, Sonesson B, Lanne T, Nilsson P, Solvig J, Loren I, et al. Prevalence of abdominal aortic aneurysm in the offspring of patients dying from aneurysm rupture. *Br J Surg.* 1992;79(11):1142-3.
19. Collin J, Walton J. Is abdominal aortic aneurysm familial? *BMJ.* 1989;299(6697):493.
20. Adams DC, Tulloh BR, Galloway SW, Shaw E, Tulloh AJ, Poskitt KR. Familial abdominal aortic aneurysm: prevalence and implications for screening. *Eur J Vasc Surg.* 1993;7(6):709-12.
21. Moher D, Cole CW, Hill GB. Definition and management of abdominal aortic aneurysms: results from a Canadian survey. *Can J Surg.* 1994;37(1):29-32.
22. van der Lugt A, Kranendonk SE, Baars AM. [Screening for familial occurrence of abdominal aortic aneurysm]. *Ned Tijdschr Geneesk.* 1992;136(39):1910-3.
23. Fitzgerald P, Ramsbottom D, Burke P, Grace P, McAnena O, Croke DT, et al. Abdominal aortic aneurysm in the Irish population: a familial screening study. *Br J Surg.* 1995;82(4):483-6.

24. Baird PA, Sadovnick AD, Yee IM, Cole CW, Cole L. Sibling risks of abdominal aortic aneurysm. *Lancet*. 1995;346(8975):601-4.
25. Larcos G, Gruenewald SM, Fletcher JP. Ultrasound screening of families with abdominal aortic aneurysm. *Australas Radiol*. 1995;39(3):254-6.
26. Jaakkola P, Kuivaniemi H, Partanen K, Tromp G, Liljestrom B, Ryyanen M. Familial abdominal aortic aneurysms: screening of 71 families. *Eur J Surg*. 1996;162(8):611-7.
27. van der Graaf Y, Akkersdijk GJ, Hak E, Godaert GL, Eikelboom BC. Results of aortic screening in the brothers of patients who had elective aortic aneurysm repair. *Br J Surg*. 1998;85(6):778-80.
28. Salo JA, Soisalon-Soininen S, Bondestam S, Mattila PS. Familial occurrence of abdominal aortic aneurysm. *Ann Intern Med*. 1999;130(8):637-42.
29. Rossaak JI, Hill TM, Jones GT, Phillips LV, Harris EL, van Rij AM. Familial abdominal aortic aneurysms in the Otago region of New Zealand. *Cardiovasc Surg*. 2001;9(3):241-8.
30. Frydman G, Walker PJ, Summers K, West M, Xu D, Lightfoot T, et al. The value of screening in siblings of patients with abdominal aortic aneurysm. *Eur J Vasc Endovasc Surg*. 2003;26(4):396-400.
31. Ogata T, MacKean GL, Cole CW, Arthur C, Andreou P, Tromp G, et al. The lifetime prevalence of abdominal aortic aneurysms among siblings of aneurysm patients is eightfold higher than among siblings of spouses: an analysis of 187 aneurysm families in Nova Scotia, Canada. *J Vasc Surg*. 2005;42(5):891-7.
32. Badger SA, O'Donnell ME, Boyd CS, Hannon RJ, Lau LL, Lee B, et al. The low prevalence of abdominal aortic aneurysm in relatives in Northern Ireland. *Eur J Vasc Endovasc Surg*. 2007;34(2):163-8.
33. Linne A, Lindstrom D, Hultgren R. High prevalence of abdominal aortic aneurysms in brothers and sisters of patients despite a low prevalence in the population. *J Vasc Surg*. 2012;56(2):305-10.
34. Sakalihasan N, Defraigne JO, Kerstenne MA, Cheramy-Bien JP, Smelser DT, Tromp G, et al. Family members of patients with abdominal aortic aneurysms are at increased risk for aneurysms: analysis of 618 probands and their families from the Liege AAA Family Study. *Ann Vasc Surg*. 2014;28(4):787-97.



35. Webster MW, Ferrell RE, St Jean PL, Majumder PP, Fogel SR, Steed DL. Ultrasound screening of first-degree relatives of patients with an abdominal aortic aneurysm. *J Vasc Surg.* 1991;13(1):9-13; discussion -4.
36. Adamson J, Powell JT, Greenhalgh RM. Selection for screening for familial aortic aneurysms. *Br J Surg.* 1992;79(9):897-8.
37. Sinha I, Cho BS, Roelofs KJ, Stanley JC, Henke PK, Upchurch GR, Jr. Female gender attenuates cytokine and chemokine expression and leukocyte recruitment in experimental rodent abdominal aortic aneurysms. *Ann N Y Acad Sci.* 2006;1085:367-79.
38. Bown MJ, Powell JT. Part two: against the motion. Evidence does not support reducing the threshold diameter to 5 cm for elective interventions in women with abdominal aortic aneurysms. *Eur J Vasc Endovasc Surg.* 2014;48(6):614-8.
39. Wilmink TB, Quick CR, Hubbard CS, Day NE. The influence of screening on the incidence of ruptured abdominal aortic aneurysms. *J Vasc Surg.* 1999;30(2):203-8.
40. Scott RA, Ashton HA, Kay DN. Abdominal aortic aneurysm in 4237 screened patients: prevalence, development and management over 6 years. *Br J Surg.* 1991;78(9):1122-5.
41. Lindholt JS, Sorensen J, Sogaard R, Henneberg EW. Long-term benefit and cost-effectiveness analysis of screening for abdominal aortic aneurysms from a randomized controlled trial. *Br J Surg.* 2010;97(6):826-34.
42. Sogaard R, Lindholt J. Evidence for the credibility of health economic models for health policy decision-making: a systematic literature review of screening for abdominal aortic aneurysms. *J Health Serv Res Policy.* 2012;17(1):44-52.
43. Multicentre Aneurysm Screening Study G. Multicentre aneurysm screening study (MASS): cost effectiveness analysis of screening for abdominal aortic aneurysms based on four year results from randomised controlled trial. *BMJ.* 2002;325(7373):1135.
44. Norman PE, Semmens JB, Lawrence-Brown MM, Holman CD. Long term relative survival after surgery for abdominal aortic aneurysm in western Australia: population based study. *BMJ.* 1998;317(7162):852-6.

45. Norman PE, Semmens JB, Lawrence-Brown MM. Long-term relative survival following surgery for abdominal aortic aneurysm: a review. *Cardiovasc Surg.* 2001;9(3):219-24.
46. Solberg S, Forsdahl SH, Singh K, Jacobsen BK. Diameter of the infrarenal aorta as a risk factor for abdominal aortic aneurysm: the Tromso Study, 1994-2001. *Eur J Vasc Endovasc Surg.* 2010;39(3):280-4.
47. Brady AR, Thompson SG, Fowkes FG, Greenhalgh RM, Powell JT, Participants UKSAT. Abdominal aortic aneurysm expansion: risk factors and time intervals for surveillance. *Circulation.* 2004;110(1):16-21.
48. Metcalfe D, Holt PJ, Thompson MM. The management of abdominal aortic aneurysms. *BMJ.* 2011;342:d1384.
49. Powell JT, Brady AR. Detection, management, and prospects for the medical treatment of small abdominal aortic aneurysms. *Arterioscler Thromb Vasc Biol.* 2004;24(2):241-5.
50. Holt PJ, Poloniecki JD, Gerrard D, Loftus IM, Thompson MM. Meta-analysis and systematic review of the relationship between volume and outcome in abdominal aortic aneurysm surgery. *Br J Surg.* 2007;94(4):395-403.
51. Golledge J, Norman PE. Current status of medical management for abdominal aortic aneurysm. *Atherosclerosis.* 2011;217(1):57-63.
52. Rughani G, Robertson L, Clarke M. Medical treatment for small abdominal aortic aneurysms. *Cochrane Database Syst Rev.* 2012;9:CD009536.
53. Cooley DA. Aortic aneurysm operations: past, present, and future. *Ann Thorac Surg.* 1999;67(6):1959-62; discussion 79-80.
54. Bhogal R DR. The Evolution of Aortic Aneurysm Repair: Past Lessons and Future Directions. In: Bush R, editor. *Aneurysmal Disease of the Thoracic and Abdominal Aorta: InTech*; 2011. p. 21-54.
55. Gage IM. The Technical Simplicity of the Matas Endo-aneurysmorrhaphy. *Ann Surg.* 1944;119(3):468-73.
56. Livesay JJ, Messner GN, Vaughn WK. Milestones in the treatment of aortic aneurysm: Denton A. Cooley, MD, and the Texas Heart Institute. *Tex Heart Inst J.* 2005;32(2):130-4.

57. Dubost C, Allary M, Oeconomos N. [Treatment of aortic aneurysms; removal of the aneurysm; re-establishment of continuity by grafts of preserved human aorta]. *Mem Acad Chir (Paris)*. 1951;77(12-13):381-3.
58. Creech O, Jr. Endo-aneurysmorrhaphy and treatment of aortic aneurysm. *Ann Surg*. 1966;164(6):935-46.
59. participants Et. Endovascular aneurysm repair and outcome in patients unfit for open repair of abdominal aortic aneurysm (EVAR trial 2): randomised controlled trial. *Lancet*. 2005;365(9478):2187-92.
60. United Kingdom ETI, Greenhalgh RM, Brown LC, Powell JT, Thompson SG, Epstein D, et al. Endovascular versus open repair of abdominal aortic aneurysm. *N Engl J Med*. 2010;362(20):1863-71.
61. Parodi JC, Palmaz JC, Barone HD. Transfemoral intraluminal graft implantation for abdominal aortic aneurysms. *Ann Vasc Surg*. 1991;5(6):491-9.
62. Greenhalgh RM, Brown LC, Kwong GP, Powell JT, Thompson SG, participants Et. Comparison of endovascular aneurysm repair with open repair in patients with abdominal aortic aneurysm (EVAR trial 1), 30-day operative mortality results: randomised controlled trial. *Lancet*. 2004;364(9437):843-8.
63. Lederle FA, Freischlag JA, Kyriakides TC, Matsumura JS, Padberg FT, Jr., Kohler TR, et al. Long-term comparison of endovascular and open repair of abdominal aortic aneurysm. *N Engl J Med*. 2012;367(21):1988-97.
64. De Bruin JL, Baas AF, Buth J, Prinssen M, Verhoeven EL, Cuypers PW, et al. Long-term outcome of open or endovascular repair of abdominal aortic aneurysm. *N Engl J Med*. 2010;362(20):1881-9.
65. Chaikof EL, Blankensteijn JD, Harris PL, White GH, Zarins CK, Bernhard VM, et al. Reporting standards for endovascular aortic aneurysm repair. *J Vasc Surg*. 2002;35(5):1048-60.
66. Tonnessen BH, Sternbergh WC, 3rd, Money SR. Mid- and long-term device migration after endovascular abdominal aortic aneurysm repair: a comparison of AneuRx and Zenith endografts. *J Vasc Surg*. 2005;42(3):392-400; discussion -1.
67. Cao P, Verzini F, Zannetti S, De Rango P, Parlani G, Lupattelli L, et al. Device migration after endoluminal abdominal aortic aneurysm repair: analysis of 113 cases with a minimum follow-up period of 2 years. *J Vasc Surg*. 2002;35(2):229-35.

68. participants Et. Endovascular aneurysm repair versus open repair in patients with abdominal aortic aneurysm (EVAR trial 1): randomised controlled trial. *Lancet*. 2005;365(9478):2179-86.
69. Fransen GA, Desgranges P, Laheij RJ, Harris PL, Becquemin JP, Collaborators E. Frequency, predictive factors, and consequences of stent-graft kink following endovascular AAA repair. *J Endovasc Ther*. 2003;10(5):913-8.
70. White GH, May J, Waugh RC, Chaufour X, Yu W. Type III and type IV endoleak: toward a complete definition of blood flow in the sac after endoluminal AAA repair. *J Endovasc Surg*. 1998;5(4):305-9.
71. Hobo R, Buth J, collaborators E. Secondary interventions following endovascular abdominal aortic aneurysm repair using current endografts. A EUROSTAR report. *J Vasc Surg*. 2006;43(5):896-902.
72. Veith FJ, Baum RA, Ohki T, Amor M, Adiseshiah M, Blankensteijn JD, et al. Nature and significance of endoleaks and endotension: summary of opinions expressed at an international conference. *J Vasc Surg*. 2002;35(5):1029-35.
73. Greenhalgh RM, Powell JT. Endovascular repair of abdominal aortic aneurysm. *N Engl J Med*. 2008;358(5):494-501.
74. Fransen GA, Vallabhaneni SR, Sr., van Marrewijk CJ, Laheij RJ, Harris PL, Buth J, et al. Rupture of infra-renal aortic aneurysm after endovascular repair: a series from EUROSTAR registry. *Eur J Vasc Endovasc Surg*. 2003;26(5):487-93.
75. Silverberg D, Baril DT, Ellozy SH, Carroccio A, Greyrose SE, Lookstein RA, et al. An 8-year experience with type II endoleaks: natural history suggests selective intervention is a safe approach. *J Vasc Surg*. 2006;44(3):453-9.
76. Jones JE, Atkins MD, Brewster DC, Chung TK, Kwolek CJ, LaMuraglia GM, et al. Persistent type 2 endoleak after endovascular repair of abdominal aortic aneurysm is associated with adverse late outcomes. *J Vasc Surg*. 2007;46(1):1-8.
77. Sidloff DA, Stather PW, Choke E, Bown MJ, Sayers RD. Type II endoleak after endovascular aneurysm repair. *Br J Surg*. 2013;100(10):1262-70.
78. Choke E, Thompson M. Endoleak after endovascular aneurysm repair: current concepts. *J Cardiovasc Surg (Torino)*. 2004;45(4):349-66.
79. Karthikesalingam A, Thrumurthy SG, Jackson D, Choke E, Sayers RD, Loftus IM, et al. Current evidence is insufficient to define an optimal threshold for intervention in

isolated type II endoleak after endovascular aneurysm repair. *J Endovasc Ther.* 2012;19(2):200-8.

80. van Marrewijk CJ, Fransen G, Laheij RJ, Harris PL, Buth J, Collaborators E. Is a type II endoleak after EVAR a harbinger of risk? Causes and outcome of open conversion and aneurysm rupture during follow-up. *Eur J Vasc Endovasc Surg.* 2004;27(2):128-37.

81. Hinchliffe RJ, Singh-Ranger R, Davidson IR, Hopkinson BR. Rupture of an abdominal aortic aneurysm secondary to type II endoleak. *Eur J Vasc Endovasc Surg.* 2001;22(6):563-5.

82. Prinssen M, Verhoeven EL, Verhagen HJ, Blankensteijn JD. Decision-making in follow-up after endovascular aneurysm repair based on diameter and volume measurements: a blinded comparison. *Eur J Vasc Endovasc Surg.* 2003;26(2):184-7.

83. van Keulen JW, van Prehn J, Prokop M, Moll FL, van Herwaarden JA. Potential value of aneurysm sac volume measurements in addition to diameter measurements after endovascular aneurysm repair. *J Endovasc Ther.* 2009;16(4):506-13.

84. Hahne JD, Arndt C, Herrmann J, Schonagel B, Adam G, Habermann CR. Follow-up of abdominal aortic aneurysm after endovascular aortic repair: comparison of volumetric and diametric measurement. *Eur J Radiol.* 2012;81(6):1187-91.

85. Aziz A, Menias CO, Sanchez LA, Picus D, Saad N, Rubin BG, et al. Outcomes of percutaneous endovascular intervention for type II endoleak with aneurysm expansion. *J Vasc Surg.* 2012;55(5):1263-7.

86. Ouriel K, Clair DG, Greenberg RK, Lyden SP, O'Hara PJ, Sarac TP, et al. Endovascular repair of abdominal aortic aneurysms: device-specific outcome. *J Vasc Surg.* 2003;37(5):991-8.

87. Verhoeven BA, Waasdorp EJ, Gorrepati ML, van Herwaarden JA, Vos JA, Wille J, et al. Long-term results of Talent endografts for endovascular abdominal aortic aneurysm repair. *J Vasc Surg.* 2011;53(2):293-8.

88. Reijnen MM, Minion DJ, Lardenoye JW. Treatment of a type IIIb endoleak in a Talent endograft using telescoping cuffs and two parallel upside-down excluder contralateral legs. *J Vasc Surg.* 2012;56(2):538-41.

89. Biebl M, Hakaim AG, Oldenburg WA, Klocker J, McKinney JM, Paz-Fumagalli R. Management of a large intraoperative type IIIb endoleak in a bifurcated endograft—a case report. *Vasc Endovascular Surg*. 2005;39(3):267-71.
90. Bucci F, Fiengo L, Valerio N, Ferdani M. Late type IIIb endoleak after endovascular aneurysm repair: case report and review of the literature. *G Chir*. 2011;32(6-7):329-33.
91. Darling RC, Messina CR, Brewster DC, Ottinger LW. Autopsy study of unoperated abdominal aortic aneurysms. The case for early resection. *Circulation*. 1977;56(3 Suppl):II161-4.
92. Participants TUSAT. Mortality results for randomised controlled trial of early elective surgery or ultrasonographic surveillance for small abdominal aortic aneurysms. The UK Small Aneurysm Trial Participants. *Lancet*. 1998;352(9141):1649-55.
93. United Kingdom Small Aneurysm Trial P. Long-term outcomes of immediate repair compared with surveillance of small abdominal aortic aneurysms. *N Engl J Med*. 2002;346(19):1445-52.
94. Lederle FA, Wilson SE, Johnson GR, Reinke DB, Littooy FN, Acher CW, et al. Immediate repair compared with surveillance of small abdominal aortic aneurysms. *N Engl J Med*. 2002;346(19):1437-44.
95. Gasser TC, Nchimi A, Swedenborg J, Roy J, Sakalihasan N, Bockler D, et al. A novel strategy to translate the biomechanical rupture risk of abdominal aortic aneurysms to their equivalent diameter risk: method and retrospective validation. *Eur J Vasc Endovasc Surg*. 2014;47(3):288-95.
96. Doyle BJ, McGloughlin TM, Miller K, Powell JT, Norman PE. Regions of high wall stress can predict the future location of rupture of abdominal aortic aneurysm. *Cardiovasc Intervent Radiol*. 2014;37(3):815-8.
97. Fillinger MF, Marra SP, Raghavan ML, Kennedy FE. Prediction of rupture risk in abdominal aortic aneurysm during observation: wall stress versus diameter. *J Vasc Surg*. 2003;37(4):724-32.
98. Stringfellow MM, Lawrence PF, Stringfellow RG. The influence of aorta-aneurysm geometry upon stress in the aneurysm wall. *J Surg Res*. 1987;42(4):425-33.

99. Dobrin PB. Pathophysiology and pathogenesis of aortic aneurysms. Current concepts. *Surg Clin North Am.* 1989;69(4):687-703.
100. Inzoli F, Boschetti F, Zappa M, Longo T, Fumero R. Biomechanical factors in abdominal aortic aneurysm rupture. *Eur J Vasc Surg.* 1993;7(6):667-74.
101. Vorp DA, Raghavan ML, Webster MW. Mechanical wall stress in abdominal aortic aneurysm: influence of diameter and asymmetry. *J Vasc Surg.* 1998;27(4):632-9.
102. Raghavan ML, Vorp DA, Federle MP, Makaroun MS, Webster MW. Wall stress distribution on three-dimensionally reconstructed models of human abdominal aortic aneurysm. *J Vasc Surg.* 2000;31(4):760-9.
103. Raghavan ML, Vorp DA. Toward a biomechanical tool to evaluate rupture potential of abdominal aortic aneurysm: identification of a finite strain constitutive model and evaluation of its applicability. *J Biomech.* 2000;33(4):475-82.
104. Fillinger MF, Raghavan ML, Marra SP, Cronenwett JL, Kennedy FE. In vivo analysis of mechanical wall stress and abdominal aortic aneurysm rupture risk. *J Vasc Surg.* 2002;36(3):589-97.
105. Venkatasubramaniam AK, Fagan MJ, Mehta T, Mylankal KJ, Ray B, Kuhan G, et al. A comparative study of aortic wall stress using finite element analysis for ruptured and non-ruptured abdominal aortic aneurysms. *Eur J Vasc Endovasc Surg.* 2004;28(2):168-76.
106. Heng MS, Fagan MJ, Collier JW, Desai G, McCollum PT, Chetter IC. Peak wall stress measurement in elective and acute abdominal aortic aneurysms. *J Vasc Surg.* 2008;47(1):17-22; discussion
107. Truijers M, Pol JA, Schultzekool LJ, van Sterkenburg SM, Fillinger MF, Blankensteijn JD. Wall stress analysis in small asymptomatic, symptomatic and ruptured abdominal aortic aneurysms. *Eur J Vasc Endovasc Surg.* 2007;33(4):401-7.
108. Harter LP, Gross BH, Callen PW, Barth RA. Ultrasonic evaluation of abdominal aortic thrombus. *J Ultrasound Med.* 1982;1(8):315-8.
109. Swedenborg J, Eriksson P. The intraluminal thrombus as a source of proteolytic activity. *Ann N Y Acad Sci.* 2006;1085:133-8.
110. Vorp DA, Lee PC, Wang DH, Makaroun MS, Nemoto EM, Ogawa S, et al. Association of intraluminal thrombus in abdominal aortic aneurysm with local hypoxia and wall weakening. *J Vasc Surg.* 2001;34(2):291-9.

111. Schurink GW, van Baalen JM, Visser MJ, van Bockel JH. Thrombus within an aortic aneurysm does not reduce pressure on the aneurysmal wall. *J Vasc Surg.* 2000;31(3):501-6.
112. Wang DH, Makaroun M, Webster MW, Vorp DA. Mechanical properties and microstructure of intraluminal thrombus from abdominal aortic aneurysm. *J Biomech Eng.* 2001;123(6):536-9.
113. Vorp DA, Mandarino WA, Webster MW, Gorcsan J, 3rd. Potential influence of intraluminal thrombus on abdominal aortic aneurysm as assessed by a new non-invasive method. *Cardiovasc Surg.* 1996;4(6):732-9.
114. Gasser TC, Auer M, Labruto F, Swedenborg J, Roy J. Biomechanical rupture risk assessment of abdominal aortic aneurysms: model complexity versus predictability of finite element simulations. *Eur J Vasc Endovasc Surg.* 2010;40(2):176-85.
115. O'Leary SA, Kavanagh EG, Grace PA, McGloughlin TM, Doyle BJ. The biaxial mechanical behaviour of abdominal aortic aneurysm intraluminal thrombus: classification of morphology and the determination of layer and region specific properties. *J Biomech.* 2014;47(6):1430-7.
116. McGloughlin TM, Doyle BJ. New approaches to abdominal aortic aneurysm rupture risk assessment: engineering insights with clinical gain. *Arterioscler Thromb Vasc Biol.* 2010;30(9):1687-94.
117. Vande Geest JP, Di Martino ES, Bohra A, Makaroun MS, Vorp DA. A biomechanics-based rupture potential index for abdominal aortic aneurysm risk assessment: demonstrative application. *Ann N Y Acad Sci.* 2006;1085:11-21.
118. Vande Geest JP, Wang DH, Wisniewski SR, Makaroun MS, Vorp DA. Towards a noninvasive method for determination of patient-specific wall strength distribution in abdominal aortic aneurysms. *Ann Biomed Eng.* 2006;34(7):1098-106.
119. Doyle BJ, Callanan A, Walsh MT, Grace PA, McGloughlin TM. A finite element analysis rupture index (FEARI) as an additional tool for abdominal aortic aneurysm rupture prediction. *Vasc Dis Prev.* 2009;6:114-21.
120. Doyle B, Coyle P, Kavanagh E, Grace P, McGloughlin T, editors. A finite element analysis rupture index (FEARI) assessment of electively repaired and symptomatic/ruptured abdominal aortic aneurysms. 6th World Congress of Biomechanics (WCB 2010) August 1-6, 2010 Singapore; 2010: Springer.



121. Raghavan ML, Webster MW, Vorp DA. Ex vivo biomechanical behavior of abdominal aortic aneurysm: assessment using a new mathematical model. *Ann Biomed Eng.* 1996;24(5):573-82.
122. Raghavan ML, Kratzberg J, Castro de Tolosa EM, Hanaoka MM, Walker P, da Silva ES. Regional distribution of wall thickness and failure properties of human abdominal aortic aneurysm. *J Biomech.* 2006;39(16):3010-6.
123. Thubrikar MJ, Labrosse M, Robicsek F, Al-Soudi J, Fowler B. Mechanical properties of abdominal aortic aneurysm wall. *J Med Eng Technol.* 2001;25(4):133-42.
124. Doyle BJ, Hoskins PR, McGloughlin TM. Computational rupture prediction of AAAs: what needs to be done next? *J Endovasc Ther.* 2011;18(2):226-9.
125. VASCOPS. VASCOPS AAA Analyser - A4 Clinics: VASCOPS; 2014 [cited 2014 12th August]. Available from: <http://www.vascops.com/en/vascops-A4clinics.html>.
126. Khosla S, Morris DR, Moxon JV, Walker PJ, Gasser TC, Golledge J. Meta-analysis of peak wall stress in ruptured, symptomatic and intact abdominal aortic aneurysms. *Br J Surg.* 2014;101(11):1350-7.
127. Raghavan ML, Kratzberg JA, Golzarian J. Introduction to biomechanics related to endovascular repair of abdominal aortic aneurysm. *Tech Vasc Interv Radiol.* 2005;8(1):50-5.
128. Frangos JA, Eskin SG, McIntire LV, Ives CL. Flow effects on prostacyclin production by cultured human endothelial cells. *Science.* 1985;227(4693):1477-9.
129. Rubanyi GM, Romero JC, Vanhoutte PM. Flow-induced release of endothelium-derived relaxing factor. *Am J Physiol.* 1986;250(6 Pt 2):H1145-9.
130. Helmlinger G, Berk BC, Nerem RM. Calcium responses of endothelial cell monolayers subjected to pulsatile and steady laminar flow differ. *Am J Physiol.* 1995;269(2 Pt 1):C367-75.
131. Malek AM, Jackman R, Rosenberg RD, Izumo S. Endothelial expression of thrombomodulin is reversibly regulated by fluid shear stress. *Circ Res.* 1994;74(5):852-60.
132. Lawrence MB, McIntire LV, Eskin SG. Effect of flow on polymorphonuclear leukocyte/endothelial cell adhesion. *Blood.* 1987;70(5):1284-90.

133. Zambrano BA, Gharahi H, Lim C, Jaber FA, Choi J, Lee W, et al. Association of Intraluminal Thrombus, Hemodynamic Forces, and Abdominal Aortic Aneurysm Expansion Using Longitudinal CT Images. *Ann Biomed Eng.* 2015.
134. Barry Doyle TM, Eamon Kavanagh,, Hoskins P. From detection to rupture: a serial computational fluid dynamics case study of a rapidly expanding, patient-specific, ruptured abdominal aortic aneurysm  
. In: Barry Doyle KM, Adam Wittek, P.M.F. Nielsen, editor. *Computational Biomechanics for Medicine Fundamental Science and Patient-specific Applications.* New York: Springer; 2014. p. 53-68.
135. Wang DH, Makaroun MS, Webster MW, Vorp DA. Effect of intraluminal thrombus on wall stress in patient-specific models of abdominal aortic aneurysm. *J Vasc Surg.* 2002;36(3):598-604.
136. Speelman L, Schurink GW, Bosboom EM, Buth J, Breeuwer M, van de Vosse FN, et al. The mechanical role of thrombus on the growth rate of an abdominal aortic aneurysm. *J Vasc Surg.* 2010;51(1):19-26.
137. Parr A, McCann M, Bradshaw B, Shahzad A, Buttner P, Golledge J. Thrombus volume is associated with cardiovascular events and aneurysm growth in patients who have abdominal aortic aneurysms. *J Vasc Surg.* 2011;53(1):28-35.
138. Fraser KH, Meagher S, Blake JR, Easson WJ, Hoskins PR. Characterization of an abdominal aortic velocity waveform in patients with abdominal aortic aneurysm. *Ultrasound Med Biol.* 2008;34(1):73-80.
139. Boyd AJ, Kuhn DC, Lozowy RJ, Kulbisky GP. Low wall shear stress predominates at sites of abdominal aortic aneurysm rupture. *J Vasc Surg.* 2015.
140. Chaudhuri A. Commentary on 'use of colour duplex ultrasound as a first line surveillance tool following Evar is associated with a reduction in cost without compromising accuracy'. *Eur J Vasc Endovasc Surg.* 2012;44(2):151-2.
141. Farr RF A-RP. *Physics for medical imaging.* Physics for medical imaging: Saunders; 2002. p. 148-82.
142. Heilberger P, Schunn C, Ritter W, Weber S, Raithel D. Postoperative color flow duplex scanning in aortic endografting. *J Endovasc Surg.* 1997;4(3):262-71.

143. Sato DT, Goff CD, Gregory RT, Robinson KD, Carter KA, Herts BR, et al. Endoleak after aortic stent graft repair: diagnosis by color duplex ultrasound scan versus computed tomography scan. *J Vasc Surg.* 1998;28(4):657-63.
144. McWilliams RG, Martin J, White D, Gould DA, Harris PL, Fear SC, et al. Use of contrast-enhanced ultrasound in follow-up after endovascular aortic aneurysm repair. *J Vasc Interv Radiol.* 1999;10(8):1107-14.
145. Wolf YG, Johnson BL, Hill BB, Rubin GD, Fogarty TJ, Zarins CK. Duplex ultrasound scanning versus computed tomographic angiography for postoperative evaluation of endovascular abdominal aortic aneurysm repair. *J Vasc Surg.* 2000;32(6):1142-8.
146. Pages S, Favre JP, Cerisier A, Pyneeandee S, Boissier C, Veyret C. Comparison of color duplex ultrasound and computed tomography scan for surveillance after aortic endografting. *Ann Vasc Surg.* 2001;15(2):155-62.
147. Raman KG, Missig-Carroll N, Richardson T, Muluk SC, Makaroun MS. Color-flow duplex ultrasound scan versus computed tomographic scan in the surveillance of endovascular aneurysm repair. *J Vasc Surg.* 2003;38(4):645-51.
148. Bendick PJ, Bove PG, Long GW, Zelenock GB, Brown OW, Shanley CJ. Efficacy of ultrasound scan contrast agents in the noninvasive follow-up of aortic stent grafts. *J Vasc Surg.* 2003;37(2):381-5.
149. Bendick PJ, Zelenock GB, Bove PG, Long GW, Shanley CJ, Brown OW. Duplex ultrasound imaging with an ultrasound contrast agent: the economic alternative to CT angiography for aortic stent graft surveillance. *Vasc Endovascular Surg.* 2003;37(3):165-70.
150. AbuRahma AF, Welch CA, Mullins BB, Dyer B. Computed tomography versus color duplex ultrasound for surveillance of abdominal aortic stent-grafts. *J Endovasc Ther.* 2005;12(5):568-73.
151. Ashoke R, Brown LC, Rodway A, Choke E, Thompson MM, Greenhalgh RM, et al. Color duplex ultrasonography is insensitive for the detection of endoleak after aortic endografting: a systematic review. *J Endovasc Ther.* 2005;12(3):297-305.
152. Iezzi R, Basilico R, Giancristofaro D, Pascali D, Cotroneo AR, Storto ML. Contrast-enhanced ultrasound versus color duplex ultrasound imaging in the follow-up of patients after endovascular abdominal aortic aneurysm repair. *J Vasc Surg.* 2009;49(3):552-60.

153. Mirza TA, Karthikesalingam A, Jackson D, Walsh SR, Holt PJ, Hayes PD, et al. Duplex ultrasound and contrast-enhanced ultrasound versus computed tomography for the detection of endoleak after EVAR: systematic review and bivariate meta-analysis. *Eur J Vasc Endovasc Surg.* 2010;39(4):418-28.
154. Ten Bosch JA, Rouwet EV, Peters CT, Jansen L, Verhagen HJ, Prins MH, et al. Contrast-enhanced ultrasound versus computed tomographic angiography for surveillance of endovascular abdominal aortic aneurysm repair. *J Vasc Interv Radiol.* 2010;21(5):638-43.
155. Perini P, Sediri I, Midulla M, Delsart P, Mouton S, Gautier C, et al. Single-centre prospective comparison between contrast-enhanced ultrasound and computed tomography angiography after EVAR. *Eur J Vasc Endovasc Surg.* 2011;42(6):797-802.
156. Cantisani V, Ricci P, Grazhdani H, Napoli A, Fanelli F, Catalano C, et al. Prospective comparative analysis of colour-Doppler ultrasound, contrast-enhanced ultrasound, computed tomography and magnetic resonance in detecting endoleak after endovascular abdominal aortic aneurysm repair. *Eur J Vasc Endovasc Surg.* 2011;41(2):186-92.
157. Karthikesalingam A, Al-Jundi W, Jackson D, Boyle JR, Beard JD, Holt PJ, et al. Systematic review and meta-analysis of duplex ultrasonography, contrast-enhanced ultrasonography or computed tomography for surveillance after endovascular aneurysm repair. *Br J Surg.* 2012;99(11):1514-23.
158. Gray C, Goodman P, Herron CC, Lawler LP, O'Malley MK, O'Donohoe MK, et al. Use of colour duplex ultrasound as a first line surveillance tool following EVAR is associated with a reduction in cost without compromising accuracy. *Eur J Vasc Endovasc Surg.* 2012;44(2):145-50.
159. Gurtler VM, Sommer WH, Meimarakis G, Kopp R, Weidenhagen R, Reiser MF, et al. A comparison between contrast-enhanced ultrasound imaging and multislice computed tomography in detecting and classifying endoleaks in the follow-up after endovascular aneurysm repair. *J Vasc Surg.* 2013;58(2):340-5.
160. Millen A, Canavati R, Harrison G, McWilliams RG, Wallace S, Vallabhaneni SR, et al. Defining a role for contrast-enhanced ultrasound in endovascular aneurysm repair surveillance. *J Vasc Surg.* 2013;58(1):18-23.

161. Rumball-Smith A, Wright IA, Buckenham TM. Strut failure in the body of the zenith abdominal endoprosthesis. *Eur J Vasc Endovasc Surg.* 2006;32(2):136-9.
162. White HA, Macdonald S. Estimating risk associated with radiation exposure during follow-up after endovascular aortic repair (EVAR). *J Cardiovasc Surg (Torino).* 2010;51(1):95-104.
163. The 2007 Recommendations of the International Commission on Radiological Protection. ICRP publication 103. *Ann ICRP.* 2007;37(2-4):1-332.
164. Wever JJ, Blankensteijn JD, Mali WPTM, Eikelboom BC. Maximal aneurysm diameter follow-up is inadequate after endovascular abdominal aortic aneurysm repair. *Eur J Vasc Endovasc Surg.* 2000;20(2):177-82.
165. Leotta DF, Paun M, Beach KW, Kohler TR, Zierler RE, Strandness DE, Jr. Measurement of abdominal aortic aneurysms with three-dimensional ultrasound imaging: preliminary report. *J Vasc Surg.* 2001;33(4):700-7.
166. Nyhsen CM, Elliott ST. Rapid assessment of abdominal aortic aneurysms by 3-dimensional ultrasonography. *J Ultrasound Med.* 2007;26(2):223-6.
167. Vidakovic R, Schouten O, Feringa HH, Dunkelgrun M, Karagiannis SE, Merks E, et al. Abdominal aortic aneurysm screening using non-imaging hand-held ultrasound volume scanner--a pilot study. *Eur J Vasc Endovasc Surg.* 2006;32(6):615-9.
168. Causey MW, Jayaraj A, Leotta DF, Paun M, Beach KW, Kohler TR, et al. Three-dimensional ultrasonography measurements after endovascular aneurysm repair. *Ann Vasc Surg.* 2013;27(2):146-53.
169. Long A, Rouet L, Debreuve A, Ardon R, Barbe C, Becquemin JP, et al. Abdominal aortic aneurysm imaging with 3-D ultrasound: 3-D-based maximum diameter measurement and volume quantification. *Ultrasound Med Biol.* 2013;39(8):1325-36.
170. Bredahl K, Long A, Taudorf M, Lonn L, Rouet L, Ardon R, et al. Volume estimation of the aortic sac after EVAR using 3-D ultrasound - a novel, accurate and promising technique. *Eur J Vasc Endovasc Surg.* 2013;45(5):450-5
171. Bihari P, Shelke A, Nwe TH, Mularczyk M, Nelson K, Schmandra T, et al. Strain measurement of abdominal aortic aneurysm with real-time 3D ultrasound speckle tracking. *Eur J Vasc Endovasc Surg.* 2013;45(4):315-23.

172. Kok AM, Nguyen VL, Speelman L, Brands PJ, Schurink GW, van de Vosse FN, et al. Feasibility of wall stress analysis of abdominal aortic aneurysms using three-dimensional ultrasound. *J Vasc Surg.* 2015;61(5):1175-84.
173. Fenster A, Downey DB, Cardinal HN. Three-dimensional ultrasound imaging. *Phys Med Biol.* 2001;46(5):R67-99.
174. Downey DB, Fenster A, Williams JC. Clinical utility of three-dimensional US. *Radiographics.* 2000;20(2):559-71.
175. Prager RW, Ijaz UZ, Gee AH, Treece GM. Three-dimensional ultrasound imaging. *Proc Inst Mech Eng H.* 2010;224(2):193-223.
176. Elliot TL, Downey DB, Tong S, McLean CA, Fenster A. Accuracy of prostate volume measurements in vitro using three-dimensional ultrasound. *Acad Radiol.* 1996;3(5):401-6.
177. Tong S, Cardinal HN, McLoughlin RF, Downey DB, Fenster A. Intra- and inter-observer variability and reliability of prostate volume measurement via two-dimensional and three-dimensional ultrasound imaging. *Ultrasound Med Biol.* 1998;24(5):673-81.
178. Tong S, Cardinal HN, Downey DB, Fenster A. Analysis of linear, area and volume distortion in 3D ultrasound imaging. *Ultrasound Med Biol.* 1998;24(3):355-73.
179. Mezger U, Jendrewski C, Bartels M. Navigation in surgery. *Langenbecks Arch Surg.* 2013;398(4):501-14.
180. Feurer R, Hengersperger C, Runyan J, Seifert C, Pongratz J, Wilhelm M, et al. Reliability of a freehand three-dimensional ultrasonic device allowing anatomical orientation" at a glance": Study protocol for 3D measurements with Curefab CS. *Journal of Biomedical Graphics & Computing.* 2012;2(2).
181. Schneider M. SonoVue, a new ultrasound contrast agent. *Eur Radiol.* 1999;9 Suppl 3:S347-8.
182. Sandford RM, Batchelder AJ, Bown MJ, Sayers RD. Pre-discharge duplex ultrasound scans detect endoleaks not seen on completion angiography after endovascular aneurysm repair. *J Endovasc Ther.* 2010;17(3):349-53.
183. Rundback JH, Nahl D, Yoo V. Contrast-induced nephropathy. *J Vasc Surg.* 2011;54(2):575-9.

184. Boykov YY, Jolly M-P, editors. Interactive graph cuts for optimal boundary & region segmentation of objects in ND images. *Computer Vision, 2001 ICCV 2001 Proceedings Eighth IEEE International Conference on*; 2001: IEEE.
185. Criminisi A, Sharp T, Blake A. Geos: Geodesic image segmentation. *Computer Vision—ECCV 2008: Springer*; 2008. p. 99-112.
186. Couprie C, Grady L, Najman L, Talbot H. Power watershed: A unifying graph-based optimization framework. *Pattern Analysis and Machine Intelligence, IEEE Transactions on*. 2011;33(7):1384-99.
187. Lorensen WE, Cline HE, editors. Marching cubes: A high resolution 3D surface construction algorithm. *ACM siggraph computer graphics*; 1987: ACM.
188. Nadolski GJ, Stavropoulos SW. Contrast alternatives for iodinated contrast allergy and renal dysfunction: options and limitations. *J Vasc Surg*. 2013;57(2):593-8.
189. Criado E, Upchurch GR, Jr., Young K, Rectenwald JE, Coleman DM, Eliason JL, et al. Endovascular aortic aneurysm repair with carbon dioxide-guided angiography in patients with renal insufficiency. *J Vasc Surg*. 2012;55(6):1570-5.
190. Abbas A, Hansrani V, Sedgwick N, Ghosh J, McCollum CN. 3D Contrast Enhanced Ultrasound for Detecting Endoleak Following Endovascular Aneurysm Repair (EVAR). *Eur J Vasc Endovasc Surg*. 2014;47(5):487-92.
191. Biasi L, Ali T, Hinchliffe R, Morgan R, Loftus I, Thompson M. Intraoperative DynaCT detection and immediate correction of a type Ia endoleak following endovascular repair of abdominal aortic aneurysm. *Cardiovasc Intervent Radiol*. 2009;32(3):535-8.
192. Harris PL, Vallabhaneni SR, Desgranges P, Becquemin JP, van Marrewijk C, Laheij RJ. Incidence and risk factors of late rupture, conversion, and death after endovascular repair of infrarenal aortic aneurysms: the EUROSTAR experience. European Collaborators on Stent/graft techniques for aortic aneurysm repair. *J Vasc Surg*. 2000;32(4):739-49.
193. Huang SG, Woo K, Moos JM, Han S, Lew WK, Chao A, et al. A prospective study of carbon dioxide digital subtraction versus standard contrast arteriography in the detection of endoleaks in endovascular abdominal aortic aneurysm repairs. *Ann Vasc Surg*. 2013;27(1):38-44.

194. Karthikesalingam A, Page AA, Pettengell C, Hinchliffe RJ, Loftus IM, Thompson MM, et al. Heterogeneity in surveillance after endovascular aneurysm repair in the UK. *Eur J Vasc Endovasc Surg.* 2011;42(5):585-90.
195. Ormesher DC, Lowe C, Sedgwick N, McCollum CN, Ghosh J. Use of three-dimensional contrast-enhanced duplex ultrasound imaging during endovascular aneurysm repair. *J Vasc Surg.* 2014;60(6):1468-72.
196. Gargiulo M, Gallitto E, Serra C, Freyrie A, Mascoli C, Bianchini Massoni C, et al. Could Four-dimensional Contrast-enhanced Ultrasound Replace Computed Tomography Angiography During Follow up of Fenestrated Endografts? Results of a Preliminary Experience. *Eur J Vasc Endovasc Surg.* 2014.
197. Arsicot M, Lathelize H, Martinez R, Marchand E, Picquet J, Enon B. Follow-up of aortic stent grafts: comparison of the volumetric analysis of the aneurysm sac by ultrasound and CT. *Ann Vasc Surg.* 2014;28(7):1618-28.
198. Fenster A, Parraga G, Bax J. Three-dimensional ultrasound scanning. *Interface Focus.* 2011;1(4):503-19.
199. Grondal N, Bramsen MB, Thomsen MD, Rasmussen CB, Lindholt JS. The cardiac cycle is a major contributor to variability in size measurements of abdominal aortic aneurysms by ultrasound. *Eur J Vasc Endovasc Surg.* 2012;43(1):30-3.
200. Bredahl K, Sandholt B, Lonn L, Rouet L, Ardon R, Eiberg JP, et al. Three-dimensional ultrasound evaluation of small asymptomatic abdominal aortic aneurysms. *Eur J Vasc Endovasc Surg.* 2015;49(3):289-96.
201. Bredahl K, Eldrup N, Meyer C, Eiberg JE, Sillesen H. Reproducibility of ECG-gated ultrasound diameter assessment of small abdominal aortic aneurysms. *Eur J Vasc Endovasc Surg.* 2013;45(3):235-40.
202. Bredahl K, Taudorf M, Long A, Lonn L, Rouet L, Ardon R, et al. Three-dimensional ultrasound improves the accuracy of diameter measurement of the residual sac in EVAR patients. *Eur J Vasc Endovasc Surg.* 2013;46(5):525-32.
203. Earnshaw JJ. Doubts and dilemmas over abdominal aortic aneurysm. *Br J Surg.* 2011;98(5):607-8.
204. Reed D, Reed C, Stemmermann G, Hayashi T. Are aortic aneurysms caused by atherosclerosis? *Circulation.* 1992;85(1):205-11.



205. Soudah E, Ng EY, Loong TH, Bordone M, Pua U, Narayanan S. CFD modelling of abdominal aortic aneurysm on hemodynamic loads using a realistic geometry with CT. *Comput Math Methods Med.* 2013;2013:472564.
206. Biasetti J, Gasser TC, Auer M, Hedin U, Labruto F. Hemodynamics of the normal aorta compared to fusiform and saccular abdominal aortic aneurysms with emphasis on a potential thrombus formation mechanism. *Ann Biomed Eng.* 2010;38(2):380-90.
207. Finol EA, Amon CH. Flow-induced wall shear stress in abdominal aortic aneurysms: Part II--pulsatile flow hemodynamics. *Comput Methods Biomech Biomed Engin.* 2002;5(4):319-28.
208. Steinman DA. Image-based computational fluid dynamics modeling in realistic arterial geometries. *Ann Biomed Eng.* 2002;30(4):483-97.
209. Teutelink A, Cancrinus E, van de Heuvel D, Moll F, de Vries JP. Preliminary intraobserver and interobserver variability in wall stress and rupture risk assessment of abdominal aortic aneurysms using a semiautomatic finite element model. *J Vasc Surg.* 2012;55(2):326-30.
210. Hippelheuser JE, Lauric A, Cohen AD, Malek AM. Realistic non-Newtonian viscosity modelling highlights hemodynamic differences between intracranial aneurysms with and without surface blebs. *J Biomech.* 2014;47(15):3695-703.
211. Bade R, Haase J, Preim B, editors. *Comparison of Fundamental Mesh Smoothing Algorithms for Medical Surface Models.* SimVis; 2006: Citeseer.
212. Dyn N, Levine D, Gregory JA. A butterfly subdivision scheme for surface interpolation with tension control. *ACM transactions on Graphics (TOG).* 1990;9(2):160-9.
213. MeshMixer. 2015.
214. MeshLab. 2015.
215. Field DA. Laplacian smoothing and Delaunay triangulations. *Communications in applied numerical methods.* 1988;4(6):709-12.
216. Vollmer J, Mencl R, Mueller H, editors. *Improved laplacian smoothing of noisy surface meshes.* Computer Graphics Forum; 1999: Wiley Online Library.
217. Taubin G, editor *Curve and surface smoothing without shrinkage.* Computer Vision, 1995 Proceedings, Fifth International Conference on; 1995: IEEE.

218. Canann SA, Stephenson MB, Blacker T. Optismoothing: An optimization-driven approach to mesh smoothing. *Finite Elements in Analysis and Design*. 1993;13(2):185-90.
219. Canann SA, Tristano JR, Staten ML, editors. *An Approach to Combined Laplacian and Optimization-Based Smoothing for Triangular, Quadrilateral, and Quad-Dominant Meshes*. IMR; 1998: Citeseer.
220. Ji Z, Liu L, Wang G, editors. A global laplacian smoothing approach with feature preservation. *Computer Aided Design and Computer Graphics*, 2005 Ninth International Conference on; 2005: IEEE.
221. Les AS, Shadden SC, Figueroa CA, Park JM, Tedesco MM, Herfkens RJ, et al. Quantification of hemodynamics in abdominal aortic aneurysms during rest and exercise using magnetic resonance imaging and computational fluid dynamics. *Ann Biomed Eng*. 2010;38(4):1288-313.
222. Doyle BJ, Morris LG, Callanan A, Kelly P, Vorp DA, McGloughlin TM. 3D reconstruction and manufacture of real abdominal aortic aneurysms: from CT scan to silicone model. *J Biomech Eng*. 2008;130(3):034501.
223. Doyle BJ, Cloonan AJ, Walsh MT, Vorp DA, McGloughlin TM. Identification of rupture locations in patient-specific abdominal aortic aneurysms using experimental and computational techniques. *J Biomech*. 2010;43(7):1408-16.
224. van den Haak RF, Hamans BC, Zuurmond K, Verhoeven BA, Koning OH. Significant Radiation Dose Reduction in the Hybrid Operating Room Using a Novel X-ray Imaging Technology. *Eur J Vasc Endovasc Surg*. 2015;50(4):480-6.
225. Clevert DA, Helck A, D'Anastasi M, Gurtler V, Sommer WH, Meimarakis G, et al. Improving the follow up after EVAR by using ultrasound image fusion of CEUS and MS-CT. *Clin Hemorheol Microcirc*. 2011;49(1-4):91-104.
226. Grant SW, Hickey GL, Grayson AD, Mitchell DC, McCollum CN. National risk prediction model for elective abdominal aortic aneurysm repair. *Br J Surg*. 2013;100(5):645-53.
227. Grant SW, Sperrin M, Carlson E, Chinai N, Ntais D, Hamilton M, et al. Calculating when elective abdominal aortic aneurysm repair improves survival for individual patients: development of the Aneurysm Repair Decision Aid and economic evaluation. *Health Technol Assess*. 2015;19(32):1-154.

